Functional Genomic Analysis of Natural Product Biosynthesis and Secretion in *Aspergillus fumigatus*

Lorna Gallagher BSc

Thesis submitted to the

National University of Ireland

for the degree of

Doctor of Philosophy

September 2010

Supervisors: Head of Department:

Prof. Sean Doyle,   Prof. Kay Ohlendieck

Biotechnology Laboratory,

Department of Biology,

National University of Ireland Maynooth,

Co. Kildare.

Dr. Kevin Kavanagh,

Medical Mycology Unit,

Department of Biology,

National University of Ireland Maynooth,

Co. Kildare.

TABLE OF CONTENTS

5. Functional characterisation of *gliK* – a component of the gliotoxin biosynthetic cluster of *Aspergillus fumigatus* 214

6. New Diagnostic Strategies for Detection of *A. fumigatus* Exposure in Humans **269**

7. Discussion **289**

8. Bibliography **296**

Declaration of Authorship

This thesis has not previously been submitted in whole or in part to this or any other University for any other degree. This thesis is the sole work of the author, with the exception of RP-HPLC and Mass spectrometry which was carried out by Prof. Thomas Larsen, Denmark technical institute, Lynby, Denmark.

_____

Lorna Gallagher BSc

Acknowleddegments

I wish to thank Prof. Sean Doyle and Dr. Kevin Kavanagh for giving me the opportunity, help and encouragement throughout my PhD years. The advice and encouragement was invaluable over the past years.

Thank you to everyone in the Biotechnology and Medical mycology lab, past and present for making the work day something to look forward to. I would like to especially thank Carol and Karen who not only helped me so much in the lab but also in life in general! I would also like to thank Grainne, Luke, Rebecca, Natasha, Fran, Cindy, Deirdre, Stephen, Emer and Tony. A special thanks to John who never failed to turn up for a coffee break and to Karen T for always joining me in the non-diet coke gang! I would also like to thank all the members of the yeast genetics and nematode genetics labs who let me "borrow" reagents in frequently occurring emergencies.

I couldn't have learnt as much if it was not for Markus and Christoph and their extensive knowledge and assistance. I would like to extend my gratitude to Prof. Thomas Larsen whose expertise in HPLC and Mass spectrometry helped so much. I would also like to thank Prof. Hubertus Haas for the Δ*sidD* strain and to Prof. Sven Krappmann for the Δ*akuB* strain and *ptrA* plasmid.

Most importantly I would like to thank my family and friends for supporting me from beginning to end. Shell and Brian, who kept me sane and made sure that I got to go to music concerts and the cinema. Thank you to Clarinda who was especially patient with me while I was writing. To my sisters, Ciara and Avril, who created enough drama to distract my parents from realising they were financially supporting me! To my extended family, thank you all so much for all the little and big things you have done for me. There are far too many of you to mention individually!

Finally, to my parents, Colette and Paul, I cannot put into words how amazing you both are. Thank you so much for everything, I hope I make you proud of me. I dedicate this thesis to you both.

Poster Presentations

Functional characterisation of gliK – a component of the gliotoxin biosynthetic cluster of Aspergillus fumigatus

Poster presentation at Society of General Microbiology – Irish Division, September 2nd – 3rd, 2010, National University of Ireland Maynooth, Maynooth, Co. Kildare. Awarded 1st Prize for presentation.

The non-ribosomal peptide synthetase, *pes1*, in Aspergillus fumigatus mediates in vitro anti-fungal drug resistance and contributes to growth ability under conditions of siderophore deficiency.

Poster presentation at 4th Advances Against Aspergillosis, February 4th – 6th, 2010, Rome, Italy.

Multiple effects of non-ribosomal peptide sythetase, *pes1*, deficiency in *Aspergillus fumigatus*.

Poster presentation at Irish fungal Meeting, 26th June 2009, University college of Dublin, Dublin 4.

Oral Presentations

Do selected nonribosomal peptide synthetases contribute to the virulence of *Aspergillus fumigatus* by protecting against oxidative stress?

Presentation at NUI Maynooth Microbiology Group Seminar, 28th Oct 2008

Do selected nonribosomal peptide synthetases contribute to the virulence of *Aspergillus fumigatus* by protecting against oxidative stress?

Presentation at NUI Maynooth Microbiology Group Seminar, 17th Dec 2007

Do selected nonribosomal peptide synthetases contribute to the virulence of *Aspergillus fumigatus* by protecting against oxidative stress?

Presentation at NUI Maynooth Departmental Seminar, NUI Maynooth, 07th May 2007

Abbreviations

aa	Amino Acid
ABPA	Allergic bronchopulmonary aspergillosis
AMM	Aspergillus Minimal Media
AmpB	Amphotericin B
ATCC	American Type Cell Culture
bp	base pairs
BSA	Bovine Serum Albumin
CADRE	Central Aspergillus Data Repository
cDNA	Complementary Dexoyribonucleic Acid
DMSO	Dimethyl sulfoxide
DNA	Deoxyribonucleic acid
DTT	Dithiothreitol
EDTA	Ethylenediaminetetraacetic acid
ELISA	Enzyme linked immunosorbant assay
FC	Fericrocin
FSC	Fusarinine C
GT	Gliotoxin
H_2O_2	Hydrogen peroxide
hph	hygromycin phosphotransferase
hr	Hour
IA	Invasive Aspergillosis
IPTG	Isoproproyl-β-DNA-thiogalactopyranoside
kb	Kilo-base
Kda	Kilo-Dalton
L	litre
LB	Luria-Bertani
mg	milligram
min	Minute
ml	millilitre
MM	Minimal Media

NADPH	Nicotinamide adenine dinuceotide phosphate
ng	nanogram
NHEJ	Non Homologous End Joining
NRP	Non-ribosomal peptide
NRPS	Non-ribosomal pepide synthetase
^{o}C	Celcius degrees
OD	Optical Density
PBS	Phosphate buffer saline
PCR	Polymerase Chain Reaction
PEG	Polyethylene Glycol
pg	picogram
rDNA	Ribosomal DNA
RIA	Reductive iron assimilation
RNA	Ribonucleic acid
RP-HPLC	Reverse Phase High Performance Liquid Chromatography
rpm	Revolutions per minute
Rt	Retention time
RT-PCR	Reverse-Transcriptaase Polymerase Chain Reaction
s	Second
SDS-PAGE	Sodium Dodecyl Sulphate Polyacrylamide Gel Electrophoresis
TAE	Tris:Acetate:EDTA
TAFC	Triacetylfusarinine C
TE	Tris:EDTA
TEMED	N,N,N1,N1-Tetramethylethylenediamine
TFA	Trifluroacetic Acid
TMB	Tetramethyl benzidine
VCR	Voriconazole
v/v	volume per volume
w/v	weight per volume
WT	Wild Type
X-gal	1,5-bromo-4-chloro-3-indoyl-β-DNA-galactosidase
μg	microgram
μl	microlitre

Summary

Aspergillus fumigatus is an opportunistic pathogen which can cause severe disease in immunocompromised patients. *A. fumigatus* produces metabolites, through a non-ribosomal peptide synthesis mechanism, including iron-chelating molecules known as siderophores and other unusual compounds such as gliotoxin. These provide the fungus with a unique strategy for survival in the host, and contribute to pathogenicity. The aim of this project was to identify interactions between non-ribosomal peptide synthetase genes (termed *pes1* and *sidD*) and to identify metabolites produced by these genes, which contribute to the virulence of *A. fumigatus* in immunocompromised patients.

A. fumigatus pes1 mutants (*pes1*) were generated in three genetic backgrounds (*akuB*, ATCC46645 and *sidD*[46645]), confirmed by Southern blot and qRT-PCR analysis. *A. fumigatus* Δ*akuB*:Δ*pes1* was significantly more sensitive to oxidative stress than wild-type (P < 0.01). It was found that, *in vitro*, either *pes1* or *sidD* significantly improved fungal tolerance to anti-fungal drugs (amphotericin B and voriconazole, respectively) which strongly suggests that either gene may play a role in mediating drug resistance/tolerance in patients. It was found that under oxidative stress conditions that this double mutant was significantly less sensitive to iron-limiting conditions than *A. fumigatus* Δ*sidD*, indicating that the peptide encoded via *pes1* is involved in the response of siderophore-deficient *A. fumigatus* to low iron availability, such as during infection. Compared to wild-type *A. fumigatus*, Δ*sidD*:Δ*pes1* was significantly less virulent than either single mutant in the *Galleria mellonella* virulence model system. Significantly, *pes1* was found to be involved in the biosynthesis of the conidial metabolite, fumigaclavine C, as this metabolite was absent in both *A. fumigatus* Δ*akuB:*Δ*pes1* and Δ*pes1*[46645].

In parallel studies, we identified a gene (*gliK*) responsible for gliotoxin biosynthesis and showed that *gliK* is involved in protecting *A. fumigatus* against oxidative stress, gliotoxin presence and secretion of gliotoxin from *A. fumigatus*. Overall, our findings may lead to improvements in therapy for patients suffering from invasive aspergillosis in the medium-to long-term.

CHAPTER 1

Introduction

1. Introduction

1.1 General Characteristics of *Aspergillus fumigatus*

Aspergillus fumigatus is a member of the *Ascomycetes* class of fungi. It is an ubiquitous soil dwelling fungus that is found mainly in decaying vegetation. Environmentally, *A. fumigatus* plays an important role in nitrogen and carbon recycling (Dagenais and Keller, 2009). *A. fumigatus* is thermostable and can survive in temperatures of up to 70 °C and still maintain growth at 55 °C (Latge, 1999). It forms septate mycelia which reproduce asexually by the production of conidial spores (Figure 1.1). The conidia are arranged in conidiophores where millions of conidia are attached in chains of eight spores (Figure 1.1) (Latge, 1999). Conidia (2 – 3 μm in diameter) are released from the conidophore and easily become airborne (Denning *et al.,* 2002). The released conidia undergo germination to form septate hyphae. *A. fumigatus* colonies are distinguishable from other fungi due to their grey-green colour as a result of the conidia pigmentation (Figure 1.1). Although generally considered to reproduce by asexual means, genes involved in the sexual cycle are present in the *A. fumigatus* genome (Dyer and Paoletti, 2005). Recently, identification of the sexual cycle in *A. fumigatus* was discovered, confirming sexual reproduction in the fungus (O'Gorman *et al.,* 2009). The genus *Aspergillus* contains over 250 species (Geiser *et al.,* 2007). However, only a small number of the species are pathogenic including *Aspergillus fumigatus, Aspergillus niger, Aspergillus terreus, Aspergillus nidulans* and *Aspergillus flavus* (Mabey *et al.,* 2004). Of these few pathogenic species, *A. fumigatus* is the most pathogenic, and is responsible for approximately 90 % of all invasive aspergillosis infections (Dagenais and Keller, 2009).
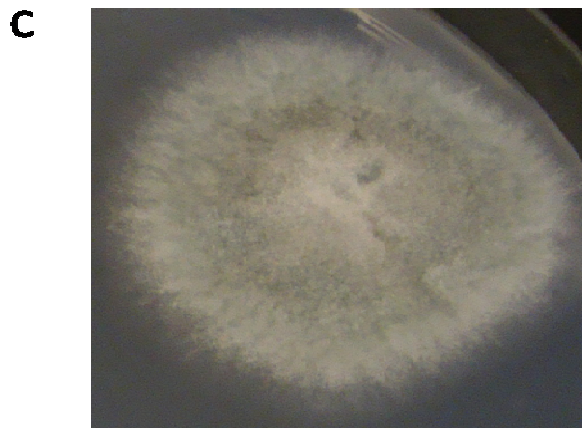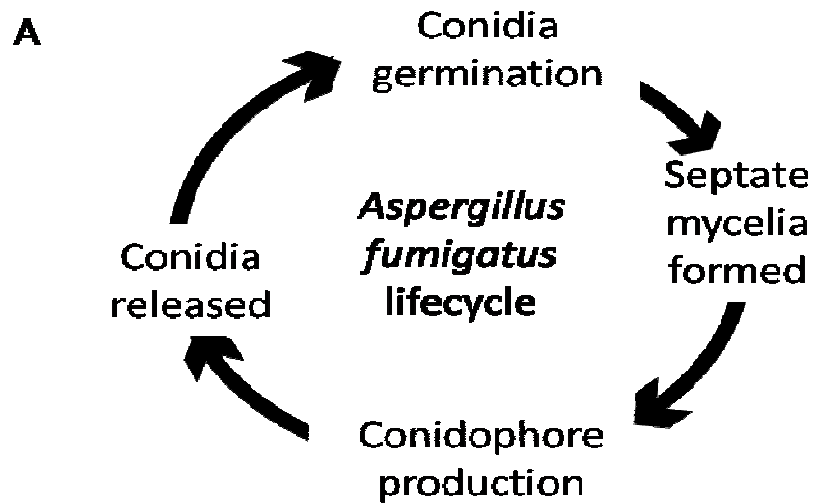
Figure 1.1: Lifecycle of *A. fumigatus* (A) The conidia released from the conidiophores germinate to form septate mycelia which produce conidiophores that release the conidia (Latge, 1999), (B) Scanning electron microscopy (SEM) of conidiophores (Taken from Latge, 2002) and (C) The grey-green colour of *A. fumigatus* due to the pigmentation of the conidia.

1.2 Pathogenesis of Aspergillus fumigatus

A. fumigatus is an opportunistic pathogen, due to the inhalation of up to 100 spores by any individual in a day. Any unchallenged conidia can lodge in the alveoli of the lungs and germinate; establishing an *Aspergillus* infection, particularly in immunocompromised individuals. The germinating conidia form a mycelial mass, begin to fill the lungs, and can potentially disseminate throughout the body. Normally, a healthy individual will clear any conidia by the innate immune response, usually by phagocytotic killing (Segal, 2007). Immunocompromised individuals are susceptible to *Aspergillus* infection as their immune system can be defective and will not clear conidia efficiently (Dagenais and Keller, 2009). The burden of this additional infection can easily result in death, thus *A. fumigatus* is one of the most virulent pathogenic fungi.

An infection by an *Aspergillus spp.* is called aspergillosis and this type of infection can be divided into degrees of severity, where invasive aspergillosis (IA) is the most fatal type of infection (Latge, 1999). Other infections include chronic cavity pulmonary aspergillosis (CCPA), and allergic bronchopulmonary aspergillosis (ABPA) and saprophytic aspergilloma (Buckingham and Hansell, 2003). Aspergilloma or "fungal ball" is a term used to describe the growth of *Aspergillus spp.* in the cavities of the lung that were created by pre-existing lung diseases or disorders such as tuberculosis or sarcodosis. Individuals with aspergilloma are usually asymptomatic and are only diagnosed by chance due to chest X-rays taken for a different pulmonary symptom (Latge, 1999). Individuals diagnosed with aspergillomas in the cavities of the chest are diagnosed with CCPA.

ABPA is a long-term hypersensitivity disorder which is a common complication in individuals with cystic fibrosis and asthma (Denning, 2001). ABPA results from

increased mucus levels within the lungs of these individuals which enables the germination of conidia. This is a persistent disease which can be distinguished from other *Aspergillus* infections due to hallmark elevation of IgE (Moss, 2002).

IA is characterised by the expansion of the aspergilloma from lung cavities into the surrounding tissue and then disseminating throughout the body. The incidence of IA has increased dramatically due to the increase in transplant and chemotherapy patients who are immunosuppressed (Baddley *et al.,* 2001; Marr *et al.,* 2002; Cordonnier *et al.,* 2006). The mortality rate associated with IA ranges from 60 – 90 % depending on the primary condition causing the immunosuppression (Latge, 1999).

1.2.1 Toxins and virulence factors associated with *A. fumigatus*

A. fumigatus can release a variety of toxins into the surrounding environment to kill other competing microorganisms (Calvo *et al.,* 2002), which the fungus uses to enhance its survival in the environment (Losada *et al.,* 2009).

The pathogenesis of *A. fumigatus* is enhanced by virulence factors. One of the best studied fungal toxins is gliotoxin, which is produced by many fungal species (Figure 1.2). It is acutely toxic with immunosuppressive properties (Sutton *et al.,* 1994). It is a member of the epipolythiodioxopiperazine (ETP) family and is characterised by a disulphide bridge across a diketopiperazine ring. Gliotoxin will be discussed further in Chapter 5.

Another important toxin found in *A. fumigatus* is fumagillin, which is an anti-tumour antibiotic which inhibits angiogenesis (Figure 1.2) (Rementeria *et al.,* 2005). It exhibits a toxic affect by inhibiting the proliferation of endothelial cells and restricts the cillary functions of the human respiratory epithelium. It works by

targeting the enzyme methionine aminopeptidase 2, and forms an irreversible bond (Bunger *et al.,* 2004). It has been recently demonstrated that fumagillin can alter neutrophil activity and therefore reduce the localised immune response (Fallon *et al.,* 2010).

Helvolic acid, otherwise known as fumigacin, is a member of a family of natural steroid antibiotics known as fusidanes, which is also produced by *A. fumgiatus* (Figure 1.2) (Rementeria *et al.,* 2005). It can have an effect on the oxidative burst of macrophages and can rupture epithelial cells (Amitani *et al.,* 1995).

Verruculogen is a member of the indole alkaloid group called tremorgens (Figure 1.2). This toxin has neurotoxic properties and is secreted from the mycelia during growth.

Fumigaclavines are metabolites produced by *Aspergillus spp.* and other fungi (Figure 1.2). There are seven members of this ergot alkaloid group, which are characterised by the four-member ergoline ring (Coyle and Panaccione, 2005), named: Agroclavine, Festuclavine, Elymoclavine, Chanaclavine, Fumigaclavine A, B and C (Frisvad *et al.,* 2009). Ergot alkaloids are associated with conidia, and represent 1 % of the conidial content (Panaccione and Coyle, 2005). There are four alkaloids identified in order of abundance in *A. fumigatus:* Fumigaclavine C, festuclavine, fumigaclavine A and fumigaclavine B. Fumigaclavine C accounts for 1.2 – 12 mg/g conidia, depending on the media used to grow the fungus. Fumigaclavine C has been shown to effect T lymphocytes by inhibiting their activation and proliferation, as well as reducing production of TNFα (Rementeria *et al.,* 2005). Fumigaclavine C will be discussed further in Chapter 4.
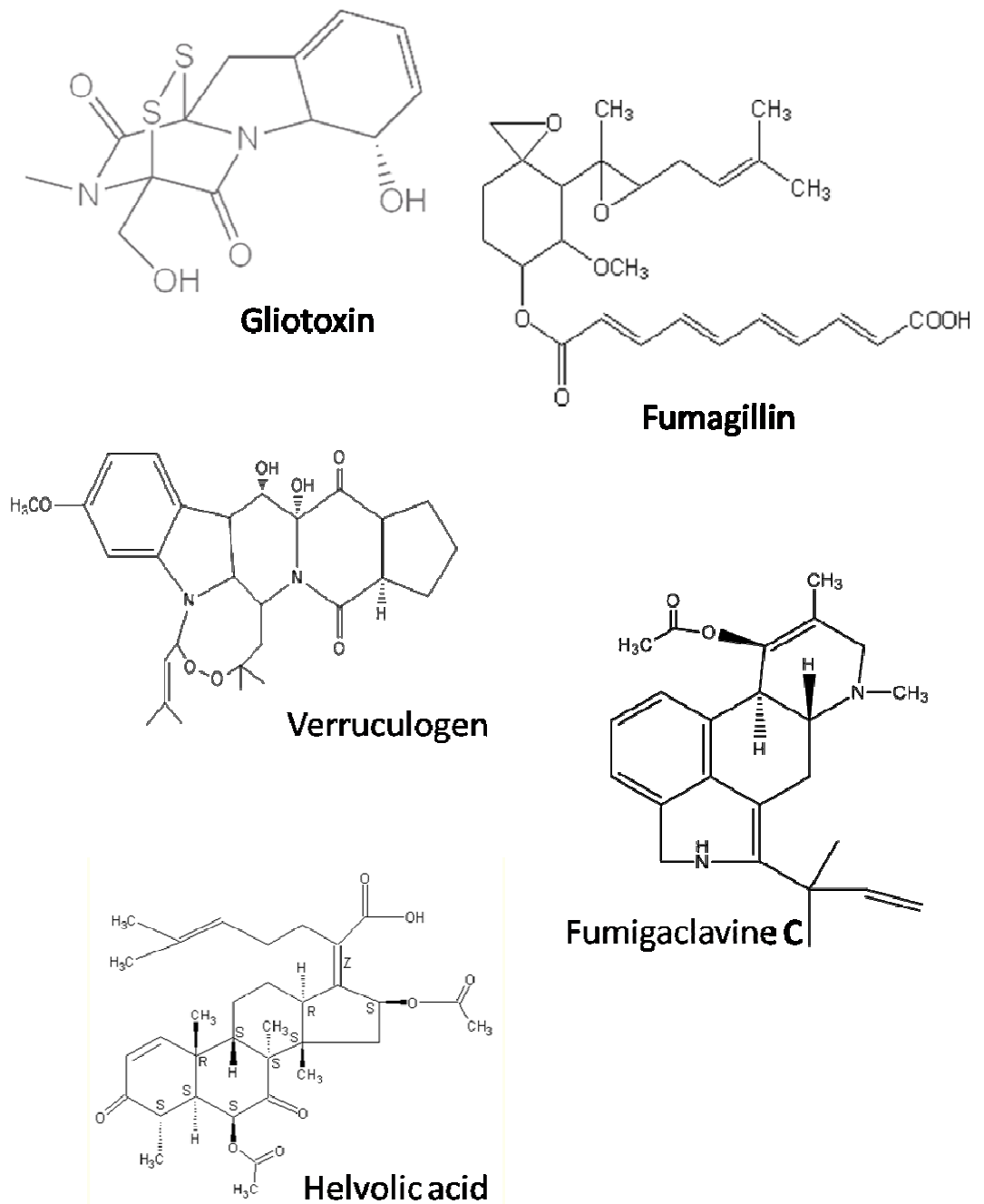
Figure 1.2: Chemical structures of toxins secreted from *Aspergillus fumigatus*.

A. fumigatus produces such a wide range of metabolites that can be classified into 24 different families (Frisvad *et al.,* 2009). Many metabolites that help the survival of *A. fumigatus* in a human host are considered to be important virulence factors. Due to the hosts immune response and sub-optimal conditions, the fungus has evolved a battery of extracellular products to acquire essential nutrients, such as iron

to survive (Losada *et al.,* 2009). Siderophores are responsible for recruiting iron in iron-depleted conditions (Howard*,* 1999). As iron is crucial for all living organisms, the ability of the fungus to ensure a constant supply of this essential metal is extremely important for fungal survival in a human host (Hissen *et al.,* 2004). The role of siderophores in fungal pathogenicity will be discussed in more detail later in this chapter.

A. fumigatus produces small basic ribosome-inactivating proteins (17 kDa), called ribotoxins, such as restrictocin, α-sarcin and mitogillin (Tomee and Kauffman*,* 2000). These inhibit protein synthesis and function by catalytically inactivating the large ribosomal subunits. Restrictocin is one of the best studied ribotoxins, and has been shown to be highly toxic to eukaryotic cell lines in the nanomolar range (Nayak *et al.,* 2001).

The metabolites involved in virulence contribute to fungal survival in the human host. Thus, identifying genes encoding metabolite biosynthesis, which contribute to the virulence of the fungus, may pinpoint possible targets for future anti-fungal therapies.

1.2.2 Current methods for detection and treatment of *A. fumigatus* infection

The current methods for detecting and treating *A. fumigatus* are invasive, expensive and can be ineffective. Therefore it is a necessity to continue searching for possible anti-fungal targets in *A. fumigatus* (Krishnan-Natesan and Chandrasekar*,* 2008). The current methods for detecting *A. fumigatus* infection are by X-ray or CT scan of the lungs, in which the mycelia mass has become so well established that the fungal mass is visible (Maschmeyer *et al.,* 2007). These methods also establish if cavities have been formed as a result of an infection. A bronchoscopy may be

performed, where tubing is sent down into the lungs, and airways, facilitating the retrieval of biopsies and fluid samples for examination (Cockrill and Hales, 1999).

Non-invasive tests include (i) Galactomannan detection, (ii) (1-3)β-glucan detection and (iii) PCR amplification of specific regions of the fungal genome. Galactomannan is a heat-stable heteropolysaccharide present in the cell wall of most *Aspergillus* and *Penicillium* species (Verdaguer *et al.,* 2007). The galactomannan assay uses EB-A2, a monoclonal antibody derived from rats, which detects the β(1,5)-linked galactofuranoside side-chain residues of the galactomannan molecule (Hope *et al.,* 2005). Using the ELISA sandwich method, detection is confirmed due to the multiple immunoreactive epitopes on an individual molecule of galactomannan. The sensitivity of the assay can be compromised due to the fact that the binding of EB-A2 requires for a positive result four or more galactofuranoside epitopes, and therefore, a sub-optimal amount of binding may not be enough for valid detection (Hope *et al.,* 2005). The galactomannan detection assay is commercially available as Platelia™ Aspergillus (Bio-Rad Laboratories, Marnes-La-Coquette, France and Bio-Rad Laboratories, Hercules, CA, USA).

(1-3)β-glucan is present in the cell wall of most fungi (Maertens *et al.,* 2007), hindering the use of this molecule as a specific *A. fumigatus* analyte. The (1-3)β-glucan molecule is able to activate the coagulation cascade, via a serine protease zymogen, within amoebocytes derived from the haemolymph of horseshoe crabs (Maertens *et al.,* 2007). The activated clotting enzyme can be detected via cleavage of synthetic chromogenic substrate, which is the basis of the assay. As the (1-3)β-glucan assay is carried out using serum specimens, consideration needs to be given to the presence of serine protease inhibitors found in human plasma, which need to be inactivated before use in the assay (Hope *et al.,* 2005). The β-glucan assay is

available in three commercial forms: Fungitell^{TM} (Associates of Cape Cod Inc., East Falmout, MA, USA), Fungi-Tec G^{TM} (Seikagaku Kogyo Corporation, Tokyo, Japan) and Wako-WB003 (Wako Pure Chemical Industries, Osaka, Japan).

PCR detection can be carried out by the use of pan-fungal primers that are used to amplify conserved regions in the DNA of fungal species. Ribosomal DNA (rDNA) is the most common target, specifically targeting the 18S (Halliday *et al.,* 2006), 28S (White *et al.,* 2006) and 5.8S genes as well as the internal transcribed spacer (ITS) regions, ITS1 and ITS2 (Lau *et al.,* 2007). PCR amplification has been used in conjunction with other diagnostic tools to enable a more sensitive and specific evaluation of *Aspergillus* infection. This includes the combination of mitochondrial PCR amplification with the galactomannan ELISA assay, named PCR-ELISA (Florent *et al.,* 2006). More specific PCR targets are being identified that can be used as a detection method for *A. fumigatus* infection but there is a lack of standardisation with these PCR assays (Thornton, 2010).

A new avenue for the detection of *A. fumigatus* infection being explored is the lateral flow device (Thornton, 2008). The basis for this type of detection is based on the murine monoclonal antibody, MAb JF5, which is raised against a protein epitope on an N-linked glycoprotein antigen present in the hyphal cell wall of *A. fumigatus.* This analyte is present in *Aspergillus* species, as well as closely related species. Unfortunately, there was weak cross-reactivity with some *Penicillium* species, but there was no cross-reactivity with antigens that are the cause of false positives in the galactomannan test (Thornton, 2008). Comparing the commercially available assays, it was found that the lateral flow device was more sensitive than the galactomannan test and the (1-3)β-D-glucan test (Wiederhold *et al.,* 2009). Therefore, the use of the

MAb JF5 may be a more selective antibody to use compared to the EB-A2 antibody in the future.

Treatment of *A. fumigatus* infection is mainly based on the principle that ergosterol is the main sterol found in fungal cell membranes, whereas cholesterol is the mammalian counterpart (Beauvais and Latge, 2001). Treatments either target ergosterol of the fungal membrane directly or inhibit ergosterol biosynthesis, leaving production of the mammalian sterol, cholesterol, intact and uninhibited. In 2001, the only drugs available for the treatment of *A. fumigatus* infections were either amphotericin B - a polyene agent, or itraconazole - an azole agent (Figure 1.3) (Beauvais and Latge, 2001). Since 2001, "second generation" azoles have been developed, namely, fluconazole, voriconazole and posaconazole (Figure 1.3).

Amphotericin B works by binding to the membrane sterols which results in the formation of pores. Beyond this, it is unclear what the precise mode of action is which causes irreversible cell damage to the fungus. Even though amphotericin B has been used for decades, there is a major drawback due to the toxic effects of its use in the mammalian host (Del Bono *et al.,* 2008). Hence, the discovery of azole alternatives was a huge advancement in the treatment of *A. fumigatus* infections (Maretens, 2004). Azole inhibition targets P450 demethylase, which is involved in the conversion of lanosterol to ergosterol (White *et al.,* 1998). This inhibition leads to the accumulation of methylated sterols and depletion of ergosterol, resulting in leakage through the cell membrane (Beauvais and Latge, 2001).

Itraconazole is a broad spectrum triazole which is less toxic than amphotericin B. It has good activity against *Candida spp.*, *Aspergillus spp.,* and other fungal pathogens (Maretens, 2004). Fluconazole can be used in mucocutaneous candidiosis

but does not have a useful activity against filamentous fungi (Maretens, 2004). Voriconazole has a wide spectrum *in vitro* activity against fungi from all clinically important pathogenic groups. Additionally, it is several-fold more active than fluconazole and itraconazole against *Candida spp.* However, resistant strains of *Candida spp.* to fluconazole and itraconazole have also shown resistance to voriconazole (Maretens, 2004). Posaconazole is a hydroxylated analogue of itraconazole. It also has a broad spectrum activity against opportunistic pathogens, including zygomycetes. It has the same activity as voriconazole and is more effective than amphotericin B, fluconazole and itraconazole (Maretens, 2004).

Caspofungin is a member of the family of echinocandins, which disrupt the cell wall synthesis of fungi by inhibiting the synthesis of $(1\text{-}3)\beta$-glucan (Heinz and Einsele, 2008). This is a different target than the other anti-fungal drugs as it does not interact with cytochrome P450, ensuring that drug-drug interactions are not a limitation for dual drug therapy. Caspofungin has showed promise in use against *Aspergillus* infections in organ transplantation patients (Groetzner *et al.*, 2008), as well as in combination therapy with voriconazole (Thomas *et al.*, 2010).

The emergence of anti-fungal drug resistance by *A. fumigatus* is of great concern, as there has been a significant rise in the frequency of azole resistant *A. fumigatus* strains since 2004 (Howard *et al.*, 2009), with many isolates displaying cross-resistance between all the current azole drugs. Even more disconcerting, is the emergence of zygomycosis, an infection by *Zygomycetes*, in patients treated with voriconazole (Kontoyiannis *et al.*, 2005). It is thought that the increase in this opportunistic mycosis is due to its resistance to voriconazole and this selective preference for zygomycosis is increasing the virulence potential of the organism (Lamaris *et al.*, 2009). Hence there is a requirement for the identification of new

11

anti-fungal drug targets that can be used to alleviate the reliance on voriconazole, and also to introduce new drugs with fewer side-effects and higher efficacy.
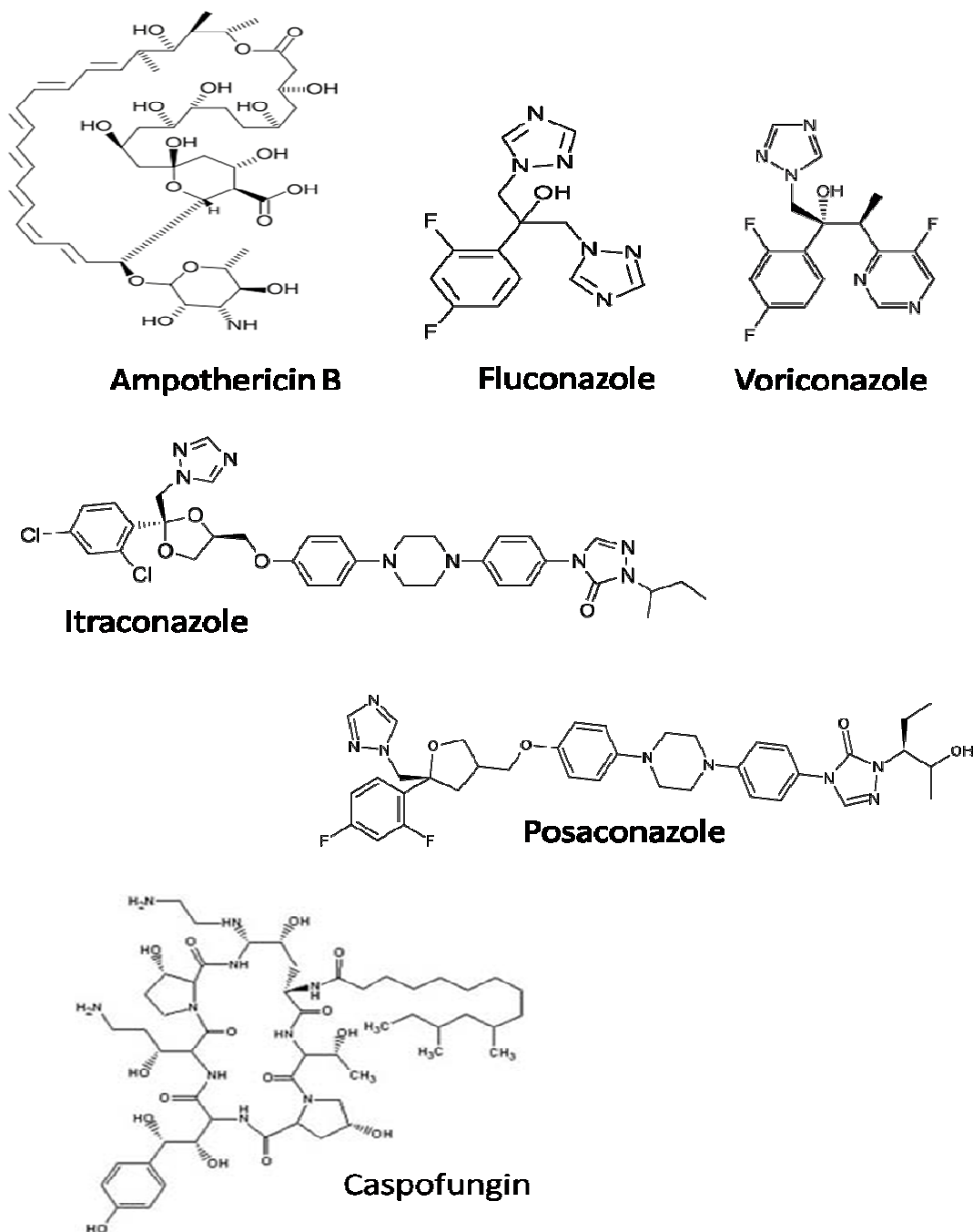
Figure 1.3: Structures of anti-fungal drugs used in the treatment of infections caused by *Aspergillus spp.* and other fungal pathogens.

1.3 Genome sequencing and identification of gene clusters

Sequencing of the genome of *A. fumigatus* (strain AF293) in 2005 has led to many important advances in the study of this pathogenic fungus, resulting in a better understanding of the fungus (Nierman *et al.,* 2005). The *in silico* annotated genome of *A. fumigatus* and other *Aspergillus* genome sequences are available at the Central Aspergillus Data Respository (CADRE) (http://www.cadre-genomes.org.uk) (Mabey *et al.,* 2004) where the genome can be analysed using ContigView, Geneview and Protview providing *in silico* information on the transcript queried by the user, such as genomic DNA (gDNA) and cDNA sequences, protein sequences, chromosome location, neighbouring genes, size of transcript, and number of introns.

The entire 29.4 Mb genome was sequenced and showed that *A. fumigatus* contains 9926 predicted genes, of which 3288 were genes with an unknown function (Nierman *et al.,* 2005). Concurrently, the genomic sequencing of *A. oryzae* was carried out (Machida *et al.,* 2005) as well as sequencing of *A. nidulans* (Galagan *et al.,* 2005). Comparative genomics was used to analyse the genome of *A. nidulans* with reference to *A. fumigatus* and *A. oryzae* (Galagan *et al.,* 2005). Two more *A. fumigatus* strains were sequenced in 2008, *A. fumigatus* A1163 and *A. clavatus* NRRL1, along with the closely related *Neosartorya fischeri* strain NRRL181 (Fedorova *et al.,* 2008). Here, it was noticed in phylogenomic analysis, that four of the virulence associated genes, a para-aminobenzoic acid synthetase, *pabaA*, a histidine kinase, *fos*-1, a polyketide synthase gene, *pksP,* involved in conidial pigment biosynthesis and a non-ribosomal peptide synthetase, *pes1,* showed accelerated evolution in the branch leading to the two *A. fumigatus* strains, indicating a positive selection for these genes as an evolutionary selection advantage.

Genes used for a common purpose are generally found in clusters in the genome (Figure 1.4), and are generally species-specific (Nierman *et al.,* 2005). There are 26 gene clusters involved in the production of secondary metabolites divided into polyketide synthetase, non-ribosomal peptide synthetase and/or dimethylallyl tryptophan synthetase genes (Nierman *et al.,* 2005; Stack *et al.,* 2007). The identification of these metabolites as 'secondary' does not signify the importance of the respective molecules, just that they are not involved in primary growth and development of the fungus (Keller *et al.,* 2005). Secondary metabolites are dispensable by the fungus on an individual basis, but are produced during specific times in the life cycle (Calvo *et al.,* 2002). Most secondary metabolite clusters contain a transcriptional regulator, indicating that the cluster regulates the expression of the genes contained within the cluster. Only 13 of these clusters have orthologues identifiable in *A. oryzae* or *A. nidulans* and even in the clusters identified, ten clusters are missing many of the genes identified in *A. fumigatus* (Nierman *et al.,* 2005). Secondary metabolite gene clusters are usually located near telomeres (Keller *et al.,* 2005). However, a major challenge still exists for the association of a particular gene cluster with production of a specific secondary metabolite.
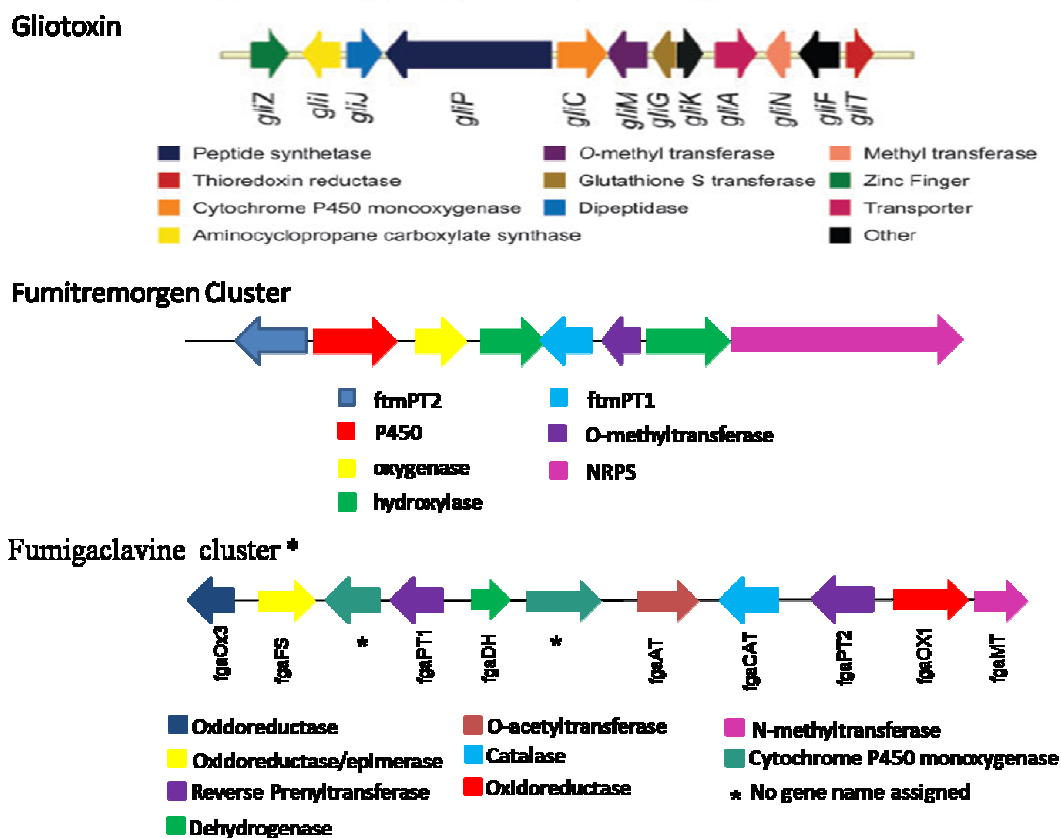
Figure 1.4: Gene clusters which encode metabolite production in *A. fumigatus*. Although gene cluster organisation is known, the functions of individual genes within clusters, or trans-acting events between clusters, remain unclear. *Cluster identified to date (Unsold and Li, 2005; Steffan *et al.,* 2009).

1.4 Non-ribosomal peptide synthetases

Non-ribosomal peptide synthetases (NRP synthetases) are multifunctional enzymes that catalyse the biosynthesis of a variety of peptides in bacteria and fungi (Figure 1.5). The products include the medically-important penicillin, from *A. nidulans* (Bok and Keller, 2004), toxins such as HC-toxin from *Cochliobolus carbonum* (Pitkin *et al.,* 1996) and gliotoxin from *A. fumigatus* (Sugui *et al.,* 2007), surfactin from *Bacillus subtilis* (Steller *et al.,* 2004) and siderophores from *A. fumigatus* (Hissen *et al.,* 2004). The wide variety of products of NRPS and the

importance of such products have stimulated much interest in the biosynthesis of these products (Bok *et al.,* 2006b).

In brief, the synthesis of non-ribosomal peptides consists of NRP synthetase gene activation, either involved in a cluster of genes or individually. The NRP synthetase enzyme generates the NRP peptide by incorporating substrates into a chain by mono- or multi-modular NRP synthetases, where each module is responsible for the generation of individual components of the final peptide. The NRP synthetase is activated by the transfer of a phosphopantetheine group (Ppant) from Coenzyme A to a specific residue in the NRP synthetase. The transfer of Ppant is facilitated by the activity of 4'-phosphopantetheinyl transferase (4'PPtase). The peptide chain generated by the NRP synthetase can then undergo modification and release from the NRP synthetase as the final NRP peptide product (Figure 1.5).
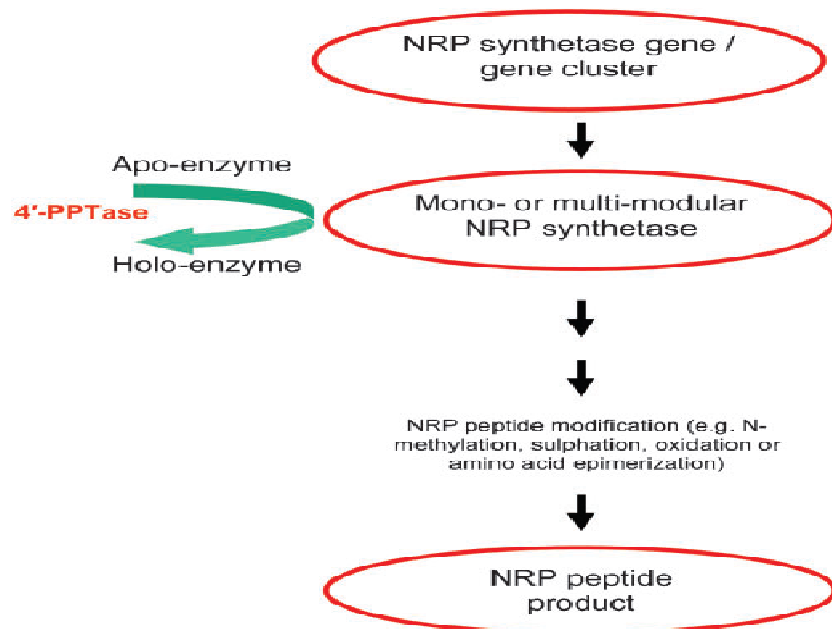
Figure 1.5: Schematic overview of the process of, and enzyme functions, involved in NRP synthesis (Stack et al., 2007).

Amino acid selection and activation in ribosomal protein synthesis is carried out by the action of tRNA synthases, whereby amino acyladenylate is converted to amino acyl-tRNA (Stachelhaus and Marahiel, 1995). The mechanism by which NRP synthetases produce peptides is similar as amino acid selection and activation is carried out by the adenylation domains in NRP synthetases, but there are two major differences in this process. Firstly, ribosomal peptide synthesis only uses the 20 proteinogenic amino acids resulting in this type of synthesis only capable of making linear chains (Stachelhaus et al., 1996), whereas, NRP synthetases are capable of using a wide variety of substrates such as fatty acids and α-hydroxy acids, as well as other non-proteinogenic and proteingoenic amino acids (Caboche et al., 2008). Secondly, ribosomal protein synthesis involves strict proof-reading to ensure the correct substrate specific for the reaction, whereas non-ribosomal synthesis shows less strict substrate selection and incorporation (Stachelhaus et al., 1999).

1.4.1 Structure arrangement and domains

NRP synthetases are composed of discrete domains, namely, adenylation (A), thiolation (T) (also known as peptidyl carrier protein (PCP)) and condensation (C). These domains group together as a distinct module of the NRP synthetase. Some NRP synthetase genes have additional domains present, such as epimerase (E) domains which are responsible for the L- to D- amino acid conversion and thioesterase (TE) domains which are involved in the release of the synthesised peptide from the NRP synthetase. Each module is responsible for the activation of a specific amino acid for protein synthesis, selected from a wide range of substrates which include more than just the 20 proteinogenic amino acids, as previously mentioned, which add to the diverse range of functions of non-ribosomally

synthesised peptides (Stachelhaus *et al.,* 1996). Furthermore, these peptides can also be modified through N-methylation, acylation, glycosylation and hererocyclic ring formation (Stachelhaus *et al.,* 1996). An NRP synthetase gene can be multi-modular where more than one module is involved in creating the entire peptide in which each individual module is responsible for incorporating one amino acid into the final peptide (Kleinkauf and Von Dohren*,* 1996). The order of the modules determines the sequence of the peptide product (Stachelhaus *et al.,* 1996). The general NRP synthetase domain arrangement is at its basic level composed of an initiation module, followed by elongation modules which build the "growing" peptide, and finishes with a termination module (Lautru and Challis*,* 2004). A diagram of the Pes1 domain architecture (Reeves *et al.,* 2006) is detailed in Figure 1.6.
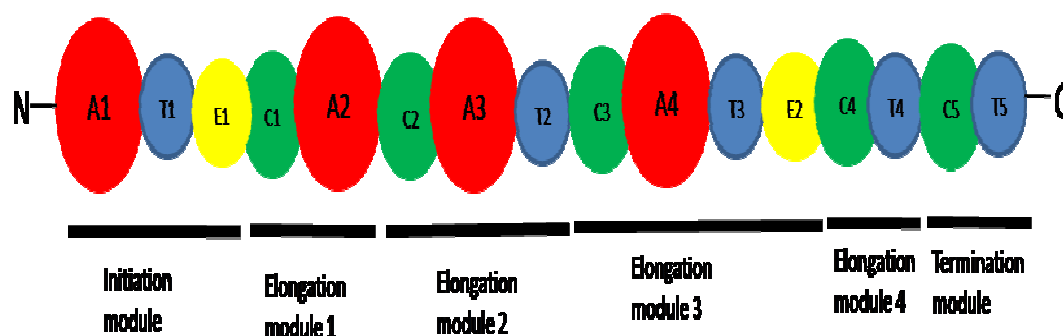
Figure 1.6: Diagram representing the Pes1 domain architecture consisting of 4 adenylation domains (A1 – A4), five thiolation domains (T1 – T5), five condensation domains (C1 – C5) and two eperimisation domains (E1 & E2).

NRP synthetases are classified into three classes: (A) linear, (B) iterative and (C) nonlinear (Figure 1.7) (Mootz *et al.,* 2002).

Linear NRP synthetase types have the classic architecture of C-A-T and the each module is only used once in the production of the peptide, as each module incorporates an individual amino acid and adds to the growing chain of the peptide.

Examples of linear NRP synthetases proteins include surfactin, cyclosporin and ACV, the penicillin precursor (Mootz *et al.,* 2002).

Iterative NRP synthetase types use the modules more than once to produce repeats of small peptides that are combined to make the final single peptide. Hence, this NRP synthetase type consists of a smaller number of modules, where each module produces the same number of peptides as the other modules within the NRP synthetase. Examples of iterative NRP synthetases proteins include enterobactin and gramicidin S (Mootz *et al.,* 2002).

Non-linear NRP synthetase types deviate from the standard linear architecture, notably by the presence of at least one unusual arrangement of the standard C-A-T domain arrangement. This deviation usually results in internal cyclizations or branch-point synthesis. Examples of non-linear NRPS synthesised peptides include syringomycin and bleomycin (Mootz *et al.,* 2002).
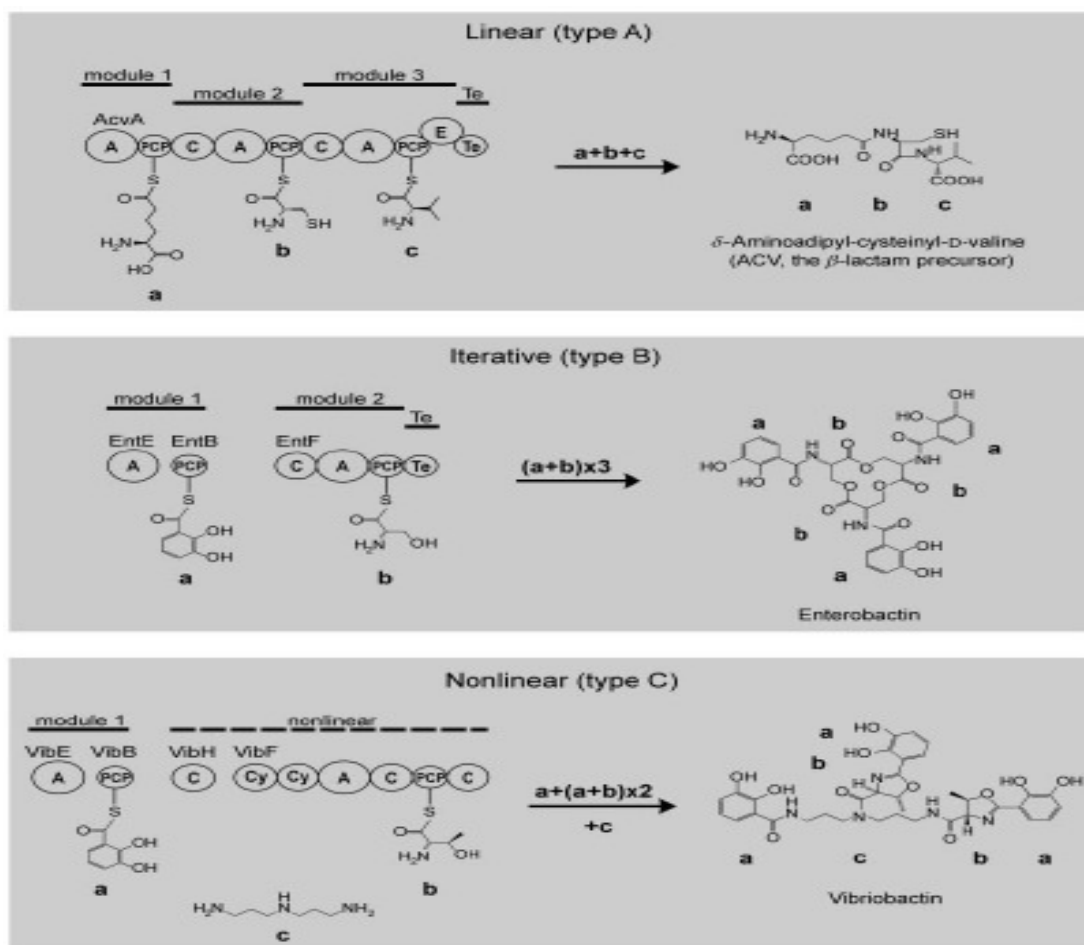
Figure 1.7: Classification of NRPS classes where the NRPS are divided into linear, iterative and nonlinear types (Mootz *et al*., 2002). The arrangement of the domains due to the specific architecture results in the variety of NRP synthetase products.

NRP synthetases are produced in an inactive apo-form and require post-translational modification to become the active halo-form (Lambalot *et al.,* 1996). The post-translational modification is carried out by transfer of a 4'-phosphopantetheine group from Coenzyme A, to a specific conserved serine residue within the thiolation domain(s) of the NRP synthetase and this reaction is catalysed by 4'-PPtase (Figure 1.8). The addition of the –SH of the Ppant group acts as a nucleophile for acylation by the adenylation domain specific substrate (Lambalot *et al.,* 1996). The 4'-PPtase was only identified recently in *A. fumigatus* (Keszenman-Pereyra *et al.,* 2003; Oberegger *et al.,* 2003; Neville *et al.,* 2005; Stack *et al.,* 2009).

Using the *A. fumigatus* 4'-PPtase, a homologue was identified in *A. nidulans* (NpgA) (Keszenman-Pereyra *et al.,* 2003). The 4'-PPTase found in *A. nidulans* (NpgA) was found to be used in a diverse range of enzymes used in primary and secondary metabolism, including the production of penicillin (Keszenman-Pereyra *et al.,* 2003; Oberegger *et al.,* 2003).
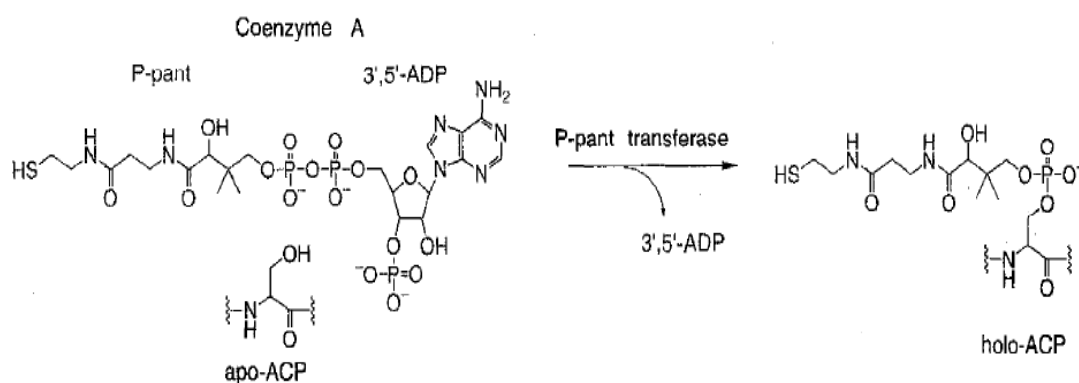
Figure 1.8: Conversion of apoprotein (apo – acyl carrier protein) to holoprotein by transfer of Ppant from Coenzyme A catalysed by 4'pptase (Lambalot *et al*., 1996)

1.4.2 Mechanisms

The mechanism by which NRP synthetase enzymes facilitate the generation of a peptide by a specific substrate has been widely studied (Meier and Burkart, 2009). The adenylation domain chooses a specific amino acid substrate via binding to a non-linear selective pocket of around 8 – 10 amino acids in the domain (Schwarzer *et al.,* 2003). These amino acids consisting of these non-linear motifs are called core motifs, found throughout the adenylation domains and are highly conserved (Table 1.1) (Schwarzer *et al.,* 2003).

Table 1.1: Core MOTIFS of NRP synthetase adenylation domains according to Schwarzer *et al*., 2003, where the core motifs are recognised by the pattern of amino acids.

NRP synthetase adenylation domain core motifs*	
A1	L(TS)YxEL
A2	LKAGxAYL(VL)P(LI)D
A3	LAYxxYTSG(ST)TGxPKG
A4	FDxS
A5	NxYGPTE
A6	GELxJGX(VL)ARGYL
A7	Y(RK)TGDL
A8	GRxPxQVKIRGxRIELGEIE
A9	LPxYM(IV)P
A10	NGK(VL)DR

* amino acids in brackets are alternative choice of amino acids that can be used to create the same core motif.

Some of the bacterial adenylation domain-specific substrates have been identified, leading to the identification of specific substrates of some bacterial NRP synthetases including gramicidin S synthetase 1, GrsA, involved in the production of gramicidin S, which has shown substrate specificity for L-phenylalanine in the adenylation domain (Conti *et al.,* 1997). The fungal adenylation domain specific substrates also remain elusive with only a handful identified, some of which are detailed in Table 1.2 (Doyle, 2009).

Table 1.2: Adenylation domain substrate specificity of fungal NRP or PK/ NRP synthetases (Taken from Doyle, 2009).

Enzyme type	Final product	Adenylation domains	Species	Reference
NRP synthetases				
SidD	TAFC	A1(N5-cis-anhydromevalonyl-N5-hydroxy-L-ornithine	*A. fumigatus*	Schrettl *et al.* (2007)
SidC	FC[a]	N5-acetly-N5-hydroxy-L-ornitine, Ser, Gly[b]	*A. fumigatus*	Schrettl *et al.* (2007)
GliP	Gliotoxin	A1 (L-Phe) and A2 (L-Ser)	*A. fumigatus*	Baliber *et al.* (2006)
Hybrid polyketide/NRP synthetases				
FUSS	Fusarin C	A1 (homoserine)	*Fusarium moniliforme*	Rees *et al.* (2007)
TENS	2-pyridone tenellin	L-Tyr[c]	*Beauveria bassiana*	Eley *et al.* (2007)
PsoA	pseurotin A	L-Phe	*A. fumigatus*	Maiya *et al.* (2007)
TdiA	terrequinone A	Arylic acid[c]	*A. nidulans*	Bok *et al.* (2006b)
CheA	cytochalasan	L-Trp	*Penicillium expansum*	Schümann *et al.* (2007)

[a] Ferricrocin (FC) can be converted to hydroxyferricrocin (HFC) by ferricrocin hydroxylase.

[b] Precise coding potential of each domain remains to be demonstrated.

[c] Proposed substrate.

Once the adenylation domain binds the specific substrate, the activated substrate is transferred to the thiolation domain (or PCP domain) (Weber and Marahiel, 2001). Here, the Ppant group from Coenzyme A is tethered to the thiolation domain, and this group accepts the activated substrate. The thiolation domain is similar to the Acyl Carrier Proteins (ACP) of fatty acid and polyketide biosynthesis. The co-factor-bound substrate is then transferred to the condensation domain. The substrate is then

attached as a thioester to the condensation domain of the following module to join the amino acid bound by that module, making the condensation domain the point where the individual peptides formed by each neighbouring module are linked together to form the final peptide (Figure 1.9) (Kleinkauf and Von Dohren, 1996).
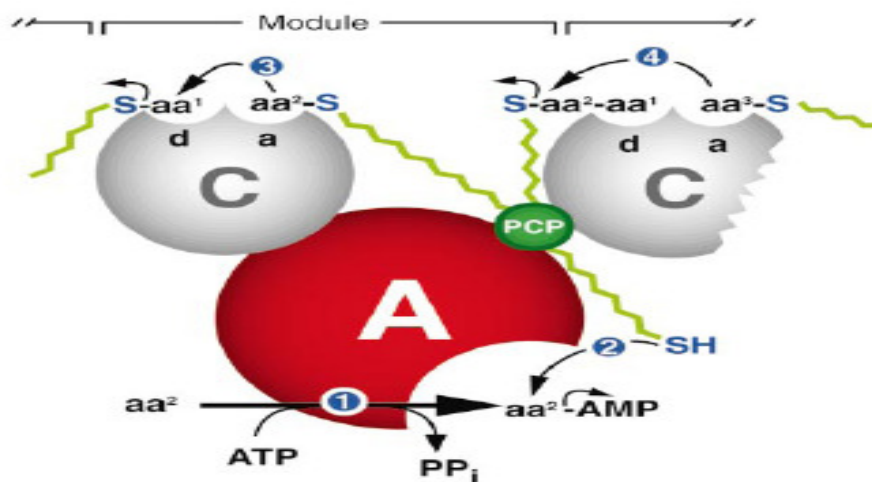
Figure 1.9: Diagram of amino acid attachment and peptide bond formation in a discrete NRP synthetase module where the reaction is carried out by (1) substrate adenylation by A-domain, (2) Thioester formation – loading of PCP (T-domain), (3) peptide bond formation by upstream C-domain and (4) Peptide bond formation by downstream C-domain. (Weber and Marahiel, 2001).

Until recently, NRP synthetase domain structure could only be determined by crystal or NMR structural investigations, which did not reveal the mechanisms by which the domains interact with each other (Koglin *et al.,* 2008). Further NMR and X-ray crystallographic structure investigations revealed the interaction between adenylation domains and the thiolation domains. It was found that the thiolation domain exists in three different conformations depending on the activity taking place; non-modified apo-PCP (A and A/H) state, A/H state and the 4'-Ppant modified holo-PCP (A/H and H) state (Koglin *et al.,* 2008). Ppant interacts with the thiolation domain in the apo-state, once the substrate is bound to the adenylation

domain; the binding of the Ppant arm to the thiolation domain changes the conformation of the thiolation domain through A/H to holo state. This conformational change allows the binding of the substrate to the Ppant arm, releasing it from the adenylation domain and transporting it by the Ppant swinging arm, via the thiolation domain to the condensation domain (Figure 1.10).

Adenylation domain specificity is the key to discovering the substrates and the final peptide products of NRP synthetase. Each adenylation domain contains a large N-terminal core domain (~450 aa) and a small C-terminal subdomain (~100 aa) The two sub-domains are connected by a hinge consisting of 5 – 10 residues (Gulick, 2009). It is thought that the adenylation domain has an open structure where the incoming amino acid substrate is able to bind, and once binding occurs, the domains rearrange into a closed formation to keep the amino acid locked to the adenylation domain where it undergoes activation (Figure 1.10). The activated amino acid is transferred to the 4'-Ppant arm tethered to the thiolation domain and this release returns the adenylation to the open conformation (Yonus *et al.,* 2008).
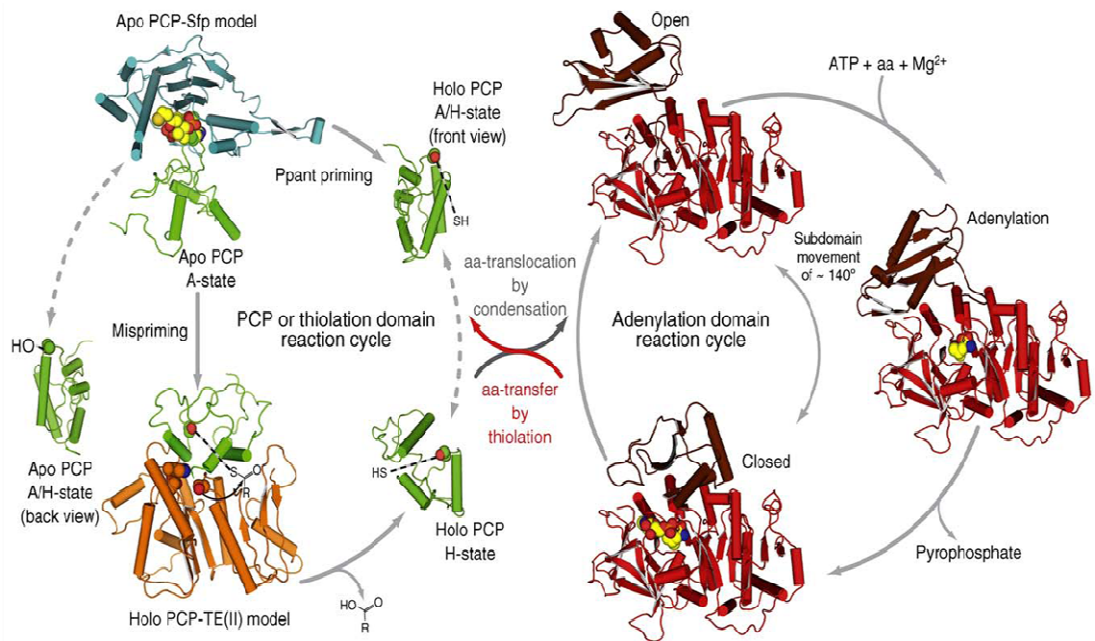
Figure 1.10: Thiolation (PCP domain) and adenylation domain cycle where the thiolation domain changes from non-modified apo-form to 4'-Ppant modified holo-form. The adenylation domain changes from an open conformation, ready to accept incoming amino acids, to a closed conformation to bind the incoming specific amino acids (Strieker *et al.,* 2010).

In 2007, the thiolation and condensation domain interaction was determined in the NRP synthetase, tyrocidine synthetase, TycC (Samel *et al.,* 2007). As the condensation domain is the point where the amino acids/peptides of neighbouring modules link to add to the growing peptide chain, it is important for the condensation domains to be able to interact directly with each other to elongate the peptide. The condensation domain was found to consist of two equally sized sub-domains in a V-shaped conformation which are connected by a small hinge region at the bottom of the V (Samel *et al.,* 2007). The V-shape allows room for the amino acid, incoming from the thiolation domain at the donor site, as well as the amino acid from the neighbouring condensation domain at the acceptor site (Figure 1.11).
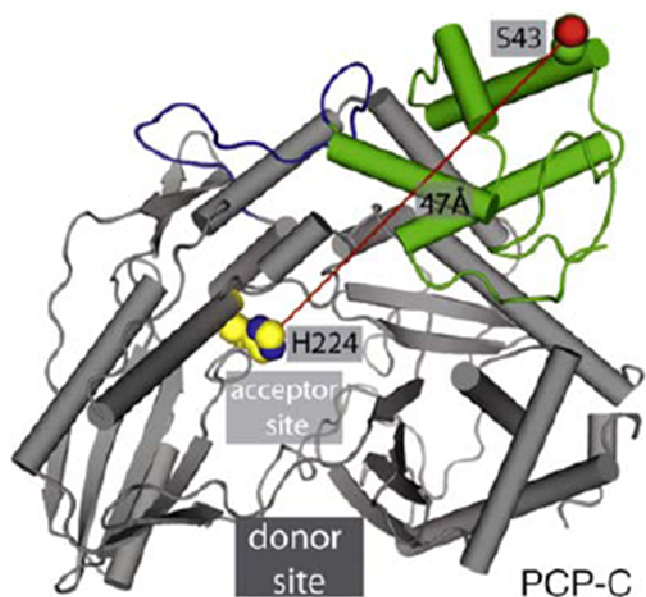
Figure 1.11: X-ray structure of the PCP and condensation di-domain of TycC, where the thiolation domain transfers the bound amino acid to the acceptor site of the condensation domain (Strieker *et al.*, 2010).

1.4.3 Functions and products

Non-ribosomal peptides have been identified in a wide range of bacteria and fungi (Doyle, 2009). With more genomes being sequenced, the identification of more NRP synthetase genes have been revealed, identifying non-ribosomally synthesised metabolites such as TAFC, ferricrocin, and bassianolide (Jirakkakul *et al.,* 2008). Cramer *et al.* (2006b) have carried out a phylogenomic analysis of the NRP synthetase genes putatively identified in *Aspergillus spp.*, in an attempt to link NRP synthetase module alignment with production specific non-ribosomal peptide products. It was shown that *A. fumigatus* contained 14 NRPS genes, of which only three had a previously assigned function (Table 1.3), namely ferrichrome (Eisendle *et al.,* 2003), gliotoxin (Cramer *et al.,* 2006a) and fumitremorgin B (Maiya *et al.,* 2006) biosynthesis. However, a gene involved in the biosynthesis of the siderophore,

triacetlyfusarinine C (TAFC), named *sidD* was predicted based on the phylogenomic analysis in the study.

Table 1.3: NRP synthetase genes identified in *A. fumigatus*, with predicted domain architecture based on in silico analysis (Cramer et al., 2006b; Stack et al., 2007).

Gene	Domain Architecture	CADRE ID	NRPS peptide product
pes1 (pesB)	ATECACATCATECTCT	AFUA_1G10380	
sidC	ATCATCATCTCTC	AFUA_1G17200	Ferrichrome
sidE	ATCATC	AFUA_3G03350	
sidD (Nps6)	ATCATC	AFUA_3G03420	TAFC
pesF	ATCATCT	AFUA_3G12920	
pesG	ATC	AFUA_3G13730	
pesH	ACATC	AFUA_3G15270	
pesI (pes3)	ATCATECATCETCATCATCATEC	AFUA_5G12730	
pesJ	C*ATC	AFUA_6G09610	
pesK (gliP)	ATCATCT	AFUA_6G09660	Gliotoxin
pesL	ATC	AFUA_6G12050	
pesM	ATCATCEATC(TE)	AFUA_6G12080	
pesN (ftmA)	ACATC	AFUA_8G00170	Fumitromorgen B
pesO	PKSNNCAT(DH4)	AFUA_8G00540	

The deletion of a NRP synthetase (*gliP*) from the *A. fumigatus* genome resulted in the loss of gliotoxin production (Cramer *et al.,* 2006a). It was determined that GliP, the NRP synthetase responsible for gliotoxin production used L-phenylalanine and L-serine as substrates in the first step of gliotoxin biosynthesis (Balibar and

Walsh, 2006). *A. fumigatus* employs siderophores for the recruitment and storage of iron, namely triacetylfusarinine C (TAFC) and ferricrocin (FC), respectively. Deletion of the NRP synthetase involved in the individual siderophore biosynthesis, *sidD* and *sidC*, respectively, resulted in the lack of production of these essential metabolites (Schrettl *et al.,* 2007). Fumitremorgin B biosynthesis begins with the NRP synthetase-mediated condensation of L-tryptophan and L-proline by FtmA (*pesN*) resulting in brevanimide F production which is the first intermediate in the biosynthesis of fumitremorgin B (Maiya *et al.,* 2006).

1.4.3.1 Siderophore biosynthesis and production for the utilisation of Iron

Iron is a metal that represents a paradox in biological organisms as it is absolutely essential for growth, yet the presence of free iron can cause the catalytic formation of reactive oxygen species (ROS) which are detrimental to the organisms that require iron to survive (Howard, 1999). Plants, animals and bacteria store iron as ferritin, phytoferritin or bacterioferritin, respectively, to counteract the toxic effects of iron (Johnson, 2008). These types of iron storage systems have not been detected in fungi, with the exception of zygomycetes (Matzanke *et al.,* 1987). Iron is most abundant in ferric (Fe^{3+}) form (Neilands, 1995), which reacts with oxygen to form insoluble ferric hydroxides, which are then unavailable for utilization by microorganisms. The acquisition of iron is considered to be a key step in the infectious process of pathogens, as iron in a host is tightly bound to proteins (Schrettl *et al.,* 2004). Pathogens must be able to obtain iron from the host which is used for metabolism and growth. In the case of *A. fumigatus,* the fungus has an ability to survive in human serum even though free iron concentrations are deemed too low to support its' growth (Gifford *et al.,* 2002). *A. fumigatus* does not have specific uptake systems for taking host iron from sources such as heme, ferritin or transferrin

(Schrettl *et al.,* 2004), it instead uses two high-affinity iron uptake systems, namely,
(i) the reductive iron assimilation (RIA) system and (ii) siderophore-assisted iron
uptake (Haas, 2003). These two systems are activated in iron starvation
environments. The RIA system reduces ferric iron (Fe^{3+}) to ferrous iron (Fe^{2+}) and
subsequently sequesters the reduced iron, whereas siderophores are low molecular
mass, ferric iron-specific chelators.

Siderophores are usually hydroxamates, characterised by the presence of N-δ-
acyl-N-δ-hydroxy-L-ornithine. There are four major hydroxamate families identified:
(i) rhodotorulic acid, (ii) coprogens, (iii) ferrichromes and (iv) fusarinines (Figure
1.12) (Haas, 2003).

Rhodotorulic acid is mainly found in basidiomyceteous yeasts and is the weakest
of the four hydroxamate siderophores for binding iron, as 1 mol of the siderophore
binds with 2 mol of iron (Haas, 2003). Coprogens are produced by a number of plant
pathogens. They are composed of N-δ-acyl-N-δ-hydroxy-L-ornithine,
anhydromevalonic acid and acetic acid, where 1 mol of the compound binds with 1
mol of iron (Renshaw *et al.,* 2002).

The important siderophores for *Aspergillus spp.* are the other two siderophores,
ferrichromes and fusarinines (Figure 1.12). Ferrichromes are cyclic peptides
containing a tripeptide of N-δ-acyl-N-δ-hydroxyornithine and a combination of
glycine, serine or alanine (Reiber *et al.,* 2005). Fusarinines are either linear or cyclic
hydroxamates where N-hydroxyornithine is N-acylated by anhydromevalonic acid
(Haas, 2003).

Fe^{3+} is classed as a hard acid due to its high charge-radius ratio, resulting in a
high affinity for hard base donor atoms such as oxygen (O) (Renshaw *et al.,* 2002).
As the ligands of siderophores are hard donors, Fe^{3+} has a high affinity for the

molecule, making siderophores a specific binder of iron. Once the iron binds to the siderophore, a thermodynamically stable complex is formed as the Fe^{3+} centre is spherically symmetric, having no directional preference for individual metal – O bonds (Renshaw *et al.,* 2002). The interaction between the iron atom and the donor atoms is largely electrostatic where the siderophore O atoms form a distorted octahedron of O atoms around the central iron atom, optimising the interaction of the positively charged metal and the negatively charged oxygen (Renshaw *et al.,* 2002).
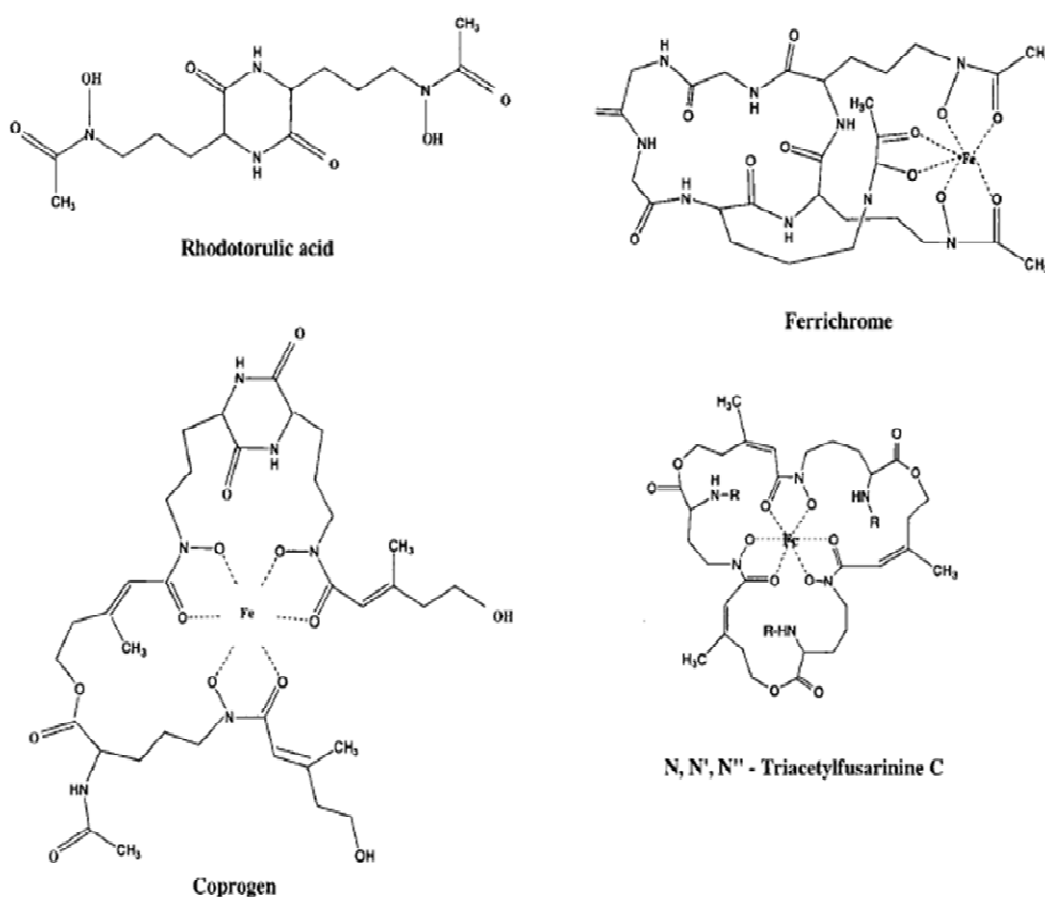
Figure 1.12: Chemical structures of hydroxamate siderophores found in fungi (Howard, 1999).

A. fumigatus produces three hydroxamate-type siderophores: extracellular fusarinine C (FSC) and TAFC, and an intracellular ferricrocin (FC) (Schrettl *et al.,* 2007). The combined iron recruitment of the RIA and siderophore systems ensures that there is a steady supply of iron for *A. fumigatus* to be a successful pathogen. Fungi such as *A. nidulans* and *A. fumigatus* produce siderophores during iron starvation conditions.

In *Aspergillus, s*iderophores were first identified in *A. nidulans* where the genome was found to contain a GATA factor, SreA, that negatively regulates the biosynthesis of siderophores and relative iron uptake (Figure 1.13) (Haas *et al.,* 1999). As SreA showed similar homology to the siderophore repressor transcription factor SRE from *Neurospora crassa* and URBS1 in *Ustilago maydis*, its identification led to the discovery of siderophores in *A. nidulans* (Haas *et al.,* 1999).
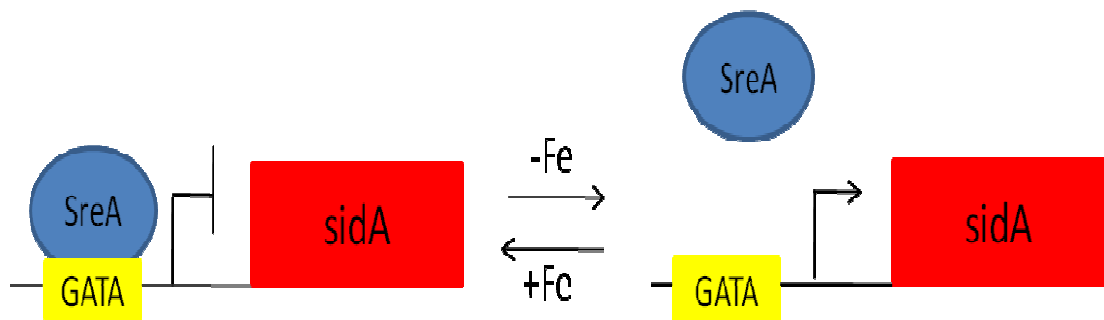
Figure 1.13: SreA binding to GATA repressing the expression of the L-ornitine N5-oxygenase (*sidA*) which is the first step of the siderophore biosynthetic pathway. The presence of iron signals for the binding of SreA to GATA, whereas reduction in iron presence signals for the release of SreA from GATA, allowing transcription of *sidA*.

In *A. nidulans* Δ*sreA* a decrease in extracellular siderophore production and an increased accumulation of the intracellular siderophore (FC) was observed (Oberegger *et al.,* 2001). This change in siderophore production caused deregulation of siderophore-bound iron uptake as well as ornithine esterase expression.

Interestingly, the lack of negative regulation from SreA did not completely deregulate extracellular siderophore production, as there was still negative regulation by the iron availability. This gave the first indication that there are additional iron regulation mechanisms besides SreA in control of siderophore production (Oberegger *et al.,* 2001).

Following the discovery that SreA was involved in regulating siderophore biosynthesis, *A. nidulans* Δ*sreA* was used to identify individual genes involved in siderophore biosynthesis, using the de-repression of the genes during iron-replete conditions (Oberegger *et al.,* 2002b). Here, *sidA* was identified, which displayed significant similarity to *sid1* of *U. maydi. sidB and sidC* were identified with fragments showing similarity to *sid2* of *U. maydis* as well as other NRPS genes (Oberegger *et al.,* 2002b). The genes, *mirA*, *mirB* and *mirC* were identified in *Saccharomyces cerevisiae* to be upregulated during iron starvation, indicating they play a role in iron acquisition for the non-siderophore producing organism (Oberegger *et al.,* 2002a).

It was established that genes involved in siderophore biosynthesis could be characterised by transcriptional induction under iron-limited conditions which were de-repressed in Δ*sreA* under iron-replete conditions (Eisendle *et al.,* 2003). As *sidA* and *sidC* completely fulfilled the terms of this characterisation, they were investigated for their role in siderophore biosynthesis in *A. nidulans* (Oberegger *et al.,* 2002b). Characterisation of *A. nidulans* Δ*sidA* and Δ*sidC* strains identified that Δ*sidA* did not produce either extracellular or intracellular siderophores, and therefore was unable to grow unless the media was supplemented with 1.5 mM $FeSO_4$.

Interestingly, media supplementation with FeCl₃ or ferric citrate was not able to restore Δ*sidA* growth. The Δ*sidC* strain was able to produce normal amounts of TAFC but completely lacked FC production, indicating involvement in the production of the intracellular siderophore (Eisendle *et al.,* 2003).

The ability of Δ*sidA* and Δ*sidC* to produce conidia was also investigated by Eisendle *et al.* (2003). Δ*sidA* was not able to produce conidia unless the media was supplemented with siderophores. Supplementation with 10 μM TAFC partially restored conidial production, whereas the presence of 10 μM FC completely restored conidial production. The Δ*sidC* strain showed a reduced level of conidiation unless the media was supplemented with FC (10 μM), which completely restored conidia production, indicating that the intracellular siderophore, FC, is essential for efficient conidiation. Furthermore, it was discovered that the Δ*sidA* and Δ*sidC* strains had an increase in intracellular iron, due to the lack FC production in both strains. This intracellular iron build up was also noted in Δ*sreA*, where the amount of iron found intracellularly was directly correlated with the extracellular iron supply. This deregulation of iron uptake causes oxidative stress in the cell and was also observed in the Δ*sidA* and Δ*sidC* strains, where the sensitivity was more notable in the Δ*sidA* strain.

Schrettl *et al*. (2004) identified an ortholog of *A. nidulans sidA* in *A. fumigatus,* also named *sidA*. In contrast to the growth deficiencies of the *A. nidulans* Δ*sidA*, the *A. fumigatus* Δ*sidA* strain was able to grow to a moderate level in iron depleted conditions. This indicates that *A. fumigatus* must possess additional iron assimilation systems that *A. nidulans* does not. *A. fumigatus* Δ*sidA* showed sensitivity towards an inhibitor of the reductive iron assimilation pathway, batho-phenanthroline-disulfonic

acid disodium salt (BPS), the genes involved in a potential RIA pathway were investigated. Screening of the *A. fumigatus* genome identified several putative metalloreductase-encoding genes, one putative ferroxidase (*fetC*) and one potential high affinity iron permease-encoding gene (*ftrA*) (Schrettl *et al.,* 2004). Deletion of *ftrA* resulted in an 8-fold increase in TAFC production, most likely due to compensation by the siderophore system where the RIA system is absent. A double mutant, Δ*sidA*:Δ*ftrA* was created, and this strain was unable to sustain any growth, even in iron-replete conditions, unless culture media was supplemented with FC, indicating that mechanisms for the uptake of available iron are essential and that *ftrA* encodes an essential component of an iron uptake system independent of the siderophore system (Schrettl *et al.,* 2004). Furthermore, in their study, the double mutant was unable to sustain growth on media containing human iron-containing sources such as haemoglobin, hemin, holotransferrin and ferritin, indicating that *A. fumigatus* double mutant does not have any specific system for the removal of iron from the host. However, previously it has been shown that *A. fumigatus* is capable of chelating iron from holotransferrin (Hissen *et al.,* 2004). This is one of the main reasons why *A. fumigatus* is classed as an opportunistic pathogen.

To investigate the role of iron acquisition in the virulence of *A. fumigatus,* both Δ*sidA* and Δ*ftrA* were tested in murine models of aspergillosis (Schrettl *et al.,* 2004). Here, the Δ*ftrA* strain was as virulent as the wild-type strain and leading to the conclusion that the reductive iron assimilation system plays no role in virulence of *A. fumigatus.* However, virulence of the Δ*sidA* strain was completely attenuated, indicating that the siderophore system is essential for virulence. A closer look at *A. fumigatus* Δ*sidA* in the lungs of mice showed that the conidia did not germinate.

Concurrently, Hissen *et al.* (2005) identified *A. fumigatus sidA* as a siderophore related virulence factor, as the wild-type strain was able to remove iron from human transferrin, compared to the Δ*sidA* strain which was unable to remove the iron from transferrin.

In 2005, *sidD* was found to be regulated by iron availability (Reiber *et al.,* 2005). The discovery of *sidD* was through a BLAST search using *sidC* as the search parameter. *sidD* was also highly similar to *sid2* of *A. oryzae.* Like the other siderophore related genes, *sidD* expression was found to be repressed in iron-replete conditions, with expression observed under iron-limiting conditions.

Ferricrocin C (FC) is a major iron storage compound in hyphae during excessive iron conditions (Eisendle *et al.,* 2006). It was found that oxidative stress caused the accumulation of intracellular iron during both iron-depleted and -replete conditions. It was noted that the increase of iron-containing FC was mediated by transcriptional upregulation of *sidC* expression, because treatments with hydrogen peroxide and paraquat under iron-replete conditions upregulated the transcription of *sidC*. Using *A. nidulans* Δ*sidC* in iron-replete conditions, it was found that there was an increase in TAFC production as well as intracellular iron content, indicating that the iron utilization within the cell was inefficient as there was nowhere for the excess iron to be stored. Importantly, it was found that the Δ*sidC* conidia were more sensitive to oxidative stress than the mycelia, which exhibited wild-type resistance. Furthermore, the Δ*sidC* conidia showed delayed germination indicating that FC plays an important role in germination. The importance of conidial siderophore storage in germination was highlighted by Charlang *et al.* (1981). Recently, it was demonstrated the FC is

involved in the intra- and trans-cellular iron distribution, where FC is used to transport iron from the hyphae to the conidia (Wallner *et al.,* 2009). The absence of FC results in iron starvation in the conidia.

The iron contained in TAFC needs to be released from the siderophore for use in the fungal cell. For this to occur, the ester bonds of TAFC are hydrolyzed, decreasing the affinity of TAFC for iron followed by the release of cleavage products, leaving the iron free within the cell to be transferred into metabolic pathways where it is utilized or to FC for storage. The hydrolysis is thought to be carried out by the TAFC esterase, EstB (Kragl *et al.,* 2007). An *A. fumigatus* Δ*estB* strain showed reduced transfer rate of iron from TAFC to FC, which in turn delayed iron-sensing and resulted in impaired growth. The Δ*estB* strain was still able to hydrolyze TAFC indicating that there are other mechanisms for the hydrolysis of TAFC, but hydrolysis is optimised by active EstB.

The siderophore biosynthetic pathway was first postulated by Plattner and Diekmann (1994) and has been significantly updated by Schrettl *et al.* (2007). The L-ornithine N^5-oxygenase gene, *sidA*, is involved in the first committed step of the biosynthesis of both intracellular and extracellular siderophores in *A. fumigatus* (Figure 1.14). Firstly, L-ornithine is converted to N^5-hydroxy-L-ornithine by L-ornithine-N^5-oxygenase encoded by *sidA* (Eisendle *et al.,* 2003). After N^5-hydroxy-L-ornithine is synthesised, the pathway splits to enable either extracellular or intracellular siderophore biosynthesis.

For the extracellular siderophore, TAFC, the N^5-hydroxy-L-ornithine is converted to N^5-cis-anhydromevalonyl-N^5-hydroxy-L-ornithine by the N^5-

transacylase, encoded by *sidF* using cis-anhydro-mevalonyl-CoA as the substrate. The N^5-cis-anhydromevalonyl-N^5-hydroxy-L-ornithine is converted to fusarinine C by the NRP synthetase, encoded by *sidD*. Fusarinine C is then converted into the extracellular siderophore, TAFC, by a N^2-transacetylase, encoded by *sidG*, using acetyl-CoA as the substrate.

For the intracellular siderophore, N^5-hydroxy-L-ornithine is converted to N^5-acetyl- N^5-hydroxy-L-ornithine, by an unidentified N5-transacylase using acetyl-CoA as the substrate. The N^5-acetyl- N^5-hydroxy-L-ornithine is converted into FC by the NRP synthetase, encoded by *sidC*, using serine and glycine as substrates. FC is converted to hydroxyferricrocin (HFC) by an unknown ferricrocin hydroxylase (Schrettl *et al.*, 2007). The enzyme SidD and the FC synthetase, SidC were identified by Reiber *et al.* (2005), and SidF and SidG were identified by Schrettl *et al.* (2007).
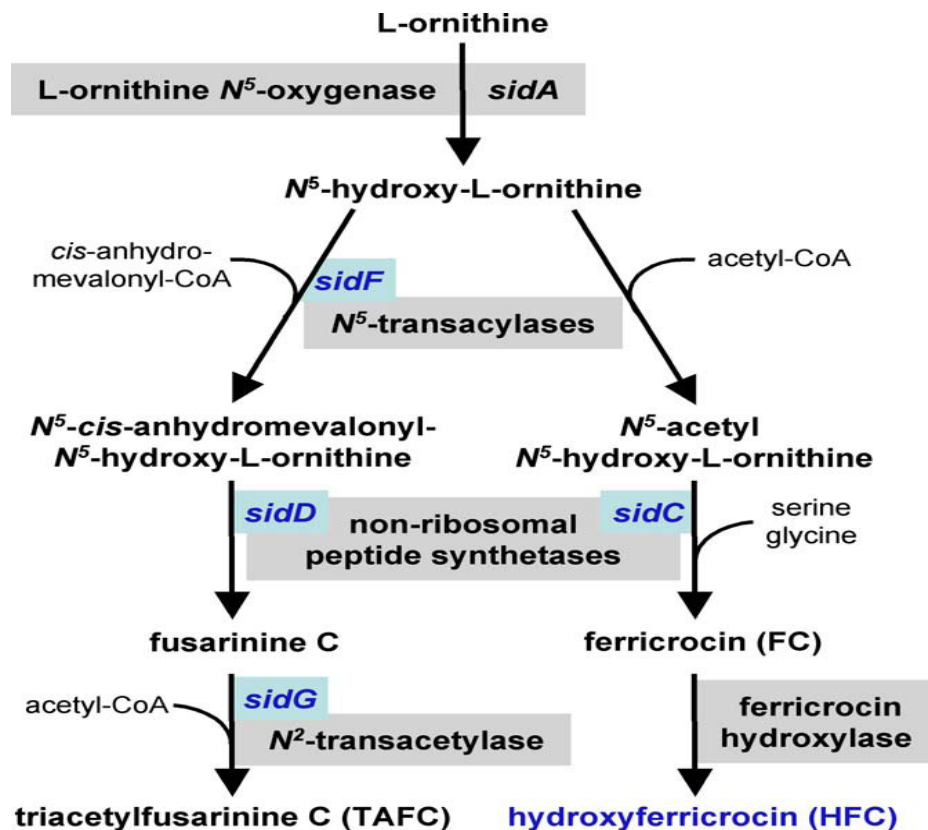
Figure 1.14: Biosynthesis of siderophores in *A. fumigatus* (Schrettl et al., 2007).

Some fungi have the ability to utilise siderophores produced by other organisms even though they do not possess the machinery to produce the siderophores themselves, such as *S. cerevisiae* (Oberegger *et al.,* 2002b). This species employs two distinct high-affinity uptake systems which are regulated by the transcriptional activators Aft1p and Aft2p. The uptake of iron requires surface metalloreductases (Fre1p and Fre4p) which reduce Fe^{3+} to Fe^{2+} (Kosman*,* 2003). The reduced iron is transported to the cell by a permease-oxidase complex (Ftr1p/Fet3p) allowing the uptake of both siderophore-bound iron and unbound reduced iron.

In *A. nidulans,* a gene encoding FreA was identified which is similar to metalloreductase, which was not regulated by SreA indicating that there are genes involved in iron availability responses other than those controlled by SreA (Oberegger *et al.,* 2002a). Many siderophore producing fungi have been identified, some of which are detailed in Table 1.4. Fungi use a wide array of siderophore types.

Table 1.4: Species of fungi which have been shown to produce either intracellular or extracellular siderophores

Siderophore producing fungi	Extracellular siderophore	Intracellular siderophore	Reference
Aspergillus fumigatus	TAFC/ fusarinine C	Ferricrocin	Nilius *et al.* (1990)
Aspergillus nidulans	TAFC/ fusarinine C	Ferricrocin	Charlang *et al.* (1981)
Aspergillus oryzae	Ferrichrysin	Ferricrocin	Yamada *et al.* (2003)
Cochliobolus heterostrophus	Coprogen/ fusarinine	Ferricrocin	Lee *et al.* (2005)
Magnaporthe grisea	Coprogen	Ferricrocin	Antelo *et al.* (2006)
Fusarinium graminearum	Coprogen/ fusarinine	Ferricrocin[a]	Oide *et al.* (2006)
Penicillium chrysogenum	Fusarinine C	Ferrichrome	Charlang *et al.* (1981)
Neurospora crassa	Coprongen	Ferricrocin	Matzanke *et al.* (1987)
Ustilago maydis	Ferrichrome	Ferrichrome	Bolker *et al.* (2008)
Schizosaccharomyces pombe	Ferrichrome	Ferrichrome	Schwecke *et al.* (2006)
Rhodotorula pilimanae	Rhodotorulic acid	Rhodotorulic acid	Muller *et al.* (1985)

[a] predicted siderophore

Intracellular siderophores are found exclusively in fungi, giving an advantage over bacteria, plants and animals which all lack a ferritin-mediated iron storage system (Haas *et al.,* 2008). The ability to scavenge for iron, mediated by siderophores, has given fungal species an advantage over other non-siderophore utilizing organisms, as they are able to recruit iron in iron-depleted conditions which facilitates growth and development that would otherwise be impossible (Hissen *et al.,* 2004). The ability of fungal strains such as *A. fumigatus* to recruit iron contributes to the virulence of the fungus. As a pathogenic organism, the siderophore system enables *A. fumigatus* to counteract oxidative stress, encountered either in the environment or by a host immune system (Eisendle *et al.,* 2006).

Oxidative stress of fungi in a host is due to the reactive oxygen species (ROS) produced by the macrophages that eliminate conidia and the hydrogen peroxide produced by neutrophil activity that kill fungal hyphae (Schaffner *et al.,* 1982). The main protective factor against oxidative killing employed by *A. fumigatus* is the presence of catalases in the conidia and mycelia (Paris *et al.,* 2003b). Catalase is an antioxidant metalloenzyme, used by all aerobic organisms in the protection against oxidative damage (Rementeria *et al.,* 2005).

A. fumigatus contains three catalases, Cat1 and Cat2 in the hyphae, and CatA in the conidia. It was demonstrated that mycelia deficient in both Cat1 and Cat2 were slightly more susceptible to hydrogen peroxide whereas the lack of CatA exhibited high sensitivity to hydrogen peroxide (Paris *et al.,* 2003b).

Iron-depleted *A. fumigatus* is more sensitive to hydrogen peroxide and inappropriate iron storage can catalyze the formation of ROS which is the reason why *A. fumigatus* Δ*sidA* and Δ*sidC* strains exhibit hypersensitivity to hydrogen

peroxide during iron-depleted growth (Schrettl *et al.,* 2007). The ability of hydrogen peroxide to kill conidia and hyphae of Δ*sidA* and Δ*sidC* was significantly higher than that of the wild-type, indicating that the siderophore conidial iron storage and the intracellular siderophore are extremely important in the protection of the fungus against oxidative stress. Human macrophages exposed to either *A. fumigatus* wild-type or Δ*sidA* conidia showed that the wild-type conidia activated a higher production of TNF-α than Δ*sidA* conidia, indicating that the siderophore system may compromise parts of the innate immune response (Seifert *et al.,* 2008). *A. fumigatus* Δ*sidD* hyphae, deficient in the extracellular siderophore, also exhibited sensitivity to hydrogen peroxide.

The catalase activity was investigated in siderophore deficient strains, and it was shown that the expression of the hyphal catalases, Cat1 and Cat2, were no different between the varying siderophore deficient strains (Δ*sidA*, Δ*sidC*, Δ*sidD*, Δ*sidF* and Δ*sidG*) and were comparable to the wild-type indicating that the oxidative stress exhibited by these strains was not due to catalase deficiency. Furthermore, the Δ*sreA* strain induced an increase in expression of Cat1 compared to the wild-type, indicating that the oxidative stress response is activated during a disruption of iron homeostasis in the fungus (Schrettl *et al.,* 2008).

The conidial catalase, CatA, showed decreased expression in the Δ*sidA* and Δ*sidC* strains but could be restored when the media was supplemented with the intracellular siderophore, FC, indicating that the decrease in catalase expression is due to the lack of FC. In transcriptional profiling, it was found that the siderophore system genes were upregulated *in vivo* during iron-depleted conditions (McDonagh *et al.,* 2008), but differential expression was not observed during exposure to hydrogen peroxide alone. The RIA system would be in use during the iron replete

conditions and the siderophore system would not need to be expressed during this time. Therefore the up-regulation of the siderophore genes during murine infection would be a better representation of the fungus in a low-iron environment coupled with oxidative stress, especially as the catalase, Cat2, was also highly upregulated during the *in vivo* profiling.

1.4.3.2 Fumigaclavine C biosynthesis and production

Many different fungi produce ergot alkaloids which result in a wide variety of clavines and lysergyl-derived ergot alkaloids being generated. The ergot alkaloid production in fungi generally results in the accumulation of ergopeptines, which are derived from non-ribosomally synthesised peptides containing lysergic acid and three amino acids. Simple amides of lysergic acid, such as ergine and ergovine can also be generated (Coyle and Panaccione, 2005).

In *A. fumigatus,* there are seven members of the ergot alkaloids produced, named: agroclavine, festuclavine, elymoclavine, chanaclavine, fumigaclavine A, B and C (Frisvad *et al.,* 2009). Ergot alkaloids are associated with conidia, and represent 1 % of the conidial content in which four alkaloids are identified, in order of abundance: fumigaclavine C, festuclavine, fumigaclavine A and fumigaclavine B (Panaccione and Coyle, 2005). Fumigaclavine C accounts for 1.2 – 12 mg/g conidia, depending on the media used to grow the fungus. Fumigaclavine C has been identified as having a mass of 366, consisting of $C_{23}H_{30}N_2O_2$ (Larsen *et al.,* 2007).

The final ergot alkaloid metabolites produced by the different fungi contain the same four member ergoline ring system, but differ in the number, type and position of the side chains (Figure 1.15). The ergot alkaloid produced by *Claviceps purpurea* is ergoamine. This was the first ergot alkaloid identified in a fungus and so is used as the metabolite that ergot alkaloids produced in other fungi are compared to. The

ergot alkaloid produced in *A. fumigatus* is Fumigaclavine C and in *Neotyphodium lolii* is ergovaline.
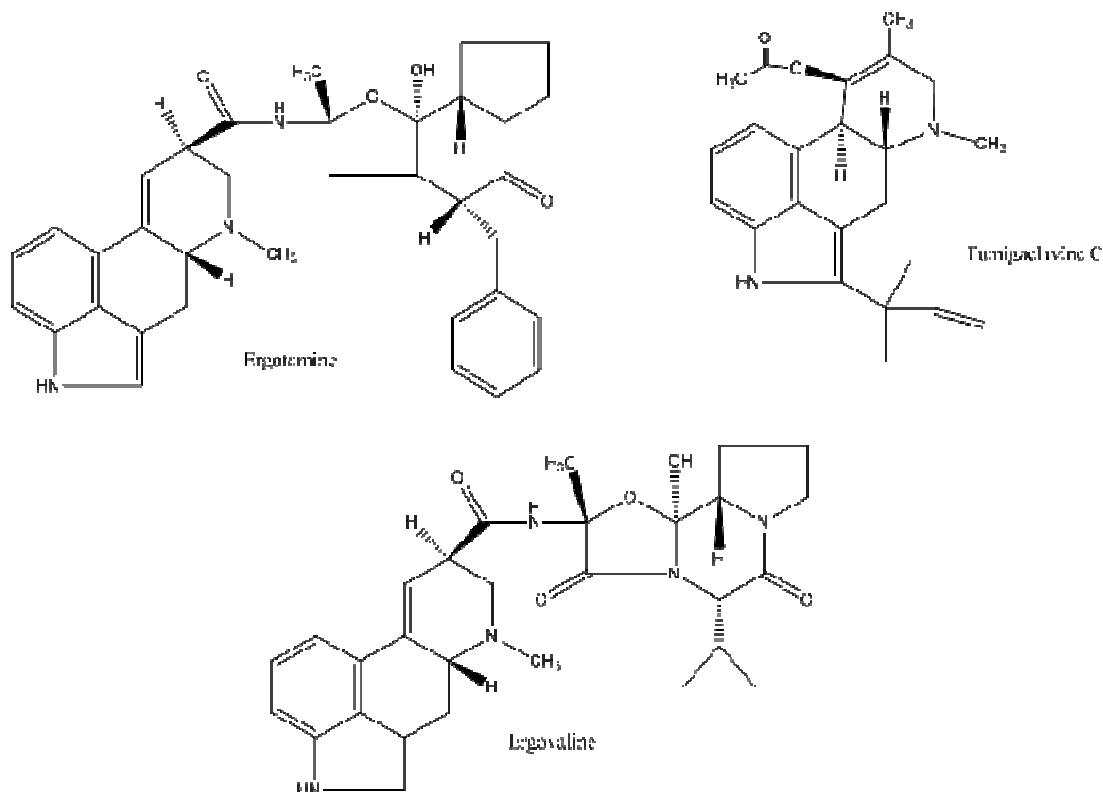
Figure 1.15: Final ergot alkaloid metabolites produced in fungal species, where ergoamine is produced by *C. purpurea*, fumigaclavine C is produced by *A. fumigatus* and ergovaline is produced by *N. lolii*.

In *A. fumigatus,* the biosynthesis of fumigaclavine C involves a complex pathway that begins with the prenylation of L-tryptophan by dimethylallyl pyrophosphate (DMAPP). This first step in the pathway was discovered due to the comparison of *A. fumigatus* production of fumigaclavine with the ergot alkaloid production in the fungus *C. purpurea* of ergoamine (Coyle and Panaccione, 2005). The biosynthesis of ergoamine in also begins with the prenylation of L-tryptophan by DMAPP. Interestingly, the final steps in the production of ergoamine involve two NRP synthetases, LspB and LspA (Ortel and Keller, 2009). The divergence between

44

these ergot alkaloid products only occurs after the production of the intermediate, chanoclavine (Coyle *et al.,* 2010). In another fungus, *N. lolii*, the production of the ergot alkaloid, ergovaline, also begins with the prenylation of L-tryptophan with DMAPP. The final product is also the result of NRP synthetase involvement. The similarities and divergence between the ergot alkaloid production in *A. fumigatus, C. purpurea* and *N. Lolii* is detailed in Figure 1.16 and will be discussed in more detail in Chapter 4.
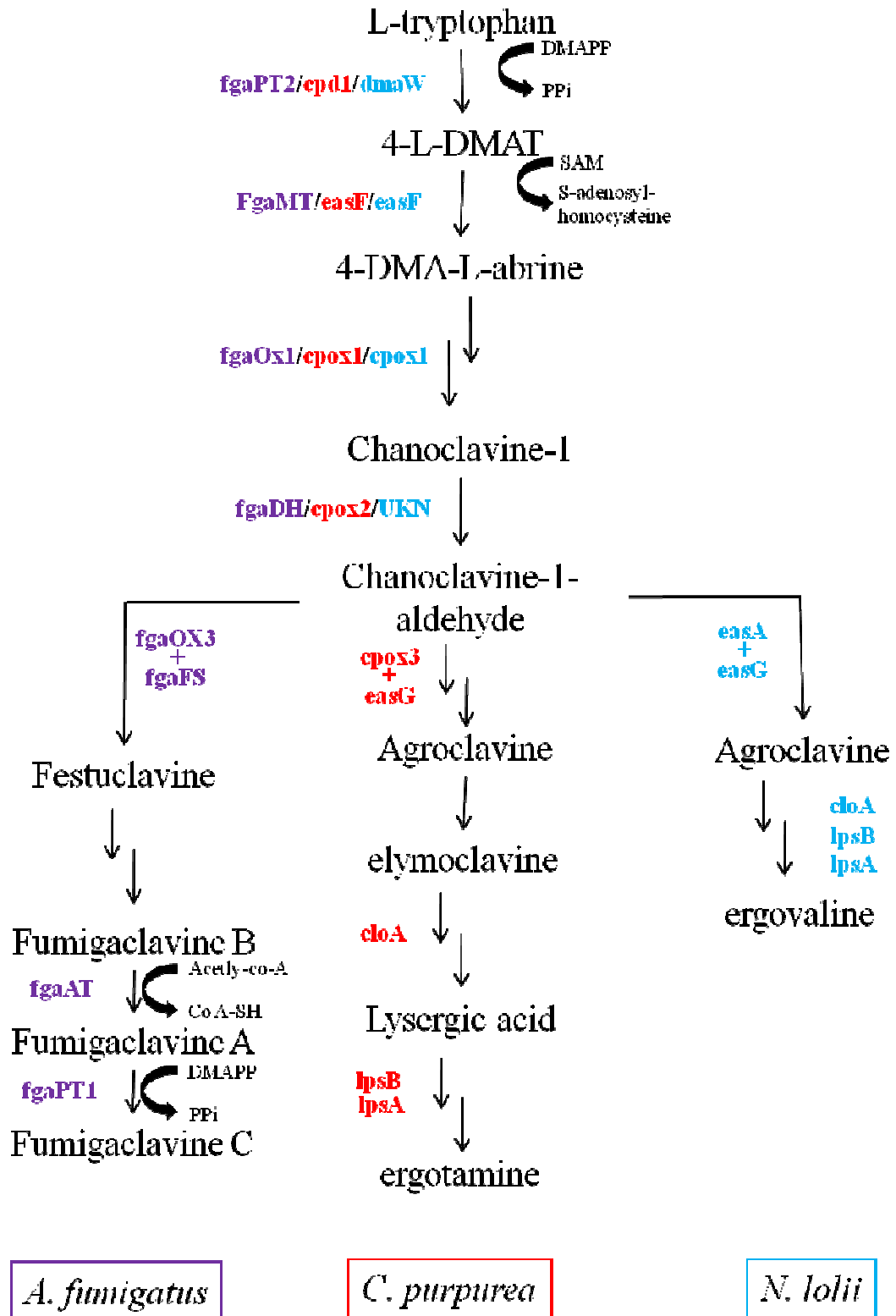
Figure 1.16: Ergot alkaloid biosynthesis in fungal species has a complex pathway with common steps initialising the pathway and diverges after the production of the intermediate chanoclavine. The function of the genes detailed is provided in the key below, where the genes involved in the production of fumigaclavine C in *A. fumigatus* are in purple, genes involved in the production of ergotamine in *C.*

purpurea are in red and the genes involved in the production of ergovaline in *N. lolii* are in blue.

Gene function	A. fumigatus	C. purpurea	N. lolli
DMAT synthase	fgaPT2	cpd1	dmaW
N-methyltransferase	fgaMT	easF	easF
Unknown	fgaOX1	cpox1	cpox1
Dehydrogenase	fgaDH	cpox2	Unknown
Unknown	fgaOX3	cpox3	easA
Unknown	fgaFS	easG	easG
monooxygenase		cloA	cloA
NRPS		lpsB	lpsB
NRPS		lpsA	lpsA*
O'-acetyltransferase	fgaAT		
Reverse prenyltransferase	fgaPT1		

1.4.3.3 Fumitremorgin biosynthesis and production

Tremorgenic mycotoxins, such as fumitremorgin B or verruculogen, result in intermittent or sustained tremors in vertebrate animals (Khoufache *et al.,* 2007). Fumitremorgins are members of a group of prenylated indole alkaloids derived from L-tryptophan and L-proline. This group includes other compounds detected in *A. fumigatus* extracts, such as tryprostatins, cyclotryprostatins and spirotryprostatins and it is thought that these compounds are derived from the diketopiperazine cyclo-L-Trp-L-Pro, known as brevianamide F (Grundmann *et al.,* 2008). The NRP synthetase encoding gene, *ftmA*, found within the cluster identified as the fumitremorgin biosynthesis cluster, was confirmed to catalyze the first step in the biosynthetic pathway of fumitremorgin B (Figure 1.17) (Maiya *et al.,* 2006). Overexpression of *ftmA* caused an accumulation of brevianamide F in *A. nidulans*. Interestingly, the *A. fumigatus* strain AF293, a clinical isolate, is not capable of producing the typical end-products such as TR-2, fumitremorgin A and B and

verrulculogen, but instead produces the intermediate fumitremorgin C (Larsen *et al.,* 2007). There is evidence that fumitremorgin B can be derived from TR-2, indicating an intermediate role for TR-2 in the biosynthesis of verruculogen (Willingale *et al.,* 1983). The production of verruculogen is variable between *A. fumigatus* isolates (Tepsic *et al.,* 1997; Kosalec *et al.,* 2005a) and although initially not found in conidial extracts (Fischer *et al.,* 2000), verruculogen is definitely a conidial metabolite (Khoufache *et al.,* 2007). It has also been established that the fumitremorgin biosynthetic cluster was down-regulated in *A. fumigatus ΔstuA,* a strain deficient in the full adaptive response to hypoxia (Sheppard *et al.,* 2005).
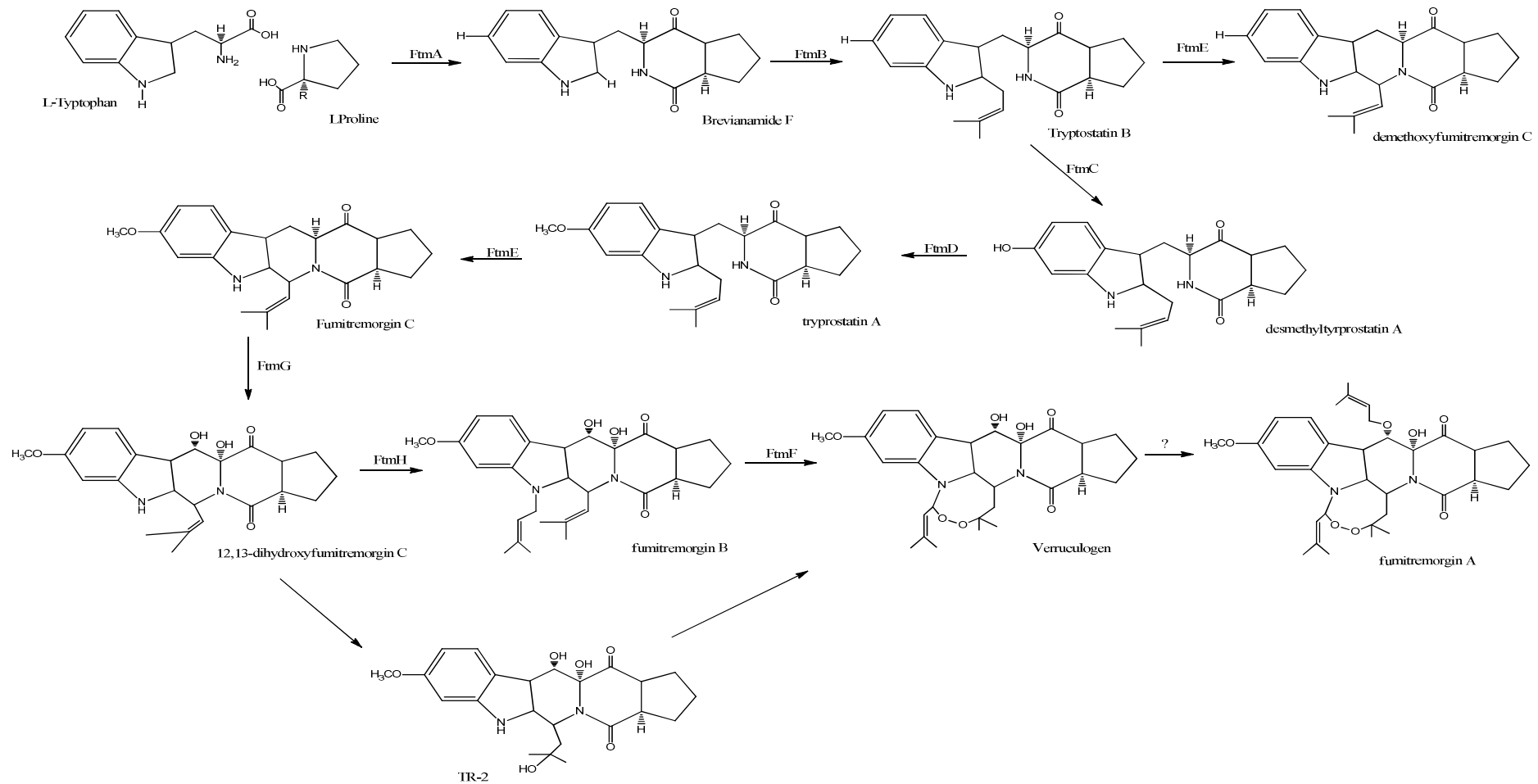
Figure 1.17: Proposed biosynthetic pathway for the fumitremorgin family of non-ribosomal peptides.

1.4.3.4 *A. fumigatus* **NRP synthetase, Pes1**

The phylogenomic study carried out by Cramer *et al.* (2006b) (Table 1.3) identified genes in *A. fumigatus* which had orthologs in other *Aspergillus* species but these genes also had no identified product or function. These genes, known to be NRP synthetases, had no identifiable product and it was unclear as to the function of the putative NRP synthetase genes. The expression analysis of the NRP synthetase genes in *A. fumigatus* AF293 was carried out to characterise the genes. In this analysis, *pes1* (AFUA_1G10380) was shown to be minimally expressed in Sabouraud media and not expressed in all other conditions tested (Cramer *et al.,* 2006b). Concurrent investigation of the *pes1* gene established it was expressed at all time points in minimal essential media (MEM) in the *A. fumigatus* strains ATCC26933, ATCC16424 and ATCC13073 (Reeves *et al.,* 2006).

This study also confirmed that *pes1* plays a role in conidial morphology and hydrophobicity whereby a *pes1* disrupted mutant exhibited reduced virulence, as well as increased sensitivity to oxidative stress. The Pes1 protein was purified from mycelial lysates of *A. fumigatus* ATCC26933 and eluted at a mass of 500 kDa. In SDS-PAGE analysis, a dominant protein band was detected using immunoaffinity-purified antibodies (IgG-Pes1) (Reeves *et al.,* 2006). The protein was approximately 33 % of the predicted mass of Pes1 and the authors indicated that this may represent the C-terminal proteolytic fragment of the protein.

The identification of the NRP peptide product encoded by *pes1* is still elusive, but *pes1* expression profiles have been generated through many transcriptional profiling studies. Large scale profile studies have been possible due to the availability of the full genomic sequencing of *A. fumigatus* and other related strains and species (Fedorova *et al.,* 2008). Genome-wide microarrays can be used to identify the effect a deleted gene has on other genes, without screening each

individual gene. Schrettl *et al.* (2008) used this method to investigate the genes regulated by the SreA transcription factor. Here, microarray analysis was conducted with RNA isolated from wild-type and Δ*sreA* strains which were grown in iron-limiting conditions for a defined period of time (12 hr) and then transferred to iron-replete conditions. As previously mentioned, SreA is a repressor of siderophore production in iron-replete conditions. This profiling identified 1147 genes that were differentially expressed in Δ*sreA*, which interestingly included *pes1* (upregulated in Δ*sreA* after 30 min). As *pes1* expression is upregulated in the absence of this regulator, this may indicate that *pes1* plays a role in the protection against oxidative stress during this sudden change in Fe^{3+} levels, potentially by signalling or interacting with siderophores or related biosynthesis genes.

Similarly, the transcriptional profiling of *A. fumigatus* Δ*laeA* strain, compared to the wild-type, revealed that this global regulator, LaeA, controlled the expression of many secondary metabolite gene clusters which included *pes1* as well as the ergot alkaloid family of fumigaclavines, gliotoxin and the fumitremorgin family (Perrin *et al.,* 2007). Interestingly, the expression of *pes1* as well as the neighbouring ABC multi-drug transporter were down-regulated in Δ*stuA*, a gene involved in the hypoxic adaptation of the fungus (Sheppard *et al.,* 2005). Also similarly to Δ*pes1*, the Δ*stuA* strain was sensitive to hydrogen peroxide, indicating that this sensitivity exhibited by Δ*stuA* may be due, in part, to the down-regulation of *pes1* expression.

1.4.3.5 Global regulation of NRPS genes

The nuclear protein, LaeA, was found to regulate the transcription of secondary metabolites in *A. fumigatus, A. nidulans* and *A. terreus* (Bok and Keller, 2004). The Δ*laeA* strain was found to exhibit wild-type growth and development, but lacked the

same level of virulence (Bok *et al.,* 2005). The decrease in virulence was associated with altered conidial morphology and lack of gliotoxin production.

Further investigation into the decreased virulence revealed that LaeA controlled the production of lovastatin in *A. terreus,* sterigmatocystin and penicillin in *A. nidulans* and gliotoxin in *A. fumigatus*, conversely the overexpression of LaeA resulted in an increase of both lovastatin and penicillin gene cluster transcription and production. LaeA production was found to be negatively regulated by two signal transduction proteins, PkaA and RasA (Figure 1.18).

As previously mentioned, transcriptional profiling of the Δ*laeA* strain compared to the wild-type showed that 13 of the 22 secondary metabolite gene clusters identified in *A. fumigatus* were down-regulated due to the absence of the regulator (Perrin *et al.,* 2007). The LaeA regulation of metabolite biosynthesis in *A. fumigatus* will be discussed further in Chapter 4.
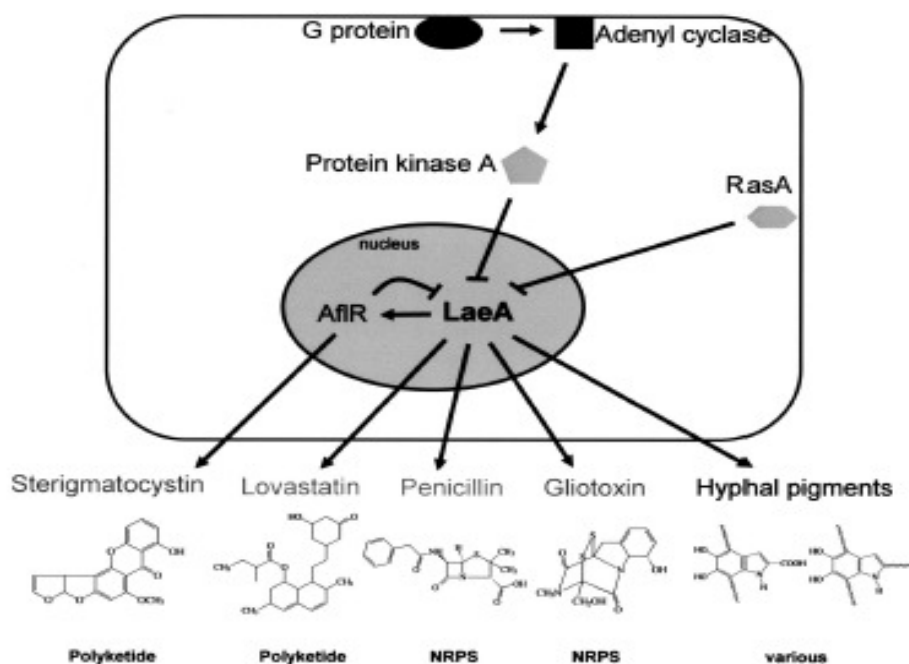
Figure 1.18: Proposed model of secondary metabolite regulation by LaeA and some of the metabolites produced under this regulation. (Taken from Bok *et al*., (2004)).

1.5 Gliotoxin

Aspergillus species produce a wide range of metabolites, including siderophores, antibiotics and toxins (Foster and Karow, 1945; Haas, 2003; Gardiner *et al.,* 2005c). One such toxin is gliotoxin, which is also produced by several other fungi, and is acutely toxic with a broad range of immunosuppressive properties (Sutton *et al.,* 1994). Gliotoxin is a member of the family of epipolythiodioxopiperazine (ETP) compounds, and is uniquely characterised by a disulphide bridge across a diketopiperazine ring (Figure 1.19). ETPs function by generating Reactive Oxygen Species (ROS) via redox cycling between the oxidized (disulphide) and reduced (dithiol) forms (Figure 1.19) (Eichner *et al.,* 1988; Gardiner *et al.,* 2005c). The disulphide bridge is thus responsible for the toxicity of the compound (Rodriguez and Carrasco, 1992). Disulphide bridge formation can be inhibited by the addition of a cellular reductant such as glutathione (GSH) or dithiothreitol (DTT), which in turn inhibit the production of the oxygen radicals, hindering the formation of the disulphide bond (Gardiner *et al.,* 2005c).
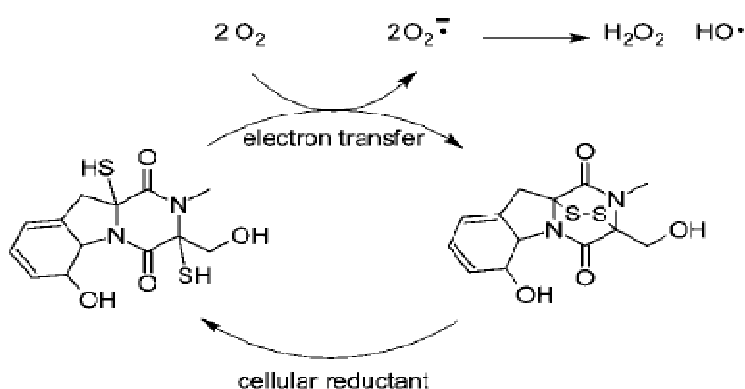
Figure 1.19: Redox cycling between the reduced (dithiol) and oxidized (disulphide) forms of gliotoxin generating reactive oxygen species (Gardiner *et al.,* 2005c).

Gliotoxin was first isolated as a product of *Gliocladium fimbriatum* by Weindling and Emerson (1936) and then in *Aspergillus spp.* (Kidd, 1947). The natural function of gliotoxin is hypothesised to be a defence mechanism against other competing organisms, such as bacteria and fungi that cannot protect themselves against gliotoxin, within the same environment (Tekaia and Latge, 2005).

Gliotoxin is regarded as one of the major immunosuppressive factors associated with *Aspergillus spp.* infections, as it causes a spectrum of effects on the host immune response such as inhibition of (i) macrophage phagocytosis (Eichner *et al.,* 1986), (ii) NADPH oxidase (Yoshida *et al.,* 2000) (iii) mitogen-activated T-cell proliferation (Mullbacher and Eichner, 1984), (iv) mast cell activation (Niide *et al.,* 2006) and (v) cytotoxic T-cell responses (Yamada *et al.,* 2000). The presence of gliotoxin also induces epithelial cell damage (Amitani *et al.,* 1995) as well as both apoptotic (Piva, 1994; Suen *et al.,* 2001) and necrotic (Hurne *et al.,* 2002) cell death in mammalian cells. Previously, it has been shown that gliotoxin can be detected in the lungs of mice experiencing aspergillosis and also in serum of patients diagnosed with invasive aspergillosis (Lewis *et al.,* 2005). Gliotoxin has also been shown to inhibit the activity of NF-κB which results in reducing neutrophil survival (Walmsley *et al.,* 2005) and its toxicity is of great interest, especially as it has been shown to induce apoptosis of cancer cells (Pan and Harday, 2007). Recently, gliotoxin has been shown to inhibit angiogenesis occurring at infection sites, in a dose dependent manner (Ben-Ami *et al.,* 2009). Furthermore, in a murine infection model, an *A. fumigatus* strain deficient in gliotoxin production due to deletion of *gliP* (which encodes a non-ribosomal peptide synthetase, one of the essential enzymes for gliotoxin biosynthesis), did not inhibit angiogenesis to the same extent as the wild-

type strain (Ben-Ami *et al.,* 2009). Therefore, it is important to understand and analyse the biosynthesis of this toxin, and determine its role in the virulence arsenal of gliotoxin-producing fungi.

The biosynthesis of gliotoxin is hypothesised to occur as described in Figure 1.20, where phenylalanine and serine are substrates for the non-ribosomal peptide synthetase, GliP, to produce cyclo-(L-phenylalanyl-L-seryl) (Balibar and Walsh*,* 2006). The next steps have been proposed to generate intermediates which have not been isolated or characterised but are thought to involve a series of sulphurisations, oxidations, chaisan rearrangement reactions, and methylation (Gardiner *et al.,* 2005c).
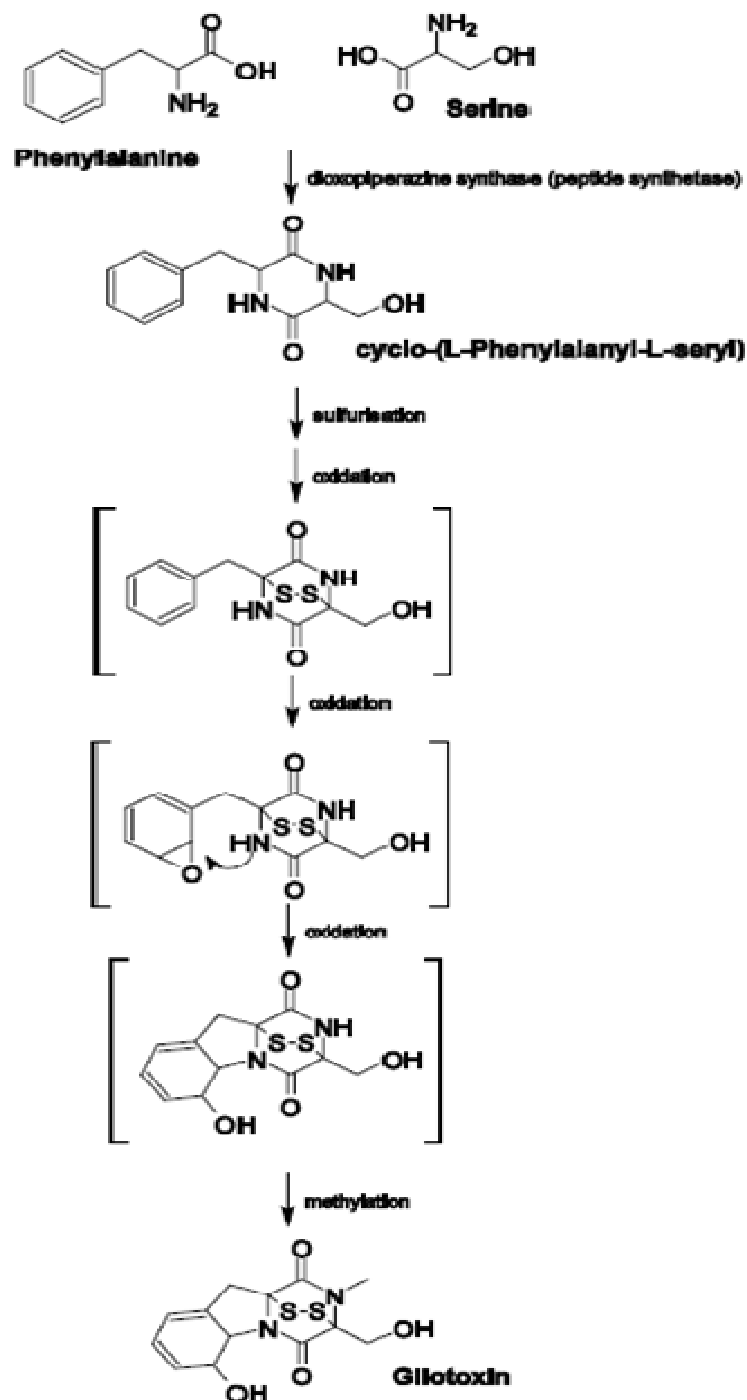
Figure 1.20: Proposed pathway for gliotoxin biosynthesis (Gardiner and Howlett, 2005a). The only known intermediate is cyclo L-phenylalanyl-L-serine. All other compounds are predicted (bracketed) and the order of reactions may not be correct.

Bioinformatic analysis has shown that the genes within the *A. fumigatus* ETP cluster are extremely similar to the sirodesmin biosynthesis gene cluster of *Leptosphaeria maculans* (Figure 1.21) (Gardiner and Howlett, 2005a). Sirodesmin PL is a toxin produced by the plant pathogen *L. maculans* which causes lesions on plant leaves and is a member of the ETP producing family (Gardiner *et al.,* 2004). Putative ETP clusters have also been identified in a range of fungi including *A. fumigatus, Penicillium lilacinaechinulatum, A. clavatus, Trichoderma virens, A. terrus, A. flavus, A. oryzae, L. maculans, T. reesei,* and *A. zeae* (Patron *et al.,* 2007).
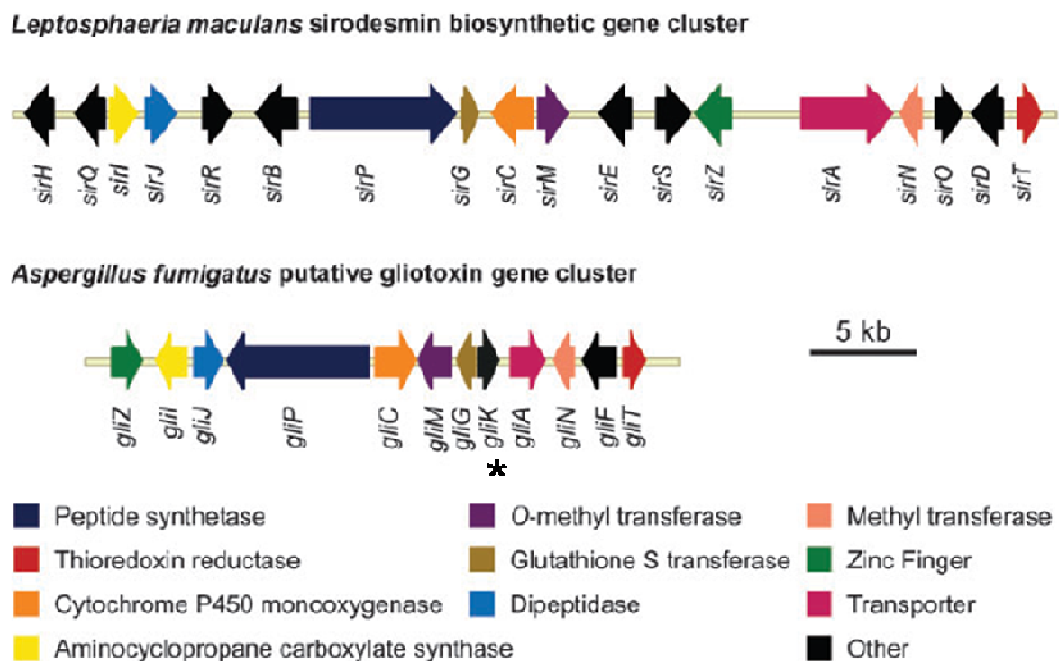
Figure 1.21: Comparison of the putative gliotoxin and sirodesmin biosynthetic gene clusters from *Aspergillus fumigatus* and *Leptosphaeria maculans*, respectively. The ''other'' category contains genes encoding cytochrome P450 monooxygenases (*gliF, sirB, sirE*), a prenyl transferase (*sirD*), an acetyl transferase (*sirH*), epimerases (*sirQ, sirR, sirS*), an oxidoreductase (*sirO*) and a gene encoding a hypothetical protein (*gliK*), as indicated by * (Gardiner *et al.,* 2005c).

1.6 Double mutations

The advantage of the double mutations can be clearly seen in the situations where separate single mutants confer no phenotypical difference from the wild-type, but the double mutation results in fatal (Kafer and Mayor, 1986) or extreme detrimental outcomes (Novak *et al.,* 1995; Fujiwara *et al.,* 2000; Belaish *et al.,* 2008; Etxebeste *et al.,* 2009; Zhang *et al.,* 2009). Double mutant strains can also show that genes involved in the same function or protein production can compensate for the absence of each other, as the double mutation results in the decrease or absence of such production (Fujiwara *et al.,* 2000; Ichinomiya *et al.,* 2002a; Ichinomiya *et al.,* 2002b; Flipphi *et al.,* 2003; Ichinomiya *et al.,* 2005). Furthermore, the double mutation of genes can reveal interactions between the separate functions or pathways showing contributing interactions that would not normally be observed. This is seen in *A. nidulans* calcium homeostasis signalling transcription factor CrzA, which is important in the adaption to osmotic stress. Here, the double mutant ($\Delta crzA$:$\Delta hogA$) was rendered hypersensitive to osmotic stress in plate cultivations, whereas the individual single mutants were not (Hagiwara *et al.,* 2008).

Double mutants created in *A. fumigatus* have involved putative virulence factors, including the mutant lacking restrictocin, a major antigen found in the urine of patients with invasive aspergillosis (IA) along with the removal of the *alp* gene encoding an alkaline protease which is subject to nitrogen, sulphur, and carbon catabolite repression and also pH regulation (Smith *et al.,* 1994). This double mutant was slightly less virulent than the wild-type strain.

A. fumigatus double mutants have also involved nutrient uptake, such as zinc acquisition from the surrounding environment. In *A. fumigatus,* the genes *zrfA* and *zrfB* were postulated to be involved in zinc transportation. The expression of *zrfA* and

zrfB was differentially down-regulated in the presence of zinc. Transcription of *zrfB* was absent at a concentration of zinc 50-fold higher that that required to halt transcription of *zrfA*. Also, the growth level of Δ*zrfA* was identical to the wild-type but the Δ*zrfB* strain had a reduction in growth (Vicentefranqueira *et al.,* 2005). In acidic conditions which omitted zinc from the media, the Δ*zrfA* strain showed the same growth potential as the wild-type but the Δ*zrfB* strain showed a reduced capability to grow. More importantly, the double mutant showed a complete growth deficiency in the acidic non-zinc media (Vicentefranqueira *et al.,* 2005). In the present study, it is proposed to dissect interaction between *A. fumigatus sidD* and *pes1* NRP synthetase by creating an *A. fumigatus* Δ*sidD*:Δ*pes1* double mutant.

1.7 Insect virulence models

Animal models such as mice and rats are routinely used to study the virulence of microorganisms due to the susceptibility of these animals to infection, including infection with *Aspergillus spp.* (Krappmann, 2006). Infection studies can vary from identification of gene production, metabolite screening and anti-fungal properties. To generate reliable, reproducible and significant results, studies using animal models can easily become costly and time-consuming. An alternative method was required to avoid high cost and other unfavourable factors associated with use of vertebrate animal models (Kavanagh and Reeves, 2004). The use of insects such as *Galleria mellonella* and *Drosophila melanogaster* as virulence models has shown good correlation with the murine virulence models (Lionakis and Kontoyiannis*,* 2005; Renwick *et al.,* 2006; Mylonakis*,* 2008; Spikes *et al.,* 2008; Jackson *et al.,* 2009; Chamilos *et al.,* 2010).

The greater wax moth, *G. mellonella,* in its larvae state has been used to test the virulence of a range of bacteria and fungi, as this model has shown strong correlation to virulence seen in murine models (Jander *et al.,* 2000; Brennan *et al.,* 2002). *G. mellonella* possesses an immune system, similar to that of the mammalian innate immune system (Kavanagh and Reeves, 2004). The immune cells of *G. mellonella* are composed of granulocytes and plasmatocytes which enable phagocytosis in a lectin-mediated manner (Tojo *et al.,* 2000). Also, similar to the mammalian immune system, is the presence of reactive oxygen species, defensins, transferrin and lyzozyme. This immune response can be used to investigate the relative pathogenicity of microorganisms, such as *A. fumigatus.* Larvae are injected with an inoculum of conidia through the cuticle of the last left proleg. The infection process can be visualised as the larvae undergo melanisation which changes the colour of the larvae from white to dark brown. The *G. mellonella* model system has previously been used to show that *A. fumigatus* strains had different relative pathogenicities, where ATCC26933 was found to be more virulent than ATCC14109, which in turn was more virulent than ATCC16424, and ATCC13073 which was the least virulent (Reeves *et al.,* 2004a). Here the virulence was attributed to the production levels of gliotoxin, which was found to vary between strains within the tissue of the larvae. The *G. mellonella* model can be used to determine virulence involvement of certain genes by comparing larval survival following infection with wild-type and mutant strains. Using the *G. mellonella* model, the *pes1* gene was shown contribute to the virulence of *A. fumigatus* in a Δ*pes1* strain, as the mutant strain exhibited a reduced virulence (Reeves *et al.,* 2006).

The fruit fly *D. melanogaster* uses cellular and humoral mechanisms in antimicrobial defence (Simon *et al.,* 2008). It releases antimicrobial peptides, one of

which, drosomycin, has high activity against filamentous fungi such as *A. fumigatus* (Chamilos *et al.,* 2008). The release of drosomycin is under the control of signals mediated by Toll, a transmembrane receptor (Simon *et al.,* 2008). The mammalian interleukin-1 receptor type I (IL-1RI), shows high similarity to the *D. melanogaster* Toll (Rock *et al.,* 1998). Toll-like receptors (TLRs) are responsible for the recognition of microorganisms and activation of the innate immune response (Birchler *et al.,* 2001). *D. melanogaster* deficient in the toll signalling pathway can be used as an infection model. The flies are fed, or injected via the dorsal thorax, with *A. fumigatus* conidia resulting in infection of the hemolymph (Lionakis and Kontoyiannis, 2005). As the flies can be used as a model of invasive aspergillosis, they can be used to assess the effect of anti-fungal drugs and also the effect of pre-incubation of one anti-fungal on the efficiency of another (Lamaris *et al.,* 2008). Here, it was concluded that pre-exposure of *A. fumigatus* AF293 conidia to voriconazole did not hinder the efficacy of posaconazole, and vice-versa. Furthermore, pre-incubation of the conidia with the anti-fungal drugs did not change the minimum inhibitory concentration (MIC) of the drug during subsequent infection. Recently, Chamilos *et al.* (2010) have shown that *A. fumigatus* strains deficient in *sidA* and *sidD*, respectively, show an attenuated virulence in the *D. melanogaster* Toll deficient model. This result was confirmed in the murine model, confirming that the *D. melanogaster* as a virulence model is a useful, cost effective and easy method of obtaining preliminary results that can be further verified in other virulence models. On the other hand, dosing and ease of use are the main drawbacks with using *D. melanogaster* as a virulence model.

1.8 Oxidative stress response

The main defence response of the host towards invading *Aspergillus spp.* is mediated by macrophage killing of the incoming conidia. The macrophage defence mechanism is mediated by the release of ROS (Segal, 2007). *A. fumigatus* and other pathogenic fungi can protect themselves from this defensive attack by mediating an oxidative stress response (Lessing *et al.,* 2007).

Activating protein (AP-1) is a family of transcription factors. The AP-1 homologue YAP1 is known as a central regulator of the oxidative stress response in *S. cerevisiae* (Qiao *et al.,* 2010). Previous work has demonstrated that *A. fumigatus* YAP1 homologue, AfYap1, contributes to oxidative stress response *in vitro* in the fungus (Qiao *et al.,* 2008). In the presence of oxidative stress, AfYap1 translocates from the cytoplasm to the nucleus in *A. fumigatus.* Proteomic analysis of *A. fumigatus* exposed to hydrogen peroxide showed that expression of 27 proteins increased and 17 exhibited decreased expression levels (Lessing *et al.,* 2007). Of the proteins that increased, the majority were associated with antioxidant defence, composed of: heat shock proteins, protein translocation apparatus, central metabolic pathways, amino acid and trehalose metabolism and proteins of the cytoskeleton. This protein profile resembles that of the protection mechanisms in *S. cerevisiae, Schizosaccharomyces pombe* and *C. albicans* (Lessing *et al.,* 2007).

All aerobic organisms are exposed to ROS and have developed enzymatic and non-enzymatic defences against them. Enzymatic defences include superoxide dismutase (SOD) and catalases, and non-enzymatic defences include the production of melanin, mannitol and trehalose (Rementeria *et al.,* 2005). SOD converts one harmful ROS, such as superoxide, to another form of ROS, namely hydrogen peroxide (Missall *et al.,* 2004). Catalases, as mentioned previously, are antioxidant

metalloenzymes which promote the conversion of hydrogen peroxide to water and molecular oxygen (Missall *et al.,* 2004). As previously mentioned, there are three catalases encoded in *A. fumigatus* which are produced during invasive aspergillosis, one conidial catalase, *catA* and two mycelial catalases, *cat1* and *cat2* (Paris *et al.,* 2003b). Cat1 and Cat2 protect *A. fumigatus* from peroxidase killing but not macrophage killing. Disruption of both genes results in a less virulent strain, whereas disruption of either catalase singularly does not change the virulence of the strain from the wild-type state (Paris *et al.,* 2003b).

Melanins are multifunctional polymers that are capable of reducing oxidants. There are two types of melanin identified in fungal pathogenesis: (i) 1,8-dihydroxynaphthalene (DHN) and (ii) 3,4-dihydroxyphenylalanine (DOPA). DHN is produced in the conidial pigment and protects from ROS and oxidative killing by macrophages (Brakhage *et al.,* 1999). DOPA is a strong antioxidant which protects against oxidative stress from macrophages (Hamilton and Gomez, 2002).

Mannitol is a polyol that scavenges for ROS *in vitro*. It has also been shown that mannitol is required for stress tolerance in *A. niger* conidiospores (Ruijter *et al.,* 2003).

Trehalose (α-D-glucopyranosyl-α-D-glucopyranoside) is a non-reducing disaccharide which accumulates during heat and oxidative stress (Fillinger *et al.,* 2001). It stabilises membranes and native proteins and prevents the aggregation of denatured proteins.

It has been shown that exposure of fungal spores or mycelia to hydrogen peroxide promotes oxidative stress (Angelova *et al.,* 2005). Oxidative stress in microorganisms cause diverse responses depending on the oxidative stress applied, due to the different oxidative stress pathways and reactions (Aguirre *et al.,* 2005).

There has also been evidence indicating a change in fungal cell morphology is due to reaction by the fungus to oxidative stress (Missall *et al.,* 2004).

In particular, it has been well documented that the NRP synthetases, *sidD* and *pes1* are involved in protection against oxidative stress (Eisendle *et al.,* 2006; Reeves *et al.,* 2006; Schrettl *et al.,* 2007).

1.9 Thesis Rationale and Objectives.

Invasive aspergillosis is a significant disease risk for immunocompromised individuals, with mortality rates as high as 90 % (Denning, 1998). Many studies are now focused on identifying novel drug targets in the organism, and the pace of functional genomic studies in *A. fumigatus* is gathering as a consequence of the availability of the entire genome sequence of *A. fumigatus* AF293 (Nierman *et al.,* 2005). The pathogenicity of *A. fumigatus* can be, in part, attributed to metabolites secreted during infection (e.g., siderophores or gliotoxin) (Willger *et al.,* 2009). Moreover, secondary metabolite, or natural product, biosynthesis represents a distinct aspect of the biochemistry of *A. fumigatus*, with respect to animals, and thus represents the focus of significant work directed towards drug target identification (Keller *et al.,* 2005).

At least 14 NRPS gene clusters have been identified in *A. fumigatus*, yet the products and functions of the majority of them still remain elusive (Cramer *et al.,* 2006b). Of the characterised NRPS products, siderophores and gliotoxin have been shown to contribute to the virulence of *A. fumigatus* (Sugui *et al.,* 2007; Haas *et al.,* 2008). However, little is known about the interaction between NRP peptides, although new studies have identified the possibility of cross-talk between NRPS clusters (Lazos *et al.,* 2010). Indeed, it is not unusual for distant genes to work

together, as in the case of the siderophore system where *sidA,* the gene involved in the first committed step of siderophore biosynthesis does not cluster with the other genes required for the biosynthesis of the siderophores, such as the NRP synthetases *sidD* and *sidC* (Schrettl *et al.,* 2004).

Previously it was established that *A. fumigatus* Δ*pes1* exhibited increased sensitivity to oxidative stress and also displayed an altered conidial morphology and hydrophobicity (Reeves *et al.,* 2006), however the NRP peptide product encoded by the NRP synthetase, Pes1, was not identified. More recent work has suggested that the increased rate of evolution of *pes1* may be associated with its pathogenicity potential (Fedorova *et al.,* 2008). Additionally, disruption of *sidD*, a siderophore synthetase which is required for TAFC biosynthesis, in *A. fumigatus* was also shown to result in increased sensitivity to oxidative stress and also play a role in virulence (Schrettl *et al.,* 2007). Thus, it was hypothesised that interplay between *pes1-* and *sidD*-encoded NRP peptides may synergistically contribute to resistance to oxidative stress in *A. fumigatus*.

The function of genes in many NRPS gene clusters remains elusive as they share neither overall, nor domain, homology with known proteins. This represents a major challenge in expanding our understanding of fungal biochemistry. An example of one such gene is *gliK* in the gliotoxin biosynthetic cluster. Consequently, deletion of this gene followed by functional analysis of the deficient fungal strain should both illuminate its function and allow assessment of any potential as a drug target.

Thus, the objectives of the work presented in this thesis are as follows:

1. Elucidation of the function of the NRP synthetase gene, *pes1*, in *A. fumigatus* by a targeted gene deletion approach, followed by comparative phenotypic analysis between wild-type and mutant strains.

2. Investigation of functional interactions between two apparently unrelated NRP synthetase genes, namely *sidD* and *pes1*, in *A. fumigatus* by generation of double-gene mutants.

3. Identification of the metabolite encoded by Pes1 in *A. fumigatus* by comparative metabolite profiling.

4. Establish a function for the gene, *gliK*, in the gliotoxin biosynthetic cluster by gene deletion in two *A. fumigatus* strains followed by extensive analysis of result mutants.

5. Develop assay systems for metabolite (TAFC) and anti-GliK IgG detection to enable future assessment of these analytes as biomarkers of fungal infection.

CHAPTER 2

Materials and Methods

2. Materials and Methods

2.1 Materials

All chemicals were purchased from Sigma-Aldrich Chemical Co. Ltd. (U.K.), unless otherwise stated. The details of the Materials used in this study can be found in Appendix I, at the back of this thesis.

2.2 Methods

2.2.1 Microbiological Methods – Strain Storage and Growth

Fungal and bacterial strains used in this study are listed in Table 2.1 and Table 2.2, respectively.

Table 2.1: Fungal strains used, including antibiotics and supplements used.

Species	Strain	Antibiotics/Supplements
A. fumigatus	ATCC46645	N/A
A. fumigatus	ATCC26933	N/A
A. fumigatus	Δ*akuB*	Hygromycin (250 μg/ml)
A. fumigatus	Δ*akuB*:Δ*pes1*	Pyrithiamine (100 ng/ml)
A. fumigatus	Δ*pes1*^{46645}	Pyrithiamine (100 ng/ml)
A. fumigatus	Δ*sidD*:Δ*pes1*	Pyrithiamine (100 ng/ml) & Hygromycin (250 μg/ml)
A. fumigatus	Δ*sidD*^{46645}	Hygromycin (250 μg/ml)
A. fumigatus	Δ*gliK*^{46645}	Pyrithiamine (100 ng/ml)
A. fumigatus	Δ*gliK*^{26933}	Pyrithiamine (100 ng/ml)
A. fumigatus	Δ*sidD*:Δ*pes1*:*pes1*^{c}	Phleomycin (40 ng/ml) & Hygromycin (250 μg/ml) & Pyrithiamine (100 ng/ml)
A. fumigatus	Δ*gliK*^{46645}:*gliK*^{c}	Phleomycin (40 ng/ml) & Pyrithiamine (100 ng/ml)

Table 2.2: Bacterial strains used, including antibiotics and supplements used.

Species	Strain	Antibiotics/Supplements
E. coli	TOP 10	Ampicillin (100 μg/ml)
E. coli	DH5α™	Ampicillin (100 μg/ml)
E.coli	pSK275	Pyrithiamine (100 ng/ml)
E. coli	pProEx™-Htb	Ampicillin (100 μg/ml)
E. coli	pAN8-1	Phleomycin (40 μg/ml)

2.2.1.1 *A. fumigatus* Growth, Maintenance and Storage

A. fumigatus strains were maintained on ME (Malt extract) agar (Section 9.1.1.3). A loop of spores from a stock spore solution was stabbed into the middle of a culture plate and plates were incubated at 37 ^{o}C for 5-7 days with periodic checking. Once full plate growth was observed, plates were sealed with parafilm, and stored inverted in a sealed plastic bag at 4 ^{o}C. For permanent storage of *Aspergillus* spores, freshly grown spores were harvested from agar plates by adding 10 ml of sterile H_2O to the conidial culture and rubbing the surface with a sterile disposable spreader to dislodge the spores. The spores were transferred to a 50 ml Falcon tube and stored at 4 ^{o}C, until required.

2.2.1.2 *E.coli* Growth, Maintenance and Storage

E. coli strains were grown on Luria-Bertani agar (Section 9.1.8) overnight at 37 ^{o}C or in Luria-Bertani broth (Section 9.1.7) at 37 ^{o}C overnight, shaking at 200 rpm. Where appropriate, media was supplemented with suitable antibiotics (Table 9.2). Bacterial strains were stored at 4 ^{o}C for short term storage.

2.2.2 Molecular Biological Methods

2.2.2.1 Isolation of Genomic DNA from *A.fumigatus*

A. fumigatus conidia were harvested from five day old plates using PBST (5 ml) (Section 9.1.4) and an aliquot of the resulting conidial suspension (100 μl) was used to inoculate 200 ml cultures of Sabouraud Dextrose Broth (Section 9.1.1.1). The cultures were incubated at 37 $^{\circ}$C for 24 hr with constant agitation. The cultures were then filtered through autoclaved miracloth and the mycelia collected. The mycelia mass was then flash frozen in liquid Nitrogen and ground to a fine powder using a pestle and mortar. The DNA extractions were carried out using the ZR Fungal/Bacterial DNA Kit supplied by Zymo Research (California, U.S.A). All buffers and reagents were supplied with the kit. For each sample, mycelia (1 g) was added to 750 μl DNA buffer in the ZR Bead Bashing tube. The tubes were vortexed rigorously for 5 minutes. The bead bashing tubes were centrifuged at 10000 x g for 1 minute. Supernatant (400 μl) was transferred to Zymo-Spin IV Spin filters in collection tubes and centrifuged at 7000 x g for 1 minute. Fungal/Bacterial DNA binding Buffer (1200 μl) was added to the filtrates in the collection tubes. Filtrate (800 μl) was transferred to Zymo-Spin IIC Columns in collection tubes and centrifuged at 10000 x g for 1 minute. The filtrate was discarded. The remaining filtrate (800 μl) was added to the Zymo-Spin IIC columns and centrifuged at 10000 x g for 1 minute. DNA Pre-Wash Buffer (200 μl) was added to the Zymo-Spin Columns in new collection tubes and centrifuged at 10000 x g for 1 minute. Fungal/Bacterial DNA wash buffer (500 μl) was added to the Zymo-Spin IIC columns and centrifuged at 10000 x g for 1 minute. The Zymo-Spin IIC columns were transferred to clean 1.5 ml microcentrifuge tubes and DNA Elution Buffer (100 μl) was added to the columns and centrifuged at 10000 x g for 1 minute to elute the DNA samples.

2.2.2.2 DNA Precipitation

2.5 X volume 100 % (v/v) ice cold ethanol and 0.1X volume 3M Sodium acetate (Section 9.1.15) was added to each DNA sample. The mixture was incubated at -20 ^{o}C for at least 30 minutes and then centrifuged at 17900 x g for 15 minutes. The supernatants were discarded and the pellets were resuspended in 100 µl 70 % (v/v) Ethanol. The samples were centrifuged at 13000 x g for 10 minutes and the supernatants were discarded and the pellets were resuspended in 16 µl sterile water. The precipitated DNA samples were stored at -20 ^{o}C until required.

2.2.2.3 Polymerase Chain Reaction (PCR)

Polymerase chain Reaction (PCR) was used to amplify fragments of DNA for cloning, transformation constructs, probes, and to test *E. coli* for recombinant plasmid presence. PCR was carried out using either Accu*Taq* LA polymerase (Sigma-Aldrich) or Expand Long Template PCR system (Roche). Annealing temperatures were estimated as *ca.* 4 ^{o}C below the melting temperature (T_m) of the primers used. Extension times used were *ca.* 1 min/kb of DNA to be synthesised. Reactions were carried out using either the Eppendorf PCR or G-Storm PCR (Roche) Systems.

The general reaction constitutes for both polymerases used was as follows:

Accu*Taq* LA polymerase

10X reaction buffer	2 µl
dNTP mix (10 µM)	2 µl
Primer 1 (100 pmol/µl)	1 µl
Primer 2 (100 pmol/µl)	1 µl
DMSO	0.8 µl
DNA template	1-10 ng
Accu*Taq*	0.2 µl
Sterile water	to a total of 20 µl

71

<u>Expand Long Template PCR system</u>

10X Reaction Buffer	5 μl
dNTP mix (5 μM)	5 μl
Primer 1 (100 pmol/μl)	2 μl
Primer 2 (100 pmol/μl)	2 μl
DNA template	1-10 ng
Expand*Taq*	1 μl
Sterile water	to a total of 50 μl

The following reaction cycle was used unless otherwise stated:

95 ^{o}C (denaturing)	1 min
95 ^{o}C (denaturing)	1 min
56 ^{o}C (annealing)	1 min
68 ^{o}C (extending)	1 min
68 ^{o}C (extending)	7 min

x 35 cycles (for the middle three steps)

2.2.2.4 Agarose Gel Electrophoresis

Agarose gel electrophoresis was used to visualise restriction digest reactions, to separate DNA for Southern analysis, to separate differently sized DNA fragments prior to purification and for estimation of DNA yield. Agarose gels were cast and run using Bio-Rad electrophoresis equipment. Agarose gels of between 0.7 – 2 % (w/v) in 1X TAE buffer (Section 9.1.12.2) were used, although for the majority of applications a 1 % (w/v) content was suitable. Powdered agarose was added to the appropriate volume of 1X TAE buffer (Section 9.1.12.2) in a 200 ml flask with loose stopper. This was then gently heated in a microwave, with frequent mixing, until the agarose had dissolved. While allowing the gel to cool, a mould was prepared by inserting the casting unit in a casting holder and sealed. A gel comb was inserted. After allowing the gel to cool to 40 - 50 ^{o}C, the molten gel was then poured into the prepared unit. Ethidium bromide (3 μl) (Section 9.1.12.3) was added to the casting unit and the gel was allowed to set on a level surface. Once set, the gel comb was

removed gently, and the gel casting unit containing the set gel was placed into the gel tank, with the wells nearer the negative (black) electrode. 1 X TAE buffer (Section 9.1.12.2) was then poured into the gel tank to fully submerge the gel.

2.2.2.5 DNA Gel Electrophoresis

DNA samples were prepared for loading by adding 5 volumes of DNA sample to 1 volume of 6 X loading dye (Section 9.1.12.4). DNA fragment size was estimated by running molecular weight markers alongside the unknown samples. Three different molecular weight markers were used throughout this study: marker VII (Roche), 2-log ladder (Roche) and 50 bp ladder (Roche). Gels were electrophoresed at 50-100 volts for 30-90 min.

2.2.3 Cloning

2.2.3.1 Preparation of competent DH5α bacterial cells

A loopful of the DH5α bacterial cells were inoculated into a 10 ml culture of LB broth (Section 9.1.7) and incubated overnight at 37 ^{o}C, shaking at 200 rpm. The culture was used to inoculate a 1 L culture of LB Broth, which was incubated at 37 ^{o}C, for 2 hr, shaking at 200 rpm. The culture was split into 4 aliquots and incubated on ice for 10 min. The cultures were then centrifuged at 2700 x g, for 10 min at 4 ^{o}C. The supernatant was discarded and the pellets were each resuspended in cold Buffer RF1 (10 ml) (Section 9.1.11.3). The suspension was incubated on ice for 30 min. The suspension was divided out into 1.5 ml Eppendorf tubes and the cells were centrifuged at 2700 x g for 10 min at 4 ^{o}C. The supernatant was discarded, and each pellet was resuspended in Buffer RF2 (3.2 ml) (Section 9.1.11.4) and kept on ice for

15 min. The cells were divided into 100 μl aliquots in Eppendorf tubes and stored at -70 °C until required.

2.2.3.2 Transformation of DNA into competent DH5α bacterial cells

Luria- Bertani agar plates (Section 9.1.8) containing Ampicillin (Section 9.1.10) were pre-heated at 37 °C for at least one hr. DH5α competent cells (50 μl) (Section 2.2.3.1) were removed from -70 °C freezer and were defrosted on ice for two minutes. DNA (1-10 ng) was added to the DH5α cells. The mixture was incubated on ice for five minutes. The mixture was spread onto the agar plates as quickly as possible and the plates were incubated at 37 °C overnight.

2.2.3.3 TOPO TA Cloning

One step cloning of PCR products were carried out using the TOPO TA Cloning kit from Invitrogen, according to the manufacturer's instructions. The principle behind one step Cloning is based on the non-template dependant activity of *Taq* polymerase that results in the addition of a single deoxyadenosine (A) to the 3' ends of the PCR products. The linearised cloning vector has single 3' deoxythymidine (T) residues therefore facilitating PCR inserts to ligate efficiently with the vector. The TOPO TA Cloning vector map is presented in Figure 2.1. The TOPO TA Cloning kit contains TOP 10 One Shot competent *E. coli* cells, Super Optimal Catabolite repression (SOC) media, TOPO vector and salt solution. Prior to cloning, TOP 10 cells were thawed on ice and LB agar plates (Section 9.1.8) containing 100 μg/ml Ampicillin (Section 9.1.10) pre- warmed in a 37 °C incubator. Genomic DNA PCR product (4 μl), Salt solution (1 μl) and TOPO vector (1 μl) were added to a sterile 0.5 ml tube and left at room temperature for 30 min. A 2 μl aliquot of this reaction

mixture was added to a vial of TOP 10 *E. coli* cells and placed on ice for 30 min. Cells were heat shocked at 42 ^{o}C for 30 s in a water bath and pre-warmed SOC media (200 µl) was added to the vial. The cell suspension was transferred to a 15 ml tube and incubated at 37 ^{o}C for 1 hr with constant agitation (200 rpm). During this incubation period, 32 µl of 5-bromo-4-chloro-3-indolyl-beta-D-galactopyranoside (X-gal) (Promega) (Southampton, UK) (40 mg/ml) was spread over the pre-warmed agar plates using a sterile glass spreader and the plates were returned to the incubator. This reagent facilitates blue/white colony screening which greatly aids in the identification of desired clones. A 50 µl aliquot of the cell suspension was spread on the selection plates using a sterile disposable spreader and the plates were incubated overnight at 37 ^{o}C. White colonies were selected and sub-cultured on to LB agar plates (Section 9.1.8) with Ampicillin (100 µg/ml) (Section 9.1.10). Colony PCR (Section 2.2.3.4) was carried out to verify the presence of the desired insert in the vector of the sample clones.
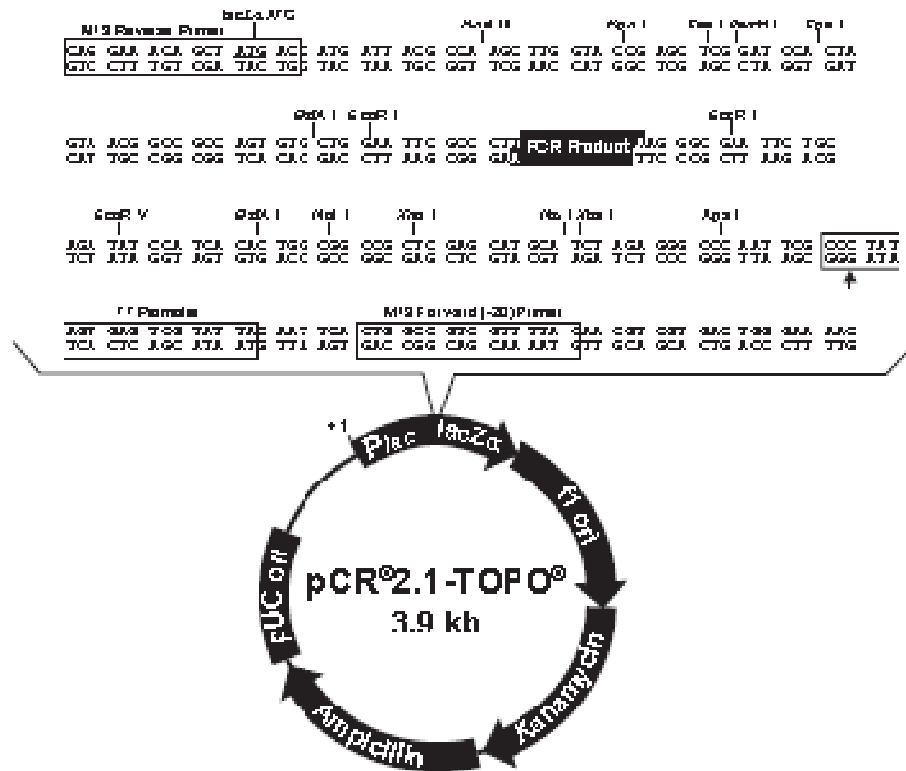
Figure 2.1: Vector map of the TOPO® TA Cloning® vector (Invitrogen, The Netherlands).

2.2.3.4 Colony PCR

Bacterial colonies observed following by transformation could be directly screened for presence of the desired plasmid by PCR. Using aseptic techniques, an isolated colony was removed using a sterile tip and placed in sterile 0.2 ml microcentrifuge tube containing a PCR Mastermix having all components necessary for PCR (Section 2.2.2.3) and also streaked onto a reference plate. Genomic DNA and DNA negative controls were included and PCR was carried out as described in

Section 2.2.2.3 with the exception that the initial denaturing step was increased to 5 min at 95 ^{o}C to allow the bacterial cells to rupture and release DNA for the PCR reaction.

2.2.3.5 Small Scale Plasmid Purification

Plasmid purification was carried out according to the Qiagen Plasmid purification manual using the QIA prep Mini-prep kit. All buffers (P1, P2, N3, PE and EB) and columns were supplied with the kit and details of buffer constituents outlined in the Qiagen Plasmid Purification Handbook. An isolated colony was picked aseptically and used to inoculate LB broth (Section 9.1.7) (3 ml) containing 100 μg/ml Ampicillin (Section 9.1.10). The culture was grown overnight at 37 °C and the cells harvested by centrifugation at 13,000 x g for 10 min at 4 °C. The supernatant was removed and the pellet resuspended in ice cold Buffer P1 (250 μl). Buffer P2 (250 μl), and Buffer N3 (350 μl) were then added and the tubes inverted 5 times prior to centrifugation at 11,000 x g for 1 min at 4 °C. The supernatant was removed, applied to the Qiaprep spin column and centrifuged at 11,000 x g for 1 min at 4 °C. The flow through was discarded and the column was washed with Buffer PE (750 μl) and centrifuged at 11,000 x g for 1 min. Once again the flow through was discarded and the DNA was eluted off the column by the addition of Buffer EB (30 μl) followed by centrifugation at 14,000 x g for 1 min. The purified plasmid was subsequently analysed by DNA gel electrophoresis (Section 2.2.2.5).

2.2.3.6 DNA Sequencing

DNA sequencing of recombinant clones was performed by Agowa genomics (Berlin, Germany) on a commercial basis.

2.2.4 RNA Analysis

2.2.4.1 RNA Isolation

A. fumigatus liquid cultures which were incubated at the required temperature and time were filtered through autoclaved miracloth and the mycelia collected. Mycelia were then flash frozen in liquid Nitrogen and ground to a fine powder in a mortar by pestle. The RNA was isolated using the RNeasy Kit supplied by Qiagen, according to the manufacturer's instructions. β-mercaptoethanol (10 μl) was added to Buffer RLC (1 ml) before RNA extraction. For each sample, Mycelia (100 mg) was placed in sterile microcentrifuge tubes. Buffer RLC (450 μl) was added the each sample vortexed vigorously. The lysates were transferred to QIAshredder spin columns. The columns were centrifuged at 17,900 x g for 2 min, and the flow through was transferred to new microcentrifuge tubes, avoiding the cell debris pellet. Ethanol (100 %, 0.5 Volume of the lysate) was added to the lysates and mixed immediately. Samples were then transferred to RNeasy spin columns, which were placed in 2 ml collection tubes. Columns were centrifuged at 10600 x g for 15 s, and the flow through was discarded. Buffer RW1 (700 μl) was added to the columns and then centrifuged at 10600 x g for 15 s, discarding the flow through. Buffer RPE (500 μl) was added to the columns and centrifuged for 15 s at 10600 x g. The flow through was discarded. Buffer RPE (500 μl) was added to the columns and centrifuged at 10600 x g for 2 min. The spin columns were removed and placed in new collection tubes and were centrifuged for 2 min at 17900 x g, to remove residual buffer collected. The columns were removed and placed in 1.5 ml microcentrifuge tubes. RNase-free water (50 μl) was added to the columns and the RNA was eluted by centrifuging the column at 10600 x g for 1 min. The RNA samples were stored at -70 ^{o}C.

2.2.4.2 RNA Gel Electrophoresis

Agarose gels (1 % (w/v)) were prepared by adding agarose (1 g) to 10 X Formaldehyde Agarose (FA) gel buffer (10 ml) (Section 9.1.13.3) and the final volume was adjusted to 100 ml with DEPC- treated water (Section 9.1.13.2). The agarose was melted in a microwave, and was allowed to cool to 65 ^{o}C. Formaldehyde (37 % (v/v)) (1.8 ml) was added to the agarose solution in a fume hood and the solution was poured into the gel tray and allowed to cool. The Formaldehyde/agarose gel was placed in an electrophoresis unit using 1X formaldehyde agarose running buffer (Section 9.1.13.4). The gel was allowed to equilibrate in the buffer for 30 min prior to use. RNA samples were prepared for loading by adding 4 volumes of RNA sample to 1 volume of 5X RNA loading buffer (Section 9.1.13.5). The samples were incubated at 65 ^{o}C for 5 min and allowed to chill on ice. Samples were loaded onto the gel and electrophoresed at 90 V for ~2 hr. Formaldehyde agarose gels were visualised on the DigiDoc RT system (Alpha Innotech).

2.2.4.3 DNase Teatment of RNA

DNase treatment of RNA was performed using a DNase kit purchased from Sigma-Aldrich. *A. fumigatus* RNA (0.5 μg) was brought to 8 μl using DEPC water (Section 9.1.13.2) in Eppendorf tubes, 1 μl of 10 X reaction buffer and 1 μl of DNase 1 were added to each of the RNA samples, which were incubated at room temperature for 15 min. Stop solution (1 μl) (supplied with kit) was added to the solutions, which were heated to 70 ^{o}C for 10 min. Samples were stored at –70 ^{o}C.

2.2.4.4 cDNA Synthesis

cDNA synthesis was performed using the SuperScript® III First-Strand Synthesis System kit, supplied by Invitrogen (California, U.S.A). All buffers and reagents were

supplied with the kit. DNase treated RNA (8 μl), 10 mM dNTP mix (1 μl), Oligo (dT) (1 μl), were added to a microfuge tube. Tubes were incubated at 65 ^{o}C for 5 min, and placed on ice for 1 min. A master mix of 10 X Reverse Transcriptase buffer (2 μl), 25 mM MgCl$_2$ (4 μl), 0.1 M DTT (2 μl) and RNase OUT recombinant RNase Inhibitor (0.9 μl), per sample, was prepared. This master mix (9 μl) was added to each RNA sample and mixed gently by pipetting. The samples were then incubated at 42 ^{o}C for 2 min. Superscript III-Reverse Transcriptase (0.25 μl) was added to each sample and mixed, prior to incubation at 42 ^{o}C for 50 min. The reaction was terminated by heating the samples to 70 ^{o}C for 15 min, and chilling the tubes on ice. RNase H (1 μl) was added to each sample and incubated at 37 ^{o}C for 20 min. The samples were stored at -20 ^{o}C.

2.2.4.5 Semi-quantitative RT-PCR

PCR was carried out on the cDNA samples as described in Section 2.2.2.3 with the *A. fumigatus* calmodulin gene serving as a control in RT-PCR experiments (Burns *et al.,* 2005).

2.2.4.6 Quantitative Real time PCR

PCR was carried out on the cDNA samples using the qPCR lightcycler system (Roche). A standard curve for each reaction was created by using a serial dilution of a cDNA sample. The dilutions were 5-fold dilutions. Once the optimum conditions were confirmed by the standard curve, the samples were used at a dilution within the serial dilution range, usually 1/25.

The expression of various genes of interest was measured against the expression of the housekeeping gene, Calmodulin (AfuA_4G10050). This quantified the level of

expression of the genes of interest relative to the house keeping gene expression, which was normalised for all the samples.

The genes of interest for this project were *pes1* (AFUA_1G10380) and *gliK* (AFUA_6G09700). The *pes1* gene is large (18.8 kb), and the region of interest is the first adenlyation domain, *A1* (1.2 kb). The PCR program used for this gene was named pes1A1, which amplified a 171 bp region. The *gliK* gene (822 bp) is relatively small compared to *pes1* and the PCR program used for this gene was gliK, which amplified a 370 bp region.

Reaction Mix

cDNA 1/25 dilution	5μl
SYBR Green	10 μl
Sterile water	2 μl
Primer 1 (5 μM)	1.8 μl
Primer 2 (5 μM)	1.8 μl

PCR Cycle (Calmodulin)

95 ^{o}C (pre-incubation)	10 min	
95 ^{o}C (denaturing)	10 sec	
55 ^{o}C (annealing)	30 sec	x 35 cycles
72 ^{o}C (extending)	30 sec	

PCR Cycle (pes1A1, gliK)

95 ^{o}C (pre-incubation)	10 min	
95 ^{o}C (denaturing)	10 sec	
60 ^{o}C (annealing)	30 sec	x 35 cycles
72 ^{o}C (extending)	30 sec	

2.2.5 Restriction Enzyme Digests

Restriction enzymes, 10 X reaction buffers, and bovine serum albumin (BSA) were obtained from either Promega (Southampton, UK) or New England Biolabs

(Ipswich, UK). Reactions were carried out according to the manufacturer's instructions, but a typical reaction was performed as follows:

DNA	1 µg
Enzyme	1 µl
10 x buffer	1 µl
BSA (10 µg/µl)	1 µl (if required)
Sterile water	to final volume of 10 µl.

The total reaction volume was always > 10 X the volume of enzyme used in order to prevent high glycerol concentrations, which could cause non-specific digestion (star activity). Reactions were typically carried out at 37 ^{o}C for 3 hr, although some enzymes required different incubation temperatures, as per the manufacturer's instructions. Digestion reactions were visualised by agarose gel electrophoresis (Section 2.2.2.5)

2.2.6 Ligation of DNA fragments

Ligation of DNA fragments was required for creating the constructs for *pes1* disruption and *gliK* deletion transformation and also for the recombinant GliK production using the pProEx™-Htb expression vector. DNA was digested (Section 2.2.5) to create compatible ends and the resultant fragments were subjected to agarose gel electrophoresis (Section 2.2.2.5). Ligation reactions were carried out using the Fast Ligase (Promega, Southampton, UK) according to the manufacturer's instructions. Ligation reactions were set up using 100 ng vector, using the following equation:

$$\frac{\text{ng Vector} \times \text{kb Insert}}{\text{kb Vector}} \times \text{Molar ratio} \frac{\text{Insert}}{\text{Vector}}$$

82

The ligations were usually carried out with molar ratios of 1:1 and 1:3 and a typical reaction was usually made up of the following, and incubated at 22 $^{\circ}$C for 2 hr:

Vector	100 ng
Insert	as per equation calculation
2X Fast ligase Buffer	12.5 µl
Fast Ligase	1 µl
Sterile water	to 25 µl

2.2.7 Transformation of selected genes of *Aspergillus fumigatus*

The bipartite method of transformation was used for the integration of the constructs into the *Aspergillus fumigatus* genome. Overall, this strategy involved three separate overlapping homologous recombination events. The general scheme of this method is outlined in Figure 2.2. The method utilises a selection marker that is only functioning by the homologous recombination of overlapping ends that unify the selection marker. The homologous recombination of the 5' and 3' flanking regions of the gene of interest are the other two locations of the homologous recombination sites.
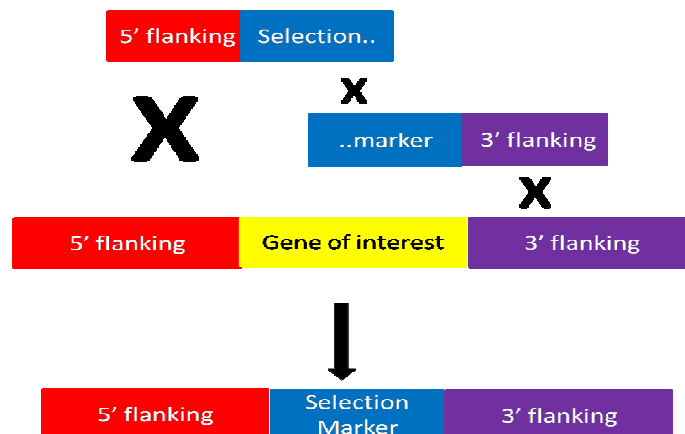
Figure 2.2: General schematic of the bipartite transformation method where the homologous recombination of the two separate fragments of the selection marker is the initial recombination site. The establishment of the complete selection marker enables the use of easy screening on the appropriate selection media. The

83

homologous recombination of the 5' and 3' flanking regions of the gene of interest direct the targeted replacement of the gene with the selection marker.

In the knock out transformations of *pes1* and *gliK*, the selection marker chosen was the pyrithiamine resistance gene, *ptrA*, excised from the plasmid pSK275 (A kind gift from Prof. Sven Krappmann, Göttingen, Germany). Pyrithiamine is an antagonist of thiamine and exposure of *Aspergillus fumigatus* to pyrithiamine is lethal to the fungus. The introduction of the pyrithiamine resistance gene produces the required thiamine, and therefore allows the transformed cell to grow in the otherwise lethal conditions.

For the reinsertion of the gene into the mutated strain the previously deleted region is PCR amplified from the wild-type strain and integrated into the TOPO vector. The plasmid is then linerised by a single restriction enzyme digestion, this is the construct used for the transformation. The selection marker is co-transformed, with the linerised construct. The transformation occurs by a single homologous recombination point. The general schematic of this complementation transformation is described in Figure 2.3.
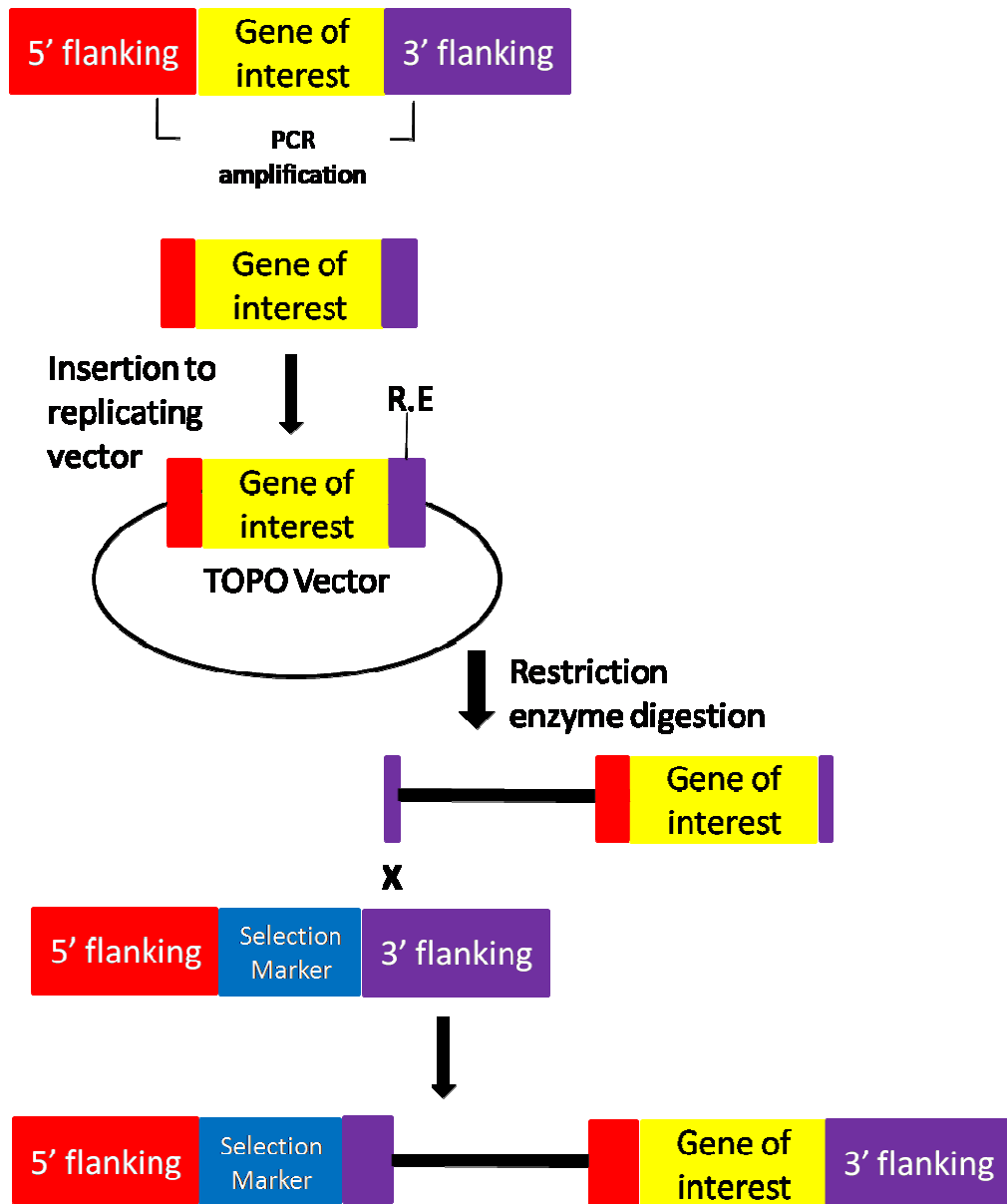
Figure 2.3: General schematic of the complementation strategies employed. The gene of interest and some of the 5' and 3' flanking region is cloned into the TOPO vector and subsequently digested with a unique restriction enzyme which cuts the 3' flanking region only. The digested vector is then used as the transformation construct where the 3' flanking region after the restriction cut is used to direct the construct to insert into the genome in the 3' flanking region after the selection marker which was already used to remove the gene previously.

2.2.7.1 Constructs for Knock out Transformations

The creation of constructs for the transformation process by the bipartite method is based on generating PCR products which contain additional restriction enzyme sites anchored onto certain primers. This enables the fragment generated by these primers to be digested and ligated to another DNA fragment, generating the final PCR products used for the transformation. The primers used for all the transformations are listed in Table 2.3.

For *pes1* transformation, the first round PCR generated products of the flanking regions used primers that incorporated restriction sites, *Pvu*I and *Kpn*I, used for a ligation site with the *ptrA* cassette (Figure 2.4). For *gliK* transformation, the first round PCR generated products of the flanking regions used primers that incorporated restriction sites, *Spe*I and *Hind*III (Figure 2.5). The flanking regions and the plasmid pSK275 were digested with the appropriate restriction enzyme and the digested PCR products were then ligated to the digested plasmid. The resultant fragments were then used as templates for the final PCR, where nested primers for the flanking regions and primers incorporated in the *ptrA* cassette were used to create the constructs used for the transformations. The final PCR products were precipitated to reduce the volume of the construct required for the transformation.

Table 2.3: Oligonucleotide primers used for the creation of constructs for the transformation of *pes1* and *gliK*.

Gene Target	Primer Name	Add on restriction sites	5' → 3' Sequence
pes1	5' forward		GTCGGCATCGGACATCTAC
pes1	5' reverse	*Pvu*I	GACGATCGGTACCATCTGCCACTCAC
pes1	3' forward	*Kpn*I	GCGGTACCCAAGGCATTGGTCTCACTG
pes1	3' reverse		CTGTAGCTTCTGGCCGAG
pes1	5' nested forward		CATGCAATCAAGGATATGG
pes1	3' nested reverse		CCTTGCACTACCAATGCTG
gliK	*gliK* 1 forward		GCATACTGTAGTCGCGGTAGA
gliK	*gliK* 4 reverse	*Spe*1	GCACTAGTGCTTTCCCCATGTTGCTTG
gliK	*gliK* 3 forward	*Hind*III	CGAAGCTTAGTCTCCATGTCTCCGATG
gliK	*gliK* 2 reverse		CGAGAGCGTGGCAAACAGAC
gliK	*gliK* 5' nested		ACGCCTCTAACATGCCATAC
gliK	*gliK* 3' nested		GTAGGTCGGCAGGTAGTACA
ptrA	optrA 1 forward		GAGGACCTGGACAAGTAC
ptrA	optrA 2 reverse		CATCGTGACCAGTGGTAC
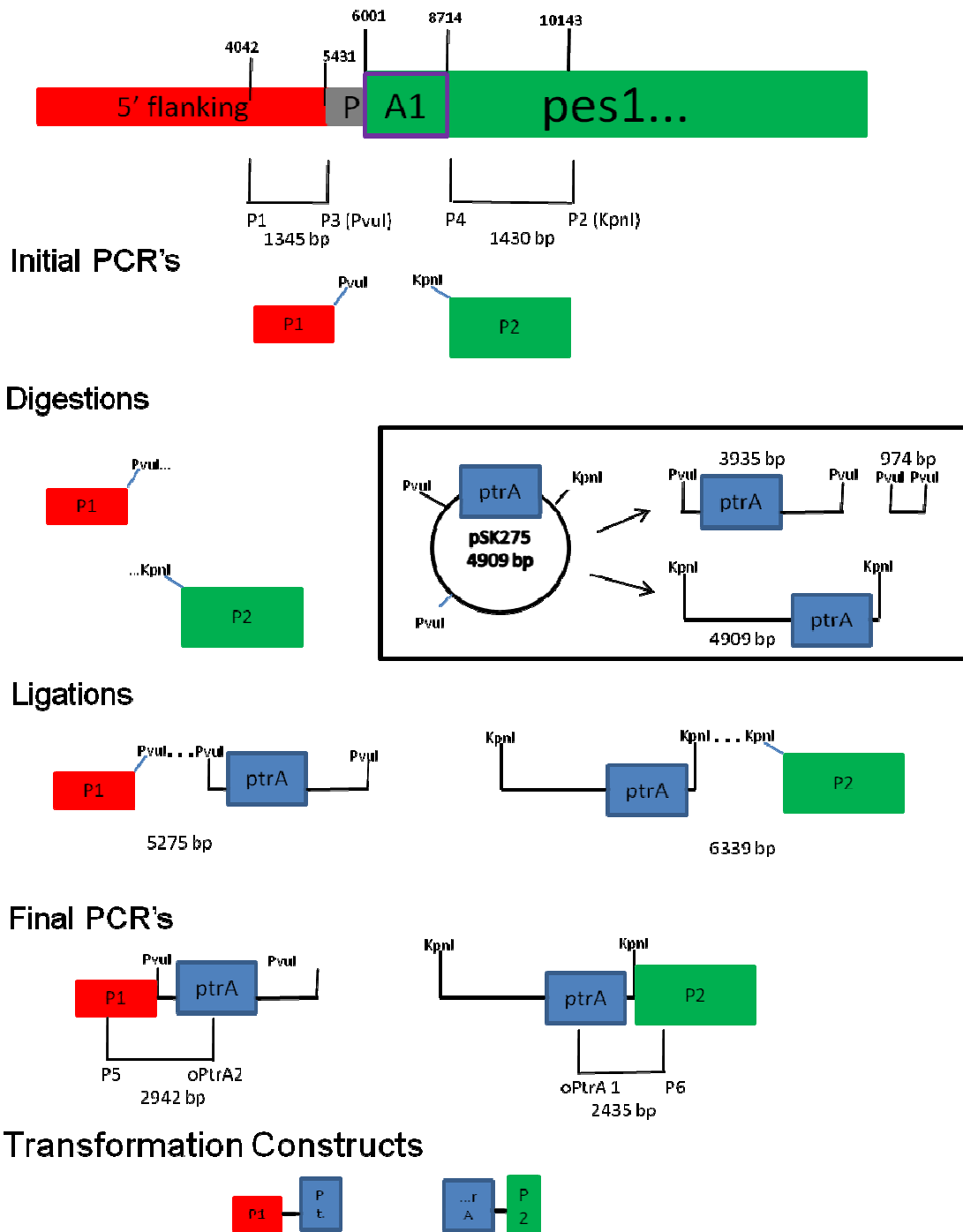
Figure 2.4: Schematic of strategy for generation of transformation constructs used in *pes1* disruption. Initial PCR products have an add-on restriction site, which is used to digest the product to facilitate ligation to the *ptrA* cassette. This is then used as a template for the final PCR products which are the Transformation constructs. The red shape depicts the PCR product generated from the 5' flanking region of *pes1*. The Green shape depicts the PCR product generated from the 3' region of *pes1*. The grey shape depicts the predicted promoter of *pes1*. The blue shape depicts the pyrithamine resistance cassette excised from the plasmid pSK275.
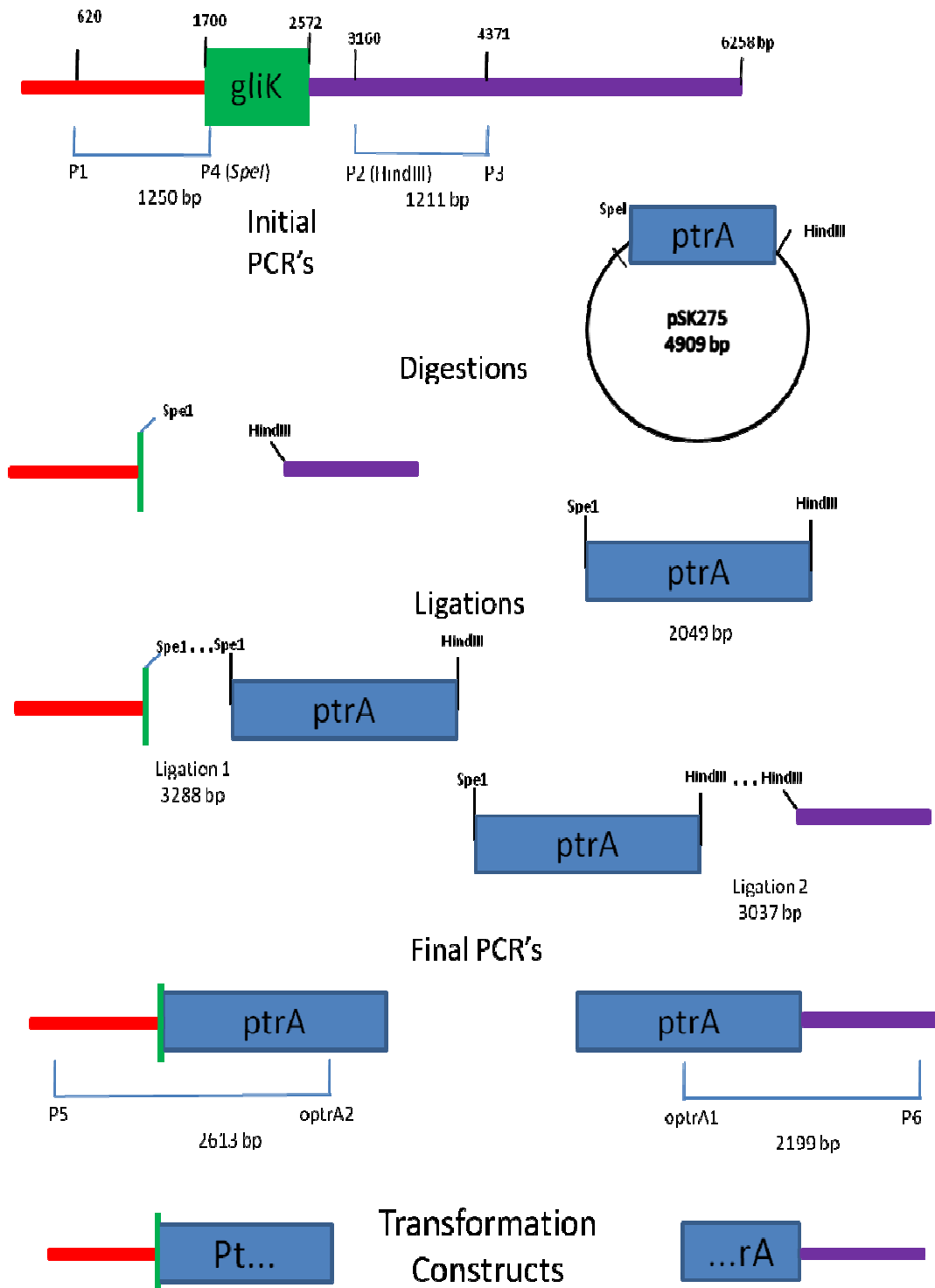
Figure 2.5: Schematic of strategy for generation of transformation constructs used in *gliK* deletion. Initial PCR products have an add-on restriction site, which is used to digest the product to facilitate ligation to the *ptrA* cassette. This is then used as a template for the final PCR products which are the transformation constructs. The red shape depicts the PCR product generated from the 5' flanking region of *gliK*. The Green shape depicts the PCR product generated from the 3' flanking region of *gliK*. The blue shape depicts the pyrithamine resistance cassette excised from the plasmid pSK275.

2.2.7.2 Constructs for complementation Transformations

The primers used for the complemented construct are listed in Table 2.4. The PCR products were inserted into the TOPO vector, and the orientation of the inserted DNA was verified. A single restriction enzyme was located within the 3' region of the inserted DNA, and the entire plasmid was linerised by digesting with this restriction enzyme. For *pes1*, the restriction enzyme was *Aar*I (Figure 2.6), and for *gliK* the restriction enzyme was *Ale*I (Figure 2.7). For the selection marker, the phleomycin resistance plasmid, pAN8-1 was used. Due to the necessity of the single restriction enzyme in the construct containing vector, it was impossible to add the phleomycin resistance cassette to the construct containing vector. Therefore, pAN8-1 was co-transformed in its circular form along with the linerised construct vector in the transformation process.

Table 2.4: Oligonucleotides used for the creation of constructs for the complementation transformation of *pes1* and *gliK*.

Gene Target	Primer Name	5' → 3' Sequence
pes1	5' nested forward	CATGCAATCAAGGATATGG
pes1	3' nested reverse	CCTTGCACTACCAATGCTG
gliK	*gliK* 5' nested forward	ACGCCTCTAACATGCCATAC
gliK	*gliK* 3' nested reverse	GTAGGTCGGCAGGTAGTACA

90
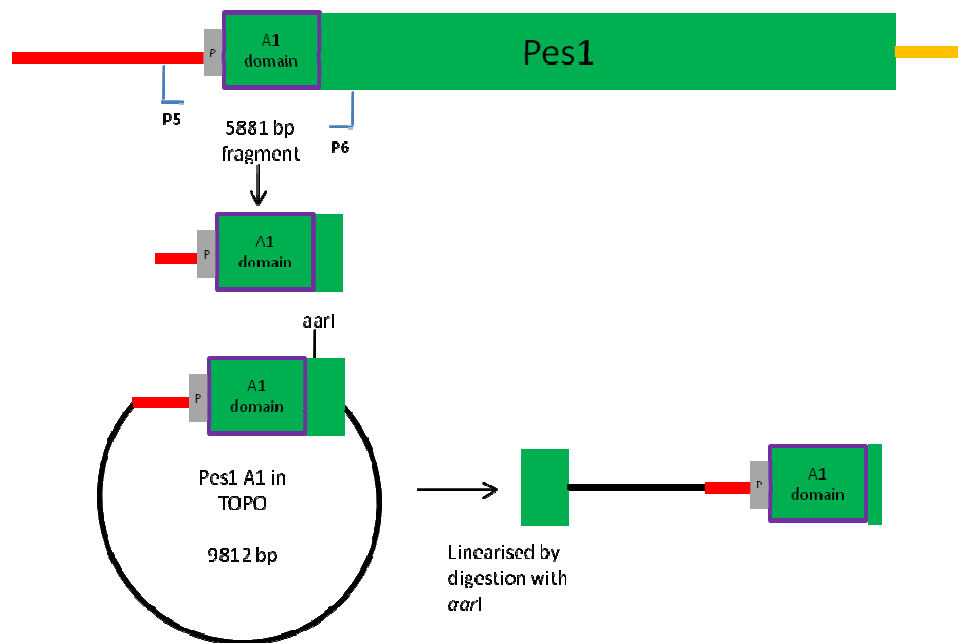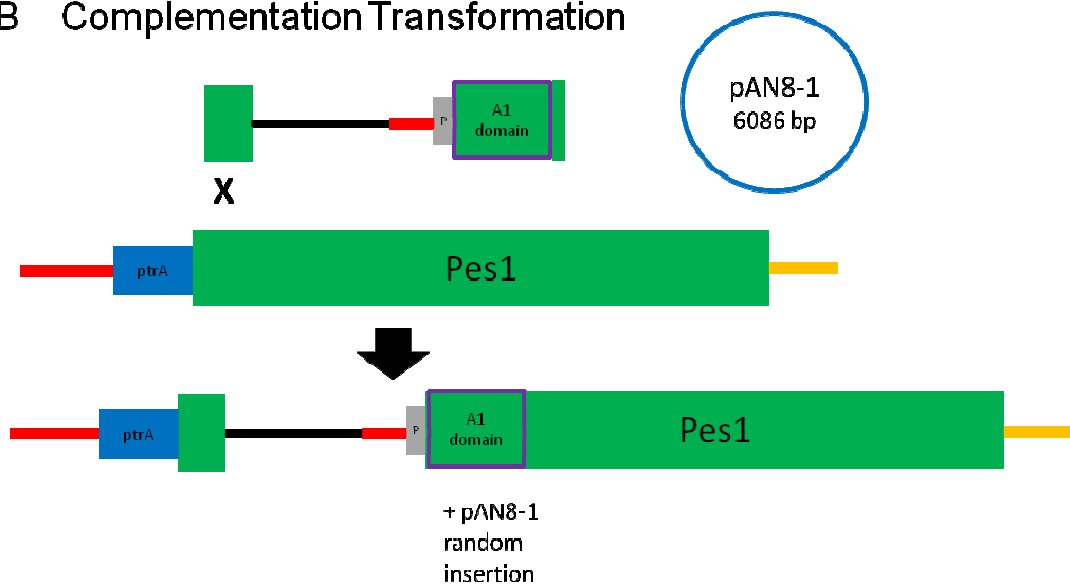
Figure 2.6: Schematics of the Complementation strategy employed for the *pes1* reconstitution transformation where (A) Schematic of the generation of the constructs for subsequent complementation and (B) Schematic of the transformation for compelementation. The red shape depicts the 5' flanking region of *pes1*. The Green shape depicts the *pes1* gene. The grey shape depicts the predicted promoter of *pes1*. The yellow shape depicts the 3' flanking region. The blue shape depicts the pyrithamine resistance cassette excised from the plasmid pSK275. The black shape depicts the Topo cloning vector.
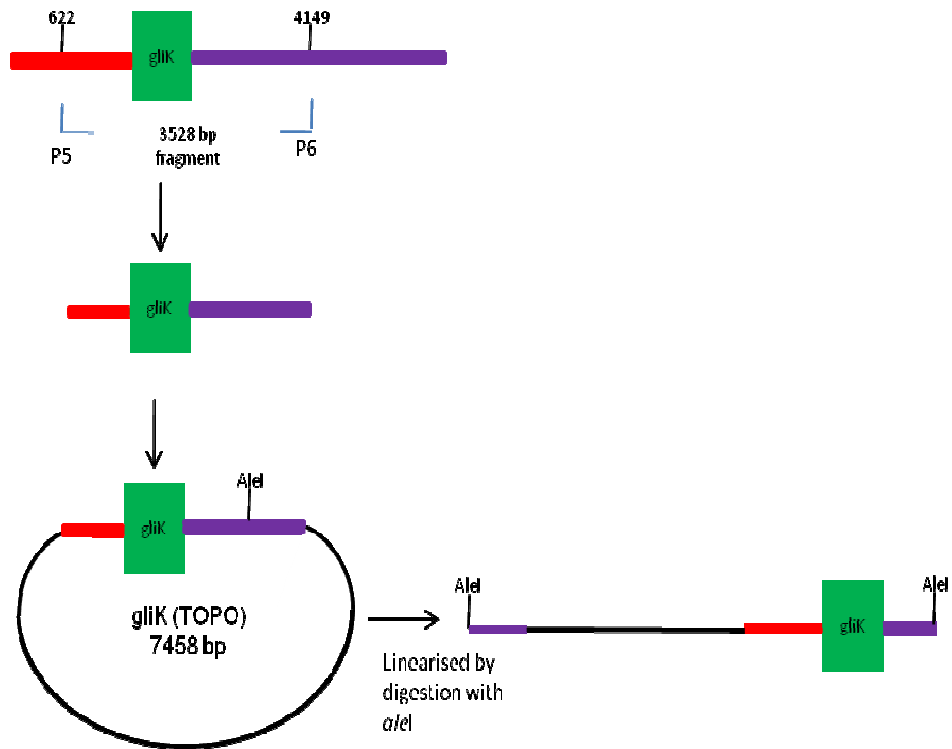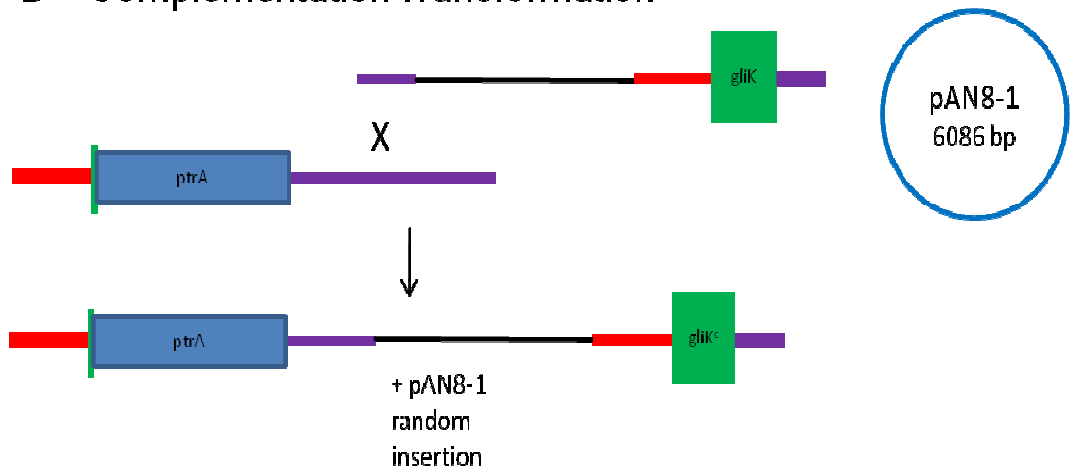
Figure 2.7: Schematic of the Complementation strategy employed for the *gliK* reconstitution transformation. The red shape depicts the 5' flanking region of *gliK*. The Green shape depicts the *gliK* gene. The purple shape depicts the 3' flanking region of *gliK*. The blue shape depicts the pyrithamine resistance cassette excised from the plasmid pSK275. The black shape depicts the Topo cloning vector.

2.2.7.3 *A. fumigatus* Protoplast Preparation

A. fumigatus conidia were harvested from 5 day old plates grown on Sabouraud agar (Section 9.1.1.1) by washing two plates with 5 ml sterile PBST (Section 9.1.4). An aliquot of the spore suspension was diluted (1/20 dilution) and counted on a haemocytometer. A 500 ml conical flask containing AMM medium (200 ml) (Section 9.1.1.6.1) was inoculated with 2×10^8 spores. The culture was incubated overnight at 37 ^{o}C, whilst shaking at 200 rpm. The mycelia were harvested through miracloth and washed through with 600 ml autoclaved distilled water. Excess water was removed by gentle blotting. Mycelia (1.5 g) was weighed out in duplicate, and each was added to 15 ml Lysis buffer containing lytic enzymes (Section 9.1.16.4.2), and then incubated at 30 ^{o}C for 3 hr, while shaking at 100 rpm. During the 3 hr, the mycelia were removed from the incubator to break up the mycelial mass by pipetting gently. After the incubation, the mycelia were placed on ice for 2 min. The mycelial solution was centrifuged at 132 x g for 18 min with the brake off. The supernatant was filtered through miracloth and brought up to 40 ml with 0.7 M KCl (Section 9.1.16.1). The solution was centrifuged at 1769 x g for 12 min with the brake off. The supernatant was poured off and discarded. The pellet was resuspended in 20 ml 0.7 M KCl (Section 9.1.16.1). The solution was centrifuged at 1769 x g for 12 min with the brake off. The supernatant was poured off and discarded. The pellet was resuspended in 70 μl Buffer L6 (Section 9.1.16.5) and then centrifuged at 58 x g for 2 min with the brake off. Finally, the protoplasts were viewed on a haemocytometer to ensure adequate yield and viability were obtained for the transformation. The protoplasts were stored on ice for up to 1 hr before use in transformation experiments.

2.2.7.4 Transformation of protoplasts

Between 2 -7 µg of 5' and 3' constructs were mixed together and the volume was brought up to 50 µl with Buffer L6 (Section 9.1.16.5) in a 50 ml Falcon tube. Protoplast (150 µl), of at least 1 x 10^7/ml were added to the constructs. Buffer L7 (50 µl) (Section 9.1.16.6) was added to the protoplast/construct mixture and was mixed by gentle shaking and placed on ice for 20 min. Buffer L7 (1 ml) (Section 9.1.16.6) was added to the mixture and left at room temperature for 5 min, to allow for recovery of protoplasts. Buffer L6 (5 ml) (Section 9.1.16.5) was added, and the mixture was left on ice until required for plating.

For the controls, protoplasts (15 µl) were added to Buffer L6 (185 µl) (Section 9.1.16.5). Buffer L7 (50 µl) (Section 9.1.16.6) was added and the mixture was mixed by gentle shaking and placed on ice for 20 min. Buffer L7 (1 ml) (Section 9.1.16.6) was added to the mixture and left at room temperature for 5 min, to allow for recovery of protoplasts. Buffer L6 (5 ml) (Section 9.1.16.5) was added, and the mixture was left on ice until required for plating.

2.2.7.5 Plating of transformation protoplasts

Regeneration agar (1.8% (w/v), 25 ml) (Section 9.1.1.8.1) containing pyrithiamine (25 µl) (Section 9.1.10) was poured into 90 mm petri dishes. The protoplasts containing the constructs mixture was brought to a final volume of 30 ml using 0.7 % (w/v) regeneration agar (Section 9.1.1.8.2), and 6 ml was poured into each of the five regeneration agar petri dishes.

For the positive controls, 1.25 ml control protoplasts were added to 0.7 % (w/v) regeneration agar (6 ml) (Section 9.1.1.8.2) and poured onto a plate containing 1.8 % (w/v) regeneration agar (25 ml) (Section 9.1.1.8.1) only and 125 µl control

protoplasts were added to 0.7 % (w/v) regeneration agar (6 ml) (Section 9.1.1.8.2) and poured onto a plate containing 1.8 % (w/v) regeneration agar (25 ml) (Section 9.1.1.8.1) only.

For the negative controls, 1.25 ml control protoplasts were added to 6 ml 0.7 % (w/v) regeneration agar (Section 9.1.1.8.2) and poured onto a plate containing 1.8 % (w/v) regeneration agar (25 ml) (Section 9.1.1.8.1) and pyrithiamine (25 µl) (Section 9.1.10).

All the plates were left upright at room temperature overnight.

2.2.7.6 Overlaying of transformation plates
0.7 % (w/v) regeneration agar (50 ml) (Section 9.1.1.8.2) containing pyrithiamine (50 µl) (Section 9.1.10) was mixed and 6 ml was poured over the 5 transformation plates, and the negative control plate. For the positive control plates, 6 ml of 0.7 % (w/v) regeneration agar (Section 9.1.1.8.2) without pyrithiamine was added to each of the plates. All the plates were incubated upside down in a 37 ^{o}C static incubator until colonies were observed through the top of the overlay layer.

2.2.7.7 Isolation of Transformant colonies
Sabouraud agar (25 ml) (Section 9.1.1.2) containing pyrithiamine (25 µl) (Section 9.1.10) was poured into 90 mm petri dishes. The individual colonies were numbered on the original plate before they were picked off with a yellow pipette tip and transferred to the new Sabouraud agar plate at a marked spot. Roughly nine individual colonies were inoculated onto each new plate. The plates were incubated at 37 ^{o}C in a static incubator until conidiation of colonies were observed.

2.2.7.8 Isolating colonies for DNA extraction

The individual putative transformant colonies were removed from the plates by using a blue pipette tip to plug out the colony along with the underneath agar, and transferring it to an Eppendorf tube containing PBST (750 µl) (Section 9.1.4). The tubes were then vortexed vigorously to release the conidia from the agar and into the solution. The conidial suspensions were stored at 4 ^{o}C until required.

2.2.7.9 Single spore isolation of transformant colonies

Putative transformants were diluted by serial dilutions ranging from 10^{-2} to 10^{-6} in filter sterilised PBST (Section 9.1.4). 100 µl of the dilutions were spread onto AMM plates (Section 9.1.1.7.1) containing pyrithiamine (100 ng/ml) (Section 9.1.10) and incubated at 37 ^{o}C in a static incubator until conidiation of colonies were observed. The individual colonies were numbered and isolated in PBST (Section 9.1.4) as described in Section 2.2.7.8 and stored at 4 ^{o}C as conidial suspensions.

2.2.7.10 Culturing transformant conidia for DNA extraction

Putative transformant conidial suspensions (500 µl) (Section 2.2.7.8) were inoculated into Sabouraud Dextrose Broth (50 ml) (Section 9.1.1.1) in a 200 ml conical flask. The cultures were incubated overnight at 37 ^{o}C, whilst shaking at 200 rpm.

2.2.7.11 Harvesting Mycelia for DNA extraction

The transformant cultures (Section 2.2.7.10) were filtered individually through miracloth to collect the mycelia. The mycelia mass was wrapped in tinfoil, and flash frozen in liquid Nitrogen. The mycelia were then crushed with a pestle, and DNA was extracted as described in Section 2.2.2.1.

2.2.8 Creation of DIG labelled probes

The probes used in the Southern Blot analysis were created by PCR with the incorporation of DIG labelled dNTP's (Roche). The oligonucleotides used are detailed in Table 2.5 and PCR was carried out as described in Section 2.2.2.3.

Table 2.5: Oligonucleotide primer sequences used to generate the probes for Southern blot analysis of transformants of *pes1* and *gliK*.

Probe name	Forward primer	Reverse primer	Size (bp)
5' *pes1*	CATGCAATCAAGGGATATGG	GACGATCGGTACCATCTGCCACTCAC	1236
pes1 KO region	CGAAACGTCCTCTTTCCTTG	TTGTGGGAAGATCTGGAAGG	1149
5' *gliK*	ACGCCTCTAACATGCCATAC	GCACTAGTGCTTTCCCCATGTTGCTTG	1096
gliK KO region	TGGGGGAATCTGGTACTTTG	ATTTAGACGCTGGCTGCTGT	1029
3' *gliK*	CGAAGCTTAGTCTCCATGTCTCCGATG	GTAGGTCGGCAGGTAGTACA	1121

2.2.9 Southern Blot Analysis

To confirm that the disruption or deletion of the gene occurred, Southern blot analysis was employed for screening the putative transformants that successfully grew on the plates containing the selection marker. The probes were created by DIG labelled PCR amplification of certain regions of the DNA allowing for the comparision of wild type and mutant strains, as described in Section 2.2.8.

For *pes*1 transformant analysis, the 5' region before and overlapping with the *ptrA* replacement cassette was probed with a 1236 bp probe homologous to the region. For distinction between successful replacement of the target region and wild

type strains, the DNA was digested with *Pvu*II which will result in different fragment sizes bound to the probe (**Error! Reference source not found.**). In this case, the wild-type strain will result in a 4234 bp fragment size, whereas a successful targeted replacement results in a fragment size of 1922 bp, due to *Pvu*II restriction site within the *ptrA* cassette. The complemented strain results in a 3812 bp fragment size as well as a 1922 bp fragment size. Also, bands observed at any other size can be deemed as untargeted integration of the replacement cassette. The *pes1* region was also probed with a 1149 bp probe homologous to the region (pes1 KO region probe, Table 2.7). The DNA was digested with *Pvu*II resulting in a 4334 bp fragment size for the wild-type, whereas the Δ*pes1* strains would not result in any band as the region bound by the probe is not present (Figure 2.9) and the complemented strain results in a 3812 bp fragment size.

For *gliK* transformant analysis, the 5' region was probed with a 1096 bp probe homologous to the region (Figure 2.10). The DNA was digested with *Pvu*I. The wild-type strain resulted in a 1926 bp fragment size, whereas Δ*gliK* resulted in a 2408 bp fragment size. The complemented strain resulted in a 2408 bp fragment as well as a 1625 bp fragment size. The *gliK* coding region was also probed with a 1029 bp probe homologous to the region (Figure 2.13). The DNA was digested with *Xba*I resulting in a 2124 bp fragment size for the wild-type, no fragment for the mutant, and a 2124 bp fragment size for the complemented strain.
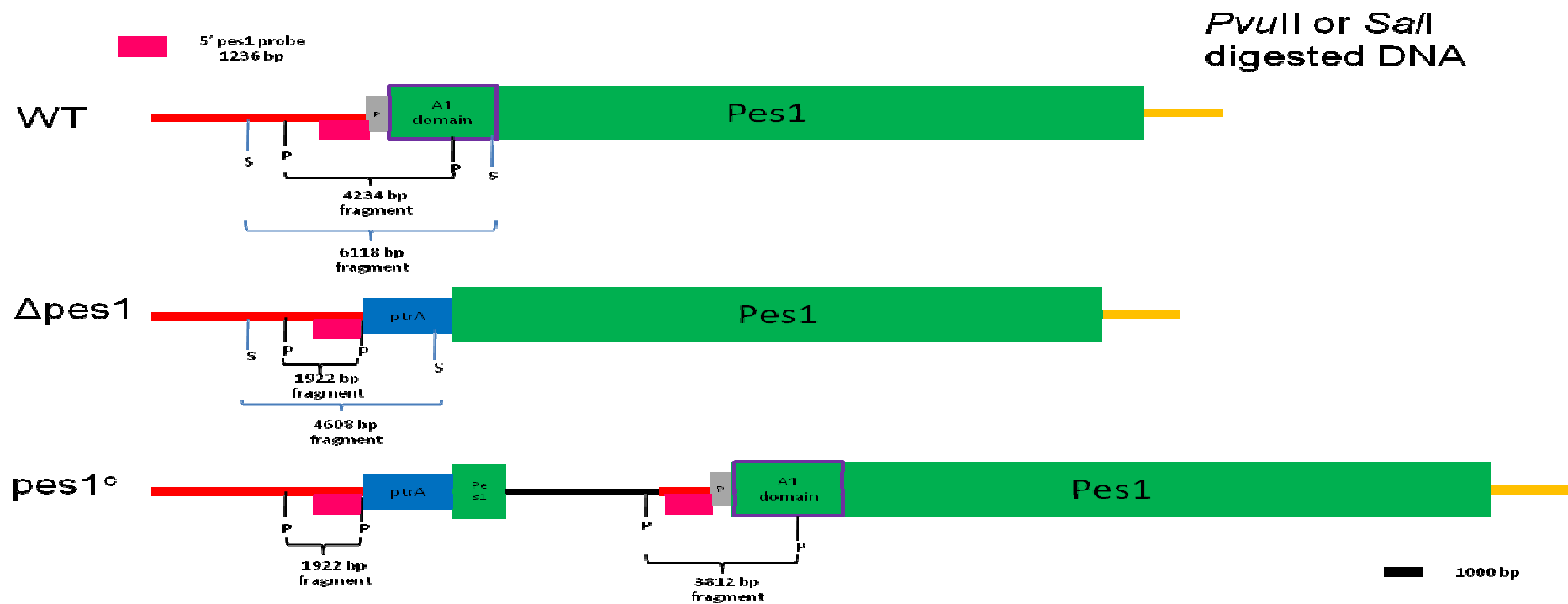
Figure 2.8: Schematic of strategy for probing with 5' *pes1* flanking region probe to use in southern blot analysis. Restriction Digestion with *Pvu*II results in fragments sizes of 4234 bp for wild-type, 1922 bp for Δ*pes1* and two fragments for *pes1ᶜ* (1922 bp and 3812 bp). Restriction Digestion with *Sal*I results in fragments sizes of 6118 bp for wild-type, 4608 bp for Δ*pes1*. *pes1ᶜ* was not screened using this resitiction enzyme. The red shape depicts the 5' flanking region of *pes1*. The Green shape depicts the *pes1* gene. The grey shape depicts the predicted promoter of *pes1*. The yellow shape depicts the 3' flanking region. The blue shape depicts the pyrithamine resistance cassette excised from the plasmid pSK275. The black shape depicts the Topo cloning vector. The pink shape depicts the 5' *pes1* flanking region probe. The symbol P shows where the *Pvu*II restriction sites are located and S shows where the *Sal*I restriction sites are located.

Figure 2.9: Schematic of strategy for probing with *pes1* coding probe to use in southern blot analysis. Digestion with *Pvu*II results in fragments sizes of 4234 bp for wild-type, no fragment for Δ*pes1* and 3812 bp for *pes1*^c^. The red shape depicts the 5' flanking region of *pes1*. The Green shape depicts the *pes1* gene. The grey shape depicts the predicted promoter of *pes1*. The yellow shape depicts the 3' flanking region. The blue shape depicts the pyrithamine resistance cassette excised from the plasmid pSK275. The black shape depicts the Topo cloning vector. The orange shape depicts the *pes1*KO region probe.
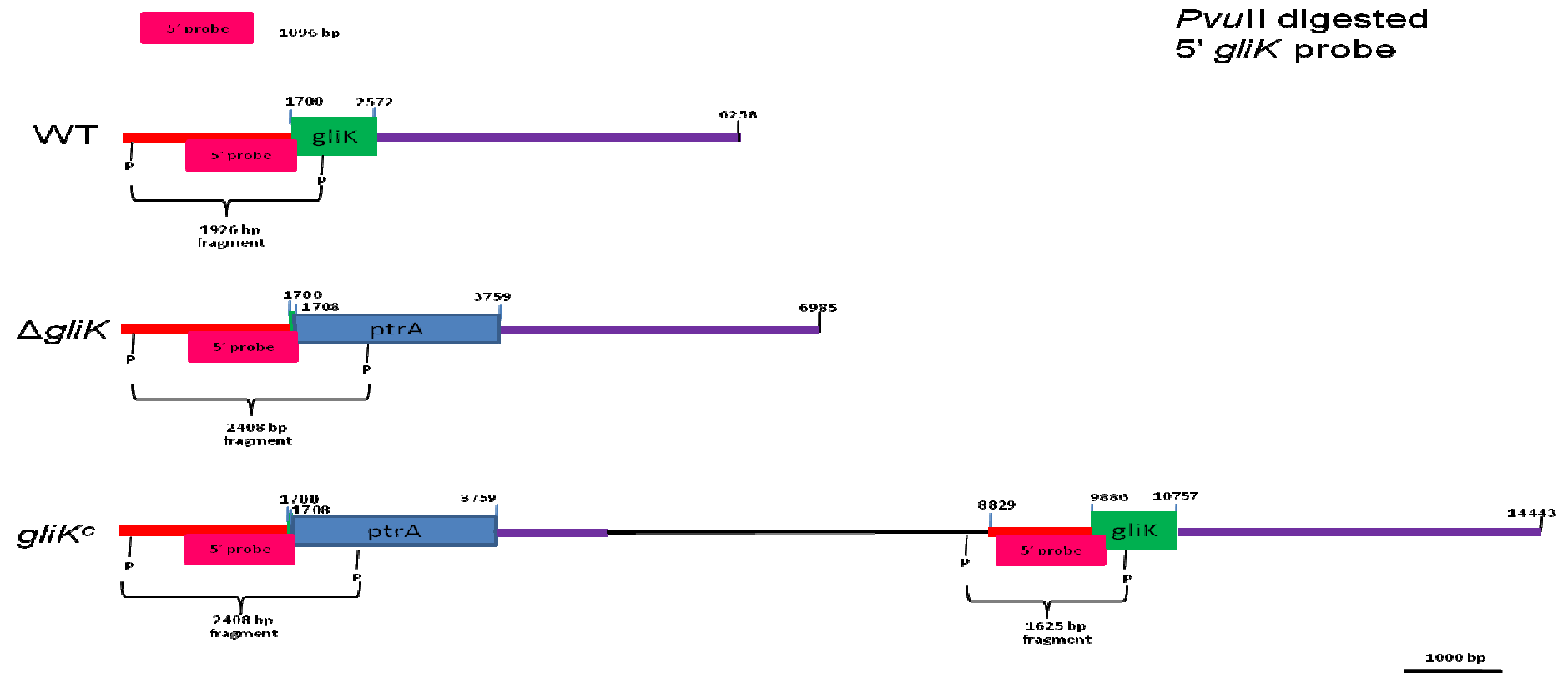
Figure 2.10: Schematic of strategy for probing with *5'gliK* probe to use in southern blot analysis. Digestion with *Pvu*I results in fragments sizes of 1926 bp for wild-type, 2408 bp for Δ*gliK* and two fragments for *gliK*ᶜ of 2408 bp and 1625 bp. The red shape depicts the 5' flanking region of *gliK*. The Green shape depicts the *gliK* gene. The purple shape depicts the 3' flanking region. The blue shape depicts the pyrithamine resistance cassette excised from the plasmid pSK275. The black shape depicts the Topo cloning vector. The pink shape depicts the gliK 5' flanking region probe.

101
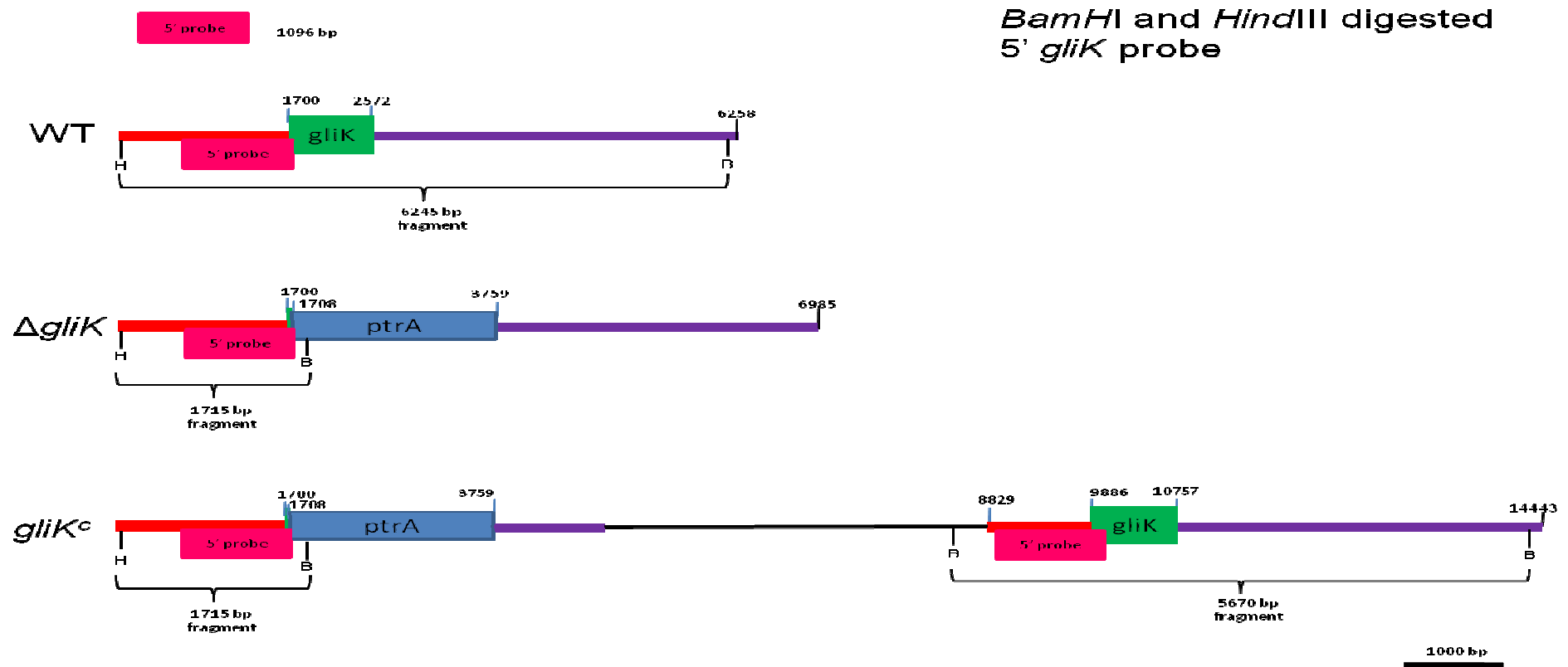
Figure 2.11: Schematic of strategy for probing with *5'gliK* probe to use in southern blot analysis. Digestion with *BamH*I and *Hind*III results in fragments sizes of 6245 bp for wild-type, 1715 bp for Δ*gliK* and two fragments for *gliK*^c of 1715 bp and 5670 bp. The red shape depicts the 5' flanking region of *gliK*. The Green shape depicts the *gliK* gene. The purple shape depicts the 3' flanking region. The blue shape depicts the pyrithamine resistance cassette excised from the plasmid pSK275. The black shape depicts the Topo cloning vector. The pink shape depicts the gliK 5' flanking region probe.
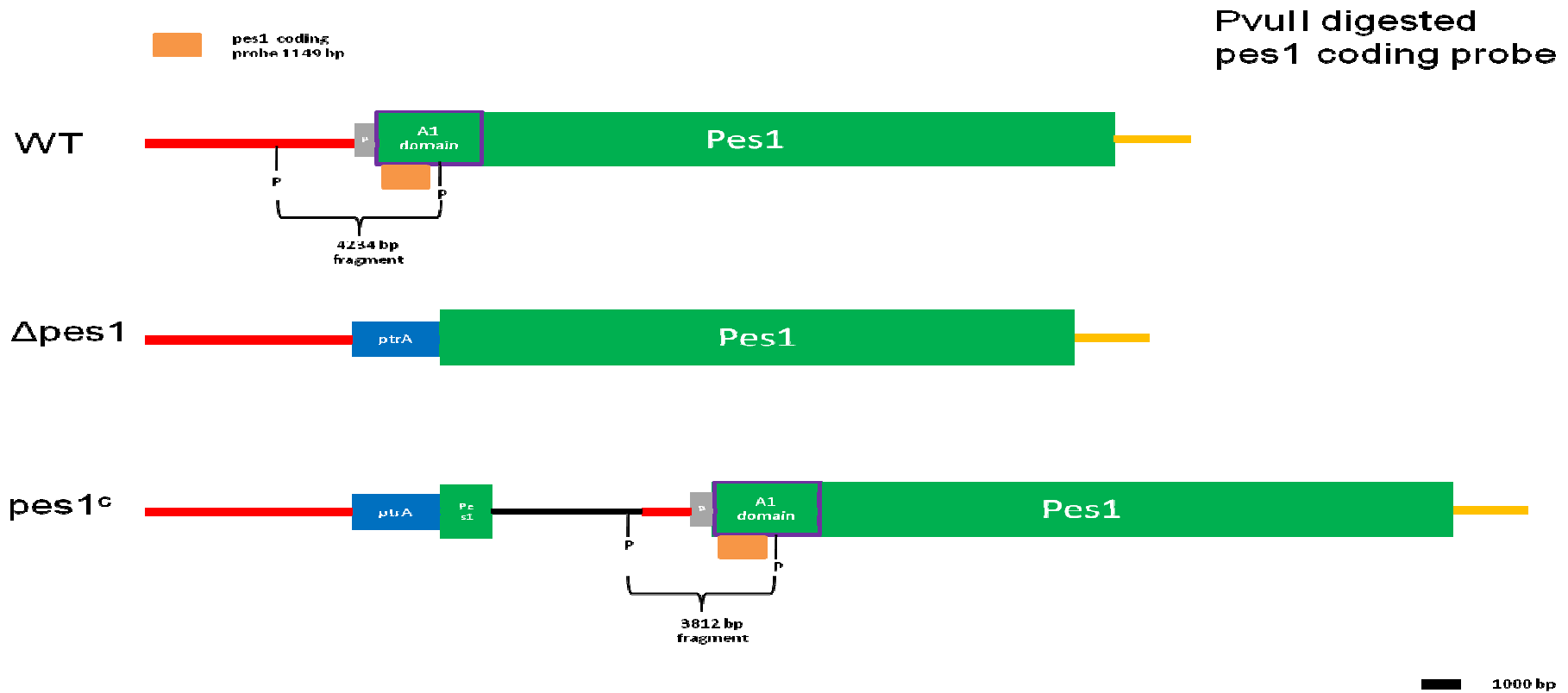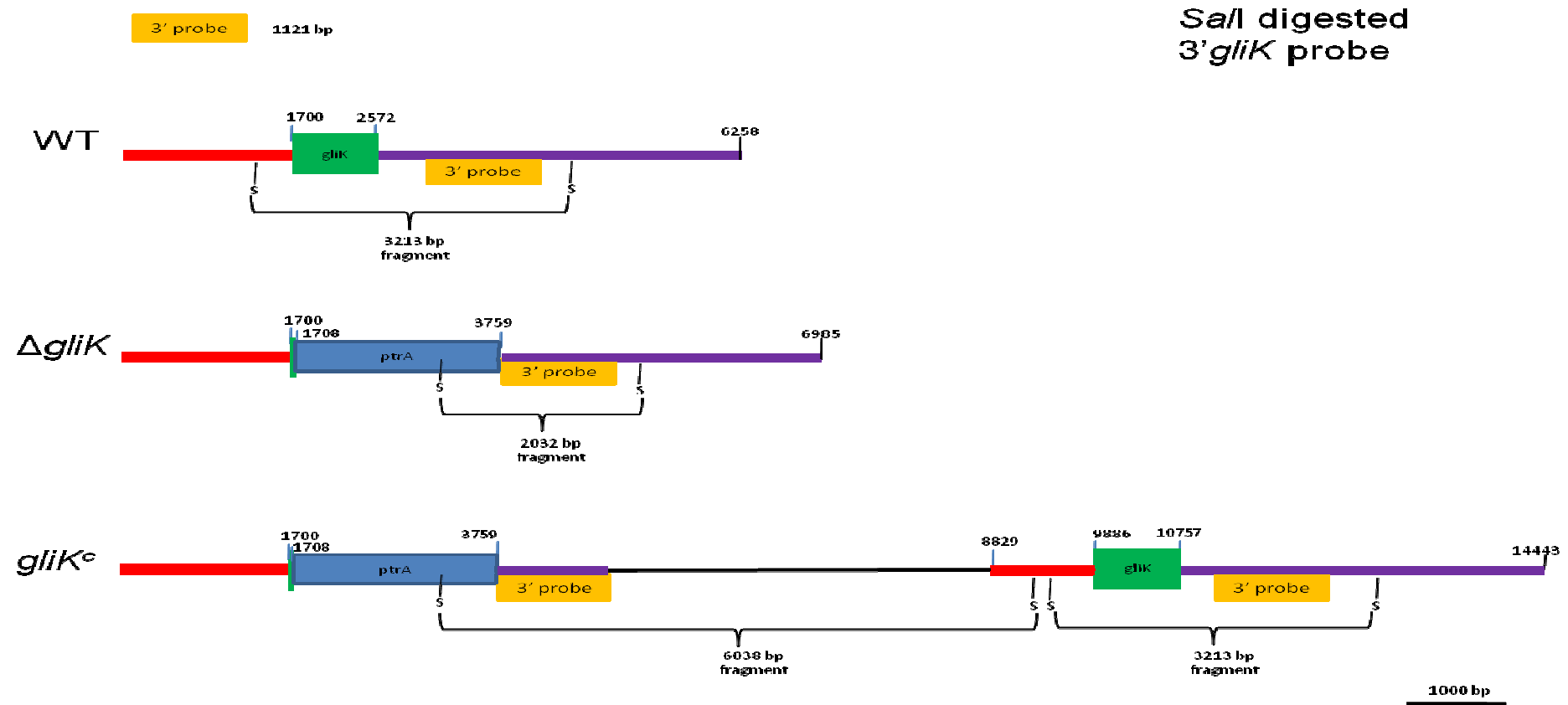
Figure 2.12: Schematic of strategy for probing with 3'*gliK* probe to use in southern blot analysis. Digestion with *Sal*I results in fragments sizes of 3213 bp for wild-type, 2032 bp for Δ*gliK* and two fragments for *gliK*[c] of 6038 bp and 3213 bp. The red shape depicts the 5' flanking region of *gliK*. The Green shape depicts the *gliK* gene. The purple shape depicts the 3' flanking region. The blue shape depicts the pyrithamine resistance cassette excised from the plasmid pSK275. The black shape depicts the Topo cloning vector. The pink shape depicts the gliK 3' flanking region probe.
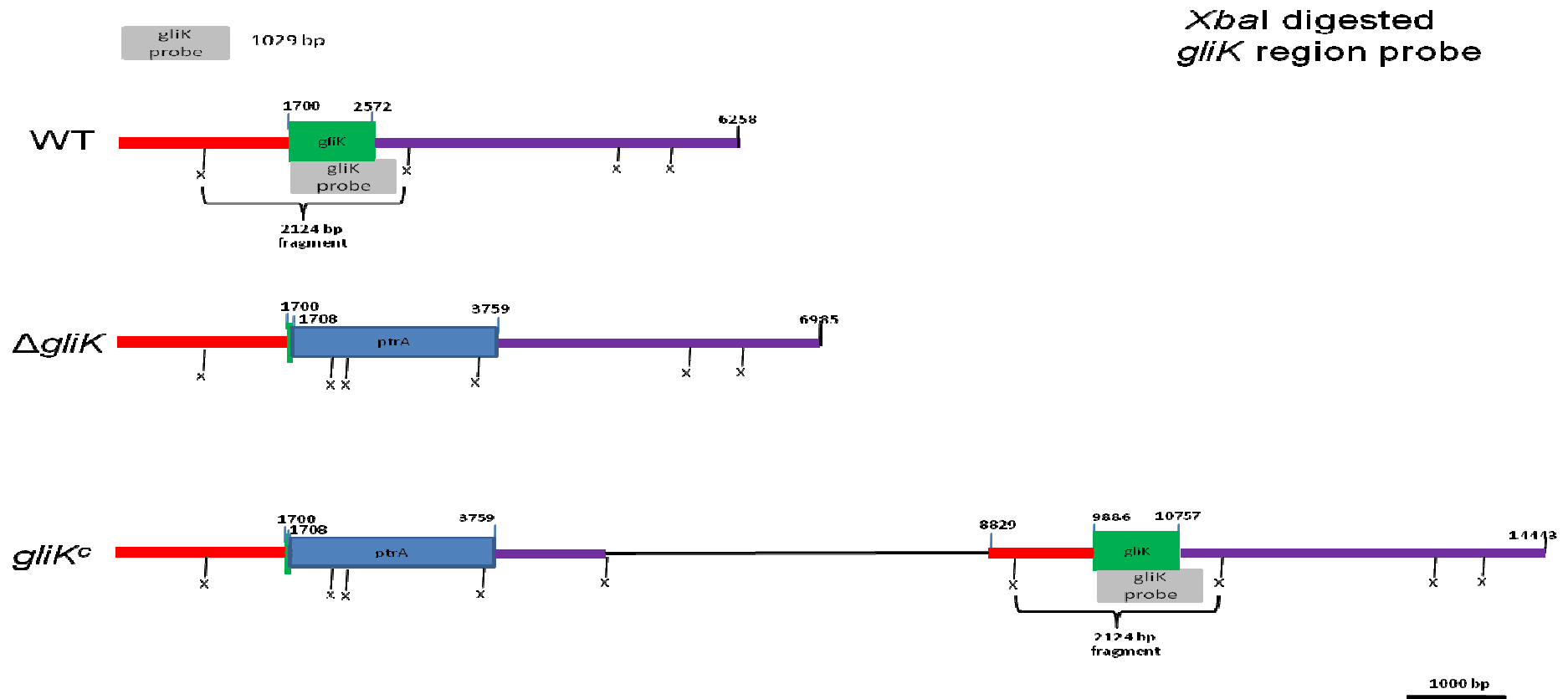
Figure 2.13: Schematic of strategy for probing with *gliK* coding region probe to use in southern blot analysis. Restriction digestion with *Xba*I results in fragments sizes of 2124 bp for wild-type, no fragment for Δ*gliK*, and 2124 bp for *gliK*^c. The red shape depicts the 5' flanking region of *gliK*. The Green shape depicts the *gliK* gene. The purple shape depicts the 3' flanking region. The blue shape depicts the pyrithamine resistance cassette excised from the plasmid pSK275. The black shape depicts the Topo cloning vector. The grey shape depicts the gliK KO region probe.

2.2.9.1 Sample Preparation

The culture was filtered through miracloth to collect the mycelia. The mycelia mass was wrapped in tinfoil, and flash frozen in liquid Nitrogen. The Mycelia were then crushed with a pestle, and DNA was extracted as described in Section 2.2.2.1, followed by DNA precipitation (Section 2.2.2.2). The concentration of the DNA was determined by measurement on the Nanodrop (Agilent, CA, USA). 600 ng DNA was digested by restriction enzyme (Section 2.2.5) for each of the samples.

2.2.9.2 Southern Blot hybridization

The digested DNA samples were separated on a 0.7 % (w/v) agarose gels (Section 2.2.2.5). Once the gels had run to completion, they were then placed in a UV crosslinker (Strategene, La Jolla, CA) and crosslinked at 80000 μjoules for 20 – 40 s. Photos of the gels was taken with the aid of a UV transilluminator. The Southern tower was assembled by filling the reservoir tanks on either side of the transfer tray with 500 ml Transfer Buffer (Section 9.1.17.1). Three sheets of Whatman paper were cut to fit across the transfer tray and into the reservoir on each side and with the exact width of the gels. The gels were then placed on the transfer tray over the Whatman paper upside down, and with the wells of the gels closest to the reservoirs. The Amersham N+ Hybond membrane (GE Healthcare, Buckingham shire, U.K) was then cut to the exact size of the individual gels and placed directly on top of the gel, ensuring that no air bubbles are trapped between the gel and the membrane. Three pieces of Whatman filter paper was then cut to the size of the individual gels and membranes and placed on top. After which, three packets of pocket tissues were placed on top of the paper. A glass plate covered all the stacks placed on the tray and a 500 g weight, usually in the form of a partially filled duran bottle, was placed on top of the stacks. Towers were left for the digested DNA to

transfer from the gel to the membrane overnight at room temperature. Generally only a maximum of 2 gels were placed in the same tower to ensure complete transfer of DNA from the gels to the membranes.

2.2.9.3 Cleaning and Blocking of the membrane

The Southern Blot stack (Section 2.2.9.2) was taken apart and the membrane and gel were removed together and placed on a clean glass plate. The position of the wells was marked onto the corresponding place on the membrane, and the gel was peeled away from the membrane. The membrane was then soaked in SSC Buffer (2X, 40 ml) (Section 9.1.17.3), and rocked gently for 10 min. The membrane was removed and placed on a clean glass plate. The membrane was then placed in a uv crosslinker (Strategene, La Jolla, CA) and crosslinked at 120000 µjoules for 20 – 50 sec. The membrane was placed in a hybaid tube with the DNA side facing inwards and pre-heated High SDS/Blocking Buffer (15 ml) (Section 9.1.17.8) was added. The membrane was rotated in a hybaid oven at 42 ^{o}C for approximately 5 hr.

2.2.9.4 Dig Probe preparation and application

Dig labelled probes were prepared by PCR using Dig labelled dNTPs. The concentration of the probe was calculated and 400 ng of the probe was heated for 8 min at 95 ^{o}C to separate the DNA duplex. Probe was added to pre-heated High SDS/Blocking Buffer (10 ml) (Section 9.1.17.8). The Buffer was discarded from the Hybaid tube containing the membrane and the probe was added. The membrane was rotated in the Hybaid oven at 42 ^{o}C overnight.

2.2.9.5 Dig detection

The membrane was removed from the Hybaid tube and placed into a container with 1X SSC/ 0.1% SDS (w/v) Solution (40 ml) (Section 9.1.17.9) and mixed by rocking for 10 min. The Buffer was discarded and replaced again and the wash was repeated for another 10 min. The blot was placed in a clean Hybaid tube with 1X SSC /0.1% (w/v) SDS Solution (30 ml) (Section 9.1.17.9) and the membrane was rotated in the hybaid oven for 15 min at 65 ^{o}C. The solution was discarded and replaced and the membrane was rotated for 15 min at 65 ^{o}C. The solution was poured off from the tube and Dig Wash Buffer (10 ml) (Section 9.1.17.10) was poured in with the membrane. The membrane was rotated for 5 min in the hybaid oven at 25 ^{o}C. The buffer was poured off from the tube and Dig Buffer 2 (10 ml) (Section 9.1.17.11) was added and the membrane was rotated in the Hybaid oven for 30 min at 25 ^{o}C. The Buffer was poured off from the tube and the Anti-Digoxigenin-Fab AP conjugate (10 ml) (Section 9.1.17.13) was added. The membrane was rotated for 30 min at 25 ^{o}C. The solution was poured off from the tube and Dig wash buffer (10 ml) (Section 9.1.17.10) was added to the tube. The membrane was rotated for 15 min at 25 ^{o}C. The wash step was repeated. The buffer was poured off from the tube and Dig Buffer 3 (10 ml) (Section 9.1.17.12) was added and the membrane was rotated at 25 ^{o}C for 5 min. The buffer was poured off from the tube and CSPD Substrate (10 ml) (Section 9.1.17.14) was added. The membrane was rotated at 25 ^{o}C for 5 min. The CSPD Substrate was collected from the tube to be reused. The membrane was removed from the hybaid tube and placed on a clean tissue briefly. The membrane was then wrapped in a single layer of cling film and incubated at 37 ^{o} C for 15 min.

2.2.9.6 Development of Southern Blot membrane

The membrane was placed in a photo developer case and an X-ray film was placed over the membrane. The blot was left to transfer to the film for 2 hr. The X-ray film was removed from the case and placed into Developer Solution (Section 9.1.18.1) for a couple of seconds or until markings were observed. The film was rinsed with water and then placed into Fixer Solution (Section 9.1.18.2). The film was then thoroughly rinsed with water and left to dry.

2.2.10 Organic Extraction from supernatants of *A. fumigatus* cultures

A. fumigatus culture supernatants (20 ml) were added to chloroform (20 ml) in 50 ml Falcon tubes which were sealed with parafilm. The mixtures were then placed on a rotating wheel overnight. The mixtures were removed and centrifuged for 10 min at 650 x g. The top layer from the mixtures were removed and discarded and the organic layers containing the supernatant organic extract were stored at -20 ^{o}C until required.

2.2.11 Rotary evaporation of Organic Extraction Samples

The supernatant organic extraction samples (~20 ml) (Section 2.2.10) were placed in an evaporation bulb and the bulb was connected to the rotary evaporation equipment whilst sitting in a water bath set to 37 ^{o}C. The chloroform evaporated leaving the dried organic extract in the bulb. The extracts were resuspended in HPLC grade Methanol (200 μl), and transferred to clean micro-centrifuge tubes and stored at -20 ^{o}C.

2.2.12 Organic extraction from plugs of *A. fumigatus* on agar plates

Organic extraction from agar plugs was carried out as described by Smedsgaard (1997) where *A. fumigatus* conidia were point inoculated onto the centre of an AMM agar plate and allowed to dry before incubating at 37 ^{o}C for 5 days. Plug extracts were removed from the agar along the radius of the plate using a cork drill, which usually yielded about six agar plugs per plate radius. The individual plugs from a plate were combined in the organic extraction buffer (Section 9.1.19) and sonicated in a sonication water bath for 60 min. The extract contained in the organic extraction buffer was removed to a clean micro-centrifuge tube and evaporated to dryness in a fume hood. The extract was resuspended in HPLC grade Methanol (400 µl), and stored at -20 ^{o}C.

2.2.13 Reverse Phase - High Performance Liquid Chromatography (HPLC) analysis

2.2.13.1 In house RP-HPLC analysis

Organic extracts from supernatant (Section 2.2.10) were analysed by reverse phase HPLC with UV detection (Agilent 1200 system), using a C_{18} RP-HPLC column at a flow rate of 1 ml/min. The general gradient used was as follows, unless otherwise stated: Acetonitrile content beginning at 5 % Acetonitrile up to 99 % Acetonitrile content over 30 min. Samples (ranging from 20 to 100 µl) were injected onto the column and the separation of the compounds was observed at 220 nm, 260 nm and 280 nm, unless otherwise stated.

2.2.13.2 External RP-HPLC analysis

HPLC separation of agar plug extractions (Section 2.2.12) was carried out by Prof. Thomas Larsen (Denmark technical university, Denmark) using a didode array

and high resolution mass spectrometry. The organic extracts were analysed using an RP-HPLC Agilent 1100 system with a Luna C_{18} II column equipped with a photo diode array detector and coupled to a LCT orthogonal time-of-flight MS with Z-spray ESI source and a LockSpray probe.

2.2.14 Gliotoxin uptake assay

The strains were cultured in MM media (20 ml) (Section 2.1.1.6.3) at 37 ^{o}C, for 24 hr. At the 24 hr time point gliotoxin (5 µg/ml) was added to the cultures and 2 ml aliquot of the supernatant was removed. The cultures were returned to the incubator and after 15 min, 2 ml supernatant was removed from the cultures. This was repeated at the 30 and 45 min timepoints. The extracted supernatants were organically extracted with 1:1 ratio of chloroform, and the extract was allowed to dry overnight in a fume hood. The dried extract was resuspended in 55 µl Methanol. The extracts were then analysed by RP-HPLC (Section 2.2.13.1) to measure the amount of gliotoxin still remaining in the supernatant. The mycelia from the cultures were lyophilized and weighted.

2.2.15 *E.coli* Expression using the pPRoEx™HTb expression vector

The PCR product of the *gliK* gene was integrated into the pPRoEx™-HTb expression vector (Figure 2.14) by linerising the vector within the multiple cloning site and ligation of the free ends of the linerised vector and the PCR product together. The orientation of the ligation was restricted to only the correct one by ensuring that that linerising digestion was conducted with two incompatible enzymes. The PCR that created the *gliK* product had add-on nucleotides that ensured that the ligation did not shift any of the subsequential amino acid expression.
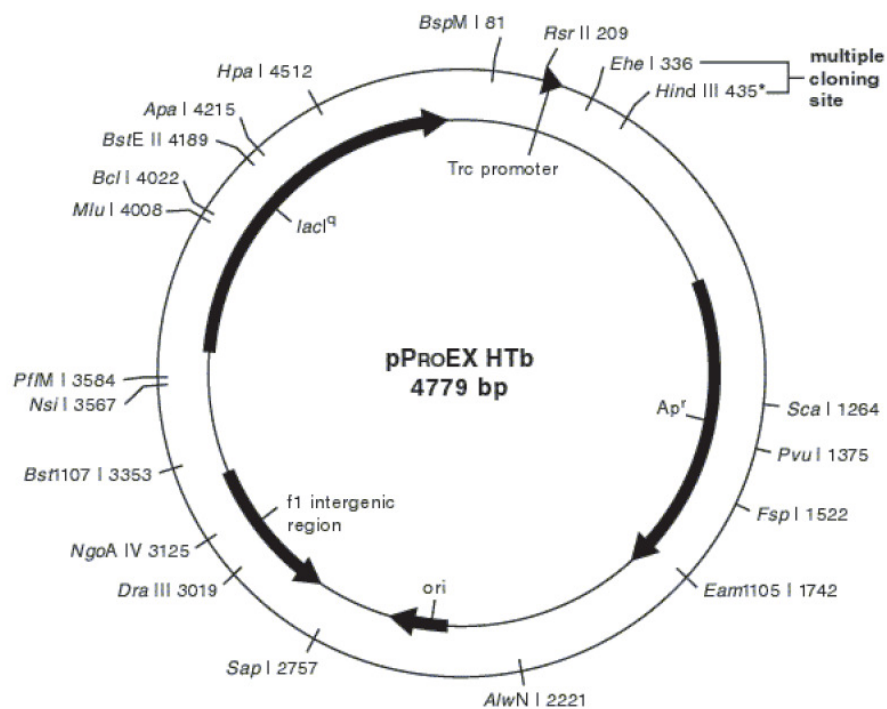
Figure 2.14: Vector map of the pPRoEx-HTb expression vector (Invitrogen).

2.2.16 Small scale induction of the recombinant pProEx:GliK Clones

Once it was verified that the pProEx:GliK vector had transformed correctly into *E. coli*, small-scale inductions were carried out to confirm GliK production. A 10 ml LB broth (Section 9.1.7) culture was set up containing 100 µg/ml ampicillin (Section 9.1.10) which was then inoculated with the pProEx:GliK plasmid and incubated overnight at 37 °C whilst shaking at 200 rpm. This culture was then used to inoculate a 50 ml LB broth culture (Section 9.1.7) containing 100 µg/ml ampicillin (Section 9.1.10). The culture was incubated at 37 °C whilst shaking at 200 rpm until an OD_{600} value of 0.5 – 0.7 was reached. Once the culture had reached the target growth level, a 1 ml aliquot was removed and kept as an un-induced aliquot used for reference. The expression was induced by adding IPTG (Section 9.1.22.1), to a final

concentration of 1 mM and the culture was incubated further, and at the time points, 1, 2 and 3 hr, 1 ml aliquots were removed, and kept as post induced time-point samples. The remaining culture was centrifuged at 3200 g at 4 ^{o}C, for 20 min and the sample aliquots were centrifuged at 17900 x g for 1 min. The supernatants were discarded and the pellets were kept at -20 ^{o}C until required.

2.2.17 Protein extraction from recombinant pProEx:GliK cultures

Lysis Buffer (9 ml) (Section 9.1.22.2) was added to every 1 g of pelleted cells. The samples were sonicated whilst sitting on ice. Lysozyme (80 µl) (Section 9.1.22.3) was added per 1 g of pellet, and the sample was incubated at 20 ^{o}C for 1 hr 45 min constantly shaking. Sodium Deoxycholate (80 µl, 120 mM) (Section 9.1.22.4) was added to the samples and incubated at 20 ^{o}C for 15 min whilst shaking. The samples were sonicated on ice. The samples were centrifuged at 12000 x g for 10 min at 4 ^{o}C. An aliquot (1 ml) was removed from the supernatant, and the rest of the supernatant was discarded. The pellets were resuspended in wash buffer (9 ml) (Section 9.1.22.5) per original 1 g. The samples were centrifuged at 12000 x g for 10 min at 4 ^{o}C. An aliquot (1 ml) of the supernatants were taken and the rest of the supernatant was discarded. The samples were resuspended in 2 M urea Buffer (2.5 ml) (Section 9.1.22.6) per original 1 g. The samples were centrifuged at 12000 x g for 10 min at 4 ^{o}C. An aliquot (1 ml) of the supernatants were taken and the rest of the supernatant was discarded. The samples were resuspended in 8 M Urea Buffer (400 µl) (Section 9.1.22.7) per original 1 g. The samples and aliquots were stored at -20 ^{o}C until required.

2.2.18 Sodium Dodecyl Suphate Polyacrylamide Gel Electrophoresis (SDS-PAGE)

SDS PAGE gels were prepared according to Table 2.6. The gels were cast using the Mini-Protean II gel casting apparatus (Biorad, CA, USA) according to the manufacturer's instructions. Lysis buffer (100 μl) (Section 9.1.23.6) was added to each of the protein extract samples (Section 2.2.17) and vortexed thoroughly. Aliquots (20 μl) of the samples were removed and Solubilisation Buffer (5X, 5 μl) (Section 9.1.23.7) was added to the aliquots. Samples were boiled for 10 min and then centrifuged briefly to collect the samples. The samples were loaded onto the gel using a Hamilton syringe. Electrophoresis begun at a setting of 80 V for about 30 min, followed by an increase to 120 V for approximately 1 hr, using 1 X running Buffer (Section 9.1.23.8.1).

Table 2.6: Components of the SDS-PAGE 12% Gels

	Stacking Gel	Resolving Gel
Reagent	12%	12%
Water	9.3 ml	6.1 ml
1.5M Tris HCl	7 ml	
0.5M Tris HCl		2.5ml
30% (w/v) acylamide	11.3 ml	1.3 ml
10% SDS	280 μl	100 μl
TEMED	23 μl	20 μl
10% APS	100 μl	200 μl

2.2.19 Coomasie Blue Staining

The gels were removed and transferred to Coomassie Blue Stain Solution (20 ml) (Section 9.1.23.9) where it was left mixing overnight. After which, the staining solution was discarded and Destain solution (20 ml) (Section 9.1.23.10) was added to the gel, and was left mixing until all the staining had been removed, which was usually 1 hr. The Destain solution was removed and the gel was left in water until required.

2.2.20 Western Blot Analysis

Nitrocellulose paper (NCP) and 6 sheets of Whatmann filter paper were cut to the size of the gel and soaked in Towbin Transfer Buffer (Section 9.1.24.1) for 15 min. The SDS-PAGE gels were removed gently from the electrophoresis unit and assembled on the transfer unit in a NCP "sandwich" containing 3 sheets of saturated filter paper, soaked NCP, SDS-PAGE gel, and another set of 3 sheets of filter paper.

Transfer occurred at 18 V for 30 min, and then the NCP was removed and placed in a container with Blocking Buffer (Section 9.1.24.2), and left gently agitating overnight. The blocking buffer was poured off and the primary antibody (anti-His$_6$ monoclonal IgG) diluted in Blocking Buffer was added to the blot and was left gently rocking for 1 hr at room temperature. The blot was then washed with 2 X 10 min washes of PBST (Section 9.1.4). The secondary HRP-conjugated antibody was diluted in Blocking buffer and added to the blot and left gently rocking for 1 hr at room temperature. The antibody was poured off and the blot was washed twice with PBST for 10 min. DAB blot developer (Section 9.1.24.5) or AEC Substrate Solution (Section 9.1.24.4.5) was added to the blot and left to rock for 10 min. The blot was removed and rinsed with distilled water and allowed to dry on filter paper.

2.2.21 Optimisation of Coating Concentration for recombinant GliK Antigen.

Microtitre plates were coated with a range of concentrations of GliK, beginning at 8 μg/ml, and double diluted down to 0.5 μg/ml. The antigen was diluted in Carbonate buffer (Section 9.1.25.1), and 100 μl was added to each well. Plates were sealed and incubated at 37 $^{\circ}$C for 2 hr. Plates were washed PBST (Section 9.1.4) and Blocking buffer (100 μl) (Section 9.1.25.2) was added to each well and incubated at 37 $^{\circ}$C for 2 hr. The blocking buffer was removed from the wells. Anti-His monoclonal antibody was diluted in Antibody Buffer (Section 9.1.25.3) at various dilutions (1/1000, 1/2500, 1/5000). The plate was incubated with 100 μl of the anti-His dilutions in the appropriate wells at 37 $^{\circ}$C for 1 hr. Plates were washed three times and TMB Substrate (Section 9.1.25.5) (100 μl) was added to each well, and incubated at room temperature for 10 min. The reaction was terminated by adding Sulphuric acid (1 N) (Section 9.1.25.6). The absorbance was measured at

wavelengths of 450 and 630 nm. The optimum coating concentration was determined for recombinant GliK antigen.

2.2.22 ELISA for Sera screening for GliK reactivity

Microtitre plates were coated with recombinant GliK (2 μg/ml) at 37 $^{\circ}$C for 2 hr. The plates were washed twice with PBST (Section 9.1.4). Blocking buffer (100 μl) (Section 9.1.25.2) were added to each well and incubated at 37 $^{\circ}$C for 2 hr, or at 4 $^{\circ}$C overnight. The blocking buffer was removed from the wells and diluted serum (100 μl, 1/100 dilution) was added to the appropriate wells. PBST (100 μl) (Section 9.1.4) was added as control to the appropriate wells. The plate was incubated at 37 $^{\circ}$C for 1 hr. The plates were washed out with PBST (Section 9.1.4) four times and the residual PBST was tapped out of the wells. The HRP-conjugated anti-human IgG (100 μl) (Section 9.1.25.4) was added to each of the wells and the plates were incubated at 37 $^{\circ}$C for 1 hr. The plates were washed with PBST (Section 9.1.4) four times and the residual PBST was tapped out. Tetramethylbenzidine (TMB) (100 μl) (Section 9.1.25.5) was added to each well and the plates were incubated for 10 min at room temperature covered in tinfoil. The reaction was stopped by adding Stop solution (100 μl, 1 N H_2SO_4) (Section 9.1.25.6) to each well. The absorbance readings were calculated using a plate reader set at 450 nm and then at 630 nm, for background subtraction. The delta OD was calculated by subtracting the readings at 630 nm from 450 nm.

2.2.23 *Galleria mellonella* Infections

The larvae of the Greater wax moth (*Galleria mellonella*) can be used as an *in vivo* method for testing the pathogenicity of microbial pathogens (Kavanagh and

Reeves, 2004). The larvae contain haemolymph which contains cells and anti-microbial peptides which respond to the invading pathogen (Morton *et al.,* 1987). In particular, haemolymph contains haemocytes, which function in a similar manner to phagocytes of mammals (Kavanagh and Reeves, 2004). Melanisation is key part of the insects defence against a wide range of pathogens. Melanin is formed in the haemocytes and is released by rupture and is activily transported to the cuticle or depositied on the invading microbe within the haemolymph (Soderhall and Cerenius, 1998). Therefore, this build up of melanin is an indication of the presence of a pathogen and can be used as a method of measuring the difference in infection by a pathogen such as *A. fumigatus* (Reeves *et al.,* 2004a) and furthermore differenciating between the wild-type and mutant strains.

The conidia were prepared by harvesting 5 day old *A. fumigatus* Sabouraud culture plates (Section 9.1.1.2) in PBST-80 (5 ml) (Section 9.1.5). The conidial suspension was centrifuged at 650 x g for 5 minutes to pellet the conidia. The supernatant was discarded and the pellet was resuspended in PBS (10 ml) (Section 9.1.3). The conidia were washed twice more with PBS and the conidia were finally resuspended in PBS (5 ml) (Section 9.1.3). The conidia were counted on a haemocytometer and the concentration was adjusted to the required amount for the inoculation. *G. mellonella* larvae were divided into groups of ten and placed in 90 mm petri dishes that contained a single sheet of filter paper. All were weighed and size matched. The larvae were inoculated through the last proleg on the left with a conidial solution (20 μl). The larvae were incubated at 30 ^{o}C and the surviving larvae were counted at predetermined time points, usually 24, 48 and 72 hr.

2.2.24 Statistical Analysis

All data was analysed using built-in GraphPad prism version 5.01 functions, as specified. The level of significance was set at $p < 0.05$ (*), $P < 0.001$ (**), and $p < 0.0001$ (***), unless otherwise stated. Post hoc comparisons between groups were performed using the Bonferroni multiple comparisons test, unless otherwise stated.

2.2.25 Software Graphing

All graphs were compiled using Graphpad Prism version 5.01, unless otherwise stated.

CHAPTER 3

Disruption of the Non Ribosomal Peptide Synthetase gene, *pes1*, in *Aspergillus fumigatus*

3. Disruption of the Non Ribosomal Peptide Synthetase gene, *pes1,* in *Aspergillus fumigatus*

3.1 Introduction

Pes1, a non-linear non-ribosomal peptide synthetase deviates from the standard $(CAT)_n$ architecture of bacterial NRPS. Previously, the *pes1* gene has been shown to be involved in the response to oxidative stress, and to have involvement in resistance to neutrophil killing (Reeves *et al.,* 2006). It is also one of 943 genes which is regulated by the global transcription factor LaeA (Perrin *et al.,* 2007), of which, 102 are deemed to be involved in secondary metabolism. Furthermore, *pes1* was found to be also regulated by StuA, a developmental regulator in *A. fumigatus* (Sheppard *et al.,* 2005) that controls the regulation of at least 94 genes.

As of yet, the product of the *pes1* gene is unknown. However, molecular techniques such as gene disruption or deletion have led to the conclusive identification of many genes in the *A. fumigatus* genome and their respective functions, such as the siderophore biosynthesis genes, *sidA*, *sidC*, *sidD*, *sidF* and *sidG* (Schrettl *et al.,* 2007) and the gliotoxin biosynthesis genes, *gliP* and *gliZ* (Bok *et al.,* 2006a; Cramer *et al.,* 2006a). Therefore, the gene disruption technique was selected to assist in identifying the *pes1* gene product.

As described in Chapter 1, there are many strategies now available for use in fungal gene deletion such as homologous recombination with a single construct and homologous recombination with two overlapping constructs utilising a split marker (Nielsen *et al.,* 2006). Site-directed modifications can be achieved by homologous recombination (HR) where the selection marker replaces the site of interest by integration with the aid of homologous recombination sequences (HRS) that flank the selection marker. The constructs which contain the HRSs are required to have at least 1 kb flanking both sides of the target site, hindering efficient construct

generation (Frandsen *et al.,* 2008). Therefore, the utilisation of the bipartite method has greatly increased the efficient generation of the constructs and increased the potential of targeted integration, while eliminating the survival of cells containing only partial integration.

As the success rate of the bipartite method is higher than other methods (Nielsen *et al.,* 2006), this strategy was employed for the disruption of *pes1*. The *pes1* gene is large, 18.8 kb, therefore the strategy chosen was to disrupt the gene, rather than a full deletion in order to prevent the expression of the gene. The predicted combined promoter and first adenylation domain were the target for deletion (3 kb). The generation of the constructs in the bipartite method involves a series of PCR, digestion and ligation steps using target DNA and a selection marker obtained from a vector (Figure 3.1).
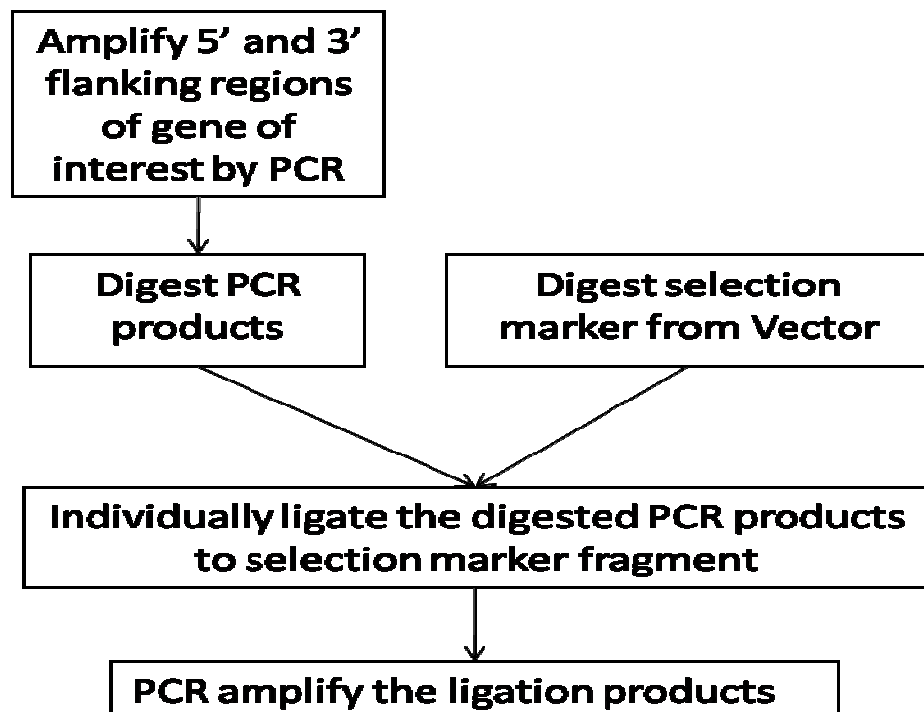

Figure 3.1: Flow diagram depicting the generation of constructs for the bipartite transformation method.

The selection marker chosen for this project was the pyrithiamine resistance gene (*ptrA*)(Kubodera *et al.,* 2000) which can be readily extracted by digestion from the pSK275 plasmid (Figure 3.2). Pyrithiamine inhibits the production of thiamine pyrophosphokinase (TPK), which is an essential co-factor in the synthesis of thiamine pyrophosphate (TPP) from thiamine. TPP is essential for enzymes involved in carbohydrate metabolism (Baker *et al.,* 2001). The product of the pyrithiamine resistance gene is able to hinder the pyrithiamine inhibition of the TPP production pathway and therefore facilitate normal growth of the fungus. The pyrithiamine resistance gene was originally isolated from *A. oryzae* and was cloned into pSK275. It is not usually expressed in other fungal species, making it a useful selection marker in many fungal transformations. The *ptrA* cassette removed from the plasmid contains the T7/lac promoter and the pyrithiamine resistance gene. Consequently, for this project where the gene disruption strategy is reliant on the selection marker, the *ptrA* gene should be highly beneficial because of its strict selection and relative ease of use. Selection of *A. fumigatus* transformants could be chosen based on resistance to pyrithiamine (100 ng/ml) (Kubodera *et al.,* 2002).
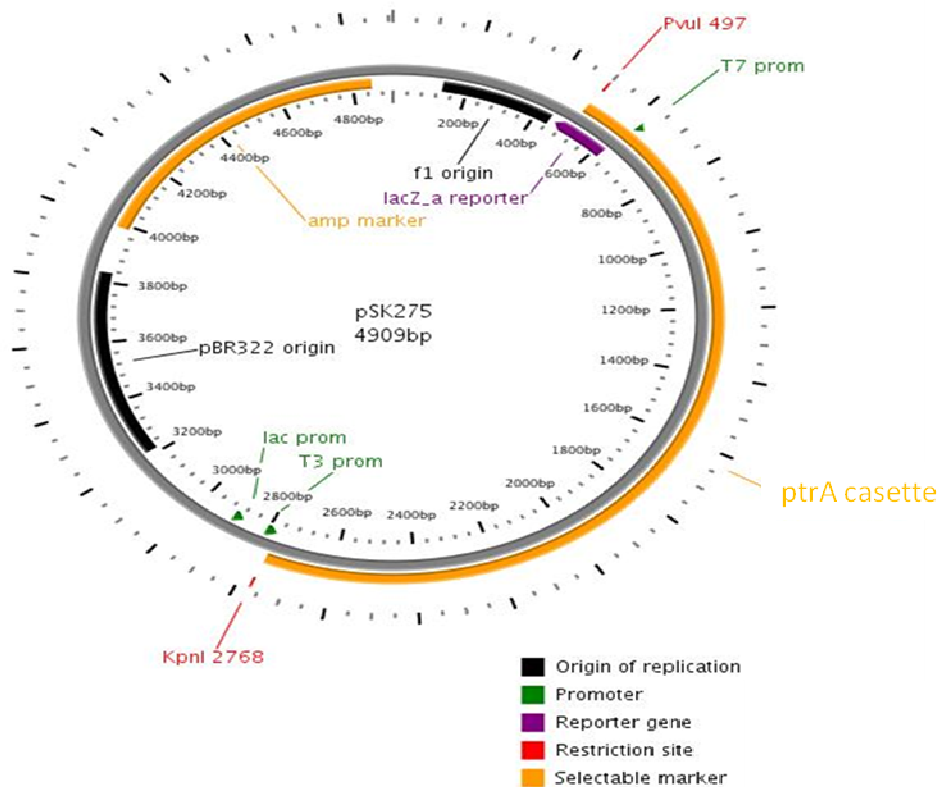
Figure 3.2: Vector map of the pyrithamine resistance pSK275 plasmid. The ptrA cassette is located from 497 bp – 2768 bp.

Three different *A. fumigatus* strains were chosen in which to disrupt *pes1* gene expression, namely ΔakuB, ΔsidD, and ATCC46645. The *A. fumigatus* ΔakuB strain is a strain that is deficient in non-homologous end joining (NHEJ) DNA repair (Krappmann *et al.,* 2006; da Silva Ferreira *et al.,* 2006a). This deficiency increases the occurrence of targeted transformations, as the strain will only integrate DNA that has a homologous target. The *A. fumigatus* ΔakuB strain has been successfully used for a number of gene deletion experiments in *Aspergillus* species (e.g. *gliP*, the NRPS involved in gliotoxin biosynthesis (Kupfahl *et al.,* 2006)*, calA,* the calcineurin A catalytic subunit (da Silva Ferreira *et al.,* 2007), and *mpkA,* a mitogen-activated protein kinase involved in cell wall signalling (Valiante *et al.,* 2008).

The *sidD* gene has been shown to be directly involved in the biosynthesis of the siderophore, Triacetylfusarinine C (TAFC) (Figure 1.14) (Schrettl *et al.,* 2004). SidD catalyses an intermediate step in the biosynthesis of TAFC by converting N^5-cis-anhydromevalanyl-N^5-hydroxy-L-ornithine to Fusarinine C (FSC) before conversion into TAFC. Fungi have two separate methods for the uptake of iron; the Reductive Iron Assimilation (RIA) method, where readily available iron is obtained from the surrounding environment and utilised by the fungus and the siderophore recruitment method where TAFC is released by the fungus in low iron conditions to scavenge for residual iron in the surrounding environment and so facilitate iron uptake by the fungus (Haas, 2003). An *A. fumigatus* Δ*sidD* mutant was created which is unable to synthesise TAFC (a gift from Prof. Hubertus Haas) (Schrettl *et al.,* 2007). It has also been shown that the *sidD* gene is indirectly involved in response to oxidative stress and directly involved with the virulence of *A. fumigatus* (Schrettl *et al.,* 2007). Previous studies have shown that siderophore related NRP synthetases may play a role in protecting *A. fumigatus* against oxidative stress as part of the host defence response (Eisendle *et al.,* 2003). NPS6, a siderophore found in the maize pathogen *Cochliobolus heterostrophus*, an ortholog of *A. fumigatus sidD*, was found to be responsible for oxidative stress resistance and virulence (Lee *et al.,* 2005). To enhance the likelihood of obtaining mutants (Δ*pes1*) with a clear phenotype, it was decided to use these strains, ΔakuB and ΔsidD, which contain additional deficiencies to ensure the best opportunity of characterising the *pes1* gene product.

Previously, it was reported that *pes1* has a similar homology to AbrePsy1 of *Alternaria brassicae* and PES of *Metarhizium anisopliae* which are responsible for the production of siderophores or destruxin (Bailey *et al.,* 1996; Guillemette *et al.,* 2004; Neville *et al.,* 2005). The initial similarity seen between these NRPS genes

lead to speculation that the *pes1* gene in *A. fumigatus* may be involved in siderophore biosynthesis in this species. However, further investigation demonstrated that *pes1* expression was unaffected by iron levels (Reeves *et al.,* 2006) and also that destruxin is not detected in *A. fumigatus* (Neville *et al.,* 2005). Thus, although *pes1* has been shown not to be involved in siderophore biosynthesis, there is no indication of a definitive function to date.

There is a possibility that fungal NRPS genes may be signalling or interacting with each other, as this type of cross-talk between NRPS clusters has been well established in bacteria (Revill *et al.,* 1995; Summers *et al.,* 1995; Madduri *et al.,* 2001). The disruption of *pes1* in *A. fumigatus* Δ*sidD* background may highlight how fungal NRPS products may interact with or signal each other, especially in relation to the oxidative stress response, i.e., the absence of both NRPS genes may enhance the effect of the *pes1* gene deficiency. As *pes1* has been shown to play a role in oxidative stress response (Reeves *et al.,* 2006), the gene product may be more likely to be identified while the fungus experiences such a stress. As mentioned in Chapter 1, there are few reports on the generation of double knock out mutants in *Aspergillus* species, the majority of which are carried out in *A. nidulans* (Stringer and Timberlake*,* 1995; Paris *et al.,* 2003a; Belaish *et al.,* 2008; El-Ganiny *et al.,* 2008). There are no reported double NRPS related mutants in *A. fumigatus*. Therefore, the production of a double mutant in *A. fumigatus* lacking *sidD* and *pes1* is of great interest as it may provide evidence that NRPS genes cross-talk and can compensate for loss of function or that certain NRPS genes may be involved in signalling to other NRPS genes not clustered together. Ultimately, the double mutation may result in severe stress for *A. fumigatus* such that the function of *pes1* may become increasingly apparent.

If the two strains, Δ*akuB* and Δ*sidD*, have significant phenotype differences, then the effect of *pes1* disruption may be undetectable, especially if the background mutation has the same phenotypical response that the *pes1* mutation may confer. The ATCC46645 strain is a clinical isolate of *A. fumigatus* and the use of this strain can give an understanding of the direct effect of losing the *pes1* product, in the absence of other deficiencies. Also, the use of a wild-type strain may show that the lack of *pes1* on its own has no obvious phenotypic disadvantage to *A. fumigatus* tentatively indicating that *pes1* acts with other NRPS products, or is compensated by another product formation.

A final step in the verification of a gene product is to reintroduce the gene into the mutant strain. If a product can be identified during phenotypic analysis, the complementation of gene should be capable of producing that product again (Steinbach *et al.,* 2006; Bok *et al.,* 2006a; Schrettl *et al.,* 2007; Ejzykowicz *et al.,* 2009). The reappearance of the relevant metabolite or phenotypic behaviour in the complemented strain is conclusive proof of the gene function.

The overall objectives of this chapter are to (i) create constructs that enable the disruption of *pes1,* (ii) utilise the bipartite transformation technique in conjunction with the pyrithiamine resistance cassette (*ptrA)* to transform *A. fumigatus*, (iii) disrupt the *pes1* gene in three different strains of *A. fumigatus,* namely*,* Δ*akuB,* Δ*sidD*, and ATCC46645 and (iv) reintroduce the deleted region of the *pes1* gene back into the Δ*sidD*:Δ*pes1* strain. The establishment of *pes1* disrupted strains will allow for comparative analysis to identify the phenotypic and metabolic components that *pes1* may play a role in, which will be investigated in Chapter 4.

3.2 Results

3.2.1 Generation of constructs by PCR

The constructs used in the creation of *A. fumigatus pes1* were generated from the flanking regions of the target DNA as described earlier in Figure 2.4. The primers used in the generation of the constructs are detailed in Table 2.3. The initial PCR steps amplified the 5' and 3' regions, respectively, of the *pes1* target region. The primers used for this amplification incorporated additional restriction sites to facilitate specific digestion and subsequent ligation of the PCR products to the pyrithiamine resistance (*ptrA*) gene. Primer 5' reverse, contained a *Pvu*I restriction site, and Primer 3' forward contained a *Kpn*I restriction site. The 5' PCR generated a fragment of 1345 bp, named P1 and the 3' PCR generated a fragment of 1430 bp, named P2 (Figure 3.3). The PCR products, P1 and P2, were gel purified to remove any non-specific products.

The plasmid pSK275 and the gel purified PCR products, P1 and P2, were digested with specific restriction enzymes (Figure 3.4). To obtain the *ptrA* gene from the plasmid pSK275, the plasmid was digested with *Pvu*I and *Kpn*I, separately. P1 was digested with *Pvu*I and P2 was digested with *Kpn*I. The digested products were gel purified for use in ligation.
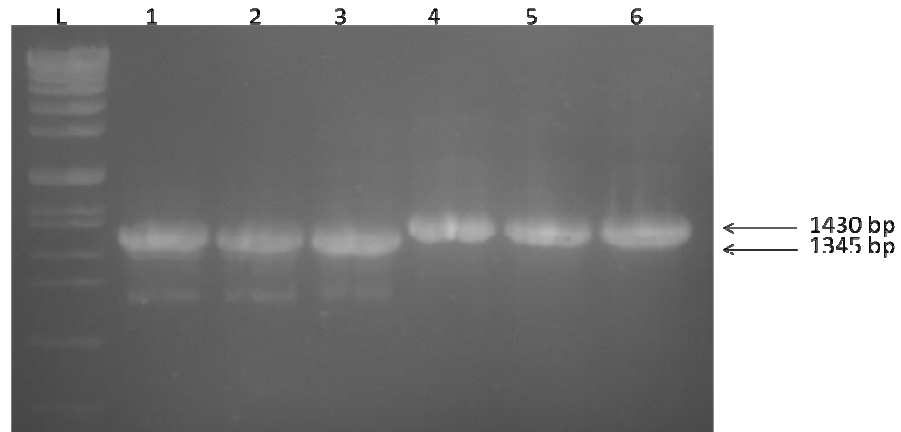
Figure 3.3: PCR products from the amplification of the 5' and 3' flanking region of the *pes1* deletion target. Lane L: Molecular weight marker ladder (Roche VII), Lanes 1-3: 5' flanking region PCR product, P1 (1345 bp), lanes 4 – 6: 3' flanking region PCR product, P2 (1430 bp).
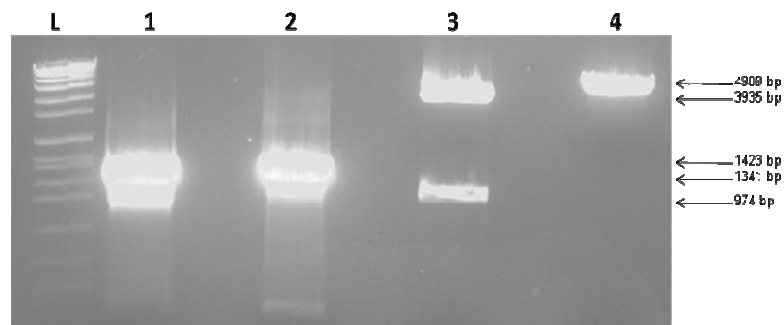
Figure 3.4: Preparation of fragments by digestion for generation of deletion constructs. Lane L: Molecular weight marker ladder (Roche VII), Lane 1: PCR product, P1, digested with *Pvu*I (1341 bp), Lane 2: PCR product, P2, digested with *Kpn*I (1423 bp), Lane 3: pSK27 digested with *Pvu*I (3935 and 974 bp), Lane 4: pSK275 digested with *Kpn*I (4909 bp).

The digested P1 product (1341 bp) was ligated with the *Pvu*I digested pSK275 (3935 bp), named ligation 1 and the digested P2 product (1423 bp) was ligated with the *Kpn*I digested pSK275 (4909 bp), named ligation 2. These ligations were used as the template for the final PCR amplification, where ligation 1 was used to create the 5' deletion construct (2942 bp) and ligation 2 was used to create the 3' deletion

construct (2435 bp) (Figure 3.5). The 5' and 3' deletion constructs were gel purified

and concentrated for subsequent protoplast transformation (Figure 3.6).
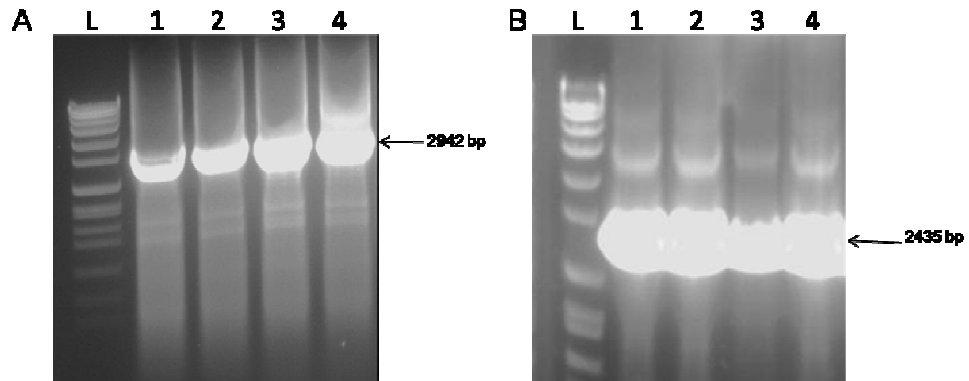
Figure 3.5: Purification of the 5' and 3' deletion constructs used in the transformation process to disrupt *pes1*. (A) Lane L: Molecular weight marker ladder (Roche VII), Lanes 1 – 4: 5' construct PCR product (2942 bp). (B) Lane L: Molecular weight marker ladder (Roche VII), Lanes 1 – 4: 3' construct PCR product (2435 bp).
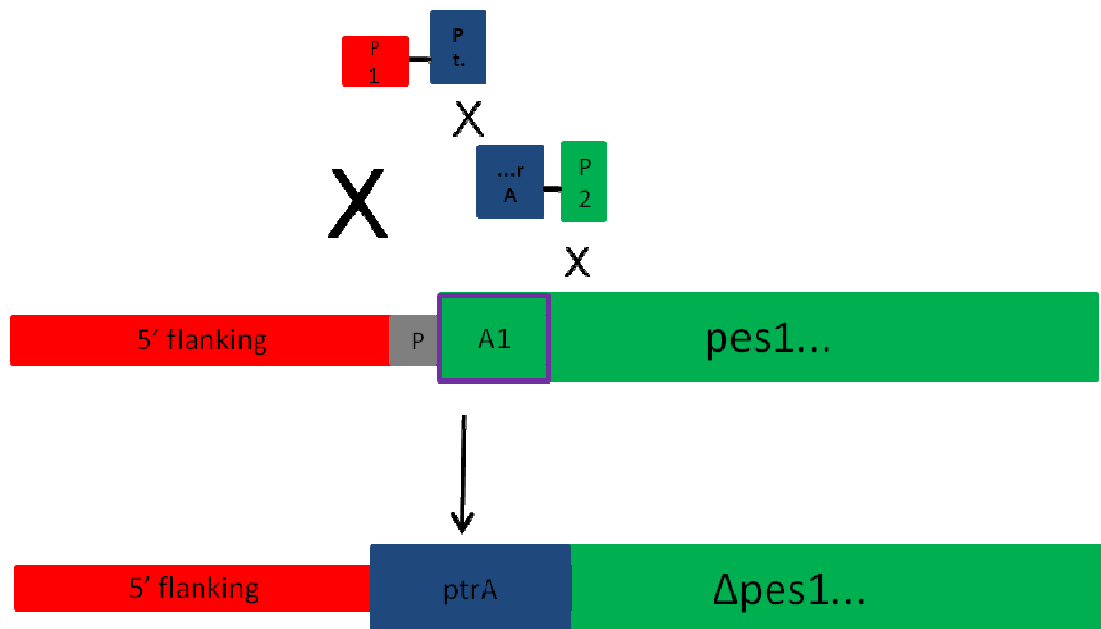
Figure 3.6: Schematic of the transformation for the disruption of *pes1* in the A. fumigatus genome. The overlapping region of the *ptr*A gene from each construct (2379 bp) is the homologous recombination site which results in the completion of the *ptr*A gene in the mutant strain. The 5' and 3' regions of the gene of interest ligated to the incomplete *ptr*A gene are the other two recombination sites which results in the targeted integration of *ptr*A into the genome.

3.2.2 Generation of DIG labelled probes by PCR for transformant identification.

The regions chosen for Southern blot analysis were the 5' region upstream of the deletion target and also a region within the deleted region (Figure 3.7). Probes were generated by PCR amplification using primers detailed in Table 2.5 containing DIG-labelled nucleotides, which allowed the probe DNA to be detectable during Southern blot analysis, as described in Section 2.2.8. The PCR products were gel extracted and purified (Figure 3.8).
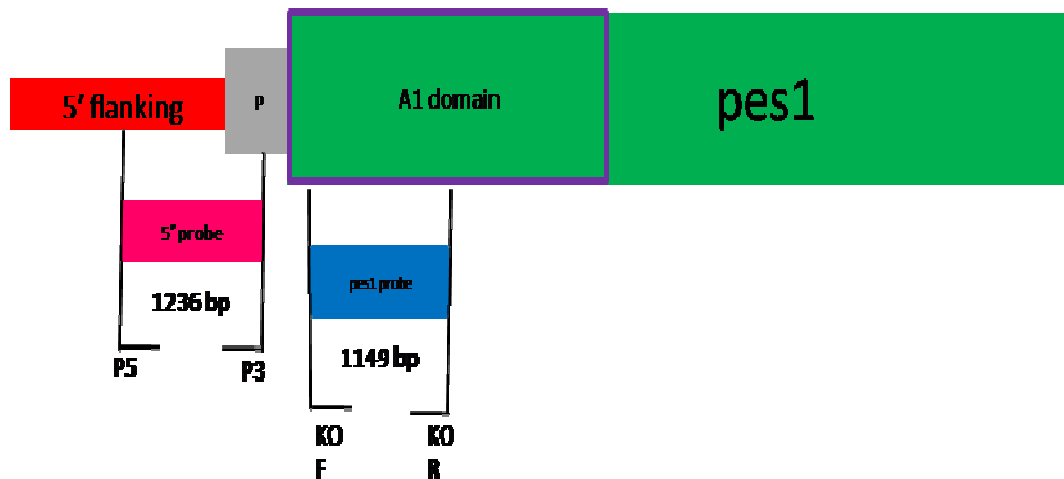
Figure 3.7: Schematic of the annealing sites of the 5' and *pes1* probes designed for pes1 that will result in different fragment binding between the wild-type and Δ*pes1* strains. The red shape depicts the 5' flanking region of *pes1*. The Green shape depicts the *pes1* gene. The grey shape depicts the predicted promoter of *pes1*. The blue shape depicts the *pes1*KO region probe. The pink shape depicts the 5'pes1 probe.
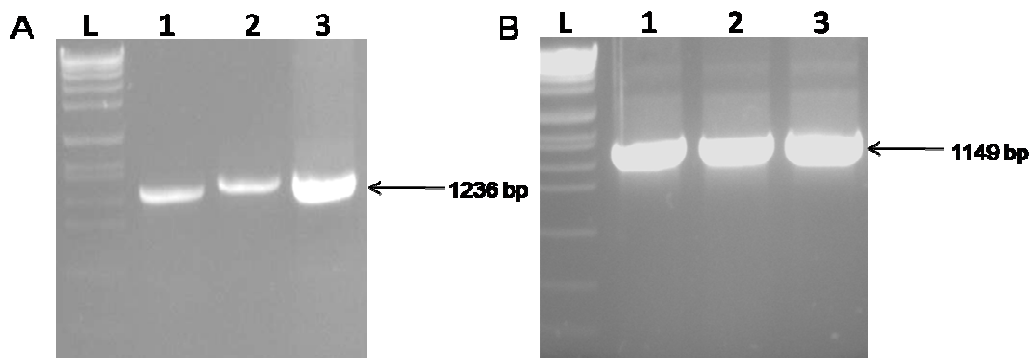
Figure 3.8: Generation of DIG labelled probes by PCR (A) PCR amplified 5' probe region of *pes1*. Lane L: Molecular weight marker ladder (Roche VIII). Lanes 1 – 3: *5' pes1* probe PCR product (1236 bp), (B) PCR amplified region of *pes1* used in the DIG labelled probe. Lane L: Molecular weight marker ladder (Roche VII). Lanes 1 – 3: *pes1* region PCR amplified product (1149 bp).

3.2.3 Protoplast transformation facilitating the disruption of *A. fumigatus pes1* by replacement of the promoter and first adenylation domain

The constructs from Section 3.2.1 were used for transformation in three different strains of *A.* fumigatus, namely Δa*kuB*, Δ*sidD,* and ATCC46645. At least 3 µg of each of the constructs were used for the individual transformation processes. Specifically, 3 µg of each construct was used for the *A. fumigatus ΔakuB* transformation, 6 µg of each construct was used for *A. fumigatus ΔsidD* transformation, and 5 µg of each construct was used for the *A. fumigatus* ATCC46645 transformation. The transformation processes were carried out as described in Section 2.2.7. The resultant transformants were initially screened on agar plates containing pyrithiamine (100 ng/ml), and are detailed in Table 3.1. The colonies that were able to grow on the media containing pyrithiamine indicated that the *ptrA* gene had integrated as a whole and conferred resistance to pyrithiamine and therefore had successfully integrated the construct fragments by recombination. The

resultant transformants were screened by Southern blot analysis for the disruption of

pes1.

Table 3.1: Summary of the screening process required for the identification of Δ*pes1* in *A. fumigatus* Δ*akuB*, Δ*sidD* and ATCC46645, respectively.

Strain	Number of putative Transformant colonies	No. of colonies Screened	Successful Transformants
ΔakuB	36	9	8
Δ*sidD*(46645)	48	10	1
ATCC46645	27	7	1

3.2.3.1 Disruption of the *pes1* gene in *A. fumigatus* Δ*akuB*

The analysis of the transformation of *A. fumigatus* Δ*akuB* was carried out on nine possible transformants (Figure 3.9). The expected band size of 4608 bp, as calculated by the *pes1* Southern strategy detailed in Section 2.2.9 (Figure 2.8), was observed in all nine transformants. One transformant contained an additional non-specific signal. A band was not detected at 6118 bp, indicating that wild-type *A. fumigatus* was not present in any of the transformants.

Figure 3.9: Identification of *A. fumigatus ΔakuB:Δpes1* strain (A) DNA digested with *Sal*I for probing by Southern blot with the 5' *pes1* probe and (B) corresponding Southern blot. Lane L: Molecular weight marker ladder (Roche VIII), Lane 1: Δa*kuB* (6118 bp), Lanes 2-10: Possible transformants (4608 bp), labelled PA 1 – 9. Transformant PA2 is marked with * below the lane.

To confirm the disruption of *pes1*, transformant PA2 was single spored as described in Section 2.2.7.8, and the first resultant individual colony was subjected to restriction digestion using *Pvu*II (Figure 3.10). The wild-type band was observed at 4234 bp and the mutant signal at 1922 bp. This confirmed that that transformant PA2.1 contained a targeted disruption of *pes1* in the *A. fumigatus* strain *ΔakuB*.
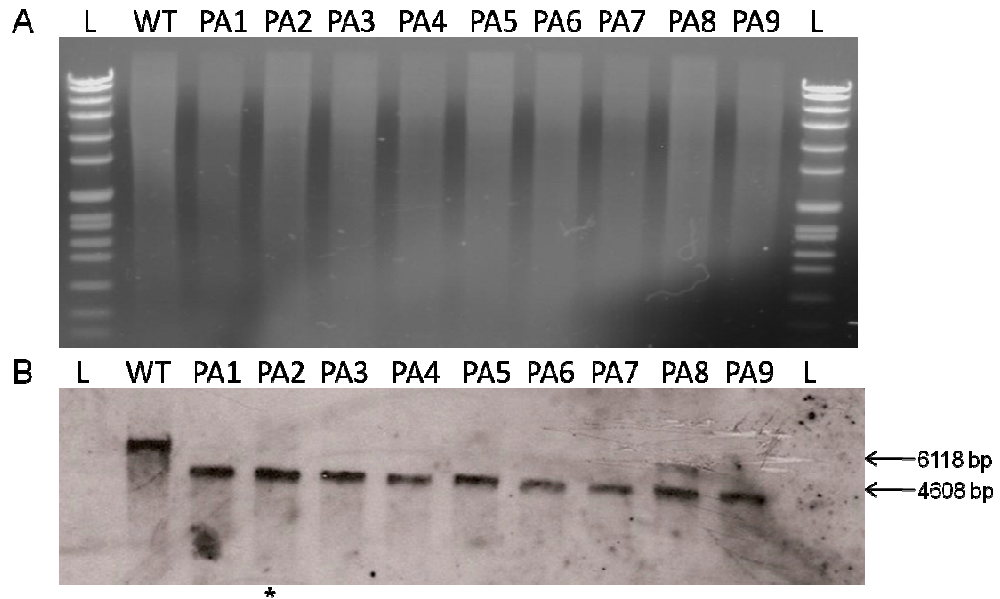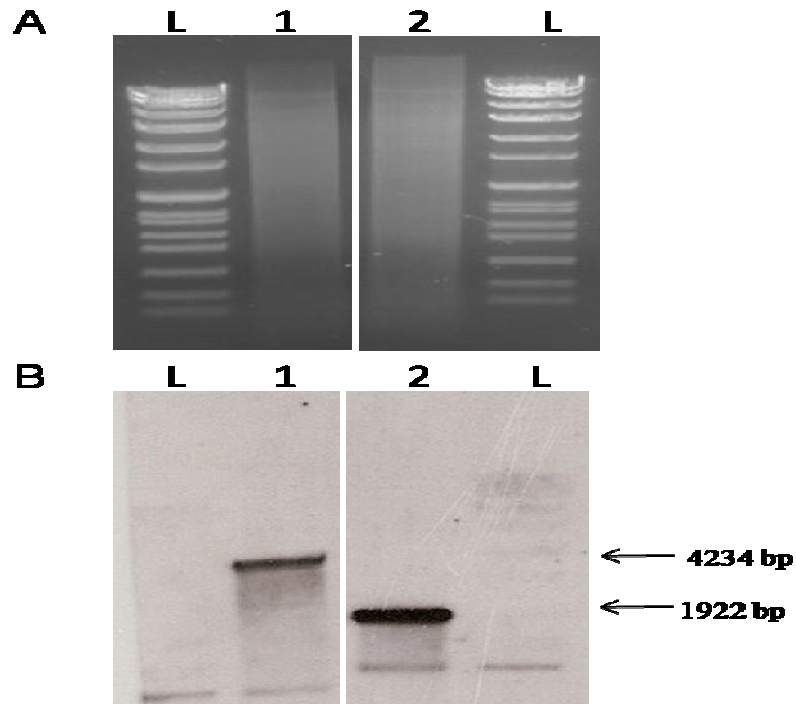
Figure 3.10: Identification of *A. fumigatus ΔakuB:Δpes1* strain (A) DNA digested with *Pvu*II for probing by Southern blot with the 5' *pes1* probe and (B) corresponding Southern blot. Lane L: Molecular weight marker ladder (Roche VIII), Lane 1: Δa*kuB* (4234 bp), Lane 2: single spored transformant PA2.1 (1922 bp).

3.2.3.2 Disruption of the *pes1* gene in the Δ*sidD* strain

The successful disruption of *pes1* in *A. fumigatus ΔakuB* confirmed the deletion constructs were functioning in *A. fumigatus.* Thus, the same strategy was used to disrupt *pes1* in the *A. fumigatus ΔsidD* (Schrettl *et al.,* 2007). The analysis of the transformation of the Δ*sidD* strain was carried out on ten putative transformants (Figure 3.11). Of the transformants, six still displayed the band at 6118 bp which indicated the presence of the *A. fumigatus* wild-type strain (PD1, 2, 3, 4, 5, and 6), and of these, one also contained the mutant band (4608 bp) (PD6), the other five contained additional non-specific bands. Two putative transformants did not contain either the wild-type or the mutant bands (PD9 and PD10), and were representative of non-targeted integrations. Transformant PD8 contained the single mutant signal (4608 bp), suggesting that the transformant may be an *A. fumigatus ΔsidD:Δpes1*

mutant. The restriction digestion of the Δ*sidD* strain resulted overactivity of the digestion and therefore was not visible on this blot, but was repeated and can be seen in Figure 3.12, Figure 3.13 and Figure 3.15.

Figure 3.11: Identification of *A. fumigatus ΔsidD:Δpes1* strain (A) DNA digested with *SalI* for probing with 5'*pes1* probe and (B) corresponding Southern blot. Lane L: Molecular weight marker ladder (Roche VII), Lane 1: ATCC46645 (6118 bp), Lane 2: Δ*sidD*, Lanes 3 – 12: possible transformants, named PD 1 – 10. Transformant PD8 is marked with * below the lane.

To confirm that the transformant PD8 was a pure mutant, the transformant was single spored as described in Section 2.2.7.8. Three of the resultant individual colonies were screened (Figure 3.12). Two of the samples still contained faint wild-type signal (6118 bp), as well as other non-specific integrations (PD8.2 and PD8.3). Sample PD8.1 exhibited no non-specific bands, but still contained the remnants of the wild-type signal. All of the transformants contained the expected Δ*pes1* mutant band (4608 bp).

Figure 3.12: Identification of *A. fumigatus ΔsidD:Δpes1* strain (A) DNA digested with *SalI* for probing with 5'*pes1* probe and (B) corresponding Southern blot. Lane L: Molecular weight marker ladder (Roche VII), WT: ATCC46645, Lanes 4 – 6: single spored transformants in Δ*sidD* strain, named PD8.1, PD8.2, and PD8.3, respectively. Transformant PD8.1 is marked with * below the lane.

Transformant PD8.1 was single spored to remove the wild-type spore contamination of the mutant spores. Six single spored colonies were analysed (Figure 3.13). The re-analysis was conducted using an alternative restriction enzyme, namely *Pvu*II. This alternative analysis resulted in a clear blot for interpretation, as the size difference between the wild-type and mutant signals is greater. All of the transformants contained the mutant signal (1922 bp). Three of the samples (PD8.1.1, PD8.1.2, and PD8.1.4) contained a non-specific signal. Transformants PD8.1.3, PD8.1.5 and PD8.1.6 were representative of single targeted integrations and

transformant PD8.1.5 was chosen as the transformant to be used as the *A. fumigatus* Δ*sidD:*Δ*pes1* strain.

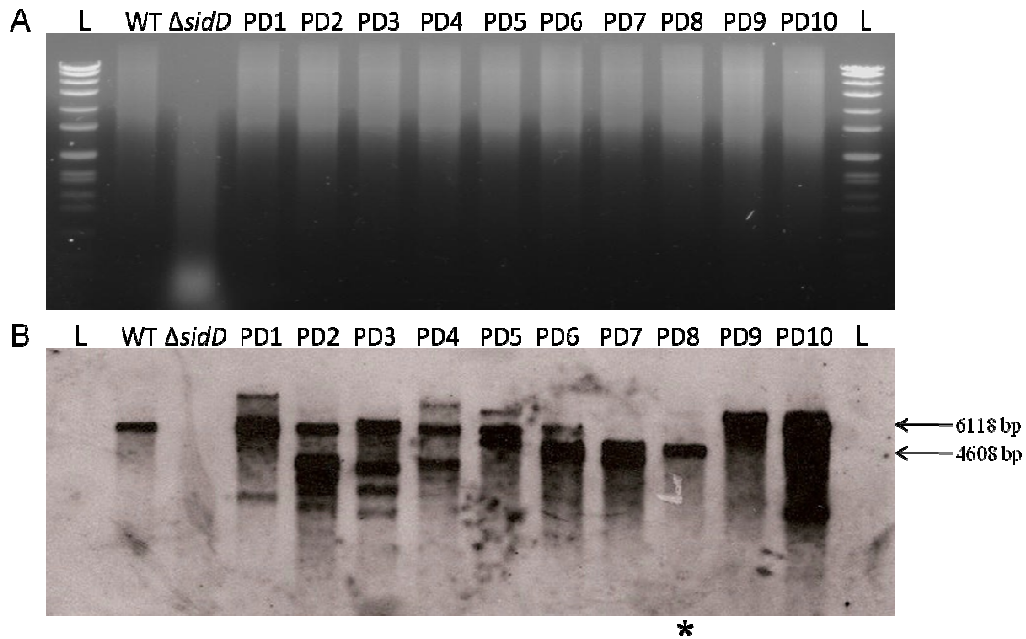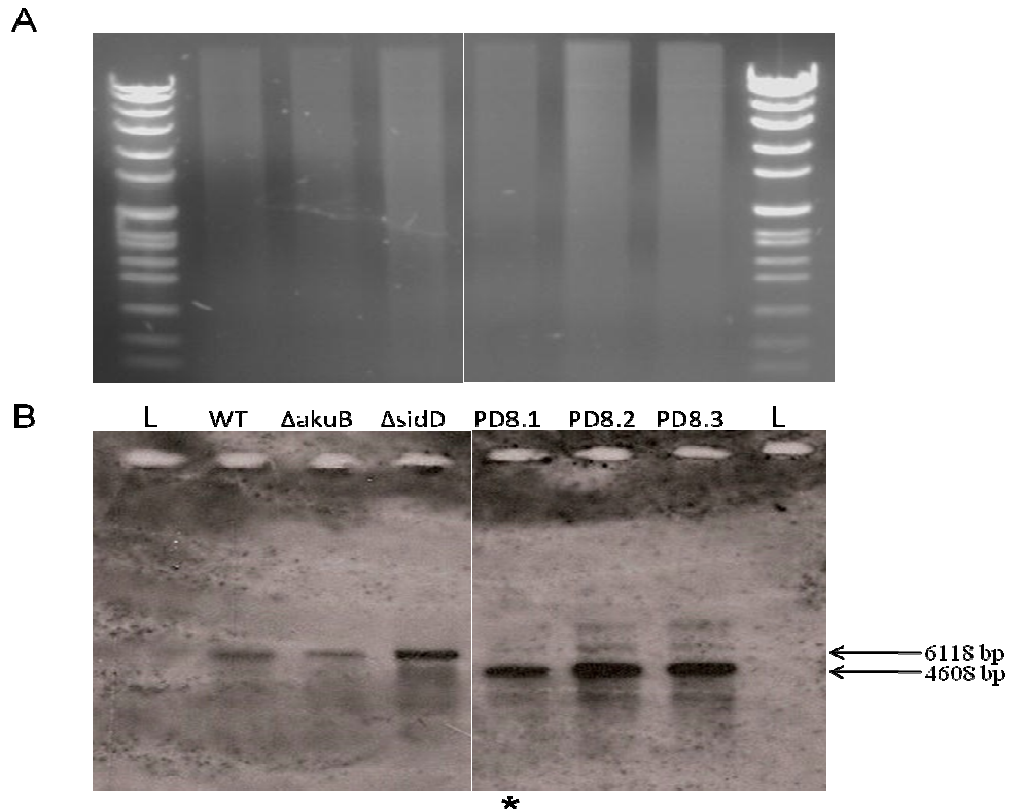**Figure 3.13:** Identification of A. fumigatus ΔsidD:Δpes1 strain (A) DNA digested with PvuII for probing with 5' *pes1* probe and (B) corresponding Southern blot. Lane L: Molecular weight marker ladder (Roche VII), Lane WT: ATCC46645, Lanes 1 – 6: Single spored PD8.1 transformants, named PD8.1.1 – PD8.1.6, Δ*pes1*(Δa*kuB*) was used as a positive control for the Δ*pes1* signal on the blot. Transformant PD8.1.5 is marked with * below the lane.

3.2.3.3 Disruption of the *pes1* gene in *A. fumigatus* ATCC46645

The previous disruptions described in Sections 3.2.3.1 and 3.2.3.2 were both in backgrounds where additional genes, *akuB* and *sidD*, respectively, had already been disrupted or deleted. Thus, it was important for classification of *pes1* function to have a strain that was representative of only *pes1* gene disruption.

Consequently, the same transformation process was used to disrupt *pes1* in the *A. fumigatus* ATCC46645 strain as was used in the generation of *A. fumigatus Δaku*B

136

and *ΔsidD*. The analysis of the *pes1* disruption in the ATCC46645 strain was performed on seven transformants (Figure 3.14), where the five of the transformants had the expected band size of the mutant (1922 bp). Only one, PW6, had no other ectopic integrations, nor did it have a band corresponding to the wild-type signal (4234 bp).
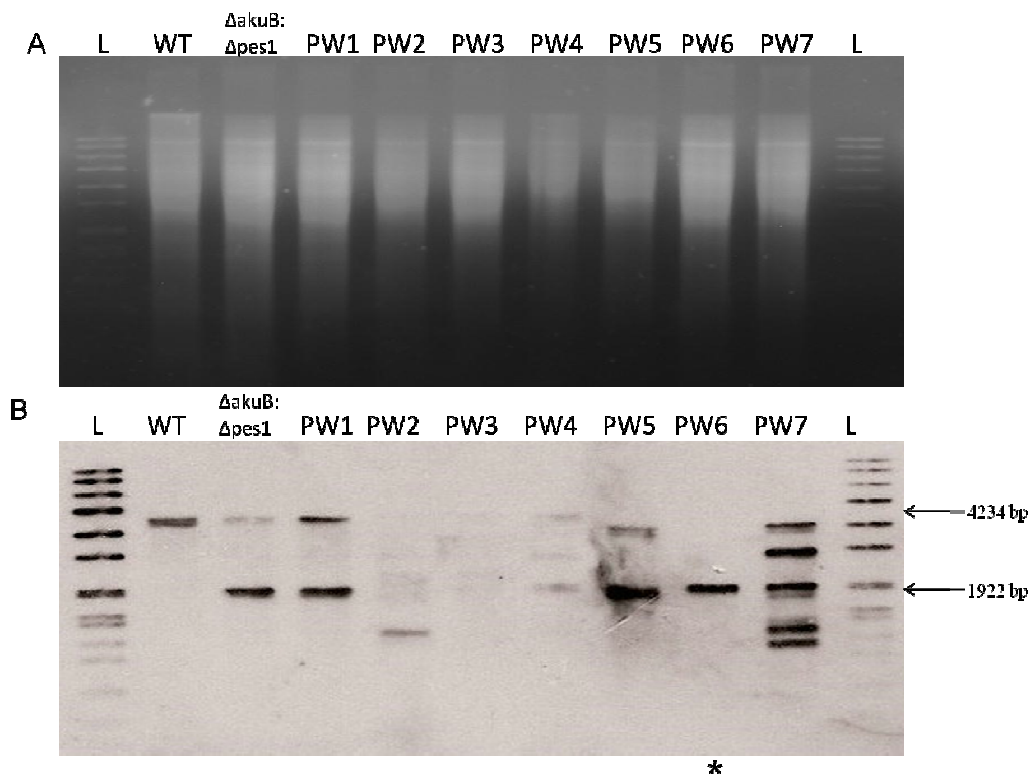
Figure 3.14: Identification of *A. fumigatus* Δ*pes1*[46645] strain (A) DNA digested with *PvuII* for probing with 5' *pes1* probe and (B) corresponding Southern blot. Lane L: Molecular weight marker dig labelled ladder (Roche VII), WT: ATCC46645, Lanes 3 – 9: possible transformants, named PW 1 – 7. PW6 is marked with * below the lane.

As transformant PW6 contained no ectopic integrations, it was re-analysed to confirm Δ*pes1* genotype (Figure 3.15). A single band corresponding to 1922 bp was evident in transformant PW6 which confirmed that it contained a targeted disruption of *pes1* in *A. fumigatus* ATCC46645.
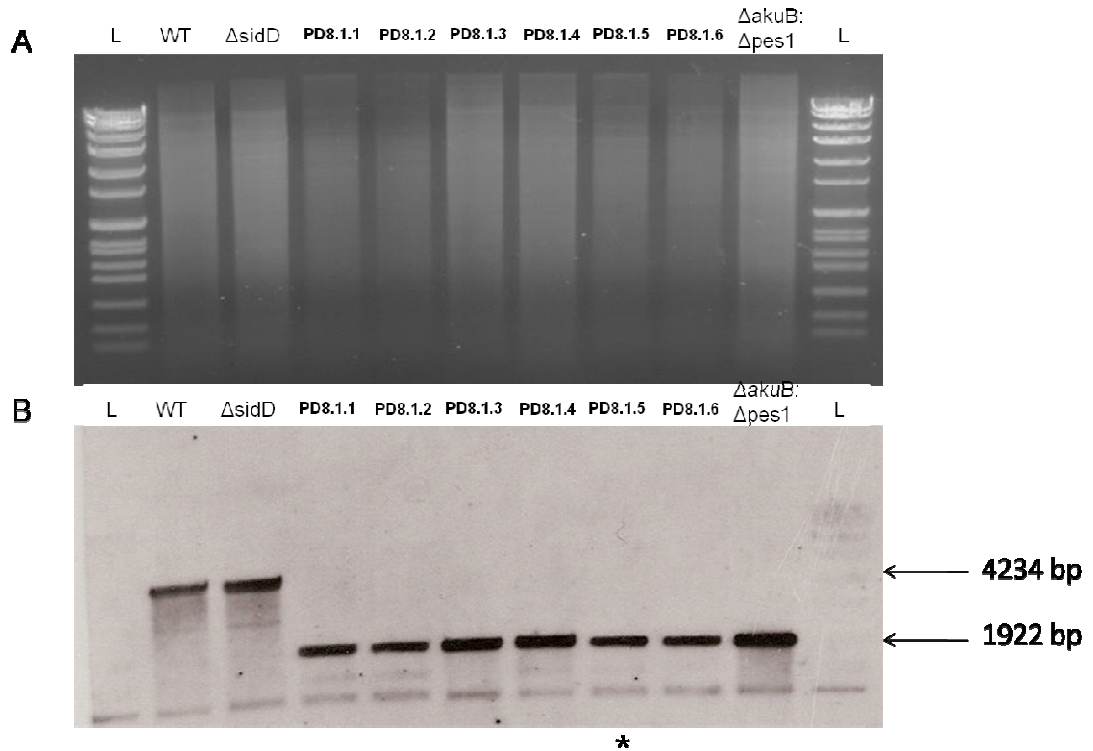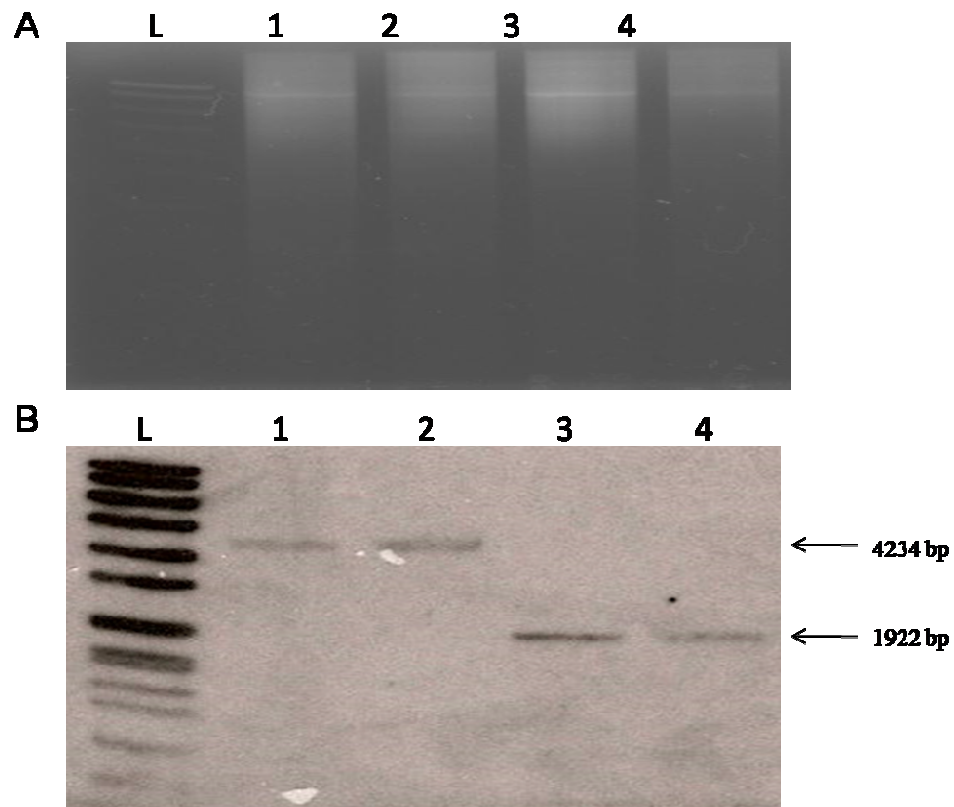
Figure 3.15: Identification of *A. fumigatus* Δ*pes1*[46645] strain (A) DNA digested with *PvuII* for probing with 5' *pes1* probe, and (B) corresponding Southern blot. Lane L: Molecular weight marker dig labelled ladder (Roche VII), Lane 1: ATCC46645, Lane 2: Δ*sidD*, Lane 3: putative transformant, PW6, Lane 4: Δ*pes1*:Δ*sidD* (PD8.1.5).

3.2.3.4 Complementation of pes1 into *A. fumigatus* Δ*sidD*:Δ*pes1*

Once it had been established that *pes1* was successfully deleted from the *A. fumigatus* Δ*akuB*, Δ*sidD*, and ATCC46645 strains, the gene was reintroduced into the genome of the Δ*sidD:*Δ*pes1* strain, to establish if any *pes1* related phenotype alterations would be restored. This would help clarify that any phenotypical differences observed between *A. fumigatus* Δ*sidD* and Δ*sidD:*Δ*pes1* that restore with the return of the gene can be attributed to the product of the *pes1*.

The reintroduction of *pes1* into the genome of *A. fumigatus ΔsidD:Δpes1* was carried out as described in Section 2.2.7.2, where the DNA encoding the deleted section of the *pes1* gene was cloned into TOPO and linearized with a unique restriction enzyme, creating a linear fragment homologous to the 3' flanking region of the *ptrA* gene (Figure 2.6), which, if targeted homologous recombination occurs, will reintroduce the relative region of *pes1* into the genome after the *ptrA* gene. This, in effect, would re-establish the *pes1* promoter and A1 region with the remainder of the disrupted *pes1* gene, thereby reconstituting the entire *pes1* gene.

The region encoding the promoter and A1 domain of *pes1* was PCR amplified using primers, P5 and P6 (Table 2.3), resulting in a 5881 bp fragment (Figure 3.16 (A)). The PCR product was gel extracted and purified. The PCR product was cloned into TOPO vector as described in Section 2.2.3.3. To verify the cloning, the modified vector was digested with the restriction enzymes *Not*I and *Sal*I which upon successful cloning would result in distinct fragments of 8393 bp and 1411 bp (Figure 3.16 (B)). After confirmation of successful cloning, the TOPO vector containing the *pes1* fragment was linearised by digestion with the restriction enzyme *Aar*I (Figure 3.16 (C)).

139
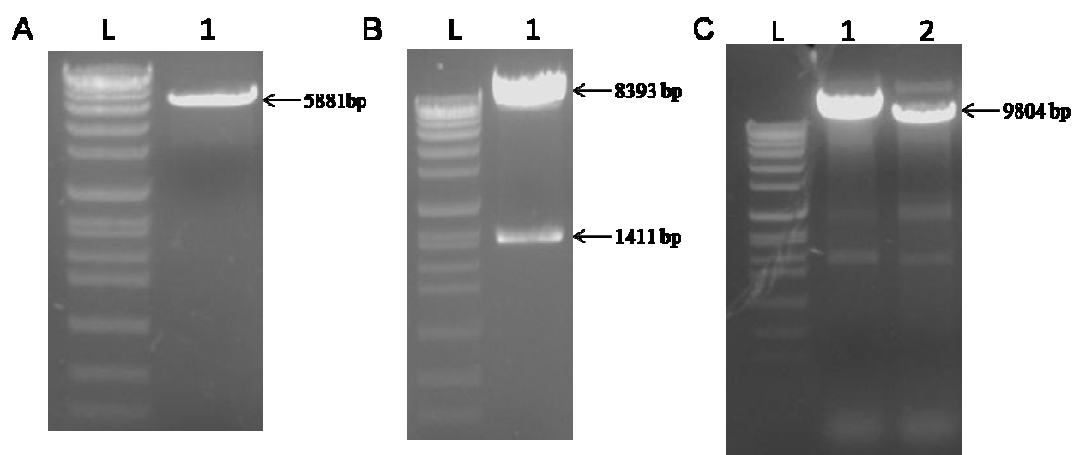
Figure 3.16: Constructs for complementation of *pes1* into the genome of Δ*sidD*:Δ*pes1*. (A) PCR amplification of the *pes1* region (5331 bp), (B) Digestion of the TOPO vector incorporating the *pes1* region with *Not*I and *Sal*I to confirm the cloning of *pes1* into TOPO (8393 bp and 1411 bp), (C) linearization of the TOPO vector incorporating *pes1* by digestion with *Aar*I (9804 bp).

The selection marker utilised in this transformation was phleomycin resistance, which was available in the plasmid, pAN8-1 (Punt and van den Hondel, 1992). As this method is dependent on the presence of unique restriction site (*AarI*) within the *pes1* region cloned into the TOPO vector, it was impossible to also incorporate a selection marker into the TOPO vector, without introducing additional *AarI* sites which are located in selection marker plasmid. Therefore, the phleomycin resistance plasmid, in its circular form, was co-transformed into *A. fumigatus* Δ*sidD:Δpes1* with the linear TOPO vector incorporating the promoter and A1 domain of *pes1* (Figure 2.6).

The regions chosen for Southern blot analysis were the 5' region upstream of the deletion target and also a region within the deleted region, which were already used in the Southern blot strategies to identify the Δ*pes1* strains. As the reconstituted strain still retained *ptrA* and also now incorporated part of the TOPO vector, the

140

binding of the 5' *pes1* probe would result in two binding fragments, 3812 and 1922

bp, and the coding region probe would result in a single fragment of 3812 bp (Figure

2.8 and Figure 2.9). These sizes are distinctly different from the binding pattern

observed in the wild-type (4234 bp) and *pes1* mutant (1922 bp) strains, and so can be

readily identified as the complemented strain, Δ*sidD:pes1^c*.

The screening for the complemented *pes1* was carried out by Southern blot

analysis as described previously, and the results are depicted in Figure 3.17.

Transformants PDC5 and PDC6, illustrate perfect examples of the *pes1^c* gene

integrated in a targeted fashion into the Δ*sidD:*Δ*pes1* strain (3812 bp and 1922 bp).

The blot showed that transformants PDC 1, 2, 3, 4, 7, 8, and 9 showed no integration

of the *pes1^c* and returned the Δ*pes1* signal (1922 bp). None of the transformants

showed contamination by a wild-type strain (4234 bp).
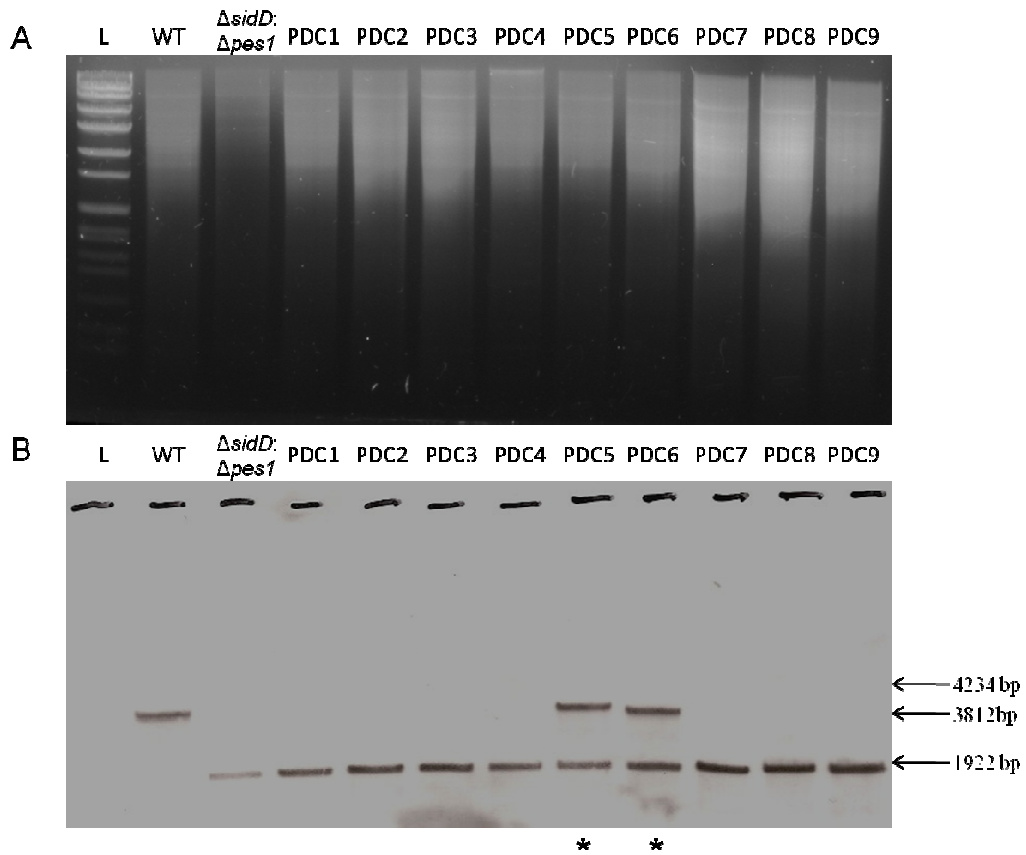
Figure 3.17: Identification of *A. fumigatus pes1^c* strain (A) DNA digested with *Pvu*II for probing with 5' *pes1* probe and (B) corresponding Southern blot. Lane L: Molecular weight marker ladder (Roche VII), WT: ATCC46645, Lanes 3 - 11: putative complemented transformants, PDC1 – 9. Transformants PDC5 and PDC6 are marked with * below the respective lanes.

The complemented transformants PDC5 and PDC6 were re-analysed by Southern analysis, whereby increased resolution of *Pvu*II-digested DNA was undertaken by increasing electrophoresis time to distinguish between the reintegrated *pes1* gene (3812 bp) and the wild-type fragment (4234 bp) (Figure 2.8), as they are similar in size (Figure 3.18). Transformant PDC5 showed that the band that was previously interpreted as the integrated *pes1* gene was in fact a non-targeted integration, as it was larger than the expected signal size of 3812 bp. Transformant

PDC6 contains the predicted banding pattern (3812 and 1922 bp, respectively) and so is confirmed as the complemented strain, *A. fumigatus* Δ*sidD:pes1ᶜ*.
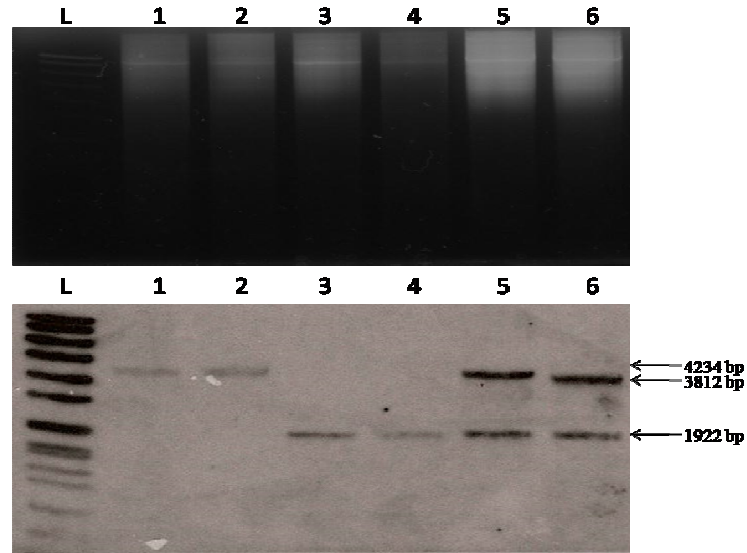
Figure 3.18: Identification of *A. fumigatus pes1ᶜ* strain (A) DNA digested with *Pvu*II for probing with 5' *pes1* probe, and (B) corresponding Southern blot. Lane L: Molecular weight marker dig labelled ladder (Roche VII), Lane 1: ATCC46645 (4234 bp), Lane 2: Δ*sidD* (4234 bp), Lane 3: Δ*pes1*⁴⁶⁶⁴⁵ (1922 bp), Lane 4: Δ*sidD:*Δ*pes1* (1922 bp), Lane 5: putative transformant PDC5, lane 6: putative transformant PDC6.

To further verify the complementation of the *pes1* gene, *A. fumigatus* ATCC46645, Δ*sidD*, Δ*pes1*⁴⁶⁶⁴⁵, Δ*sidD:*Δ*pes1* and Δ*sidD:pes1ᶜ* strains were probed for the *pes1* region that was deleted in the mutants and reintroduced in the complemented strain. For the wild-type strains, this would result in a detection of a fragment of 4234 bp, Δ*pes1* strains would yield no signal, and the complemented strain would result in a restriction fragment of 3812 bp. This blot is depicted in Figure 3.19, where the expected patterns were observed.
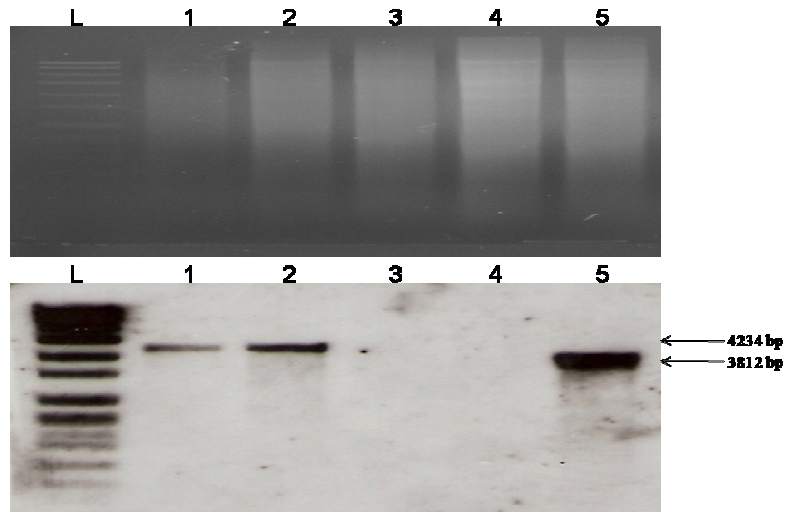
Figure 3.19: Verification of the *A. fumigatus* mutant and complemented strains. (A) DNA digested with *Pvu*II for probing with *pes1* coding region probe and (B) corresponding Southern blot. Lane L: Molecular weight marker dig labelled ladder (Roche VII), Lane 1: ATCC46645, Lane 2: Δ*sidD*, Lane 3: Δ*pes1*[46645], Lane 4: Δ*sidD:*Δ*pes1*, Lane 5: Δ*sidD:pes1*[c].

Overall, these results confirm disruption of *pes1* in *A. fumigatus* ATCC46645 and Δ*sidD*, respectively*,* as well as reconstitution of the gene in Δ*sidD*: Δ*pes1* to yield *A. fumigatus* Δ*sidD:pes1*[c].

144

3.3 Discussion

The intention of the work described here was to establish a transformation strategy that would target a disruption of the *pes1* gene in *A. fumigatus*. The constructs generated to carry out such transformation are specific for each gene target and therefore the creation of the DNA fragments required is a tedious but essential step in a successful transformation. The constructs need to be between 0.5 and 1 kb in length, with the partial selection marker ligated via a specific restriction enzyme site. The correct ligation is essential as this is the template for the final PCR that creates the constructs, as an inefficient ligation will result in partial amplification of the template, where the target flanking region or the partial selection marker amplifies separately. The bipartite method (Nielsen *et al.,* 2006) reduces the number of PCR steps used as there are only two rounds of PCR in comparison to the three rounds used in the double joint method (Yu *et al.,* 2004). This reduction of the PCR steps reduces the possibility of incorporating unwanted mutations that may occur from amplification with DNA polymerase (Nielsen *et al.,* 2006). This bipartite method was used to create the three different *A. fumigatus* Δ*pes1* mutant strains, Δ*akuB*:Δ*pes1*, Δ*sidD*:Δ*pes1* and Δ*pes1*^{46645} which were disrupted by removing the first adenylation domain of the gene. The *pes1* gene was restored using a linearised vector containing the missing adenylation domain, resulting in the complemented strain, Δ*sidD:pes1*^{c}.

Advances in the transformation of *Aspergillus spp.* have improved the transformation rate where construct generation has increased the likelihood of targeted integration, rather than ectopic integrations (Kuwayama *et al.,* 2002; Yu *et al.,* 2004; Nayak *et al.,* 2006; Nielsen *et al.,* 2006). As the bi-partite method relies on three homologous recombination events, namely the recombination of *ptrA* and then

the 5' and 3' flanking regions of the target DNA, respectively, the success rate of such a task is quite low. Furthermore, the number of transformants able to grow on the selective media is low, due to the inability of transformants containing only partial integrations to survive on the selection media. Any colonies that do grow on the selective media are expected to be the result of the recombination of the selection marker and very likely the result of successful integration of both constructs (Nielsen *et al.,* 2006). The transformation method generally used in fungal genetic manipulations is the PEG-mediated transformation of protoplasts. This method has been unchanged for the last 20 years and although the exact mechanisms of the PEG system are unknown, this method of DNA uptake into the genome gives an advantage over other fungal transformation methods such as *Agrobacterium tumefaciens* and electroporation as mentioned in Chapter 1.

Fungal transformation was carried out in *A. fumigatus ΔakuB* initially, to verify if it was possible to disrupt such a large gene, in a targeted fashion. Using *A. fumigatus ΔakuB* background for the disruption of *pes1* confirmed that the constructs and transformation method chosen were capable of this targeted disruption. The *pes1* disruption in *A. fumigatus ΔakuB* resulted in all nine transformants screened containing the targeted disruption, with only one of the nine also containing an additional integration. The drawback with using *A. fumigatus ΔakuB* in transformations is that the *akuB* mutation itself may have an impact on fungal growth and development. Previously, it was demonstrated that the phenotype of the NHEJ deficient strains had no altered morphology and extremely mild sensitivities to genotoxins including methyl methanesulphonate (MMS) and UV (Ninomiya *et al.,* 2004; Nayak *et al.,* 2006) but these investigations were not in-depth analysis and the alterations that the strain may be harbouring could impinge upon the phenotypical

analysis of a further gene deletions. Indeed, Nielsen *et al.* (2008) have pointed out that gene targeting carried out in NHEJ deficient strains should ideally be followed by a restoration of the NHEJ activity before characterisation of the mutant strain.

Once it was established that this transformation method and construct choice was effective in the disruption of *pes1* in a targeted manner, the transformation was carried out using *A. fumigatus* Δ*sidD*, which yielded more transformant colonies than the *A. fumigatus* Δ*akuB* transformation. However, the screening of the first ten colonies identified only one as being a single targeted integration. Thus, the other colonies growing on the selective pyrithiamine were most probably due to ectopic integrations of the constructs, with reconstitution of *ptrA*. An important factor to consider in double deletion strategies is the presence of the selection marker already utilised for the first gene deletion. In this case, *sidD* had been replaced with the hygromycin resistance gene, *hyg*, and therefore, the use of this selection marker is ruled out for any subsequent mutation in this strain (Schrettl *et al.,* 2007). As there are a limited number of selection markers to choose from for fungal transformations, the number of different transformations that can be carried out on the same strain is restricted to the number of selection markers available.

It was also important to have a wild-type disrupted version of the Δ*pes1* for comparative purposes, and therefore, the *pes1* gene was disrupted in the *A. fumigatus* ATCC46645 clinical isolate strain. This transformation resulted in the lowest number of colonies and also had a low rate of targeted integration, where only one out of seven colonies screened was representative of the correct integration.

The *pes1* gene was previously disrupted (Reeves *et al.,* 2006), by replacing the second adenylation domain with a zeocin-*pyrG* cassette using the double joint PCR (DJ-PCR) method (Yu *et al.,* 2004). The DJ-PCR method integrates a single

construct into the target genome, which has greater potential, than bi-partite constructs, to integrate randomly into the genome, as well as by targeted integration. The screening method, in that study, for transformation was carried out by Southern blot and RT-PCR of the deleted region of *pes1*, verifying the mutant inability to transcribe the *pes1* gene, but did not verify that the transformation event was solely targeted to the *pes1* gene region. As there is potential for ectopic integrations, it is essential to verify that only a single targeted transformation event has occurred before phenotypic analysis. For this reason, the method of screening transformations by Southern blot analysis of the 5' or 3' flanking regions, as adopted herein, immediately highlights any non-specific integration and such transformants can be ruled out of further analysis. The work presented in this chapter confirms the specificity of the bipartite method.

NRP synthetase genes are restricted to bacterial and fungal species, which allows for the prediction of gene function in one species by comparing to the orthologs observed in other species, as in the case of identifying the gliotoxin biosynthetic cluster in *A. fumigatus* which was found by its similar homology to the sirodesmin biosynthesis cluster in *Leptosphaeria maculans* (Gardiner and Howlett, 2005a). But this type of investigation can only be carried out if the orthologs have a defined function. The majority of NRPS-related genes identified in *A. fumigatus* have either undefined orthologs or no orthologs available, making analysis difficult as there is no indication of the function of the NRP synthetase under investigation. Therefore, gene deletion by transformation can facilitate the identification of a gene function by comparing the phenotypic and metabolic difference observed between the wild-type and mutant strains.

Microarray studies have shown that the *pes1* gene is one of the genes upregulated in stressful environments such as hypoxia (Gardiner and Howlett, 2005a; Willger *et al.,* 2008). Here, the SrbA transcription factor was investigated for regulation of genes during hypoxic condition, by creating a *srbA* deficient strain. In the analysis, *pes1* expression had the highest increase in fold change expression (23.36) of all the genes investigated in the wild-type during hypoxia compared to the *ΔsbrA* strain. This would indicate that Pes1 is involved in the stress response and perhaps defence in such conditions. Interestingly, Pes1 is also regulated by the transcription factor LaeA, where *pes1* expression is downregulated in a Δ*laeA* strain (Perrin *et al.,* 2007). LaeA is a global regulator of secondary metabolites in many *Aspergillus spp*. and is also involved in controlling the expression of certain virulence factors (Bok *et al.,* 2005). *laeA* encodes a nuclear protein that is required for the expression of genes involved in sterigomycystin, penicillin, lovastatin and gliotoxin biosynthesis (Bok and Keller, 2004). Also, *pes1* expression is severly downregulated in Δ*stuA* strain. StuA is one of the proteins that regulate the morphogenesis and virulence in *A. fumigatus* and the *ΔstuA* strain is susceptible to the application of hydrogen peroxide (Sheppard *et al.,* 2005).

The downregulation of *pes1* in *A. fumigatus* Δ*laeA* and absence of expression in *A. fumigatus* Δ*stuA* suggests that *pes1* is responding to changes in transcription factor presence and external factors, indicating that *pes1* expression may only be activated when the surrounding environment deviates from optimal conditions. If this is valid, then the function of *pes1* may not be observed unless the fungus is experiencing a stress, either an internal change in transcription factor signalling or an external stress environment. Therefore, the generation of the double mutant *A.* fumigatus Δ*sidD*:Δ*pes1* where the *pes1* deficiency is in addition to the extracellular

siderophore deficiency, may result in a distinctive phenotype of the double deficiency, and may potentially reveal the *pes1* function by comparison to the wild-type strain and also the single Δ*sidD* strain. As the product of the *sidD* gene is already defined as being involved in the biosynthesis of fusarinine C (FC), one of the intermediates of the biosynthesis of the extracellular siderophore, TAFC, the different phenotypes between *A. fumigatus* Δ*sidD* and Δ*sidD:*Δ*pes1* can be accredited to the *pes1* deficiency. Chapter 4 further characterises the *A. fumigatus* Δ*pes1* mutants and presents phenotypical and metabolite analysis of the *pes1* disrupted mutants with the overall goal of identifying the nature and function of the Pes1 peptide.

CHAPTER 4

Phenotypic analysis of *A. fumigatus* Δ*pes1* mutant strains

4. Phenotypic analysis of *A. fumigatus* Δ*pes1* mutant strains

4.1 Introduction

Certain fungal metabolites display antimicrobial activity, hence it has been hypothesized that they serve as a defence mechanism against other micro-organisms in the environment (Waring and Beaver, 1996). Cramer *et al.* (2006b) have used phylogenomics and functional genomics to identify NRP synthetase genes in five *Aspergillus* species, focusing on *Aspergillus fumigatus*. In the phylogenetic investigation, 14 NRP synthetase genes were identified, including *pes1* (named NRPS1 in the study) (AFUA_1G10380). The adenylation domains of *pes1* were shown to cluster repeatedly with the same uncharacterised NRP synthetase genes from other *Aspergillus* species; including *A. nidulans, A. terreus, A. oryzae,* and *A. flavus.* Real time PCR analysis by Cramer *et al.* (2006b) showed that *pes1* expression was only detected in liquid cultures of Sabouraud broth, using *A. fumigatus* Af293. Concurrently, Reeves *et al.* (2006) confirmed *pes1* expression, using RT-PCR analysis, in cultures of Minimal Essential Media (MEM) containing Foetal Calf Serum (FCS) (5 % v/v) using *A. fumigatus* ATCC26933, ATCC16424 and ATCC13073, where *pes1* expression varied between the strains analysed. These two studies have highlighted that the expression of *pes1* is not constitutive and therefore, that there is regulated production of the metabolite encoded by *pes1*.

The regulation of secondary metabolite production has been identified in *A. nidulans* where production of sterigmatocystin and aflatoxin are controlled by G protein-cyclic AMP-protein kinase A regulation (Hicks *et al.,* 1997). As decribed in Chapter 1 (Section 1.4.4), LaeA is a global regulator in *A. fumigatus* and other fungi, and is required for secondary metabolite production (Bok and Keller, 2004). Importantly, it was established that LaeA is responsible for the regulation of gene

expression during vegetative growth and sporulation in *A. fumigatus* (Bok *et al.,* 2005). The loss of LaeA resulted in impaired virulence in *A. fumigatus* which correlated with the loss of secreted factors from the fungus, including cell wall structural components such as hydrophobins, and pigments which confer resistance to phagocytic killing. Here, it was also hypothesised that molecules secreted from conidia may impart resistance to phagocytosis and that characterisation of conidial metabolites missing from *A. fumigatus* Δ*laeA* may provide more insight into this phenomenon.

Perrin *et al.* (2007) have established a genome-wide comparison of the genes regulated by the LaeA transcription factor by comparing *A. fumigatus* Δ*laeA* with its cognate wild-type, which established the genes regulated by the global regulator. In this study, expression of *pes1* was down-regulated in the *A. fumigatus* Δ*laeA* strain. Also, expression of the genes found in the gliotoxin, fumitremorgin B and ergot alkaloid biosynthetic clusters was down-regulated. Thus, it has been suggested that reduction in virulence of the Δ*laeA* strain is most likely attributed to the combined loss of the array of metabolites that are not produced in the absence of LaeA induction.

Sheppard *et al.* (2005) generated an *A. fumigatus* Δ*stuA* strain which resulted in the production of abnormal conidiophores. StuA is a member of the APSES (Asm1p, Phd1p, Sok2p, Efg1p and StuAp) group of transcription factors that are key regulators of fungal development (Dutton *et al.,* 1997). Transcriptional profiling of the Δ*stuA* strain indicated that 104 genes were differentially expressed in the mutant strain compared to the wild-type and complemented strains. *pes1* was one of the genes identified as differently expressed in the Δ*stuA* strain, whereby *pes1* expression was downregulated, but not absent, indicating that while StuA may influence the expression of *pes1*, it does not completely control *pes1* expression. Interestingly, the biosynthetic cluster encoding genes involved in the production of the tremorgenic mycotoxin,

fumitremorgin B, was found to be StuA dependant. Furthermore, *A. fumigatus* Δ*stuA* was susceptible to oxidative stress following exposure to hydrogen peroxide, but only showed a trend towards reduced virulence.

Taken together, *pes1* expression was down-regulated in both Δ*laeA* and Δ*stuA* strains, where each of these transcription factors are associated with the regulation of secondary metabolite production. As mentioned in Chapter 3, *pes1* was previously disrupted which resulted in a mutant that has reduced virulence in the *Galleria mellonella* insect model system, increased sensitivity to oxidative stress and neutrophil-mediated phagocytosis (Reeves *et al.*, 2006). This pattern of reduced virulence is similar to the Δ*stuA* strain, indicating that *pes1* may play a role in downstream activity consequent to *stuA* expression. Also, *A. fumigatus* Δ*pes1* displayed altered conidial morphology and hydrophobicity, similar to that of the *A. fumigatus* Δ*laeA* strain, indicating that the altered conidial morphology observed in Δ*laeA* may be in-part due to the down-regulation of *pes1* expression (Figure 4.1) (Bok *et al.*, 2005; Reeves *et al.*, 2006). The indication that *pes1* may function downstream of these transcription factors gives an insight into the potential function of this NRP synthetase gene.
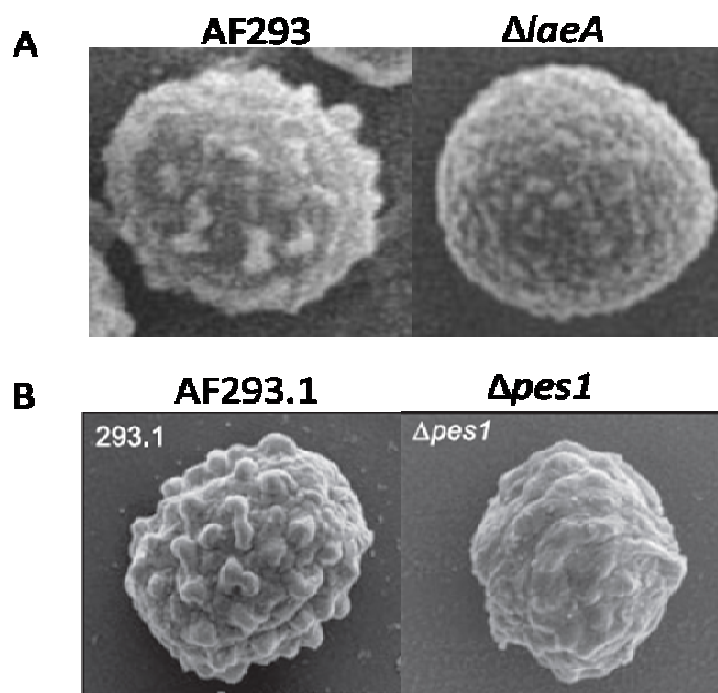
Figure 4.1: Scanning electron micrographs of conidia (approx 3 μm in diameter) of (A) wild-type Af293 and Δ*laeA* (Bok *et al.,* 2005) and (B) wild-type Af293.1 and Δ*pes1* (Reeves *et al.,* 2006) showing the similar conidial surface alterations in the Δ*laeA* and Δ*pes1* strains.

Furthermore, another NRPS deficient strain, Δ*sidD* results in a similar phenotype to Δ*pes1*, which also exhibits sensitivity to oxidative stress with reduced virulence (Schrettl *et al.,* 2007). As described in Chapter 1, *sidD* is the NRP synthetase involved in the production of the extracellular siderophore TAFC. Cramer *et al.* (2006b) reported that *sidD* was the most expressed NRP synthetase during incubation with macrophages, indicating that the production of TAFC plays a role in protecting the organism during the infection process of the fungus from the immune response of the human host. Using the Δ*sidD* strain as a background to disrupt *pes1* may highlight possible NRP synthetase peptide interaction or signalling, especially in relation to the similar observed response to oxidative stress in the separate single mutants (Reeves *et al.,* 2006; Schrettl *et al.,* 2007). As mentioned in Chapter 3, identification of the Pes1–encoded NRP peptide may be possible due to the potential accumulative effect of the double mutant.

Consequently, *pes1* disruption was carried out in three different strains, *A. fumigatus ΔakuB*, *ΔsidD* and ATCC46645, as detailed in Chapter 3. The resultant phenotypical observations were used to further characterise the function of *pes1*. To investigate the elusive function of *pes1*, the strains lacking a functional *pes1* gene, were subjected to extensive phenotypical analysis, which included exposure to oxidative stress agents such as hydrogen peroxide, as well as anti-fungals and gliotoxin, a toxin produced by *A. fumigatus* which has been indicated as a cause of oxidative stress (Schrettl *et al.,* 2010).

The objective of the work presented in this chapter is to compare phenotypic and metabolite differences between the wild-type and respective mutant strains. This involved (i) identifying *pes1* expression by real time PCR, (ii) establishing growth differences after exposure to anti-fungals, oxidative stress and other agents, (iii) use of *Galleria mellonella* as a model of infection and (iv) identifying metabolites produced by RP-HPLC and LC-MS-DAD.

4.2 Results

4.2.1 Real time PCR determination of *pes1* expression

The expression of *pes1* has previously been demonstrated at the 24, 48, and 72 hr time-points in various isolates of *A. fumigatus* by RT-PCR (Reeves *et al.*, 2006). As the *pes1* transcript is large, sections of the gene were selected in order to investigate the relationship between fungal growth and *pes1* expression. As the *A. fumigatus* Δ*pes1* strains disrupted herein lacked the predicted promoter and first adenylation domain, a region of the first adenylation domain (*pes1A1,* hereafter *pes1*) (Figure 2.4) was chosen to be the region amplified in the PCR analysis. Relative quantification of *pes1* gene expression was calculated by comparison to the constitutively expressed Calmodulin gene (calm) (AFUA_4G10050). This gene is expressed at the same level regardless of time-point, media, or additive (Burns *et al.*, 2005). Therefore, the expression of the gene of interest can be compared to the expression of calmodulin and the difference is expressed as a ratio, where the expression of calmodulin is adjusted to 1 and the expression of the gene of interest is expressed as a ratio compared to calmodulin expression.

Firstly, the expression of *pes1* was measured in the *A. fumigatus* strain ATCC46645 in different liquid media types, namely, Sabouraud media (SAB), Minimal media (MM), and Aspergillus Minimal media (AMM). The cultures were grown for 24, 48 and 72 hr (Figure 4.2). There is only low expression of *pes1* in Sabouraud media at 24 and 48 hr, and no expression detectable at 72 hr. The expression of *pes1* in MM media is approximately the same at 24 and 48 hr, whereas the expression level drops at 72 hr. The highest expression of *pes1* was seen in AMM media, where the highest expression was seen at 48 hr. The expression decreased to zero at 72 hr.
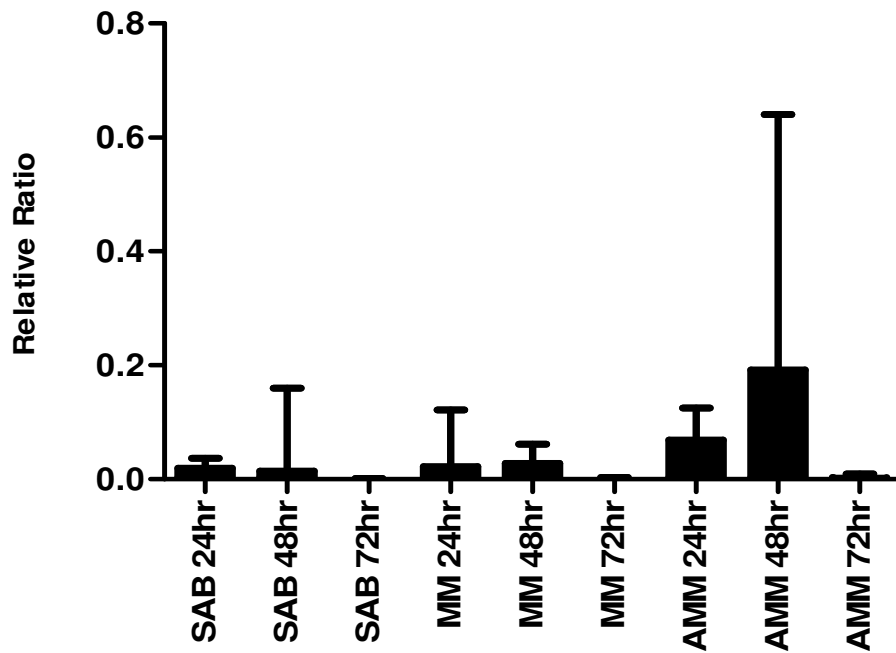
Figure 4.2: qRT-PCR analysis of *pes1* expression at 24, 48 and 72 hr in *A. fumigatus* ATCC46645 cultured in various media types at 37 °C.

Secondly, if successful, the disruption of *pes1* in the genome *A. fumigatus* ATCC46645 and Δ*sidD*[46645] should result in the absence of expression of the *pes1* gene. As AMM gave the greatest expression of *pes1*, this medium was chosen to establish an absence of *pes1* expression in the mutant strains. Since *pes1* expression was evident at 24 hr in AMM, this time-point was selected for subsequent analysis. *A. fumigatus* ATCC46645 and Δ*sidD*[46645] expressed *pes1*, whereas Δ*pes1*[46645] and Δ*sidD*:Δ*pes1* did not, confirming the disruption of *pes1* from the genome of these mutant strains. The complemented strain, Δ*sidD:pes1*[c], exhibited the highest expression of *pes1* (Figure 4.3).
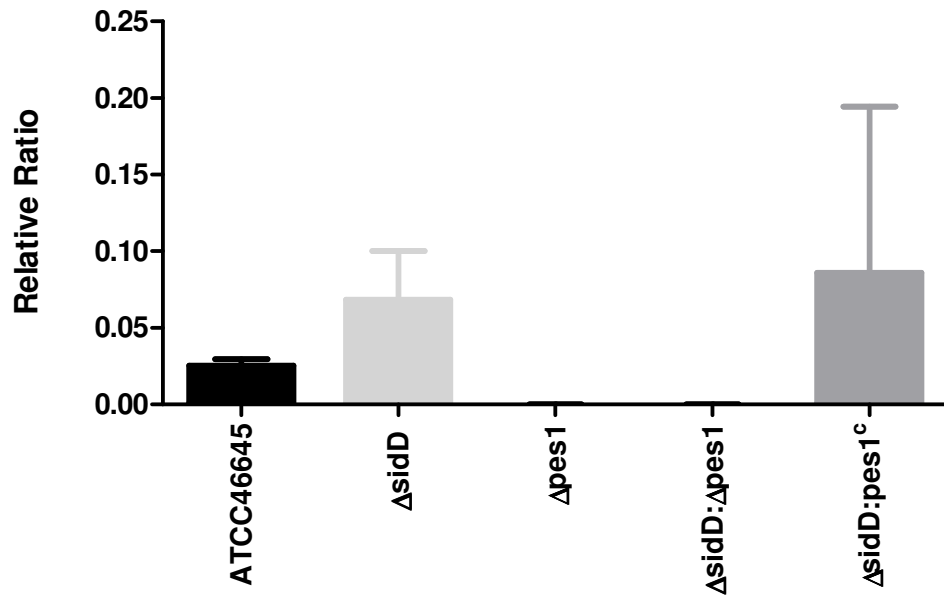
Figure 4.3: qRT-PCR analysis of *pes1* expression in *A. fumigatus* ATCC46645, Δ*sidD*[46645], Δ*pes1*[46645], Δ*sidD*:Δ*pes1* and Δ*sidD*:*pes1*[c] in AMM in 37 ^{o}C at 24 hr. The relative expression of *pes1* in ΔsidD had a 2.69 fold change higher than the expression of *pes1* in *A. fumigatus* ATCC46645. The expression of *pes1* had a 3.38 fold change higher in ΔsidD:pes1[c] than the expression of *pes1* in *A. fumigatus* ATCC46645. The analysis confirmed the disruption of *pes1* in ATCC46645 and ΔsidD as the Δ*pes1* expression in the Δ*pes1* and Δ*pes1*:Δ*sidD* strains was complely absent (*n* = 3).

AMM liquid cultures of *A. fumigatus* ATCC46645, Δ*sidD*[46645], and Δ*sidD*:*pes1*[c] were treated with hydrogen peroxide (1 mM final conc.) at 21 hr and the culture was harvested 3 hr later. The expression of *pes1* was evident (Figure 4.4), however exposure of *A. fumigatus* to hydrogen peroxide caused a decrease in *pes1* expression for all strains. The final concentration of hydrogen peroxide (1 mM) was chosen to ensure that the fungus was capable of maintaining growth and production of mycelia for the extraction of RNA.
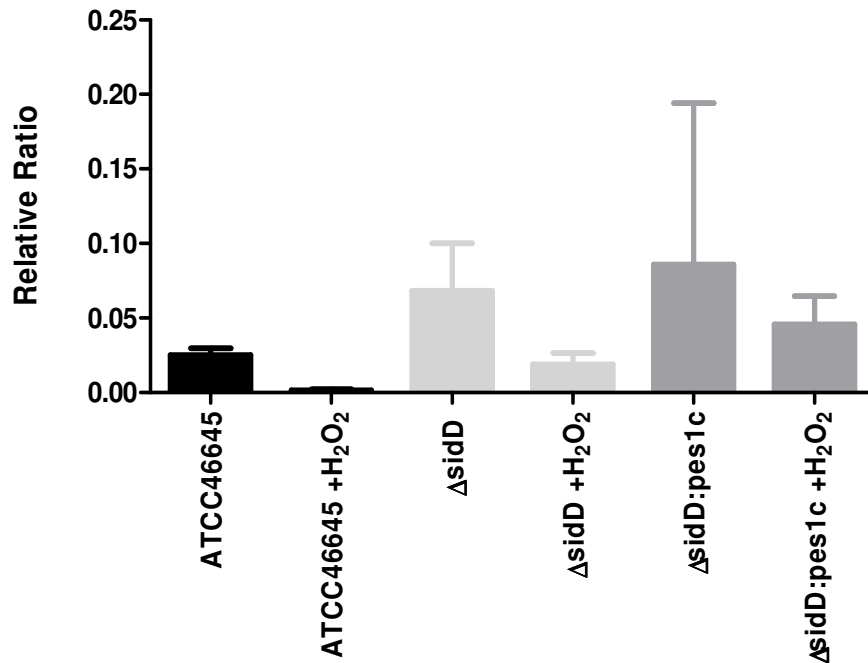
Figure 4.4: qRT-PCR analysis of *pes1* expression in *A. fumigatus* ATCC46645, *ΔsidD*[46645] and *ΔsidD:pes1*[c], with and without hydrogen peroxide (1 mM) spiked into the media.

4.2.2 Assessment of *A. fumigatus* Δ*pes1* susceptibility to oxidative stress and anti-fungal exposure

Reeves *et al.* (2006) showed that *pes1* plays an important role in oxidative stress response and virulence of *A. fumigatus*. Here, to further clarify these findings, *A. fumigatus* Δ*akuB* and Δ*akuB*:Δ*pes1* were exposed to hydrogen peroxide and various anti-fungal drugs, namely voriconazole and amphotericin B. The strains were also subjected to gliotoxin exposure to investigate if the toxin had any deleterious effect on the *pes1* deficient strains in this background.

4.2.2.1 Plate assays of A. fumigatus Δ*akuB*:Δ*pes1*

Initially, it was observed that *A. fumigatus* Δ*pes1* was only capable of maintaining 83 % growth compared to its wild-type, Δ*akuB*, but this growth difference was not

deemed significant (Figure 4.5). After 72 hr growth on AMM plates, there was a significant difference in the radial growth of *A. fumigatus* Δ*akuB:*Δ*pes1* strain compared to Δ*akuB*, when hydrogen peroxide (2 mM) was present (P < 0.01) (Figure 4.5). The presence of this concentration of hydrogen peroxide reduced *A. fumigatus* Δ*pes1* growth by 80 %, compared to the wild-type which, itself, was reduced by 40 %. *A. fumigatus* Δ*pes1* was unable to grow at 3 mM hydrogen peroxide, however, as the wild-type strain was only capable of 20 - 40 % growth at this concentration, this was not deemed significant. Neither strain was capable of growth at 4 mM hydrogen peroxide. At the lower hydrogen peroxide concentration (1 mM), both strains were capable of equivalent radial growth.
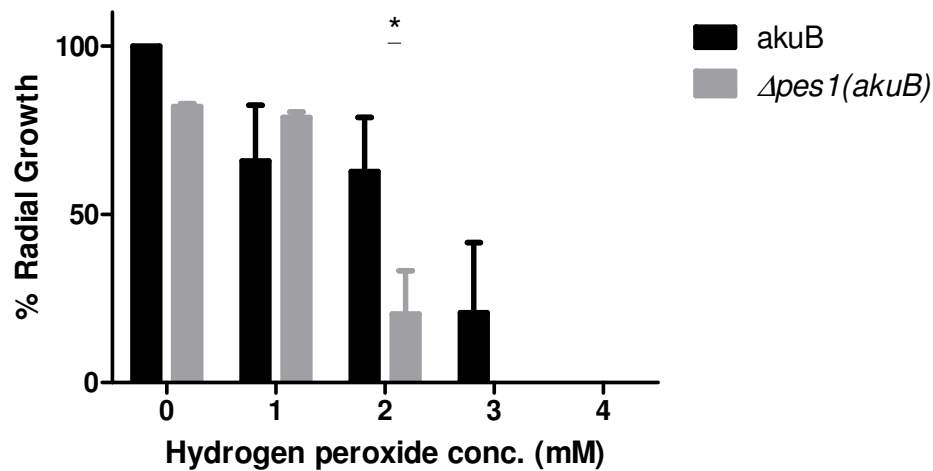
Figure 4.5: Effect of hydrogen peroxide on the growth of *A. fumigatus* Δ*akuB* and Δ*akuB:*Δ*pes1*, respectively. Significant growth inhibition of Δ*akuB:*Δ*pes1* was evident at 2 mM hydrogen peroxide compared to the wild-type, *akuB* (* = P < 0.01)(*n* = 4).

After 72 hr growth on AMM plates, there was a significant decrease in the radial growth of *A. fumigatus* Δ*akuB:*Δ*pes1* compared Δ*akuB* when voriconazole was present in the medium (Figure 4.6). The difference in radial growth was significant even at the lowest concentration of voriconazole (0.05 μg/ml) (P < 0.01). The difference is highly

significant when the voriconazole concentration was increased to 0.15 and 0.25 µg/ml, respectively (P < 0.001). The *akuB* background strain also exhibits a decrease in radial growth (~ 50 %) at the highest voriconazole concentration used (0.25 µg/ml), indicating that *A. fumigatus* is sensitive to high concentrations of voriconazole, under the experimental conditions used, as would be expected.
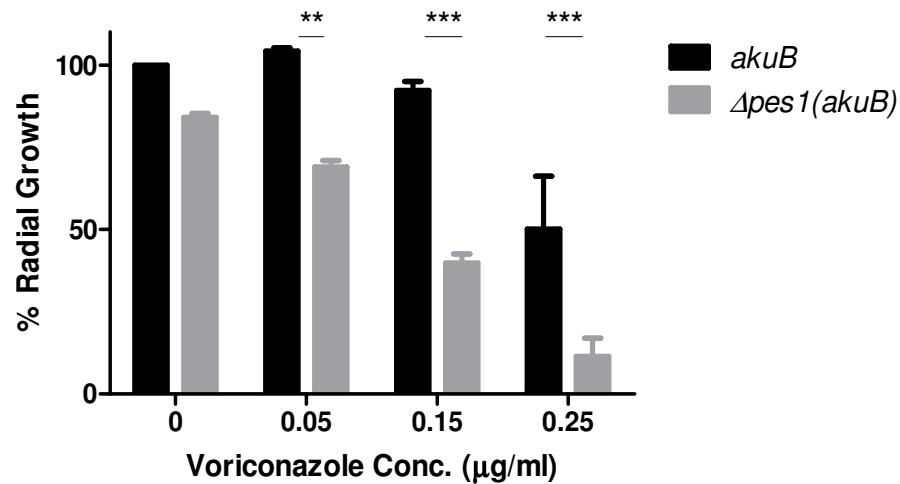
Figure 4.6: Effect of voriconazole (0 – 0.25 µg/ml) on the growth of *A. fumigatus* Δ*akuB* and Δ*akuB:*Δ*pes1*, respectively. Significant growth inhibition of Δ*akuB:*Δ*pes1*, compared to Δ*akuB*, is evident (** = P < 0.01, *** = P < 0.001)(n = 6).

After 72 hr growth on AMM plates, there was a significant decrease in the radial growth of *A. fumigatus* Δ*akuB:*Δ*pes1* compared to Δ*akuB* when amphotericin B was present in the media (Figure 4.7). *A. fumigatus* Δ*akuB* increased in radial growth at the lower concentrations of amphotericin B, 0.15 and 0.25 µg/ml, respectively, whereas *A. fumigatus* Δ*akuB:*Δ*pes1* decreased in radial growth significantly (P < 0.001) at these concentrations of amphotericin B. At the higher concentrations of amphotericin B, growth of *A. fumigatus* Δ*akuB* decreased but not to the same extent as Δ*akuB:*Δ*pes1* (P < 0.01).
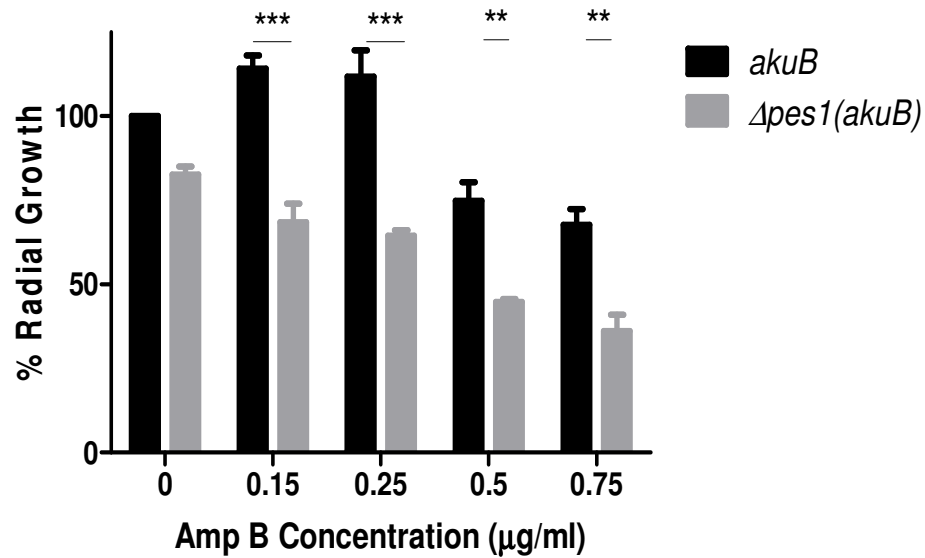
Figure 4.7: Effect of amphotericin B on the growth of *A. fumigatus* Δ*akuB* and Δ*akuB:*Δ*pes1*, respectively. Significant growth inhibition of Δ*akuB:*Δ*pes1*, compared to Δ*akuB*, is evident at 0.15 – 075 μg/ml amphotericin B (** = P < 0.01, *** = P < 0.001)(*n* = 2).

After 72 hr on AMM plates in the presence of gliotoxin (0 – 20 μg/ml), there was no significant growth difference between *A. fumigatu*s Δ*akuB* and Δ*akuB:*Δ*pes1* strains (Figure 4.8).
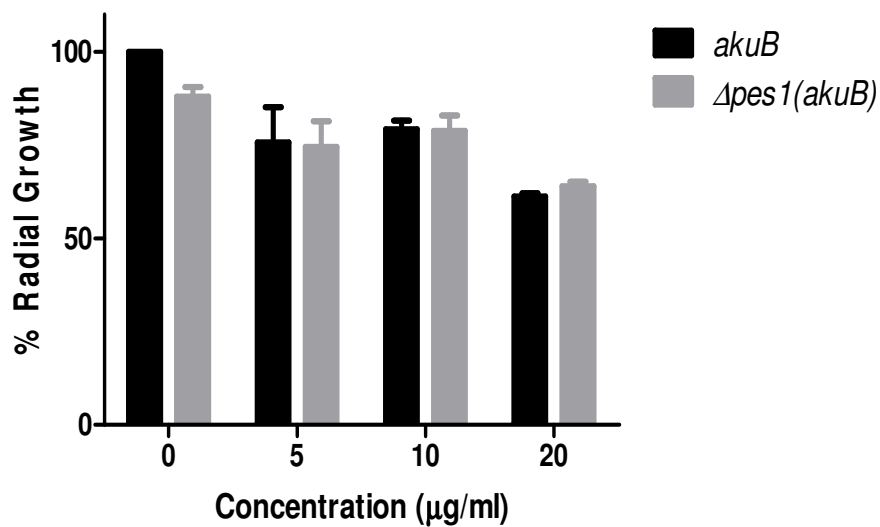
Figure 4.8: Effect of gliotoxin on the growth of *A. fumigatus* Δ*akuB* and Δ*akuB:*Δ*pes1*, respectively. No significant growth inhibition of Δ*akuB:*Δ*pes1* is evident (*n* = 4).

Both strains were still maintaining over 50 % growth at the highest concentration of gliotoxin (20 μg/ml), and the reduction in growth is significantly different from the growth observed without gliotoxin added, where Δ*akuB* was capable of 61 % growth (P < 0.001) and Δ*akuB*:Δ*pes1* was capable of 63 % growth (P < 0.05) (Figure 4.9).
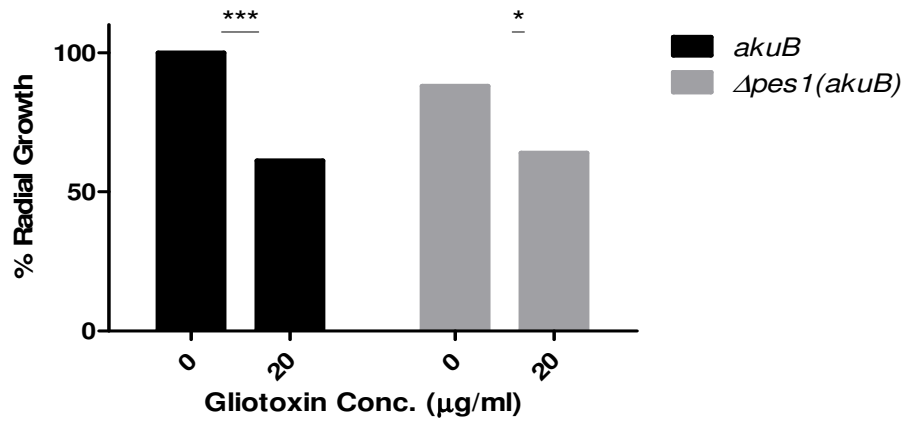
Figure 4.9: Effect of gliotoxin on the growth of *A. fumigatus* Δ*akuB* and Δ*akuB*:Δ*pes1*, respectively. Significant growth inhibition was evident at 20 μg/ml gliotoxin application for both strains (*** = P < 0.001, * = P < 0.05). Redrawn from Figure 4.8 for clarity.

4.2.2.2 Phenotypic analysis of *A. fumigatus* Δ*pes1*[46645]

After 72 hr growth on AMM plates in the presence of hydrogen peroxide (0 – 4 mM), there was no significant growth difference between the *A. fumigatus* ATCC46645 and Δ*pes1*[46645] strains (Figure 4.10).
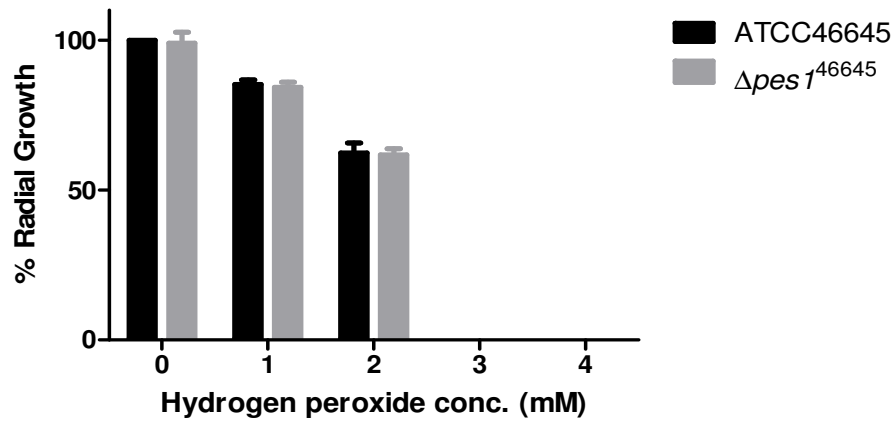
Figure 4.10: Effect of hydrogen peroxide on the growth of *A. fumigatus* ATCC46645 and Δ*pes1*[46645], respectively. No significant growth inhibition of Δ*pes1*[46645] was evident (*n* = 4).

After 72 hr on AMM plates in the presence of voriconazole, there was a significant decrease in the radial growth of *A. fumigatus* Δ*pes1*[46645] compared to ATCC46645 when voriconazole was present in the media (Figure 4.11). The difference is significant when the voriconazole concentration is 0.15 μg/ml ($P < 0.05$). Both strains were incapable of growth at 0.25 μg/ml concentration of voriconazole.
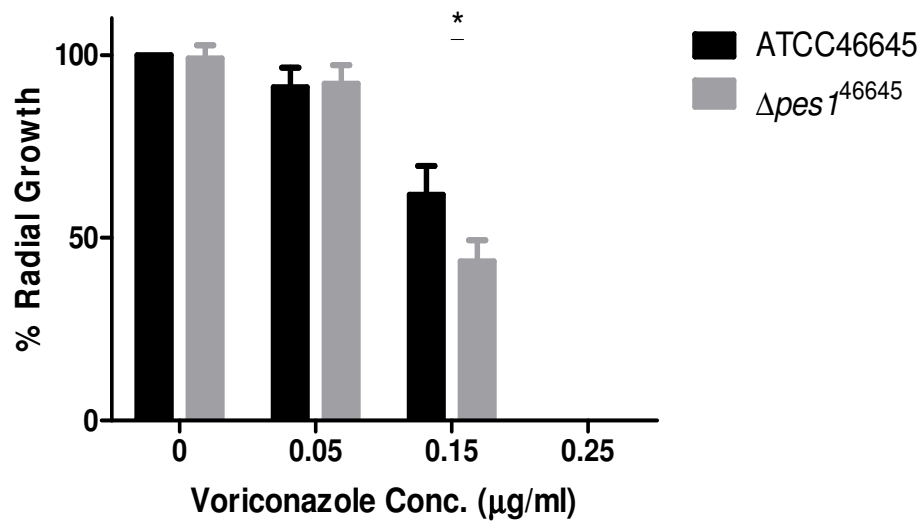
Figure 4.11: Effect of voriconazole on the growth of *A. fumigatus* ATCC46645 and Δ*pes1*[46645], respectively. Significant growth inhibition of Δ*pes1*[46645] was evident in the preence of voriconazole (0.15 μg/ml), compared to *A. fumigatus* ATCC46645 (* = P < 0.05) (*n* = 4).

After 72 hr growth on AMM plates in the presence of amphotericin B (0 – 0.75 μg/ml), there was no significant growth difference between the *A. fumigatus* ATCC46645 and Δ*pes1*[46645] strains (Figure 4.12).
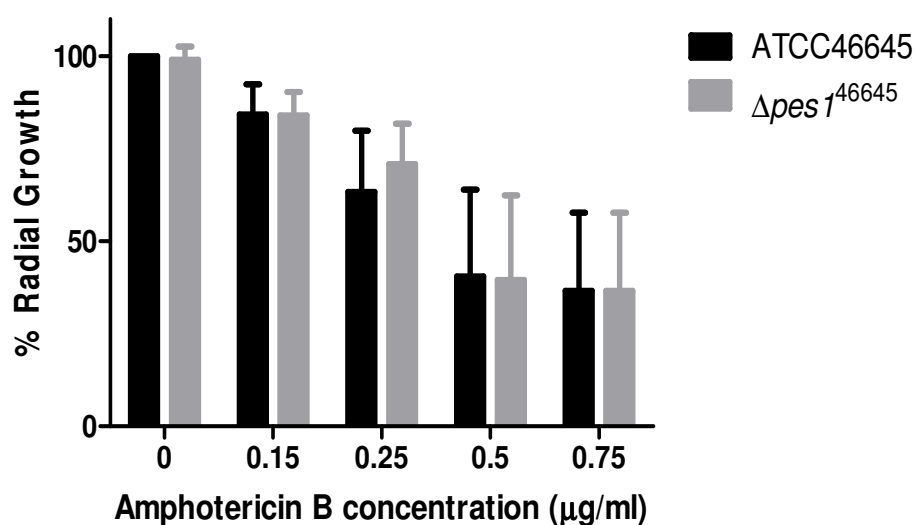
Figure 4.12: Effect of amphotericin B on the growth of *A. fumigatus* ATCC46645 and Δ*pes1*[46645], respectively. No significant growth inhibition of Δ*pes1*[46645] was evident (*n* = 4).

4.2.2.3 Phenotypic analysis of *A. fumigatus* double mutant, Δ*sidD*:Δ*pes1*

After 72 hr growth on MM plates in the presence of hydrogen peroxide, significant growth difference was observed between ATCC46645 and Δ*sidD*[46645] and also between ATCC46645 and Δ*sidD*:Δ*pes1* at a concentration of 2 mM hydrogen peroxide (P < 0.001) (Figure 4.13), however there was no significant difference in radial growth between *A. fumigatus* Δ*sidD*[46645] and Δ*sidD*:Δ*pes1*.
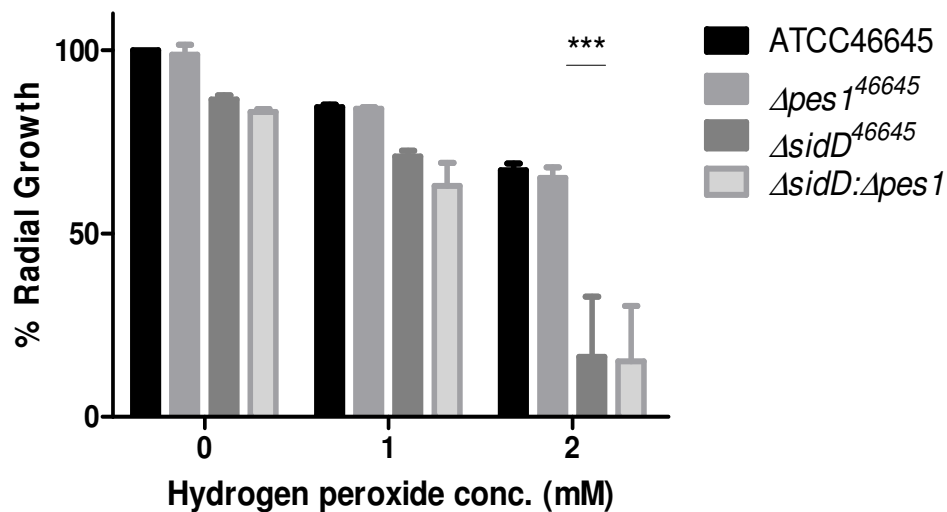
Figure 4.13: Effect of hydrogen peroxide on the growth of *A. fumigatus* ATCC46645, *Δpes1*[46645], Δ*sidD*[46645], and Δ*sidD*:Δ*pes1*, respectively. Significant growth inhibition of Δ*sidD*[46645] and Δ*sidD:*Δ*pes1* was evident at the highest concentration of hydrogen peroxide (2 mM), compared to wild-type (*** = P < 0.001) (*n* = 3).

After 72 hr growth on MM plate in the presence of voriconazole (0 – 0.5 µg/ml), significant growth differences were observed between ATCC46645 and Δ*sidD*[46645] and also between ATCC46645 and Δ*sidD*:Δ*pes1* at a concentration of 0.05 µg/ml voriconazole (P < 0.001) (Figure 4.14). At the higher concentration of 0.15 µg/ml voriconazole, there was a significant growth difference between ATCC46645 and Δ*sidD*[46645] (P < 0.01). There was also lower significant growth difference between ATCC46645 and Δ*pes1*[46645] and also between ATCC46645 and Δ*sidD*:Δ*pes1* at this concentration of voriconazole, but to a lesser extent (P < 0.05). No significant growth differences were observed between Δ*pes1*[46645], Δ*sidD*[46645] and Δ*sidD*:Δ*pes1* indicating that there is no additive effect of voriconazole sensitivity in Δ*sidD*:Δ*pes1*.
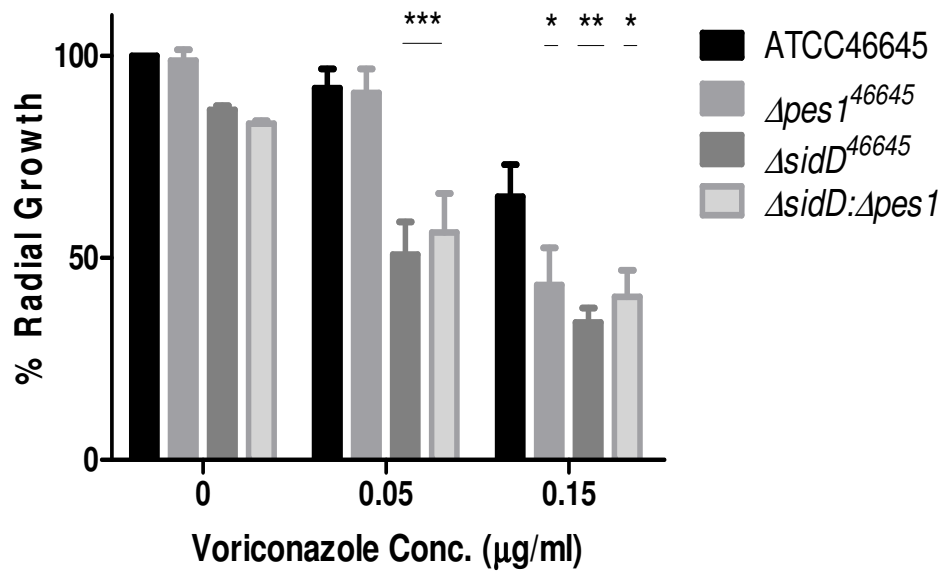
Figure 4.14: Effect of voriconazole on the growth of *A. fumigatus* ATCC46645, *Δpes1*[46645], Δ*sidD*[46645], and Δ*sidD*:Δ*pes1*, respectively. Significant growth inhibition of Δ*sidD*[46645] and Δ*sidD*:Δ*pes1* was evident (*** = $P < 0.001$, ** = $P < 0.01$, * = $P < 0.05$) ($n = 3$).

After 72 hr growth on MM plates in the presence of amphotericin B (0 – 0.75 µg/ml), significant growth differences were observed between *A. fumigatus* ATCC46645 and Δ*sidD*:Δ*pes1* at 0.15 µg/ml concentration ($P < 0.05$) (Figure 4.15). No other significant growth differences were observed.
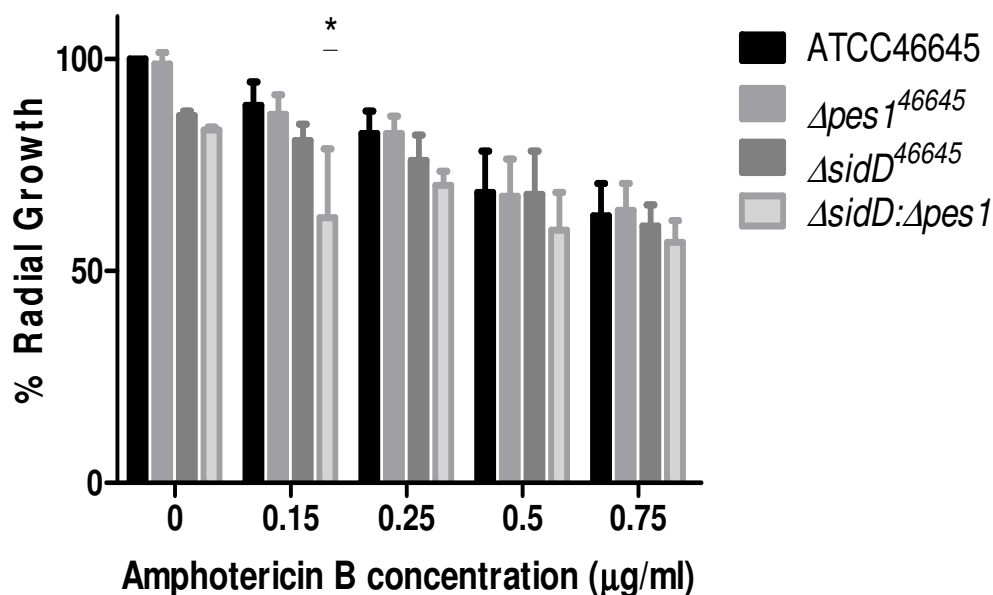
Figure 4.15: Effect of amphotericin B on the growth of *A. fumigatus* ATCC46645, Δ*pes1*[46645], Δ*sidD*[46645], and Δ*sidD*:Δ*pes1*, respectively. Significant growth inhibition of Δ*sidD*:Δ*pes1* was evident at the lowest concentration of amphotericin B (0.15 μg/ml) (* = P < 0.05) (*n* = 3).

4.2.3 Evaluation of culture media type and iron on fungal growth

Conidia (~100 spores/ 10 μl) were inoculated onto agar plates of AMM or MM, which differed in their respective nitrogen sources. AMM media contained ammonium tartrate as the nitrogen source, whereas MM media contained L-glutamine. L-glutamine is involved in the production of L-ornithine (Jones, 1985), which is used in the first committed step in siderophore biosynthesis (Eisendle *et al.*, 2003). Consequently, *A. fumigatus* Δ*sidD* and Δ*sidD*:Δ*pes1* were unable to grow on AMM (Figure 4.16), unless a high concentration of iron was present in the media(1.5 mM). The high concentration of iron (1.5 mM) is 150 times the concentration of iron used in standard *Aspergillus* growth medium (Eisendle *et al.*, 2003).

On media containing L-glutamine, the Δ*sidD*[46645] and Δ*sidD*:Δ*pes1* strains were capable of significant growth in the presence of low levels of iron (10 μM) (Figure

4.16). The iron supply limitation coupled with the potential absence of the *pes1* peptide product caused a trend towards an accumulative detrimental effect in this low iron condition. Therefore, Minimal media containing L-glutamine was used for all further plate assay experiments using *A. fumigatus* Δ*sidD* and Δ*sidD*:Δ*pes1*, to ensure all strains were capable of measureable growth in the basic media.

As expected, in the presence of bathophenanthroline disulfonic acid disodium salt (BPS), both *A. fumigatus* Δ*sidD* and Δ*sidD*:Δ*pes1* were unable to grow as BPS chelates all available iron (Figure 4.16). Therefore due to the absence of *sidD,* the mutant strains are unable to produce TAFC to remove the iron bound to BPS and are incapable of surviving in the absence of iron. The same result was observed, as expected, in the iron deficient (-Fe) media (Figure 4.16).

A

Effect of media type on *A. fumigatus* Δ*sidD radial growth*

Ammonium tartrate

Legend:
- ATCC46645
- ΔsidD[46645]
- ΔsidD:Δpes1

B

Effect of media type on *A. fumigatus* Δ*sidD radial growth*

L-glutamine

Legend:
- ATCC46645
- *ΔsidD*[46645]
- *ΔsidD:Δpes1*
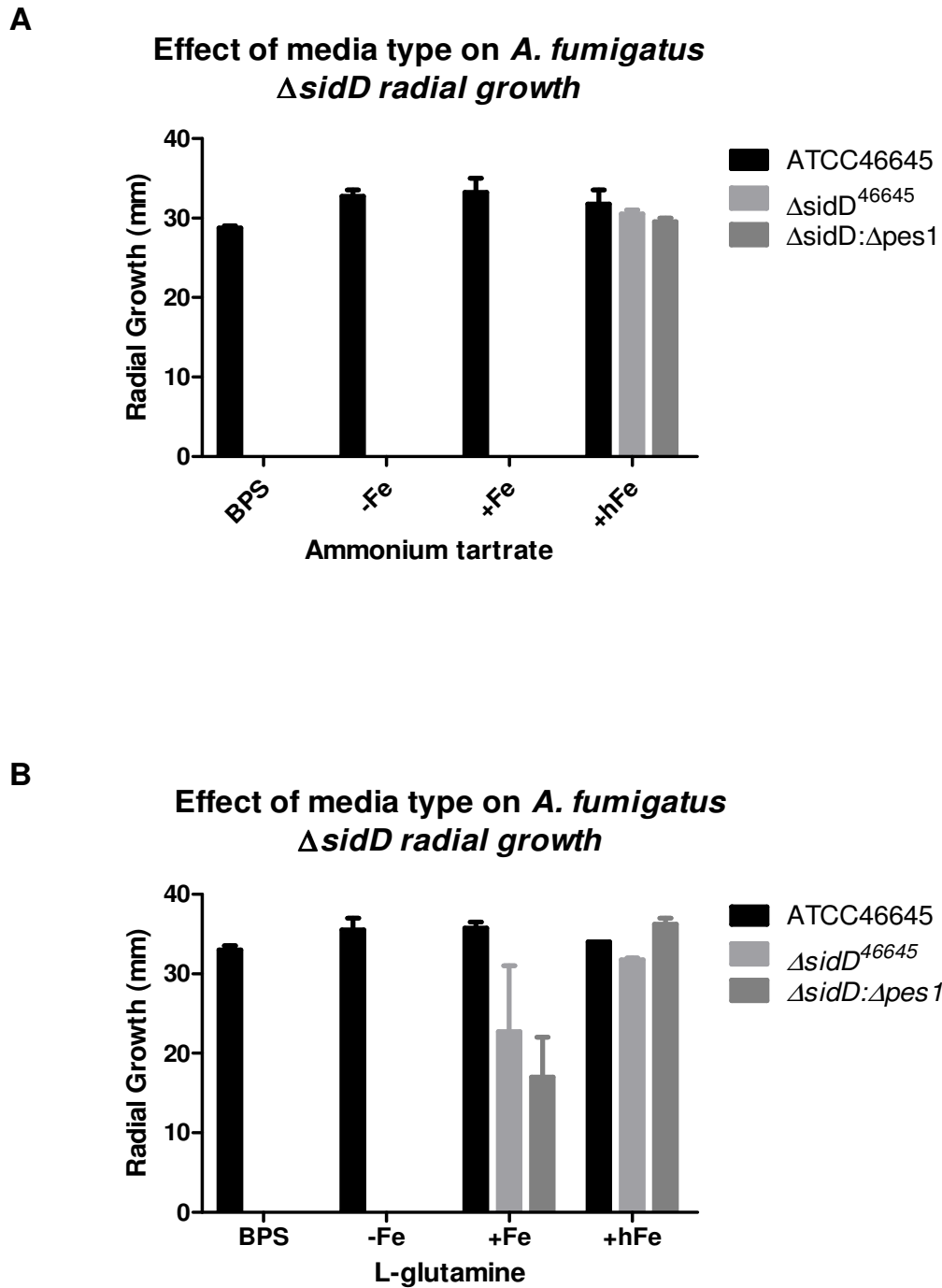
Figure 4.16: Effect of media type in conjunction with increasing levels of iron available, on *A. fumigatus* growth containing Δ*sidD*. (A) radial growth on media containing ammonium tartrate. (B) radial growth on media containing L-glutamine in conjunction with increasing levels of iron available. Iron availability is noted as BPS: iron chelator; -Fe: No iron added to media; +Fe: 10 μM $FeSO_4$; and +hFe: 1.5 mM $FeSO_4$ Significant difference in radial growth is observed in Δ*sidD* and Δ*sidD*:Δ*pes1* strains, compared to wild-type, between the two media types (P < 0.001) (*n* = 2).

Furthermore, the source of iron plays an important role in the radial growth capabilities of *A. fumigatus* Δ*sidD*[46645] and Δ*sidD*:Δ*pes1* (Figure 4.17). Conidia (100 spores/ 10μl) were inoculated onto plates containing a low concentration of iron (10 μM), Δ*sidD*[46645] and Δ*sidD*:Δ*pes1* were unable to grow when the iron source was $FeCl_3$, whereas, when $FeSO_4$ was the iron source, these strains were capable of maintaining some growth, although this growth was still significantly different from *A. fumigatus* ATCC46645. Notably, Δ*sidD*:Δ*pes1* showed a trend towards a lower capability of growth in the iron limited condition, compared to Δ*sidD*, when both growth rates were compared to the wild-type ($P < 0.001$ and $P < 0.01$, respectively). Both iron sources at the higher concentration (1.5 mM) resulted in restoration of full growth for both *sidD* deficient strains. This iron-dependant growth capability has been noted previously in *Aspergillus spp.* (Eisendle *et al.*, 2003).
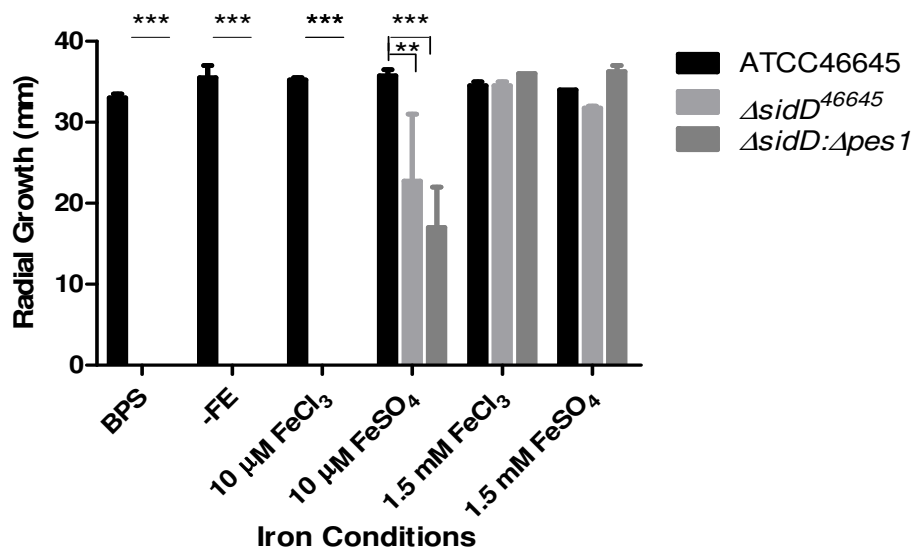
Figure 4.17: Effect of the source of iron in minimal media on *A. fumigatus* ATCC46645, Δ*sidD*[46645] and *ΔsidD:Δpes1* (*** = $P < 0.001$, ** = $P < 0.01$) (*n* = 2).

After 72 hr growth on minimal media with L-glutamine as the nitrogen source, an interaction between growth and hydrogen peroxide and available iron was observed. *A. fumigatus* ΔsidD[46645] and ΔsidD:Δpes1 were unable to grow in the absence of iron in conjunction with the presence of hydrogen peroxide at different concentrations (0 – 4 mM) (P < 0.001), due to the absence of *sidD* (Figure 4.18).
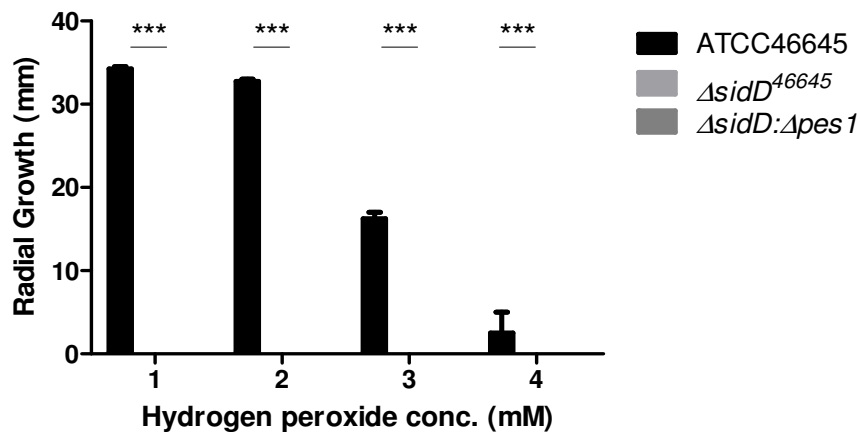
Figure 4.18: Effect of hydrogen peroxide on the growth of *A. fumigatus* ATCC46645, ΔsidD[46645], ΔsidD:Δpes1 without iron present in the media (*** = P < 0.001) (*n* = 2).

Supplementing with $FeCl_3$ (10 μM) did not restore the growth of either ΔsidD[46645] or ΔsidD:Δpes1 (P < 0.001) (Figure 4.19 (A)). The addition of a higher concentration of $FeCl_3$ (1.5 mM) resulted in 100 % growth capabilities of all strains in all concentrations of hydrogen peroxide used (0 – 4 mM) (Figure 4.19 (B)). Using $FeSO_4$ (10 μM) as the iron source, growth of *A. fumigatus* ΔsidD[46645] and ΔsidD:Δpes1 was observed at lower concentrations of hydrogen peroxide (0 – 2 mM) (P < 0.01), although the double mutant appeared to grow slightly better under these conditions (Figure 4.19 (C)). The addition of a higher concentration of $FeSO_4$ (1.5 mM) resulted in 100 % growth of all strains in all concentrations of hydrogen peroxide tested (0 – 4 mM) (Figure 4.19 (D)).
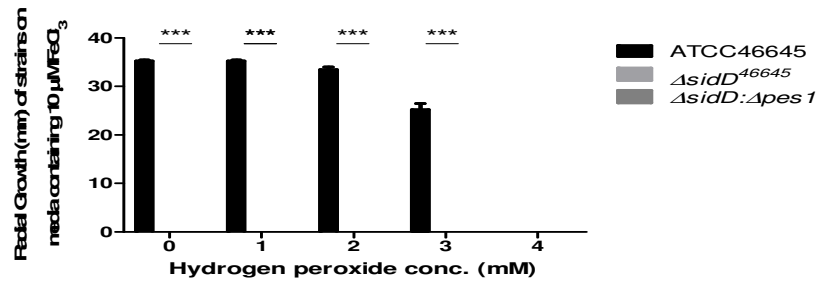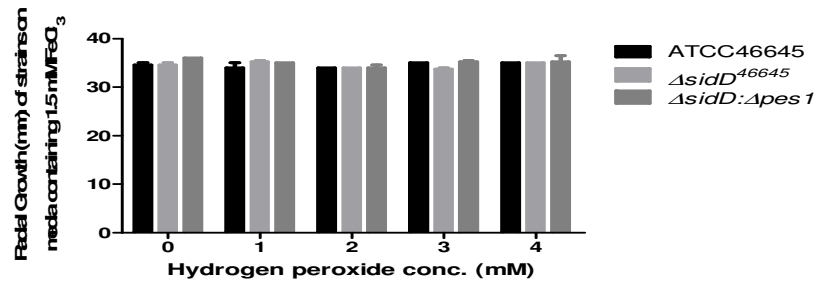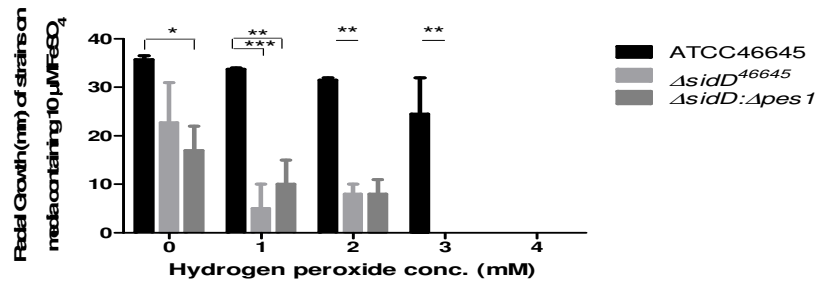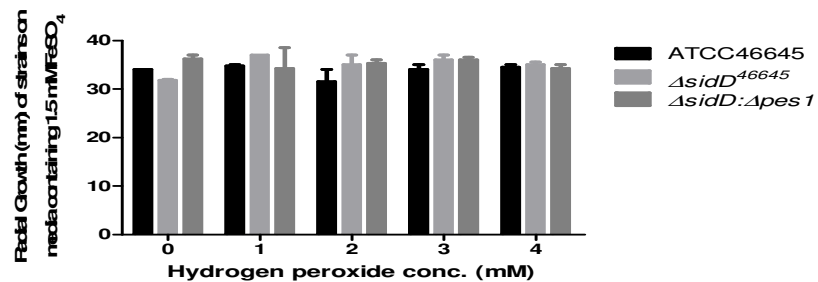
Figure 4.19: Effect of hydrogen peroxide on the growth of *A. fumigatus* ATCC46645, $\Delta sidD^{46645}$, $\Delta sidD$:$\Delta pes1$ in conjunction with different iron sources (A) radial growth on increasing hydrogen peroxide with 10 μM FeCl$_3$ as the iron source, (B) radial growth on increasing hydrogen peroxide with 1.5 mM FeCl$_3$ as the iron source, (C) radial growth on increasing hydrogen peroxide with 10 μM FeSO$_4$ as the iron source, (D) radial growth on increasing hydrogen peroxide with 1.5 mM FeSO$_4$ as the iron source (*** = $P < 0.001$, ** = $P < 0.01$, * = $P < 0.05$) ($n = 2$).

Interestingly, growth of *A. fumigatus* ATCC46645 in hydrogen peroxide (3 mM) is the same regardless of the iron source used (Figure 4.20). Without iron present, ATCC46645 is capable of a maximum radial growth of ~16 mm, whereas the addition of iron (10 μM), the radial growth reached ~25 mm and the addition of the higher concentration of iron (1.5 mM) resulted in a radial growth of ~35 mm, on either iron source.
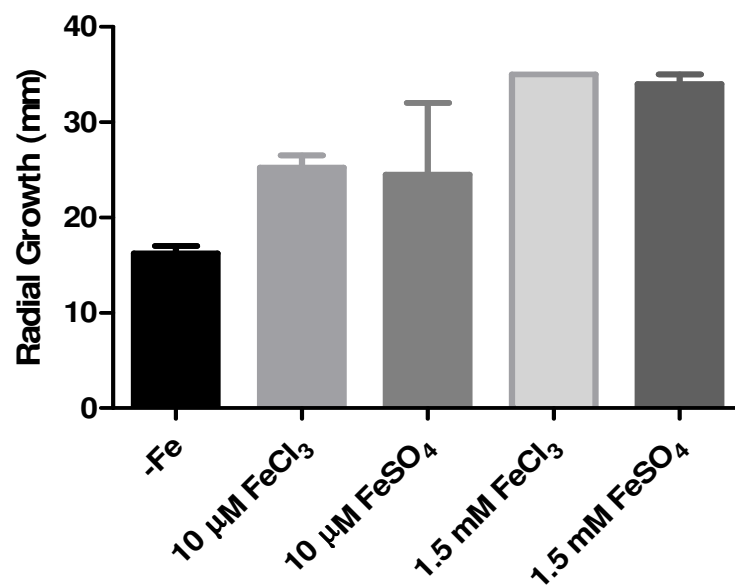
Figure 4.20: Effect of the source of iron in conjunction with the exposure to hydrogen peroxide (3 mM) on the growth of *A. fumigatus* ATCC46645.

4.2.4 Galleria infection model

Galleria mellonella larvae are used as a model system for the innate immune response of mammals to infection with *A. fumigatus* and to assess the relative virulence of fungal mutants (Kavanagh and Reeves, 2004). The larvae were injected with conidia (1×10^6) and incubated for up to 72 hr at 30 $^{\circ}$C, as described in Section 2.2.25 and were inspected at 24, 48 and 72 hr for survival. The melanisation of the larvae was easily observed indicating the presence of *A. fumigatus* is causing an immune response within the larvae. The difference between *A. fumigatus* ATCC46645 and $\Delta sidD^{46645}$, $\Delta pes1^{46645}$ and $\Delta sidD$:$\Delta pes1$ was clear at the 48 hr time point (Figure 4.21 and Figure 4.22).
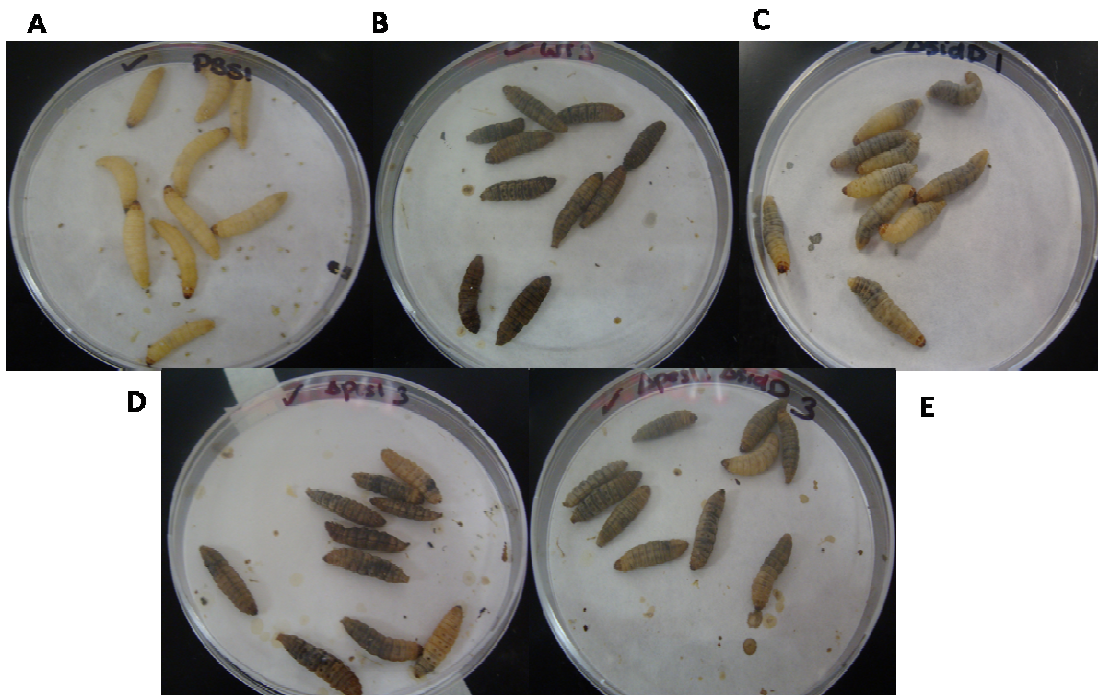
Figure 4.21: *Galleria mellonella* larvae displaying different levels of melanisation due to injection of *A. fumigatus* conidia (48 hr) (A) PBS control; (B) ATCC46645; (C) $\Delta sidD^{46645}$; (D) $\Delta pes1^{46645}$; and (E) $\Delta sidD$:$\Delta pes1$.

Survival curves, representative of three independent experiments, are shown in Figure 4.22. All the larvae showed similar survival rates at 24 hr. At 48 hr the difference between the strains became more evident. The *A. fumigatus* strains clustered into two groups at the 48 hr time point with a low survival rate group consisting of ATCC46645 (25 % survival), Δ*pes1*[46645] (30 %), and Δ*sidD:pes1*[c] (33 %). The second group had a higher survival rate consisting of Δ*sidD*[46645] (48 %), and Δ*sidD:*Δ*pes1* (53 %). Indicating that *sidD* plays a more important role in the pathogenicity of *A. fumigatus* than *pes1*. Mortality (100 %) was observed for all larvae after 72 hr incubation, except for the PBS controls.
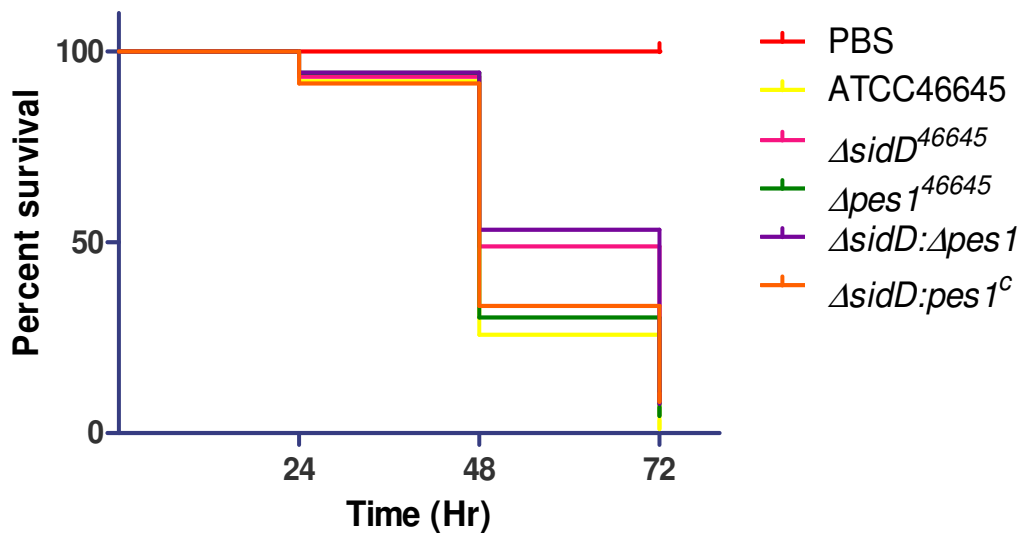
	Δ*sidD*	Δ*pes1*	Δ*sidD* : Δ*pes1*	Δ*sidD :pes1*[c]
ATCC46645	*** P=0.001	NS	*** P=0.0002	NS
Δ*sidD*		* P=0.028	NS	NS
Δ*pes1*			** P=0.0082	NS
Δ*sidD* : Δ*pes1*				NS

Figure 4.22: Survival of *Galleria mellonella* larvae infected with *A. fumigatus* ATCC46645, Δ*sidD*[46645], Δ*pes1*[46645], Δ*sidD*:Δ*pes1* and Δ*sidD*:*pes1*[c] and relevant significance table (* = P < 0.01, ** = P < 0.01, *** = P < 0.001) (*n* = 90).

4.2.5 Identification of non-ribosomal peptide encoded by *A. fumigatus pes1*

Pes1, as an NRP synthetase, is highly likely to be involved in the biosynthesis of a low molecular mass metabolite. Thus, culture supernatants were examined for the presence of such a metabolite, by comparing the metabolite profile from culture supernatants of the *A. fumigatus* wild-type strain to the *pes1* mutant strains. Supernatants were collected from liquid cultures and subjected to organic extraction as described in Section 2.2.10. Organic extracts were fractionated by Reversed Phase – High Performance Liquid Chromatography (RP – HPLC), as described in Section 2.2.13.1. Initial results revealed a similar metabolite profile from wild-type and mutant strains (Figure 4.23).

For a more detailed analysis, the strains were grown on AMM agar plates and point inoculated into the centre of the plate and incubated for five days at 37 ^{o}C. Organic extraction of agar plugs were taken and organic material was extracted as described in Section 2.2.12 (Smedsgaard, 1997). The extracts were analysed in triplicate in collaboration with the Denmark Technical Institute, by LC-MS-DAD, as described in Section 2.2.13.2. Figure 4.24 details the RP-HPLC chromatograms for *A. fumigatus* wild-type and Δ*pes1* strains.
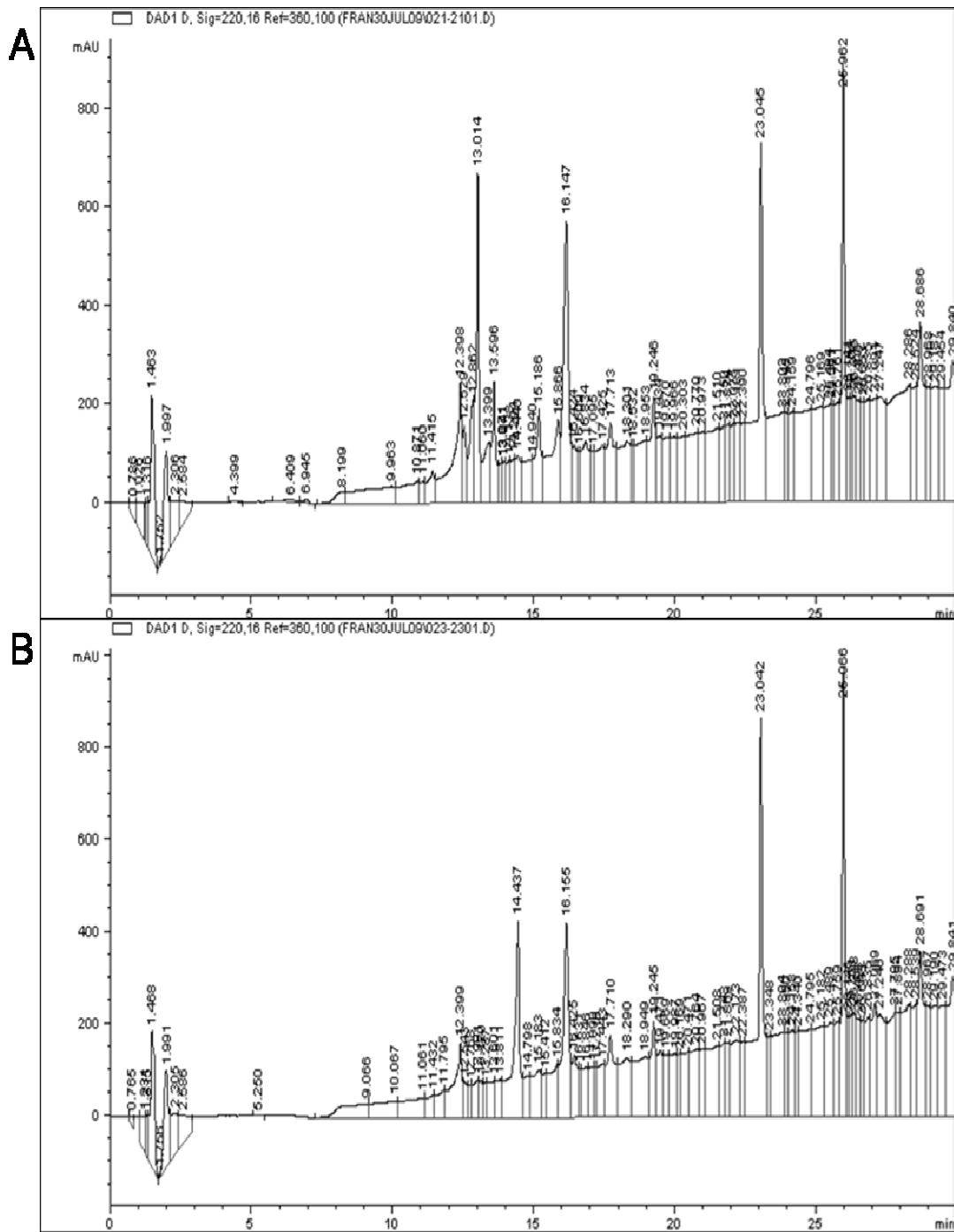
Figure 4.23: HPLC chromatograms detailing the fractionation of metabolites from supernatant organic extractions of *A. fumigatus* liquid cultures for the identification of the *pes1* product, at 220nm. (A) ATCC46645 and (B) Δ*pes1*[46645], which show extremely similar metabolite profiles.

Fumigaclavine C was present in both *A. fumigatus* Δ*akuB* and ATCC46645 but absent in both Δ*akuB:*Δ*pes1* and Δ*pes1*[46645] (Figure 4.24 and Figure 4.25). The RP-HPLC chromatograms clearly demonstrate that the wild-type strains produce a high amount of fumigaclavine C, whereas in the mutant strains, fumigaclavine C is completely absent. This significant observation represents the first confirmation of *A. fumigatus pes1* involvement in the biosynthesis of a specific metabolite.

Fumigaclavine C is the final product of a complex biosynthetic pathway (Unsold and Li, 2005) and it was suspected that loss of fumigaclavine C production might result in increased levels of putative biosynthetic intermediates or related fumigaclavines. Thus, the presence of additional metabolites was assessed during these fractionations. Fumigaclavine A was present in all strains, and production appeared to be increased in *A. fumigatus* Δ*akuB*:Δ*pes1* compared to Δ*akuB*, however Δ*pes1*[46645] produced the same level of fumigaclavine A as ATCC46645 (Figure 4.24 and Figure 4.25). An unidentified metabolite with a mass of 309 (retention time 5.17 min) is only observed in Δ*akuB* and is absent in all the other strains (Figure 4.24 and Figure 4.25). TR-2 and fumitremorgin C are absent in Δ*akuB*, but present in Δ*akuB*:Δ*pes1* (Figure 4.24) whereas both metabolites are present in ATCC46645 and Δ*pes1*[46645], with a slight increase in production in *Δpes1*[46645] (Figure 4.25). Fumitremorgin B and A are absent in all strains. Verruculogen is present in all strains, but the production is increased in both Δ*pes1* strains (Figure 4.24 and Figure 4.25).
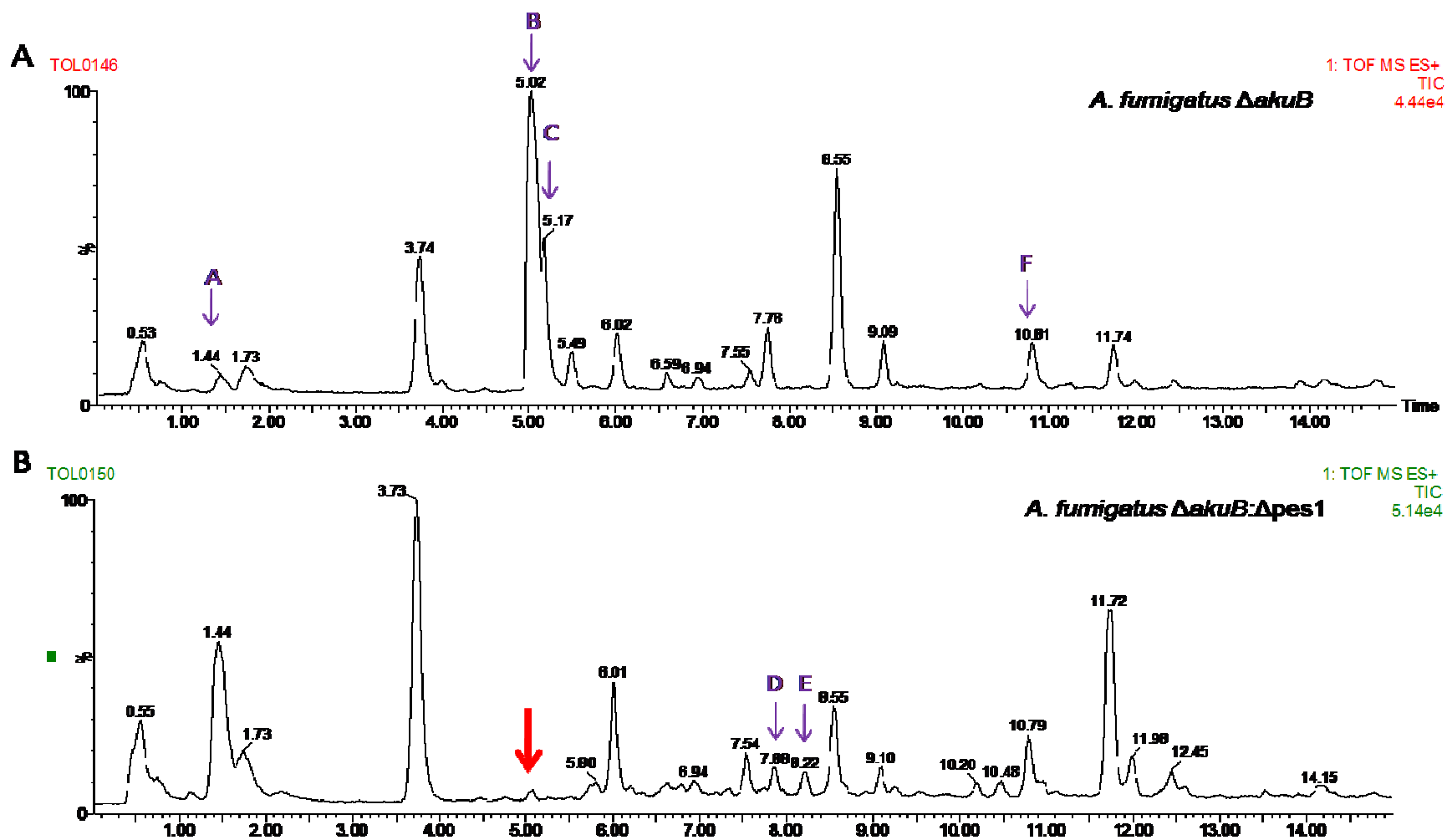
Figure 4.24: Total ion chromatograms (0 – 15 min) representative of metabolites detected from *A. fumigatus* (A) Δ*akuB* and (B) Δ*akuB*:Δ*pes1*. Major differences between the chromatograms are annotated as follows; A; Fumigaclavine A (1.44 min), B; Fumigaclavine C (5.02 min), C; unknown peak (m/z 309) (5.17 min), D; TR-2 (7.88 min) E; Fumitremorgin C (8.22 min) and F; Verruculogen (shouldering peak 10.96 min). Red arrow highlights the absence of fumigaclavine C in Δ*akuB*:Δ*pes1*.
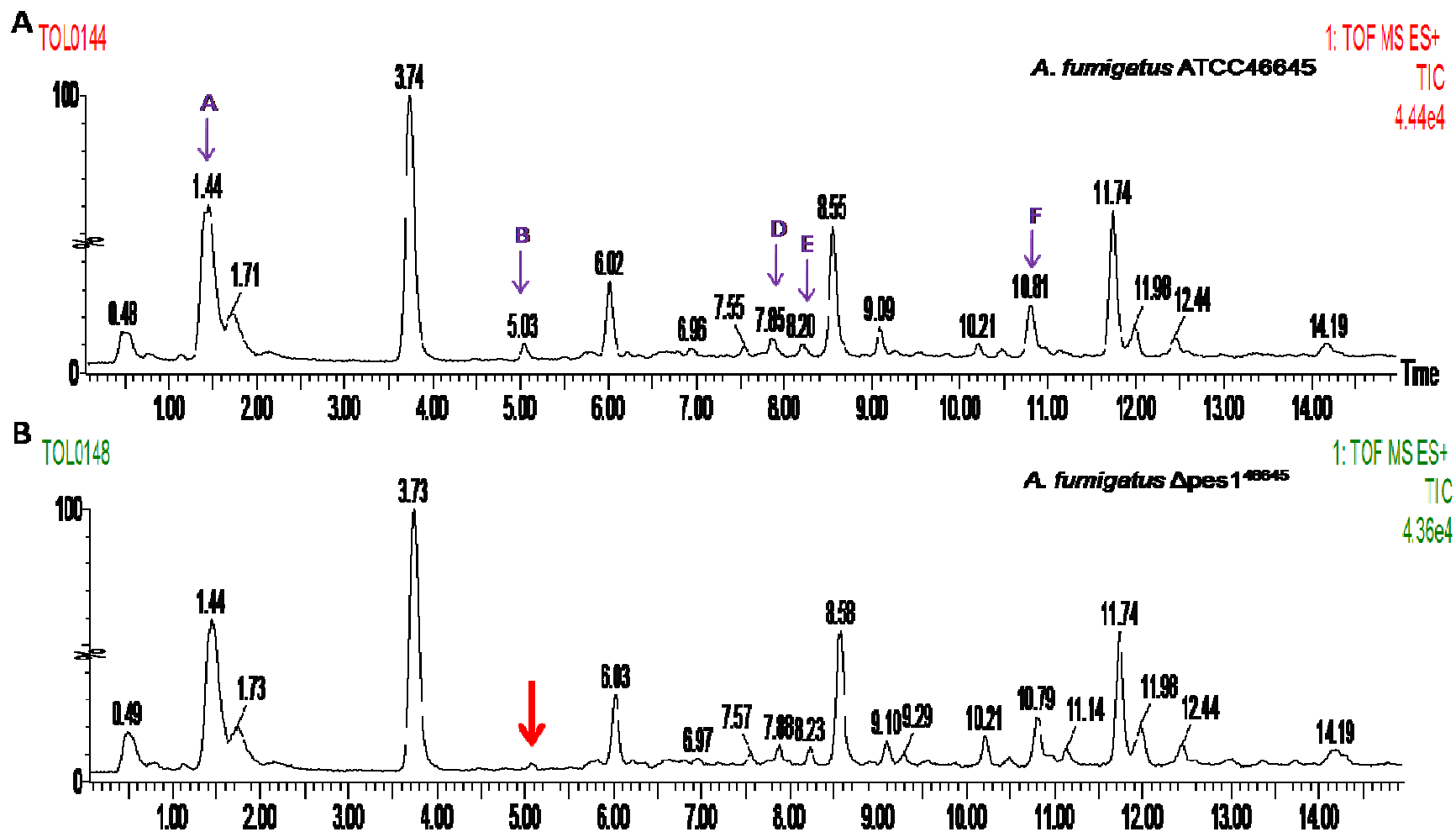
Figure 4.25: Total ion chromatograms (0 – 15 min) representative of metabolites detected from *A. fumigatus* (A) ATCC46645 and (B) *Δpes1*[46645]. Major differences between the chromatograms are annotated as follows; A; Fumigaclavine A (1.44 min), B; Fumigaclavine C (5.03 min), D; TR-2 (7.88 min) E; Fumitremorgin C (8.22 min) and F; Verruculogen (shouldering peak 10.96 min). Red arrow highlights the absence of fumigaclavine C in *Δpes1*[46645].

Identification of each of the metabolites was confirmed by searching for the specific mass of each metabolite. Fumigaclavine C was identified by searching for a mass of 367 $[M+H]^+$, where the fumigaclavine C peak was observed at a retention time of 5.03 min. This peak was absent in the $\Delta pes1$ strains (Figure 4.26). Fumigaclavine A was identified by searching for a mass of 299 $[M+H]^+$, and was identified in all strains at a retention time of 1.44 min (Figure 4.27). Fumitremorgin C was identified at m/z 390 $[M+H]^+$ and also by UV spectrophotometry (Figure 4.28). TR-2 was identified at m/z 394 $[M-2xH_2O+H]^+$ and also be UV spectrophotometry (Figure 4.28). Verruculogen was identified by ion trace mass spectrometry, where it was identified at m/z 512 $[M+H]^+$ with a retention time of 10.97 min and also at m/z 494 $[M-H_2O+H]^+$ with a retention time of 10.96 min (Figure 4.29). Verruculogen elutes slightly later than, and appears as a shoulder of, the pseurotin A or D peaks (m/z 432 for $[M+H]^+$) at 10.79 and 10.81 min. A summary of all metabolites identified is detailed in Table 4.1.
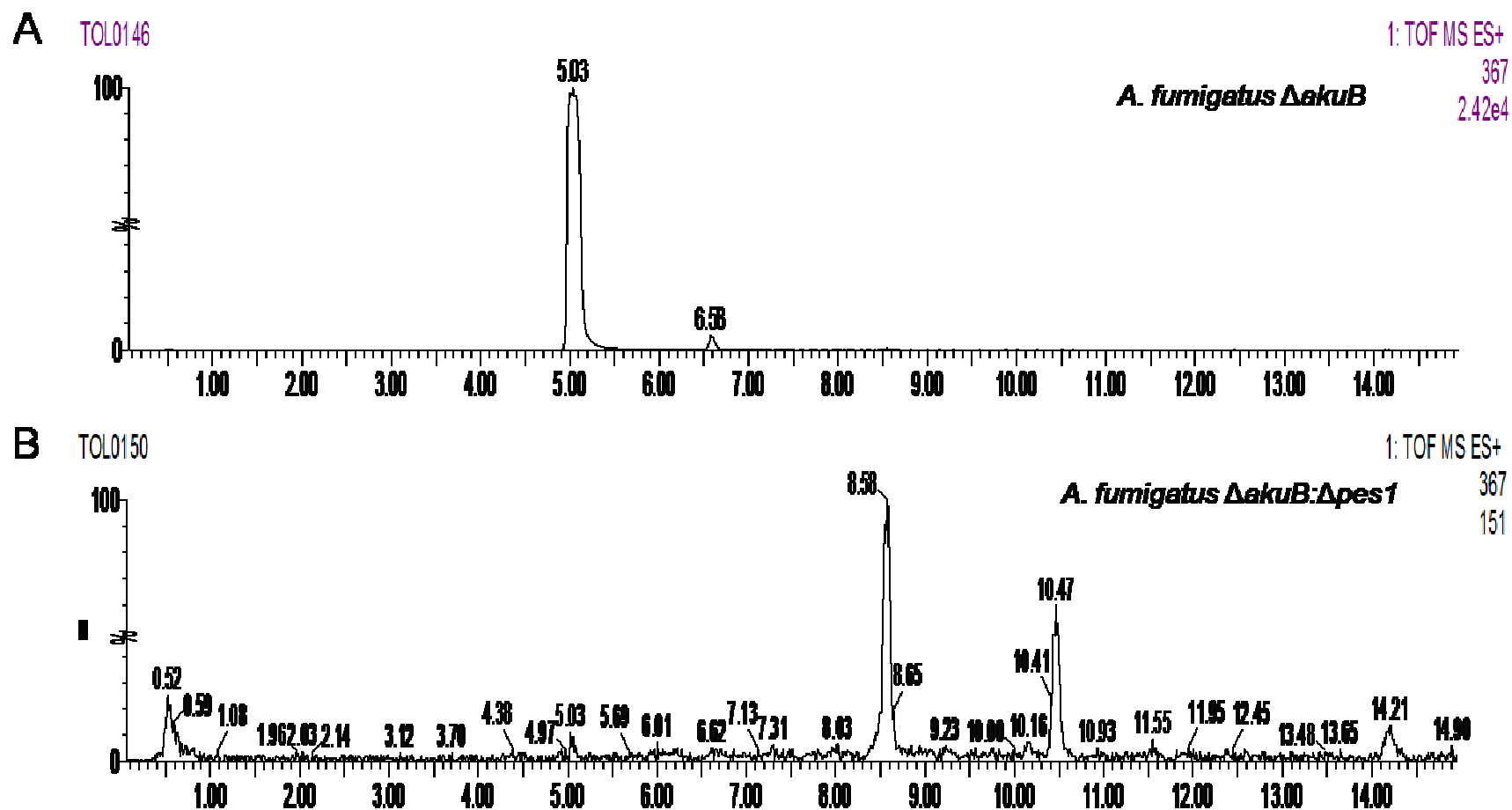
Figure 4.26: Fumigaclavine C identification by mass spectrometry. (A) Fumigaclavine C in *A. fumigatus* Δ*akuB* identifying at m/z 367 [M+H]$^+$ (retention time 5.03 min) and (B) absence of relevant peak in Δ*akuB*:Δ*pes1* strain.
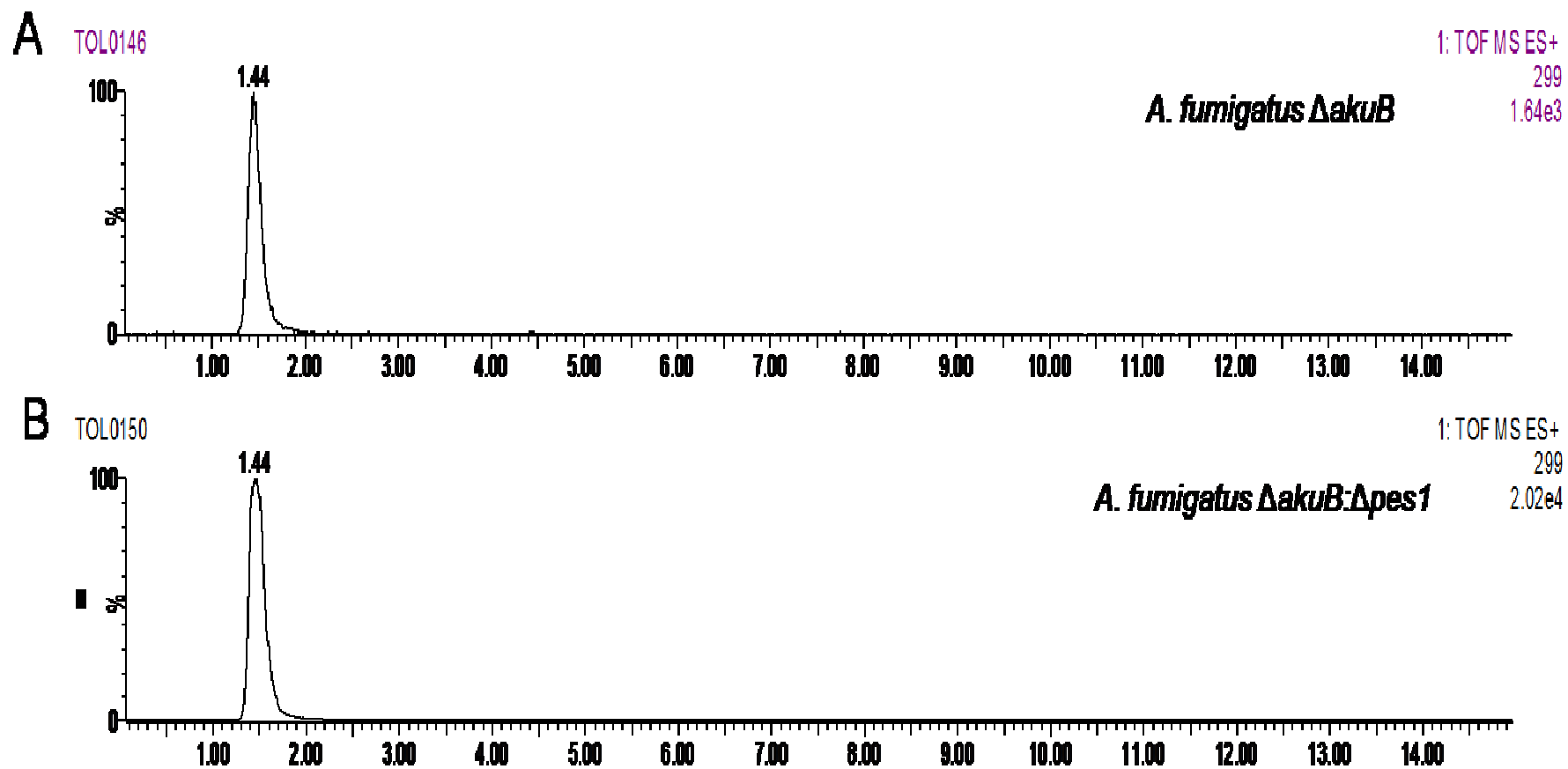
Figure 4.27: Identification of fumigaclavine A by mass spectrometry. (A) fumigaclavine A in *A. fumigatus ΔakuB* at m/z 299 [M+H]$^+$ (retention time 1.44 min) and (B) Fumigaclavine A in *A. fumigatus ΔakuB:Δpes1* at m/z 299 [M+H]$^+$ (retention time 1.44 min).
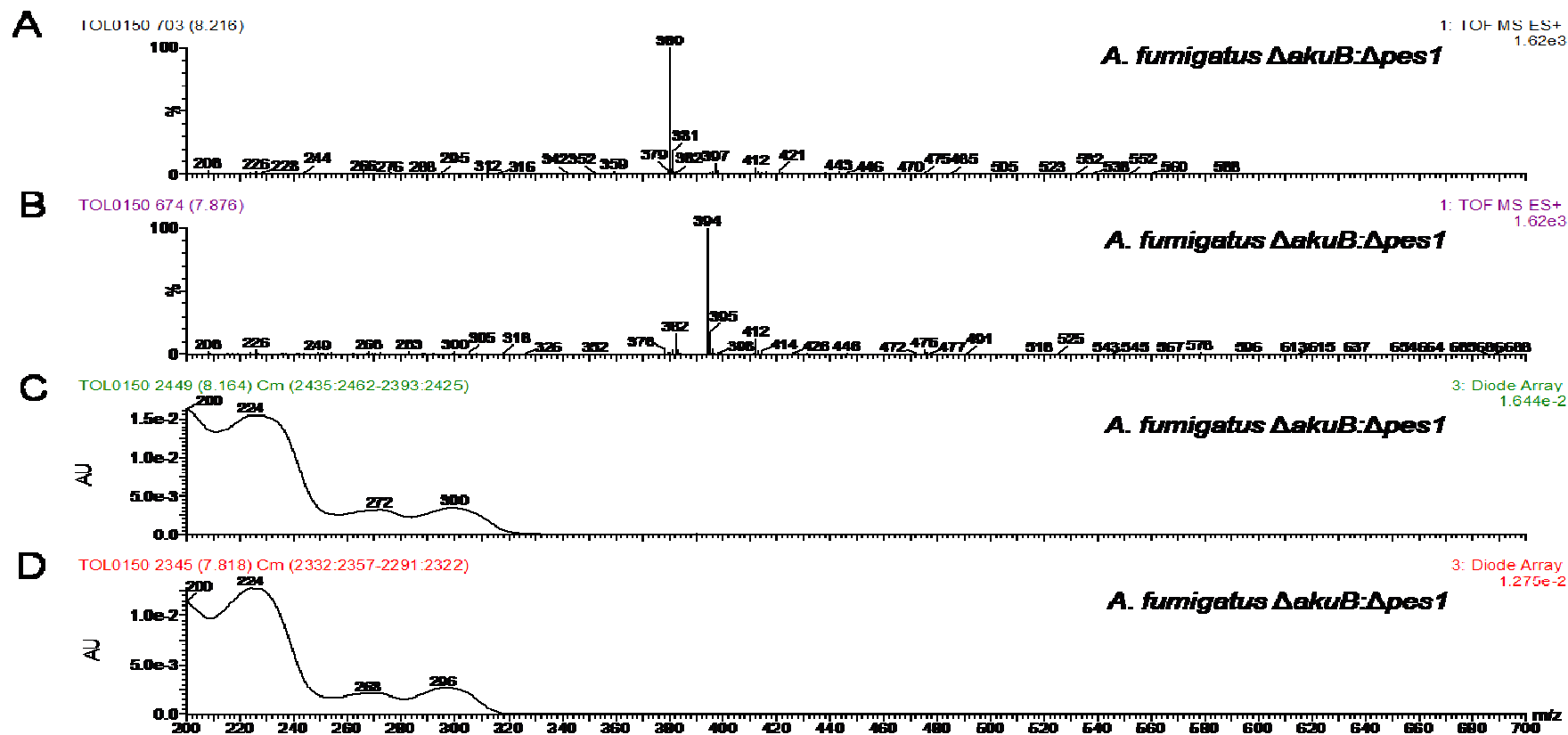
Figure 4.28: Mass spectrometry and UV spectrophotometry identifying TR-2 and fumitremorgin C in Δ*akuB*:Δ*pes1*. (A) Mass spectrometry identification of fumitremorgin C, iontrace m/z 380 [M+H]$^+$, (B) Mass spectrometry identification of TR-2, iontrace m/z 394 [M-2xH$_2$O+H]$^+$, (C) UV spectrophotometry confirming the identity of fumitremorgin C and (D) UV spectrophotometry confirming the identity of TR-2.
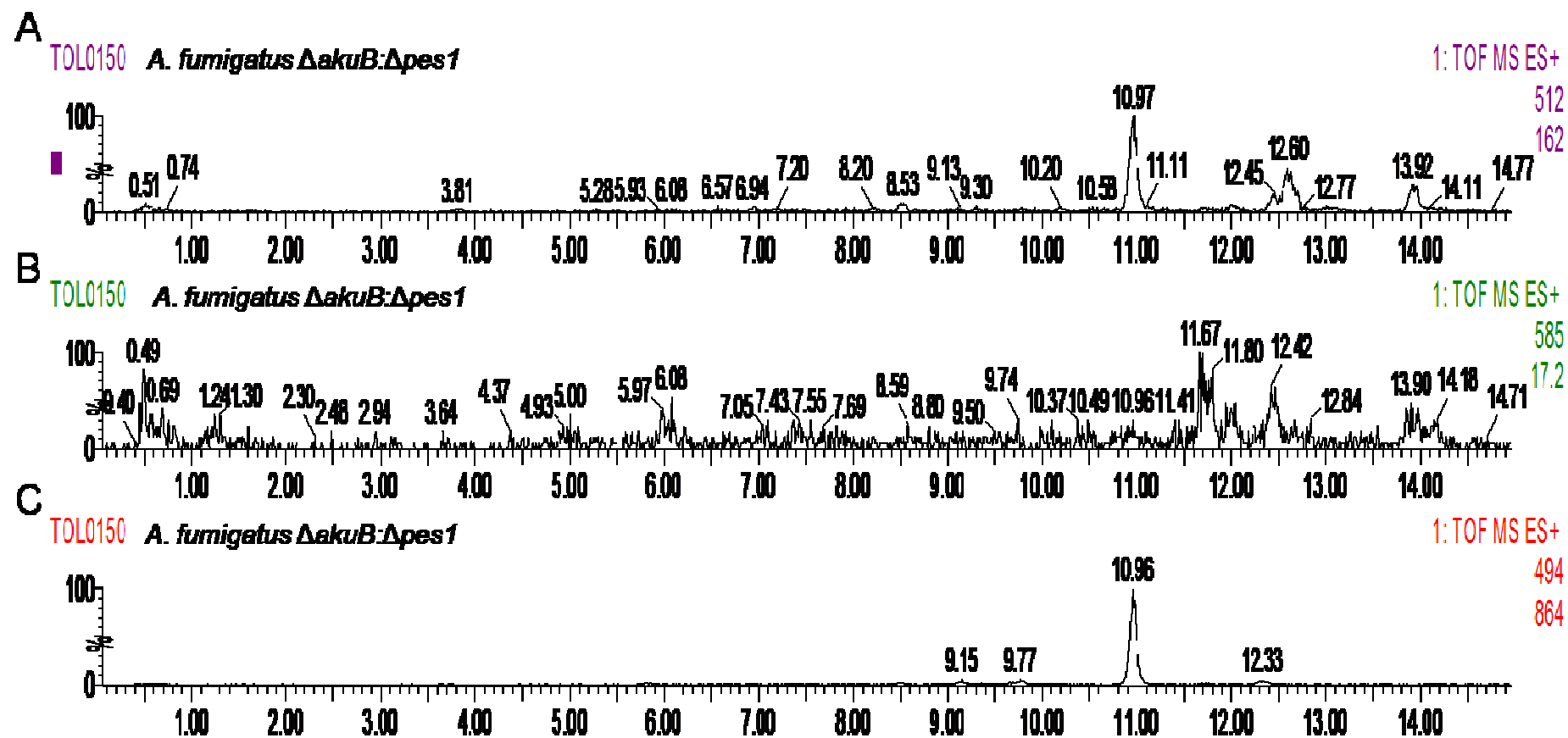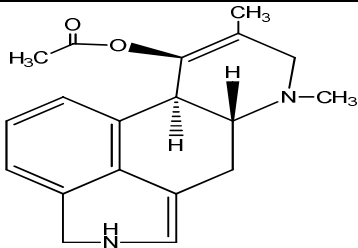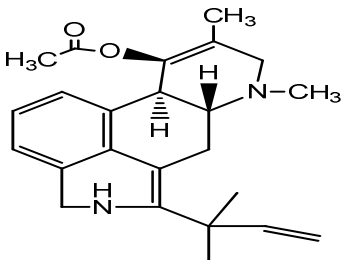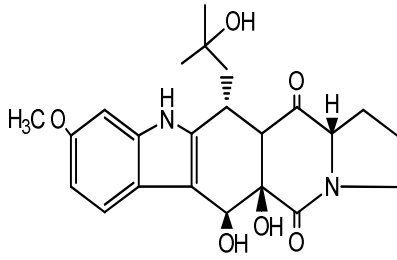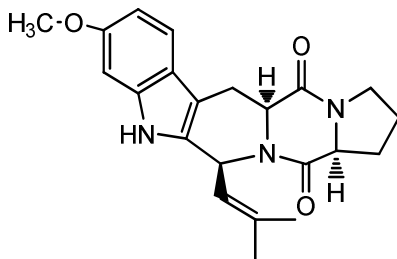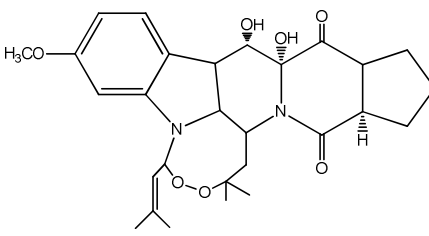
Figure 4.29: Verruculogen identification by mass spectrometry. (A) iontrace identification m/z 512 [M+H]$^+$ where verruculogen is identified at 10.97 min, (B) iontrace identification m/z 585 [M+CH$_3$CN+Na]$^+$, and (C) iontrace identification m/z 494 [M-H$_2$O+H]$^+$ where verrucululogen is identified at 10.96 min.

Table 4.1: Metabolites produced by wild-type (Δ*akuB* and ATCC46645) and Δ*pes1* (*ΔakuB* and ATCC46645).

Metabolite	Retention time	Structure
Fumigaclavine A	1.44 min	
Fumigaclavine C	5.02 min	
Peak (m/z 309)	5.17 min	Unknown
TR-2	7.88 min	
Fumitremorgin C	8.22 min	
Verruculogen	10.96 min	

The relative production of each metabolite identified was compared between wild-type and respective Δ*pes1* strains and is detailed in Table 4.2.

Table 4.2: Ion count of metabolites identified by mass spectrometry in *A. fumigatus* wild-type and Δ*pes1* strains.

| Metabolite | *A. fumigatus* | | | |
	Δ*akuB*	Δ*akuB*:Δ*pes1*	ATCC46645	Δ*pes1*[46645]
	Ion Count			
Fumigaclavine C	2.42e4	Absent	1.18e3	Absent
Fumigaclavine A	1.64e3	2.02e4	1.94e4	1.90e4
Fumitremorgin C	114	1.73e3	750	1200
TR-2	-	-	865	1100
Verruculogen	90.1	162	450	548

Table 4.1 and 4.2 summarise the findings of the LC-mass spectrometry metabolite profiling of *A. fumigatus* wild-type and Δ*pes1* strains. Table 4.1 shows the nomenclature, LC retention time and structure of all relevant metabolites. The similarity between fumigaclavine A and C is notable. Table 4.2 clearly shows that fumigaclavine C is absent in both Δ*pes1* mutants and allows us to conclude that *pes1*, in part, mediates fumigaclavine biosynthesis and the absence of fumigaclavine C contributes to phenotypic differences between *A. fumigatus* wild-type and Δ*pes1*.

4.3 Discussion

The disruption of *pes1* in *A. fumigatus* has provided an opportunity to investigate the possible functions of the gene. The disruption of this gene was not lethal to the fungus in any of the strains used, and therefore demonstrates that *pes1* production is not essential for primary growth and development of the fungus. The disruption of *A. fumigatus pes1* was confirmed by real-time PCR expression analysis. Plate assay analysis showed that the disruption of *pes1* in *A. fumigatus* Δ*akuB*, ATCC46645 and Δ*sidD*^{46645} resulted in strains which had different sensitivities to hydrogen peroxide (H_2O_2), voriconazole (VCR) and amphotericin B (AmpB) where Δ*akuB*:Δ*pes1* has the greatest sensitivity in the presence of all three ($P < 0.01$ at 2 mM H_2O_2, $P < 0.001$ at 0.15 μg/ml VCR, and $P < 0.001$ at 0.15 μg/ml AmpB). *A. fumigatus* Δ*pes1*^{46645} does not display the same sensitivities to hydrogen peroxide or amphotericin B, only displaying sensitivity toward voriconazole ($P < 0.01$ at 0.15 μg/ml). Whereas, Δ*sidD*:Δ*pes1* is more sensitive in the presence of hydrogen peroxide ($P < 0.001$ at 2 mM) than the other disrupted strains, but is less sensitive to voriconazole ($P < 0.01$ at 0.15 μg/ml) and amphotericin B ($P < 0.01$ at 0.15 μg/ml). Interestingly, at the lower concentration of voriconazole (0.005 μg/ml), Δ*sidD*:Δ*pes1* is more sensitive than Δ*pes1*^{46645} ($P < 0.001$), where Δ*pes1*^{46645} displays the same growth capabilities as the wild-type, ATCC46645. It was observed that the Δ*sidD*^{46645} and Δ*sidD*:Δ*pes1* strains required supplementation with L-glutamine rather than ammonium tartrate in iron limited (10 μM) conditions and that the iron source was also significantly important for the growth capabilities of these strains. Iron sulphate was able to maintain approximately 50 % growth for *A. fumigatus* Δ*sidD*^{46645} ($P < 0.001$) and Δ*sidD*:Δ*pes1* ($P < 0.0001$), whilst iron chloride was still ineffective in restoring growth, unless the iron concentration was increased to 1.5 mM. Furthermore, iron

sulphate combined with a low hydrogen peroxide concentration (1 mM or 2 mM) resulted in growth reduction of $\Delta sidD^{46645}$ and $\Delta sidD$:$\Delta pes1$ (P < 0.001) compared to the wild-type, ATCC46645. Infection studies using the insect host *G. mellonella* showed that the virulence of *A. fumigatus* is reduced due to the absence of the *sidD* gene (P = 0.001), and a further reduction in virulence was observed in the double mutant $\Delta sidD$:$\Delta pes1$ (P = 0.0002). Finally and most significantly, HPLC analysis determined that the strains $\Delta akuB$:$\Delta pes1$ and $\Delta pes1^{46645}$ were deficient in fumigaclavine C which for the first time implicates a role for *pes1* in fumigaclavine C biosynthesis.

The expression pattern of *pes1* was investigated to establish the optimal media and time point for *pes1* expression, which would therefore potentially produce the Pes1-encoded NRP product. The relationship between the level of *pes1* expression and the amount of the Pes1-encoded NRP product is not known. The expression of *pes1* was analysed by real-time PCR in the strain *A. fumigatus* ATCC46645 grown in Aspergillus minimal media (AMM), Minimal media (MM) and Sabouraud media (SAB). The expression pattern of *pes1* had been previously examined by Cramer *et al.* (2006b) and Reeves *et al.* (2006) where a range of media types and strains were used in their respective expression analysis. There was no expression of *pes1* in *A. fumigatus* AF293 cultured in Czapek's broth or RPMI, and minimal expression using Sabouraud media (Cramer *et al.,* 2006b). Whereas using MEM + FCS culture media for culturing *A. fumigatus* ATCC26933, ATCC16424, and ATCC13073 resulted in expression of *pes1*, with different levels between the strains (Reeves *et al.*, 2006). As the previous expression analysis conducted did not include the strains used in the disruption of *pes1* for this project, the expression of *pes1* in *A. fumigatus* ATCC46645 was profiled using a variety of media types and range of time-points.

The expression of *pes1* in *A. fumigatus* ATCC46645 was highest in cultures of all media types at either 24 or 48 hr, with a decrease at 72 hr. The lowest overall expression was observed in Sabouraud media, whereas in MM, there was a slight increase in expression of *pes1*. The highest expression was seen in AMM media, in 24 and 48 hr, with 48 hr having the highest expression. The real-time PCR analysis of *pes1* confirmed that *pes1* expression was not detected in the mutant strains, *A. fumigatus* Δ*pes1*[46645] and Δ*sidD*:Δ*pes1*, and also the restoration of expression of *pes1* in the complemented strain, Δ*sidD*:*pes1*[c]. This analysis confirms the Southern blot analysis of the mutants detailed in Chapter 3.

pes1 has previously been shown to confer protection against oxidative stress (Reeves *et al.*, 2006). In plate assays, there was a significant decrease in radial growth of *A. fumigatus* Δ*akuB*:Δ*pes1* compared to Δ*akuB* at 2 mM hydrogen peroxide (P < 0.01). This is in contrast to the application of hydrogen peroxide to *A. fumigatus* ATCC46645 and Δ*pes1*[46645], where there was no difference observed between the wild-type and respective mutant strain. Additionally, *A. fumigatus* Δ*sidD*[46645] and Δ*sidD*:Δ*pes1* exhibited a significant decrease in radial growth compared to ATCC46645 (2 mM hydrogen peroxide) (P < 0.001). Clearly, there is strain variability between Δ*akuB* and ATCC46645, in so far as, ATCC46645 is less sensitive to exogenous hydrogen peroxide.

In voriconazole plate assays, *A. fumigatus* Δ*akuB*:Δ*pes1* was sensitive to the presence of this anti-fungal, compared to the wild-type, Δ*akuB*. Even at the lowest voriconazole concentration (0.05 μg/ml), there was a significant decrease in growth (P < 0.01) of Δ*akuB*:Δ*pes1*. The higher concentrations of voriconazole (0.015 & 0.25 μg/ml) resulted in a further decrease in radial growth in Δ*akuB*:Δ*pes1* (P < 0.001).

For Δ*pes1*[46645], there was also a significant decrease in radial growth compared to *A. fumigatus* ATCC46645 at 0.15 µg/ml ($P < 0.05$). Interestingly, both *A. fumigatus* ATCC46645 and Δ*pes1*[46645] were incapable of growth at 0.25 µg/ml voriconazole, whereas *A. fumigatus* Δ*akuB* was capable of approximately 50 % growth and Δ*akuB*:Δ*pes1* was capable of about 10 % growth. *A. fumigatus* Δ*sidD*[46645] and Δ*sidD*:Δ*pes1* were capable of between 40 – 50 % growth in 0.05 and 0.15 µg/ml voriconazole, respectively. This indicates that the sensitivity towards voriconazole is more pronounced in Δ*sidD*, compared to Δ*pes1*[46645], as there is a greater decrease in radial growth in Δ*sidD*[46645] than Δ*pes1*[46645]. This sensitivity of Δ*sidD* towards voriconazole has not been observed previously. The Δ*sidD*:Δ*pes1* strain has the same radial growth as Δ*sidD*[46645], indicating that the sensitivity towards voriconazole is not an accumulative effect in the double mutant. Furthermore, in transcriptome analysis of *A. fumigatus* gene expression during exposure to voriconazole, the expression of *pes1* was found not to be significantly changed (da Silva Ferreira *et al.,* 2006b). This highlights the importance of focused studies which can vary the conditions to analyse selected specific genes at the same time, whereas global studies are capable of screening many genes in one condition at the same time.

In the amphotericin B plate assays, *A. fumigatus* Δ*akuB*:Δ*pes1* was sensitive to even the lowest level (0.15 µg/ml) ($P <0.001$), compared to the background strain, Δ*akuB* and this sensitivity was observed at all concentrations used ($P < 0.01$). This was in contrast to *A. fumigatus* ATCC46645 and Δ*pes1*[46645] where there was no difference in radial growth between the wild-type and mutant strain. *A. fumigatus* Δ*sidD*[46645] and Δ*sidD*:Δ*pes1* were also capable of maintaining similar growth, as were ATCC46645 and Δ*pes1*[46645]. However, at 0.15 µg/ml, Δ*sidD*:Δ*pes1* exhibited a

decrease in radial growth compared to ATCC46645 (P < 0.05). Reeves *et al.* (2004) showed that the presence of amphotericin B was in part responsible for an increase in the production of gliotoxin, and suggested that this may be due to pores created in the membrane by amphotericin B binding to the membrane sterols. This pore creation may be an advantage to the fungus in the presence of low concentrations of amphotericin B, as the wild-type strain was capable of over 100 % radial growth compared to growth on media-only plates, indicating that there is an advantage for the fungus to grow in the presence of low concentrations of amphotericin B. Potentially, growing the strains in liquid media containing amphotericin B, and measuring the gliotoxin secretion may provide more insight to the possibility of amphotericin B enhancing gliotoxin production.

The addition of gliotoxin did not have any impact on the radial growth of *A. fumigatus* Δ*akuB*:Δ*pes1*, indicating that *pes1* peptide production or function is not inhibited by the presence of gliotoxin. This also shows that the phenotypic results observed are specifically due to the absence of Pes1 production in *A. fumigatus* and not as a result of the transformation process itself, which should not interfere with the expression and function of other genes.

On media plates without additives, *A. fumigatus* Δ*akuB*:Δ*pes1* was only capable of maintaining 81 % radial growth compared to Δ*akuB*, indicating that mutations in this strain may result in higher sensitivities to hydrogen peroxide, voriconazole and ampothericin B, especially if the gene deleted or disrupted is involved in conferring protection against these agents. As mentioned in the previous Chapter, the characterisation of mutations conducted in the Δ*akuB* background should be carried

out after *akuB* has been restored (Nielsen *et al.,* 2008). The radial growth phenotypes observed in the *A. fumigatus* ATCC46645 and $\Delta sidD^{46645}$ and respective $\Delta pes1$ mutations, were less sensitive to hydrogen peroxide and anti-fungals, than the strains containing the *akuB* mutation, indicating that *akuB* strain may already exhibit sensitivities to these agents, and that the disruption of *pes1* could be adding to the sensitivities observed. This "unmasking" of the effect of the presence of hydrogen peroxide or anti-fungals in a sensitive strain, enhances the effect due to the absence of *pes1*, whereas in the other wild-type strain, ATCC46645, the mutation did not display any phenotypical difference when grown in the same conditions. Indeed, the $\Delta akuB$ strain had a slower growth rate than ATCC46645 and after 72 hr resulted in a smaller radial diameter on minimal media, 31.8 (±0.125) mm and 38.25 (±1.898) mm, respectively. Therefore, the use of the $\Delta akuB$ strain may be beneficial in the preliminary screening of phenotypic results, as this strain may potentiate the sensitivities of the mutated strain and indicate a possible line of enquiry in further phenotypic analysis.

A. fumigatus ATCC46645 and $\Delta pes1^{46645}$ exposed to hydrogen peroxide have the same growth capabilities, whereas the hydrogen peroxide inhibition assay conducted by Reeves *et al.* (2006) showed that the diameter of the inhibition zones increased as the dose of hydrogen peroxide increased, but that the effect was more pronounced in the *A. fumigatus* $\Delta pes1$ strain, compared to the wild-type AF293.1. As the hydrogen peroxide is placed in "pockets" in the agar and subsequently, *A. fumigatus* conidia are applied to the plate, the conidia of the mutant strain isolated onto the plate would be capable of growing on the agar away from the hydrogen peroxide pockets. In the hydrogen peroxide plate assays described here, the conidia were inoculated together

onto one spot on the plate, and the hydrogen peroxide was distributed throughout the agar at a specific concentration. Theoretically, activation of protective mechanisms against the presence of hydrogen peroxide may occur earlier than in inhibition zone assays, as well as conidia protecting other conidia due to clumping in one location resulting in similar sensitivities seen between *A. fumigatus* ATCC46645 and Δ*pes1*[46645]. Also, once mycelia begin to form the difference between wild-type and mutant becomes negligible, especially if *pes1* is a conidial-related gene, as the mycelial will activate alternative oxidative stress resistance genes, such as the catalases (Paris *et al.,* 2003b).

The media type plays an important role in the growth capabilities of *A. fumigatus.* This was especially highlighted in the different growth patterns observed for *A. fumigatus* Δ*sidD*[46645] and Δ*sidD*:Δ*pes1* in AMM compared to MM media types. *A. fumigatus ΔsidD*[46645] and Δ*sidD*:Δ*pes1* were not able to grow on AMM in the lower iron concentration (10 μM), but were able to maintain some growth on MM at this iron concentration (P < 0.001). Both strains were capable of maintaining similar growth capabilities as the wild-type, ATCC46645 when the iron concentration was increased (1.5 mM) on either media types. The difference between the two media types is the source of nitrogen. In AMM, the nitrogen source is ammonium tartrate and in MM, the nitrogen source is L-glutamine. L-glutamine can be used to synthesis L-ornithine, which is converted to N^5-hydroxy-L-ornithine during the first step of siderophore biosynthesis (Jones, 1985). As L-glutamine plays a role in the siderophore biosynthesis process, iron utilisation by the *sidD* deficient strains was investigated. The iron source also plays an important role in the growth capabilities of siderophore utilising organisms. It has been established that *A. nidulans* can

197

acquire iron from iron sulphate and not iron chloride (Eisendle *et al.*, 2003). Similar results were observed during this project, where *A. fumigatus* Δ*sidD* and Δ*sidD*:Δ*pes1* were capable of growth in the low iron concentration (10 μM) when the iron source was iron sulphate but not capable of any growth when the iron source was iron chloride (P < 0.001). Maximum growth was observed with both iron sources when the iron concentration was increased (1.5 mM). As the Δ*sidD* strains cannot utilise the siderophore system of recruiting iron (Schrettl *et al.*, 2007), the reductive iron assimilation (RIA) system (Howard, 1999) is solely relied upon for the iron recruitment. The source of iron is obviously important at the lower concentrations available, whereas at the higher concentrations, ample iron is available to utilise and does not restrict the growth of *A. fumigatus* Δ*sidD*, as the siderophore system is not required in this iron replete condition.

Previously, Schrettl *et al* (2007) demonstrated that the siderophore deficient strains were sensitive to oxidative stress. In particular, it was shown that Δ*sidD* was sensitive to hydrogen peroxide in plate assays with various iron concentrations. As the *pes1* gene is putatively thought to also be involved protection against oxidative stress (Reeves *et al.*, 2006), *A. fumigatus* ATCC46645, Δ*sidD*[46645] and Δ*sidD*:Δ*pes1* strains were exposed to increasing amounts of hydrogen peroxide with and without the presence of iron from different sources and at different concentrations. The wild-type strain is able to compensate for the lack of iron by utilising the siderophore system (Haas *et al.*, 1999), and resist the oxidative stress response. Evidently, the lack of the extracellular siderophore system is too much of a stress for the Δ*sidD*[46645] strain to grow, and consequently, the Δ*sidD*:Δ*pes1* strain also unable to maintain growth. It was therefore investigated if the supplementation with different iron sources and concentration would restore growth in the mutant strains.

Interestingly, *A. fumigatus* Δ*sidD*[46645] and Δ*sidD*:Δ*pes1* strains grown on media containing hydrogen peroxide (1 – 2 mM) in conjunction with 10 μM iron sulphate resulted in both strains capable of 20 % radial growth compared to ATCC46645 (P < 0.01), whereas growth on media containing hydrogen peroxide in conjunction with 10 μM iron chloride did not result in any growth (P < 0.001). In the presence of the higher iron concentration (1.5 mM) from either sources, both Δ*sidD*[46645] and Δ*sidD*:Δ*pes1* strains were capable of maintaining the same radial growth as ATCC46645 in the presence of any of the hydrogen peroxide concentrations used (1 – 4 mM). Upon the addition of a high concentration of iron, all strains no longer required the siderophore system, and therefore experienced only a single stress (hydrogen peroxide) instead of multiple stress factors. Therefore, Δ*sidD*[46645] acts exactly like the wild-type during the iron replete conditions, regardless of the type of iron supplied, which enables Δ*sidD*:Δ*pes1* to maintain full growth capabilities. The lower concentration of $FeSO_4$ (10 μM) is not enough iron supplementation to maintain the iron acquisition through the reductive iron assimilation (RIA) system, and requires the activation of the siderophore system when the available iron is used up. However, the initial iron acquisition by RIA enables the fungus to maintain some growth in the presence of hydrogen peroxide. This demonstrates the essential nature of iron recruitment by the fungus during oxidative stress, which counteracts the accumulative detrimental effect of the absence of a second gene, *pes1*, known to facilitate resistance to oxidative stress.

The *G. mellonella* insect host model has been used to study the virulence of bacteria (Jander *et al.,* 2000) and fungi (Cotter *et al.,* 2000; Reeves *et al.,* 2004a), as an alternative to using murine models. There is a good correlation between the *G.*

mellonella and murine response to fungal infection (Brennan *et al.*, 2002). As described in Chapter 1, the larvae of *G. mellonella* exhibit a similar innate immune response to that of a human in response to a pathogen (Kavanagh & Reeves, 2004). Reeves *et al.* (2004a) used the *G. mellonella* host model as a method of determining the virulence of *A. fumigatus*. The *G. mellonella* host system was also used to compare *A. fumigatus* AF293.1 and Δ*pes1*. Here, the virulence of Δ*pes1* was shown to be reduced compared to the wild-type, 48 hr post injection (Reeves *et al.*, 2006). As part of this project, the *A. fumigatus* ATCC46645, Δ*sidD*[46645], Δ*pes1*[46645] and Δ*sidD*:Δ*pes1* strains were used to infect *G. mellonella* larvae to determine the virulence of each strain. After 48 hr, there was significantly different survival rates between the strains, where *G. mellonella* infected with *A. fumigatus* Δ*sidD*[46645] (49 %) and Δ*sidD*:Δ*pes1* (53 %) displayed the highest survival rates. *A. fumigatus* Δ*pes1*[46645] (30 %) and Δ*sidD*:*pes1*[c] (33 %) infected larvae had similar survival rates. *A. fumigatus* ATCC46645 infected larvae displayed the lowest survival rate (25 %), which was expected.

A reduced virulence was observed in all mutants compared to the wild-type strain, with Δ*sidD*[46645] (P = 0.001) and Δ*sidD*:Δ*pes1* (P = 0.0002) being the most significant. These results show that *pes1* and *sidD* play an important role in the virulence of *A. fumigatus* and the combined loss of these genes contribute to the greatest virulence diminution in *A. fumigatus*. As the larvae injected with either Δ*sidD*[46645] or Δ*sidD*:Δ*pes1* conidia showed the greatest survival rate, it is a possibility that *sidD* plays a greater role than *pes1* in the pathogenicity of *A. fumigatus*, with *pes1* playing a contributing role. This virulence difference between the mutant strains is observed in the higher survival rate of *A. fumigatus* Δ*sidD*[46645] infected larvae compared to the Δ*pes1* infected larvae (P = 0.028). All the larvae,

irrespective of the strains, reached 100 % mortality after 72 hr incubation, indicating that attenuated virulence was not achieved by the absence of these genes individually or combined, and that the invasion capacity of these *A. fumigatus* mutant strains remained intact.

The creation of mutant strains gave rise to the opportunity of analysing the metabolites produced by wild-type and mutant strains by RP-HPLC and mass spectrometry. Initially, the culture filtrates were analysed by RP-HPLC with the aim to identify and compare secreted metabolites in the wild-type and Δ*pes1* mutant strains, as this method has previously identified metabolites such as brevianamide F (Maiya *et al.,* 2006) and Pseurotin A (Maiya *et al.,* 2007) in *A. fumigatus*. However, this analysis showed no difference between the strains. Subsequently, agar plate plug extractions of *A. fumigatus* Δ*akuB* and ATCC46645 and their respective *pes1* mutation strains, Δ*akuB*:Δ*pes1* and Δ*pes1*[46645], were taken following the protocol of Smedsgaard (1997). This extraction method ensures the inclusion of conidial and mycelial related metabolites, which would have been excluded in the culture filtrate analysis, as well as profiling the metabolites secreted into the agar (Smedsgaard and Nielsen*,* 2005). The agar plug extractions of all strains were subjected to RP-HPLC and mass spectrometry analysis. Both *A. fumigatus* Δ*akuB*:Δ*pes1* and Δ*pes1*[46645] were deficient in fumigaclavine C production, compared to the corresponding wild-type strains. As mentioned in Chapter 1, fumigaclavine C is one of seven ergot alkaloids produced by *A. fumigatus.* Therefore, the presence of the proposed fumigaclavine C precursor, fumigaclavine A, was searched for and observed in all strains, wild-type and mutant. Interestingly, the production of fumigaclavine A was increased in Δ*akuB*:Δ*pes1*, whereas Δ*pes1*[46645] produced the same amount of this

metabolite as ATCC46645. As the mutant strains are both capable of producing fumigaclavine A but not fumigaclavine C, the biosynthesis of this metabolite is reliant on the presence of the NRP synthetase, Pes1, and therefore for the first time, establishes a role for this NRP synthetase in the biosynthesis of fumigaclavine C.

Considering the involvement of the NRP synthetase, Pes1, in the biosynthesis of fumigaclavine C, the biosynthetic cluster of the ergot alkaloid identified in *A. fumigatus* was reviewed to clarify a role for Pes1 in Fumigaclavine C biosynthesis. Previously, the *A. fumigatus* fumigaclavine biosynthetic cluster was identified by the cloning and overexpression of the dimethylallyltryptophan synthase encoded by *fgaPT2* (AFUA_2G18040) (Unsold and Li, 2005). This gene showed significant identity (54 %) to *cpd1*, the dimethylallyltryptophan synthase, of *Claviceps purpurea*. Genes surrounding *fgaPT2* also had significant similarity to other genes involved in the ergot alkaloid synthase (EAS) cluster of *C. purpurea*, including *fgaOX3* (53 % identity to *cpox3*), *fgaOX1* (41 % identity to *cpox1*), *fgCAT* (57 % identity to *cpcat2*) and *fgaOX2* (66 % identity to *cpox2*) (Unsold & Li, 2005). *fgaDH* has an identity of 78 % to *cpox2* of *C. purpurea* (Wallwey *et al.,* 2010). The genes spanning from AFUA_2G17960 to AFUA_2G18060 in the genome were therefore identified as members of the *A. fumigatus* ergot alkaloid biosynthetic cluster (Figure 4.30).

C. purpurea produces the ergot alkaloid, lysergic acid and derivatives of this are ergopeptides such as ergoamine (Riederer *et al.,* 1996). Most of the chemistry of ergot alkaloids has been studied using *C. purpurea,* as the biosynthetic gene cluster for ergot alkaloids was discovered in this fungus (Tudzynski *et al.*, 1999). The

cluster was identified by genomic walking with a starting point at *cpd1* (previously known as *dmaW*) (Tudzynski *et al.*, 1999).

Another member of the ascomycota, *Neotyphodium lolii*, produces similar ergot alkaloids, named ergovaline and its derivatives such as ergine (Wang *et al.,* 2004). Interestingly, the *C. purpurea* and *N. lolii* ergot alkaloid biosynthetic clusters both contain at least one NRP synthetase. The biosynthetic cluster of *C. purpurea* contains three NRP synthetases, *lpsA, lpsB* and *lpsC*. *lpsA* is a trimodular NRP synthetase and *lpsB* is a monomodular NRP synthetase, whereas *lpsC* is also a trimodular NRP synthetase but has not been assigned a function in the biosynthesis of ergot alkaloids in *C. purpurea*. In *N. lolii*, only the *lpsB* gene is present in the cluster, but Southern blot analysis has identified the presence of the *lpsA* gene in the genome (Fleetwood *et al.,* 2007).

The *A. fumigatus* ergot alkaloid cluster does not contain any NRP synthetase genes and there is extensive gene rearrangement between the ergot alkaloid gene clusters in all three species, as depicted in Figure 4.30, which details the ergot alkaloid gene clusters identified in *A. fumigatus, C. purpurea* and *N. lolii*, with the general gene function of each strain indicated by the same colour across the three individual clusters. As there has been frequent gene renaming within all three clusters, this is the first time that the separate clusters are displayed together which shows the most recent gene names associated with putative functions. The information was compiled from publications that either displayed one or two of the clusters (Haarmann *et al.,* 2005; Lorenz *et al.,* 2007), or had all three clusters but no gene function alignment (Fleetwood *et al.*, 2007). *A. fumigatus* contains three genes in the centre of the cluster which are not present in the other clusters, namely an O-

acetyltransferase, *fgaAT,* involved in the conversion of fumigaclavine B to fumigaclavine A (Liu *et al.,* 2009) and two cytochrome P450 monooxygenases, which have not been assigned a function. Also different in the *A. fumigatus* cluster is the presence of a second reverse prenyltransferase, *fgaPT1* (Unsold and Li*,* 2006). The dioxygenase, *easH,* was determined to be a pseudogene in *A. fumigatus* (Fleetwood *et al.*, 2007), and therefore is not included in the proposed biosynthetic gene cluster schematic (Figure 4.30).

A. fumigatus
Fumigaclavine cluster

fgaOx3 · fgaFS · * · fgaPT1 · fgaDH · * · fgaAT · fgaCAT · fgaPT2 · fgaOX1 · fgaMT
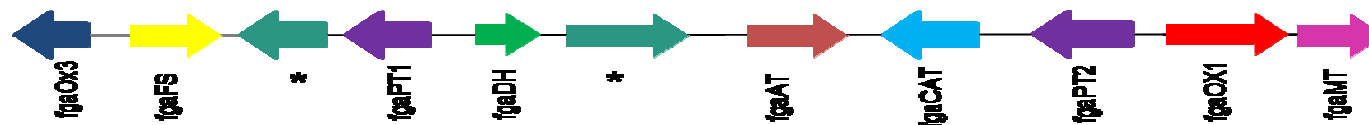
C. purpurea
Ergoamine cluster

lpsC · cppox3 · lpsB · cloA · cppat2 · cppox2 · cppox1 · easF · easG · cpd1 · easH · lpsA

N. lolli
Ergovaline cluster

easH · easA · easG · easF · cppox1 · lpsB

cloA · dmaW · lpsA

Not shown, as location relative
to the EAS cluster is unknown

Legend:
- ■ Oxidoreductase
- ■ Oxidoreductase/epimerase
- ■ Reverse Prenyltransferase
- ■ Dehydrogenase
- ■ O-acetyltransferase
- ■ Catalase
- ■ Oxidoreductase
- ■ Dioxygenase
- ■ N-methyltransferase
- ■ Cytochrome P450 monoxygenase
- ■ NRPS (monomodular)
- ■ NRPS (multimodular)
- * No gene name assigned

Figure 4.30: Proposed biosynthetic gene clusters of ergot alkaloid synthase genes in *A. fumigatus, C. purpurea* and *N. lolii* (Coyle and Panaccione, 2005; Haarmann *et al.,* 2005; Unsold and Li, 2005; Fleetwood *et al.,* 2007; Lorenz *et al.,* 2007).

The ergot alkaloid pathway is complex and not fully understood, differing between alkaloid producers (Figure 4.31 and Figure 4.32). The ergot alkaloid biosynthetic pathways of *A. fumigatus* and *N. lolii* have a common origin with *Clavicipitaceous* fungi, where there is a homolog in the initial determinant step of converting L-tryptophan to 4-L-DMAT (Coyle and Panaccione, 2005). In *C. purpurea* the biosynthetic production of the ergot alkaloid ergoamine begins with the prenylation of L-tryptophan with Dimethylallyl pyrophosphate (DMAPP) by the dimethylallyltryptophan (DMAT) synthetase, Cpd1, to result in 4-L-DMAT. This is then converted to 4-DMA-L-abrine by the N-methyltransferase, EasF. This is then converted to chanoclavine-1 by undetermined steps, but which include the oxidoreductase, Cpox1. The chanoclavine-1 is converted to chanoclavine-1-aldehyde by the dehydrogenase, Cpox2. This then undergoes steps which include the oxidoreductase, Cpox3 and an unknown reaction carried out by EasG which result in the production of agroclavine. This is then converted to elymoclavine by unknown reactions. Elymoclavine is the converted to paspalic acid by the cytochrome P450 monoxygenase, CloA. The orientation of the COOH acid is changed by an unknown spontaneous reaction and results in the production of lysergic acid. The conversion of lysergic acid to ergotamine is catalyzed by the monomodular NPR synthetase, LpsB, and the multimodular NRP synthetase, LpsA, where the lysergic acid is combined with three amino acids, usually alanine, phenylalanine and proline. It was established that derivatives of ergotamine could be synthesised by replacing the first two amino acids, alanine and phenylalaine with alternative amino acids, but that proline was essential for LspA activation (Walzel *et al.,* 1997). The proposed biosynthetic pathway of ergtoamine is detailed in Figure 4.31.
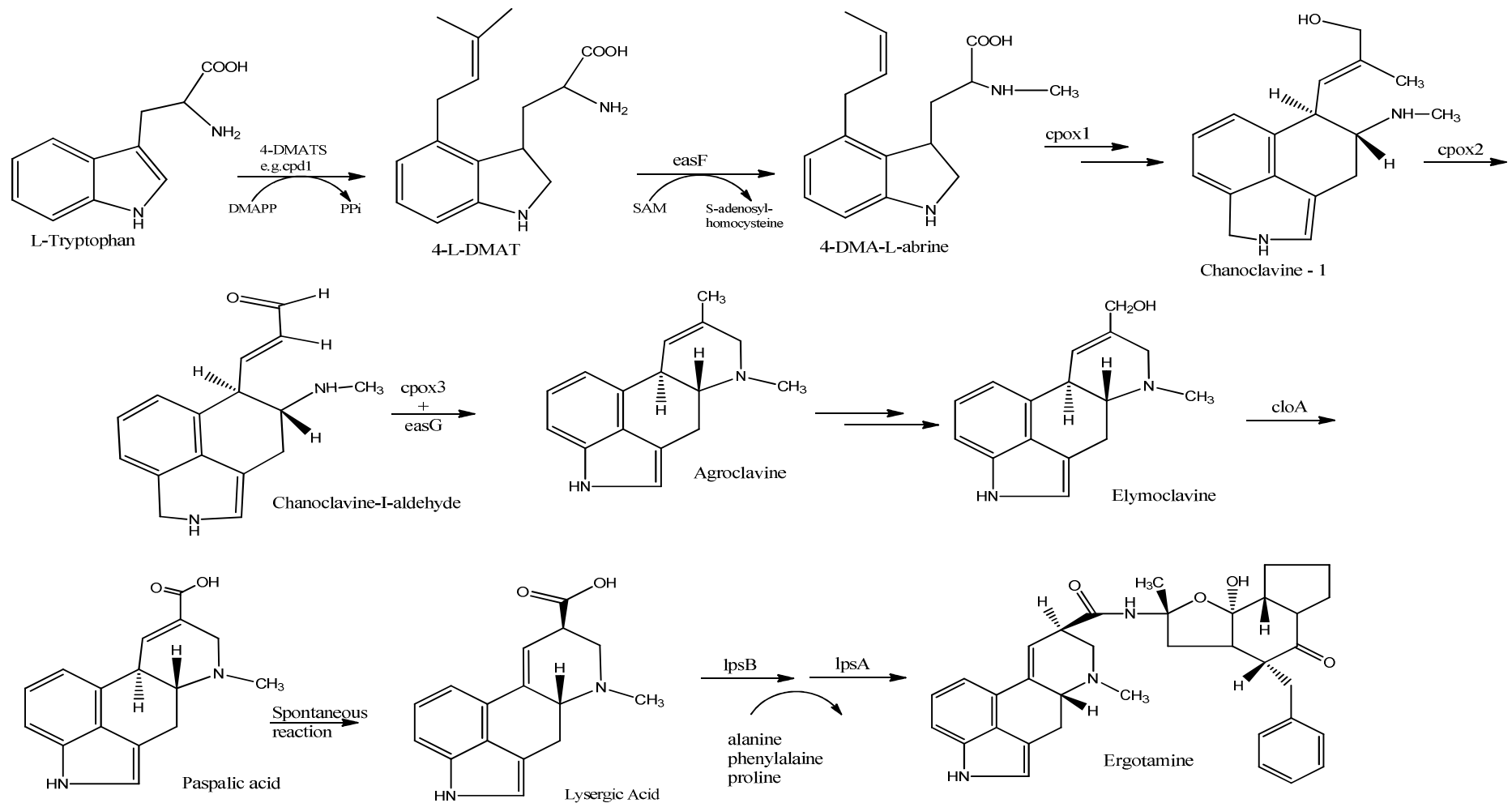
Figure 4.31: Proposed biosynthetic pathway of ergotamine, an ergot alkaloid in *C. purpurea.* (Riederer *et al.,* 1996; Walzel *et al.,* 1997; Correia *et al.,* 2003; Coyle *et al.,* 2010).

In *A. fumigatus* the biosynthetic production of fumigaclavine C also begins with the prenylation of L-tryptophan with DMAPP by the DMAT synthase, *fgaPT2* to result in 4-L-DMAT. This is converted to 4-DMA-L-abrine by the N-methyltransferase, FgaMT. This is converted to chanoclavine-1 by undetermined steps, but which include the oxidoreductase, FgaOx1. The chanoclavine-1 is converted to chanoclavine-1-aldehyde by the dehydrogenase, FgaDH. This then undergoes steps which include the oxidoreductase, FgaOX3 and an unknown reaction carried out by FgaFS which results in the production of festuclavine (also known as agroclavine). It is from this point that the ergot alkaloid biosynthesis deviates from that of *C. purpurea.* Festuclavine is converted to fumigaclavine B by unknown reactions. Fumigaclavine B is converted to fumigaclavine A by the O-acetyltransferase, FgaAT. Fumigaclavine A is converted to fumigaclavine C by a reverse prenyltransferase, FgaPT1. The proposed biosynthetic pathway of fumigaclavine C in *A. fumigatus* is detailed in Figure 4.32.
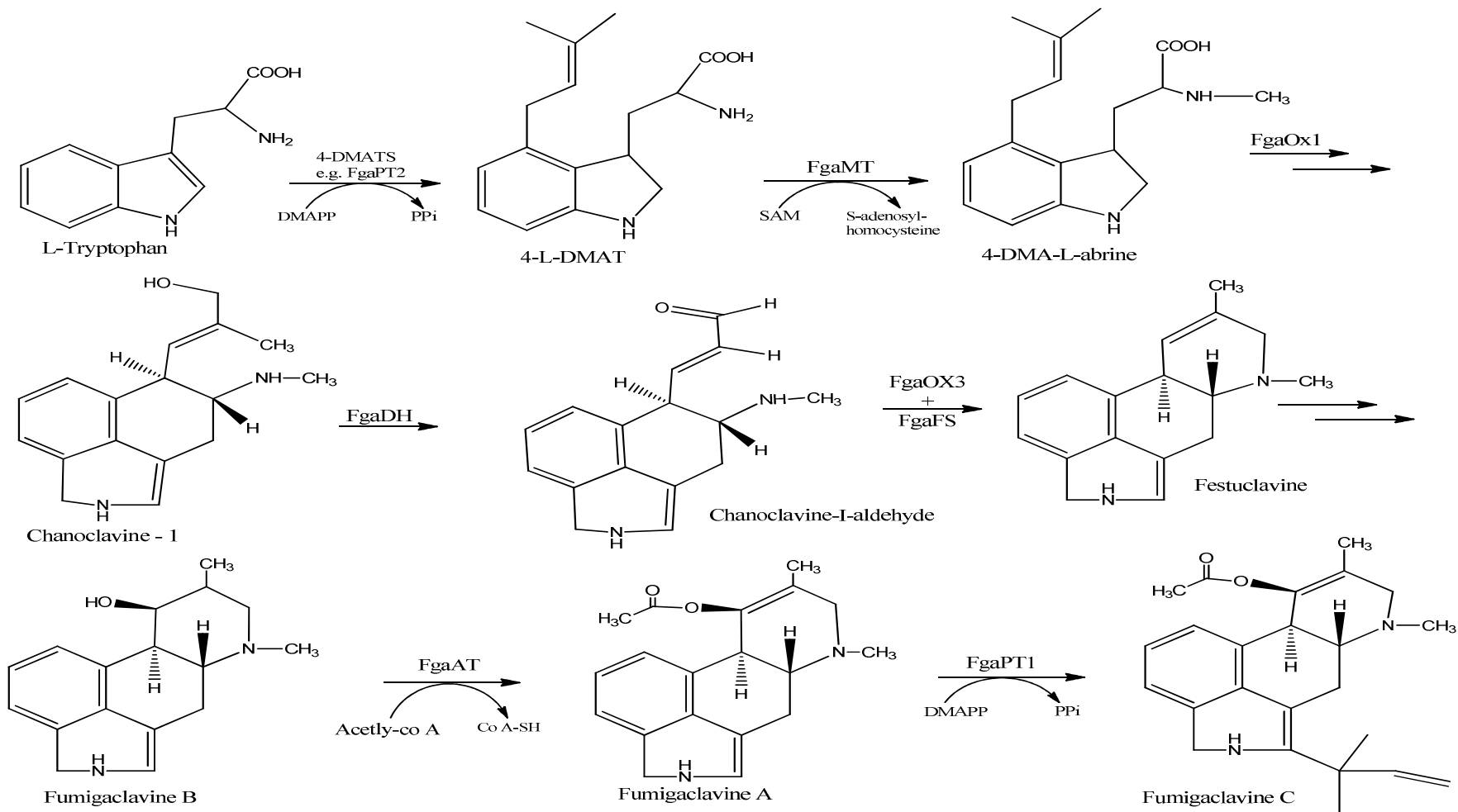
Figure 4.32: Proposed biosynthesis pathway of the ergot alkaloid, fumigaclavine C, in *A. fumigatus* (Unsold and Li, 2006; Rigbers and Li, 2008; Coyle *et al.,* 2010; Wallwey *et al.,* 2010).

The ergot alkaloids were confirmed to be associated with the conidia, as an *A. fumigatus ΔbrlA* strain, unable to produce conidiophores, did not produce any ergot alkaloids (Coyle *et al.,* 2007). *pes1* was previously identified as a gene involved in conidial morphology and hydrophobicity (Reeves *et al.*, 2006). As the absence of *pes1* expression, a known conidial related gene, is causing the lack of production of the conidial related metabolite, fumigaclavine C, the biosynthesis of this metabolite must require the involvement of the NRP synthetase, *pes1*, at some unknown stage during the biosynthetic process.

An *A. fumigatus* Δ*laeA* strain, deficient in the global transcription factor is unable to produce any of the fumigaclavine products (Perrin *et al.*, 2007). Interestingly, *pes1* expression is down-regulated in Δ*laeA*, which enables us to conclude that down-regulation of *pes1* in Δ*laeA* leads to the decrease in the production of these metabolites, specifically fumigaclavine C. The similarities between the Δ*laeA* and Δ*pes1* strains have been noted recently in relation to the involvement of metabolites in the pathogenicity of *A. fumigatus*, in a study concentrating on the association of LaeA mediated phagocytosis with the hydrophobin layer of conidia in *A. fumigatus* (Dagenais *et al.*, 2010). Also, as *pes1* expression is down-regulated in an *A. fumigatus* Δ*stuA* strain, which also exhibits conidial morphology differences, which may be a result of the down-regulation of *pes1* (Sheppard *et al.,* 2005).

The *A. fumigatus* fumigaclavine biosynthetic cluster has been extensively studied (Willingale *et al.,* 1983; Unsold and Li, 2006; Kato *et al.,* 2009; Maiya *et al.,* 2009; Steffan *et al.,* 2009) but there are still a number of undefined reaction steps, and genes in the cluster with unknown functions. As *pes1* is a multimodular non-linear NRP synthetase, and the biosynthesis of ergotamine in *C. purpurea* involves a

trimodular NRP synthetase (*lpsA*), it is possible that *pes1* shares a common ancestor with the NRP synthetase, *lpsA*. The NRP synthetases involved in ergotamine biosynthesis use lysergic acid as a specific substrate, activated through the NRP synthetase, *lpsB*, which sequentially adds three amino acids to the activated lysergic acid, suggesting that there are four peptide synthetase domains on the LPS multienzyme complex (Walzel *et al.*, 1997). Pes1 contains four adenylation domains for binding individual amino acids and has a non-linear type organisation, indicating that it may bind a complex peptide amongst its substrates, and may use domains more than once in the peptide production process (Section 1.4.1, Figure 1.6). *A. fumigatus* also has two monomodular NRP synthetases, *pesG* and *pesL*. Interestingly, in an *A. fumigatus* Δ*pesL* mutant strain, the production of fumigaclavine C is absent (Karen O'Hanlon – personal communication), indicating that this monomodular NRP synthetase may have a common origin with the monomodular NRP synthetase also found in *C. purpurea* (*lpsB*).

In *A. fumigatus* Δ*pes1*, the production of the precursor fumigaclavine A is unhindered, which strongly indicates that *pes1* absence is most likely preventing the conversion of fumigaclavine A to fumigaclavine C by the reverse prenyltransferase, FgaPT1. FgaPT1 has strict specific substrate specificity (Unsold and Li, 2006). *In vitro* experimentation directly reacted the substrate, fumigaclavine A with the reverse prenyltransferase, resulting in the production of fumigaclavine C (Unsold and Li, 2006). Possibly, *in vivo*, the direct interaction of substrate and transferase may not occur as easily, and may require the tethering of the substrate to an NRP synthetase, such as Pes1 for the reaction to occur. As the production of the precursor of fumigaclavine C, fumigaclavine A is not inhibited, *pes1* absence may interfere with

the prenylation step. Furthermore, analysis of *A. fumigatus ΔfgaPT2* mutant which could not convert L-tryptophan to 4-L-DMAT revealed a small quantity of chanaclavine still being produced, even though this is thought to be one of the intermediates further along the biosynthetic pathway, indicating that there may be an alternative pathway to fumigaclavine C type products (Unsold and Li, 2005).

Conversely, *in vitro* experimentation found that methylation of L-tryptophan could be induced resulting in the production of L-abrine. This in turn was accepted by FgaPT2 as a substrate for prenylation. But the methyltransferase FgaMT, would not accept L-tryptophan as a substrate unless it was previously prenylated, indicating the substrate specificity required in ergot alkaloid production (Rigbers and Li, 2008). As these reactions were carried out *in vitro*, the full biosynthetic reaction cannot be easily defined, especially if an NRP synthetase is involved.

Alternatively, fumigaclavine A may be produced by an alternative Pes1-independent pathway.

The *A. fumigatus* fumigaclavine biosynthetic cluster most likely has a common origin with the ergotamine biosynthetic cluster from *C. purpurea*, which contains NRP synthetases. The extensive gene rearrangement seen in the *A. fumigatus* fumigaclavine cluster may have resulted in the translocation of the NRP synthetase genes to other parts of the genome which remain intimately involved in the biosynthesis of the ergot alkaloid, fumigaclavine C. Evidence for this type of cluster cross-talk is beginning to emerge in the literature (Lazos *et al.*, 2010).

In summary, phenotypic analysis of disrupted *A. fumigatus pes1* in three strains namely, Δ*akuB*, Δ*sidD* and ATCC46645 resulted in (i) sensitivity to hydrogen

peroxide, voriconazole and amphotericin B to varying degrees between the different strains, (ii) an inability of the Δ*sidD*:Δ*pes1* strain to maintain similar growth capabilities as Δ*sidD* during iron limiting conditions, (iii) an additive sensitivity of the *pes1* disruption in the Δ*sidD* background towards amphotericin B, (iv) a decrease in virulence in all mutant strains compared to the wild-type, and (v) the absence of fumigaclavine C production in Δ*pes1* strains.

The ergot alkaloid production in *A. fumigatus* was not thought to involve NRP synthetases, even though the *C. purpurea* ergot alkaloid biosynthetic cluster, which was used to identify the *A. fumigatus* ergot alkaloid cluster, contains two functional NRP synthetases. We propose that gene rearrangement within the *A. fumigatus* cluster masked the potential NRPS involvement. The exact mechanism by which Pes1 is involved in the production of fumigaclavine C is still unknown, but this "cluster cross-talk" between *pes1* and the fumigaclavine C cluster has implications for all the undefined NRP synthetase genes in *A. fumigatus.*

CHAPTER 5

Functional characteristaion of *gliK* – a component of the gliotoxin biosynthetic cluster of *Aspergillus fumigatus*

5. Functional characterisation of *gliK* – a component of the gliotoxin biosynthetic cluster of *Aspergillus fumigatus*

5.1 Introduction

There is significant identity between the *A. fumigatus* gliotoxin biosynthetic cluster and the *L. maculans* sirodesmin biosynthetic cluster, including, *gliZ*, the zinc finger transcriptional regulator (Bok *et al.,* 2006a); *gliP*, the nonribosomal peptide synthetase; *gliG*, the glutathione S-transferase; *gliN*, the methyl transferase; *gliM*, the O-methyl transferase; *gliC*, the cytochrome P450 monooxygenase; *gliI*, the aminocyclopropane carboxylic acid synthase; *gliJ*, the dipeptidase; and *gliT*, the thioredoxin reductase which are all thought to be genes required for ETP biosynthesis. Three other genes in the gliotoxin cluster have no orthologs in the sirodesmin cluster, and these are: *gliF*, a cytochrome P450 monooxygenase; *gliA*, the multi facilitator superfamily (MFS) transporter; and *gliK*, a protein of unknown function.

gliF, encoding an extra P450 monooxygenase, may be involved in the addition of the hydroxyl group to the phenylalanine residue in an indirect manner, where the hydroxyl group is derived from one of the intermediates, as this is the function of *sirE* found in the sirodesmin cluster, which also encodes for an additional P450 monoxygenase (Gardiner and Howlett, 2005a).

The *A. fumigatus* gliotoxin cluster contains a MFS transporter (*gliA*), whereas, the *L. maculans* sirodesmin cluster contains an ABC (ATP-Binding Cassette) (*sirA*) transporter (Gardiner and Howlett, 2005a). This is interesting as it suggests that the same type of toxin is produced in a similar manner and yet has a different class of transporter. MFS transporters are more common than ABC transporters in fungal genomes, and this is especially true of *A. fumigatus* where there are 45 ABC transporters compared to 275 MFS transporters (Chang *et al.,* 2004). The MFS-type

transporters have been associated with the production of aflatoxins (*Aspergillus spp., aflT*), HC-toxin (*Cochliobolus carbonum, TOXA*), trichothercenes (*Fusarium sporotrichioides,* TRI12), cercosporins (*Cercospora kikuchii,* CFP) and poxilline *(Penicillium poxilli, paxT)* (Pitkin *et al.,* 1996; Alexander *et al.,* 1999; Callahan *et al.,* 1999; Young *et al.,* 2001; Chang *et al.,* 2004)*.* Previously it has been shown that, in sirodesmin production by *L. maculans*, the ABC transporter (*sirA*) is not essential for sirodesmin production but facilitates self protection (Gardiner *et al.,* 2005b). Here, it was shown that the expression of *sirA* is controlled by the mechanism that regulates the other genes in the cluster and also by sirodesmin itself. Conversely, *aflT*, a gene encoding the MFS transporter for aflatoxin in *A. parasiticus,* was not involved in the toxin production, nor was it essential for aflatoxin secretion, indicating that there may be other components involved in the transportation of toxins in association with the MFS type transporter. This study also indicated that the expression of the transporter was not controlled by the cluster transcription factor, but by the FadA-dependent G-protein signalling pathway (Chang *et al.,* 2004).

Previous studies have involved disruption of individual genes from the *A. fumigatus* gliotoxin cluster, and have identified that gliotoxin production was completely absent when the transcription factor, *gliZ*, was deleted (Bok *et al.,* 2006a) and also when *gliP*, the NRP synthetase was deleted (Kupfahl *et al.,* 2006; Cramer *et al.,* 2006a; Sugui *et al.,* 2007; Spikes *et al.,* 2008). Gliotoxin production was restored with the reconstitution of the respective deleted gene. These studies definitively confirmed that the cluster discovered in *A. fumigatus* was responsible for the production of gliotoxin. The expression of all cluster components except *gliP* was restored when exogenous gliotoxin was applied to the Δ*gliP* mutant (Cramer *et al.,*

2006a); indicating that gliotoxin itself can potentially regulate the cluster expression, in conjunction with the transcription factor.

The hypothetical protein, encoded by *gliK*, in the gliotoxin biosynthetic cluster found in *A. fumigatus* has not been characterised to date. Organisms which contain the MFS transporter rather than an ABC transporter associated with gliotoxin production, also have a *gliK*-type gene adjacent, or nearby (Patron *et al.,* 2007), whereas organisms that contain the ABC transporter do not contain a *gliK* gene within the cluster (Table 5.1). Therefore, it is possible that the protein encoded by *gliK* may be involved in the efflux of ETP toxins by the MFS transporter and its presence adjacent to the MFS transporter (*gli*A*)* makes it an interesting choice of study.

Table 5.1: Transporter types involved in gliotoxin production and their association with *gliK* (Patron *et al.,* 2007).

ABC & MFS	ABC	MFS + *gliK*	MFS only
A. flavus	*L. maculans*	*A. fumigatus*	*A. clavatus*
A. oryzae	*T. reesei*	*P. lilacinoechinulatum*	*C. globusum*
	A. zeae	*A. clavatus*	
		T. virens	
		A. terreus	

Consequently, it was of interest to investigate the role of *gliK* in *A. fumigatus*. This investigate was initiated by the deletion of the entire *gliK* gene (872 bp) and replacement with the pyrithiamine resistance selection marker, *ptrA* (2051 bp) (Figure 2.5). Thus, the *gliK* gene was deleted in two different *A. fumigatus* strains, ATCC46645 and ATCC26933, both of which are human clinical isolates. Clinical isolates of *A. fumigatus* have been shown to vary in their ability to produce gliotoxin (Kupfahl *et al.,* 2008). ATCC46645 is generally regarded as a non- to low-gliotoxin

producing strain, even though it possesses the genes for normal production, and ATCC26933 has been shown to produce significant amounts of gliotoxin (Reeves *et al.,* 2004a). Therefore, to generate *gliK* deficient mutants which originate from strains with different gliotoxin producing capabilities could elucidate the role of this functionally uncharacterised component of the gliotoxin biosynthetic cluster.

5.2 Results

5.2.1 Generation of constructs for the transformation of *gliK*

The constructs used for the creation of the *gliK* deficient mutants were generated from the flanking regions of the *gliK* gene (Figure 2.5). The flanking regions were amplified by PCR to generate the 5' flanking region, PCR1 (1250 bp), and the 3' flanking region, PCR2 (1211 bp). The primer sets for the flanking region PCR amplification contained unique restriction sites to facilitate specific digestion for subsequent ligation of the PCR products to the pyrithiamine resistance selection marker gene, *ptrA*; the reverse primer in the 5' flanking region contained a *Spe*I restriction site, and the forward primer in the 3' flanking region contained a *Hind*III restriction site. The *ptrA* gene was digested from the pSK275 plasmid by digestion with *Spe*I and *Hind*III.

The PCR reactions were optimised by using the three different reaction buffers provided with the Expand Long template PCR system (Roche). The PCR products, PCR1 and 2 were gel purified to remove any non-specific products (Figure 5.1).
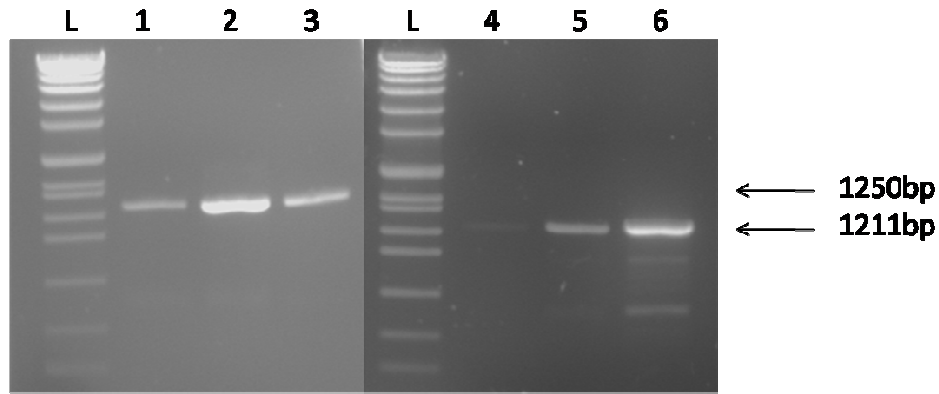
Figure 5.1: PCR products of the flanking region of the *gliK* deletion target, amplified using the three different reaction buffers provided. Lane L: Molecular weight marker ladder (Roche VII), Lanes 1 – 3: 5' flanking region PCR1 products (1250 bp), Lanes 4 – 6: 3' flanking region PCR2 products (1211 bp).

The PCR products were digested with the appropriate restriction enzyme, specifically, PCR1 was digested with *Spe*I (1243 bp) and PCR2 was digested with *Hind*III (1208 bp) (Figure 5.2) and the plasmid pSK275 was digested with both *Spe*I and *Hind*III simultaneously, to yield the *ptrA* gene which was contained within the smaller fragment (2049 bp) (Figure 5.3). The double digestion of the pSK275 plasmid increased the probability of the subsequent ligations to occur in the preferred orientation, as the digested fragment has a different restriction site at each alternative end, thereby reducing the number of unintentional ligations.
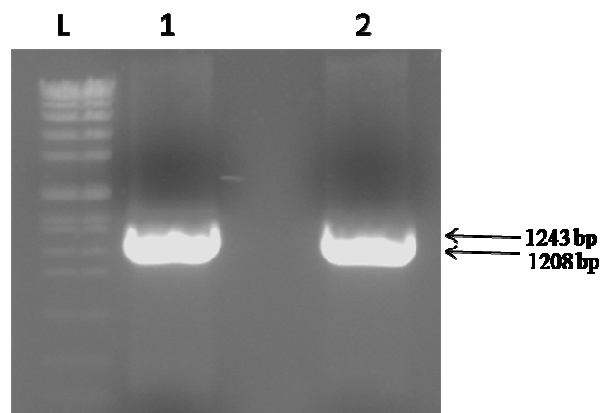
Figure 5.2: Digested PCR products. Lane L: Molecular weight marker ladder, Lane 1: PCR1 product digested with *Spe*I (1243 bp), Lane 2: PCR2 product digested with *Hind*III (1208 bp)
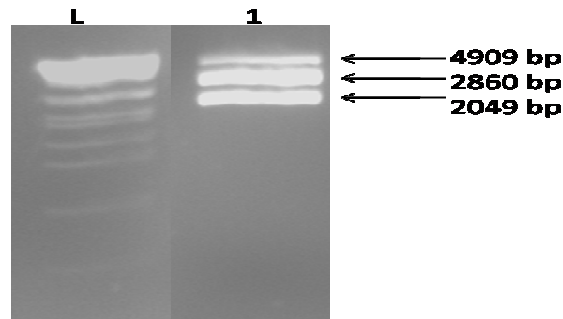
Figure 5.3: Plasmid pSK275 digested with *Spe*I and *Hind*III to release the *ptrA* gene. Lane L: Molecular weight marker ladder (Roche VII), Lane 1: digested pSK275; *ptrA* gene (2049 bp), plasmid backbone (2860 bp), undigested plasmid (4909 bp)

The digested PCR products (Figure 5.2) were ligated to *ptrA* (2049 bp). The *Spe*I digested PCR1 product was ligated to the *Spe*I digested side of *ptrA*, named ligation 1, and the *Hind*III digested PCR2 product was ligated to the *Hind*III digested side of *ptrA*, named ligation 2. These ligations were used as the templates for the final PCR amplifications where ligation 1 was used to create the 5' construct (2616 bp) and ligation 2 was used to create the 3' construct (2199 bp) (Figure 5.4) for subsequent protoplast transformation. The 5' and 3' constructs were gel purified and precipitated.
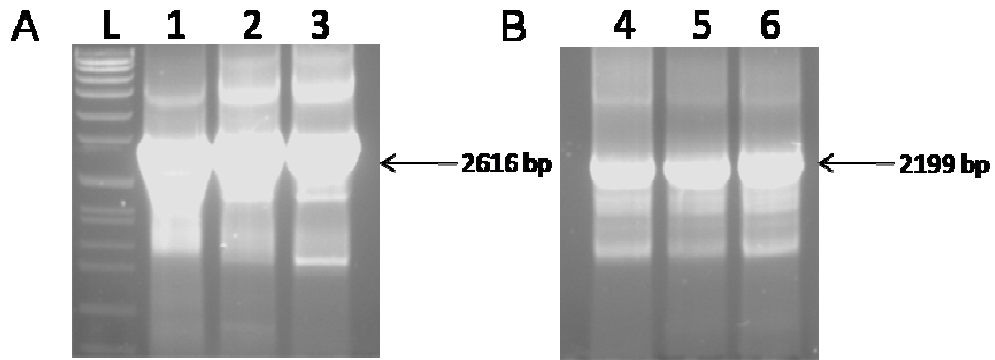
Figure 5.4: Final PCR products used for the deletion of *gliK* (A) Lane L: Molecular weight marker ladder (Roche VII), Lanes 1 – 3: Final PCR product of the 5' construct (2616 bp), (B) Lanes 4 – 6: Final PCR product of the 3' construct (2199 bp).

5.2.2 Generation of DIG-labelled probes by PCR for transformant identification.

The regions chosen for Southern blot analysis were the 5' region upstream of *gliK,* the 3' region downstream of *gliK* and also a selected region within the *gliK* deletion target itself. The probes were generated by PCR and contained DIG-labelled nucleotide bases, as described in Section 2.2.8. The PCR products were gel extracted and purified (Figure 5.5).
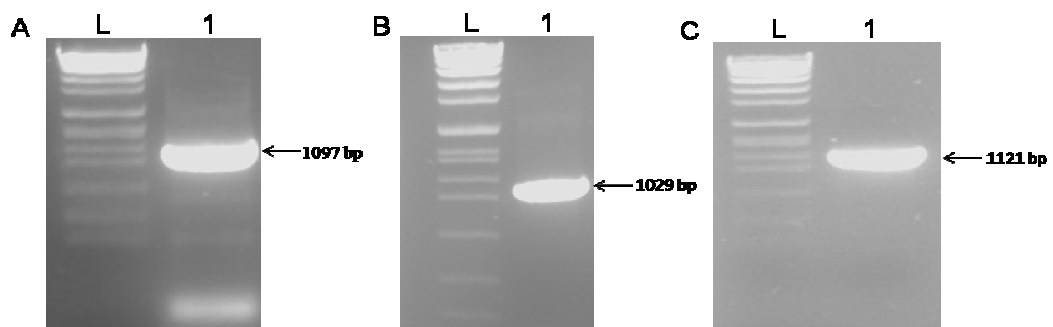
Figure 5.5: DIG labelled probes for use in transformant screening. (A) 5' *gliK* probe: Lane L: Molecular weight marker ladder (Roche VII), Lane 1: 5' *gliK* probe PCR product (1097 bp), (B) *gliK* coding region probe: Lane L: Molecular weight marker ladder (Roche VII), Lane 1: *gliK* coding region probe PCR product (1029 bp), (C) 3' *gliK* probe PCR product (1121 bp).

220

5.2.3 Protoplast transformation of *A. fumigatus* facilitating the deletion of the *gliK* gene.

The constructs were transformed into two different strains of *A. fumigatus*, with differing gliotoxin-producing capabilities, namely ATCC46645 and ATCC26933. At least 2.5 µg of each of the constructs were used for the individual transformation processes. Specifically, 3.4 µg of each construct was used for the ATCC46645 transformation and 2.5 µg of each construct was used for ATCC26933 transformation. The transformation process was carried out as described in Section 2.2.7. For both strains, the transformations were carried out twice. The resulting potential transformants are detailed in Table 5.2. The resultant transformants were screened on pyrithiamine plates (100 ng/ml) and colonies were screened by Southern blot analysis for the absence of *gliK*.

Table 5.2: Colony numbers screened in the deletion of *gliK* from two different strains of *Aspergillus fumigatus*.

Strain	No of Transformation Experiments	Number of putative Transformant colonies	No. of colonies screened	Successful Transformants
ATCC46645	2	65	65	0
		64	48	1
ATCC26933	2	27	27	0
		31	31	1

5.2.3.1 *gliK* deletion in the ATCC46645 strain

The results depicted in Figure 5.6 show the analysis of 14 possible transformants. The expected signals are detailed in Figure 2.12. Of the putative transformants, six

retained the wild type signal (3217 bp), eight exhibited non-specific banding, five contained the expected mutant signal (2032 bp) along with other non-specific banding and two contained the mutant signal only.
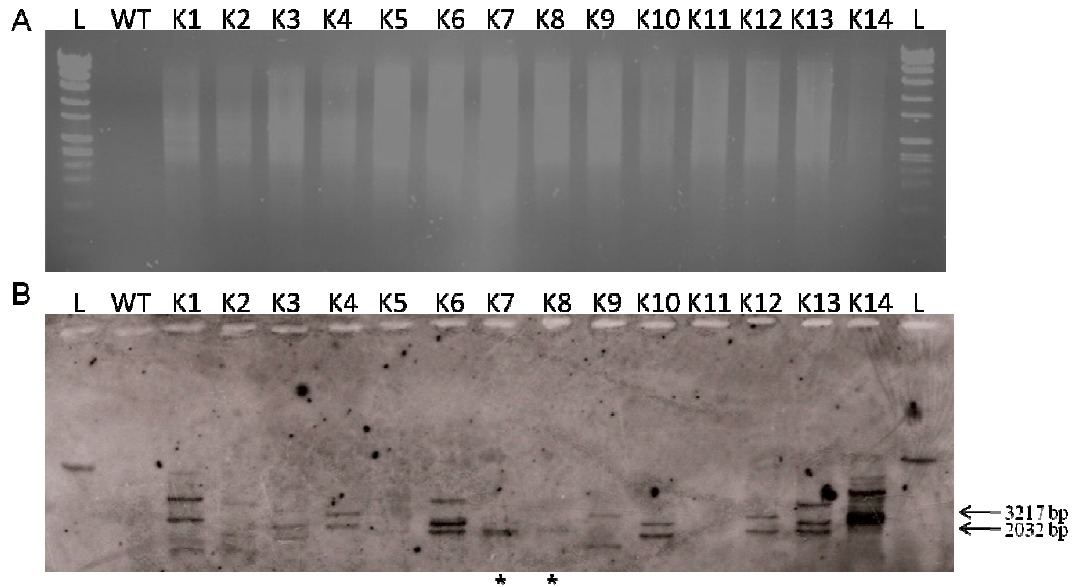
Figure 5.6: Identification of *A. fumigatus* Δ*gliK*[46645] by Southern blot analysis. (A) DNA digested with *Sal*I for probing by Southern blot with the 3'*gliK* probe and (B) corresponding Southern blot. Lane L: Molecular weight marker ladder (Roche VIII), Lane 1: ATCC46645 (3217 bp), Lanes 2-15: Possible transformants (2032 bp), named K1 - 14. Transformants K7 and K8 are marked by * below the respective lanes.

The potential deletion mutants, K7 and K8, were single-spored and re-analysed using different restriction enzymes, to confirm the single targeted integration (Figure 2.12). The single-spored colonies of K7 did not result in any definitive bands upon the Southern analysis. The single-spored colonies of K8, resulted in three of the clones containing only the wild-type signal (6245 bp), and one containing the expected band for the targeted integration, and was named K8.1 (1715 bp) (Figure 5.7). There was also some non-specific binding which occurred using this analysis,

which resulted in bands appearing around 6245 bp, which can be seen in the ladder lane.
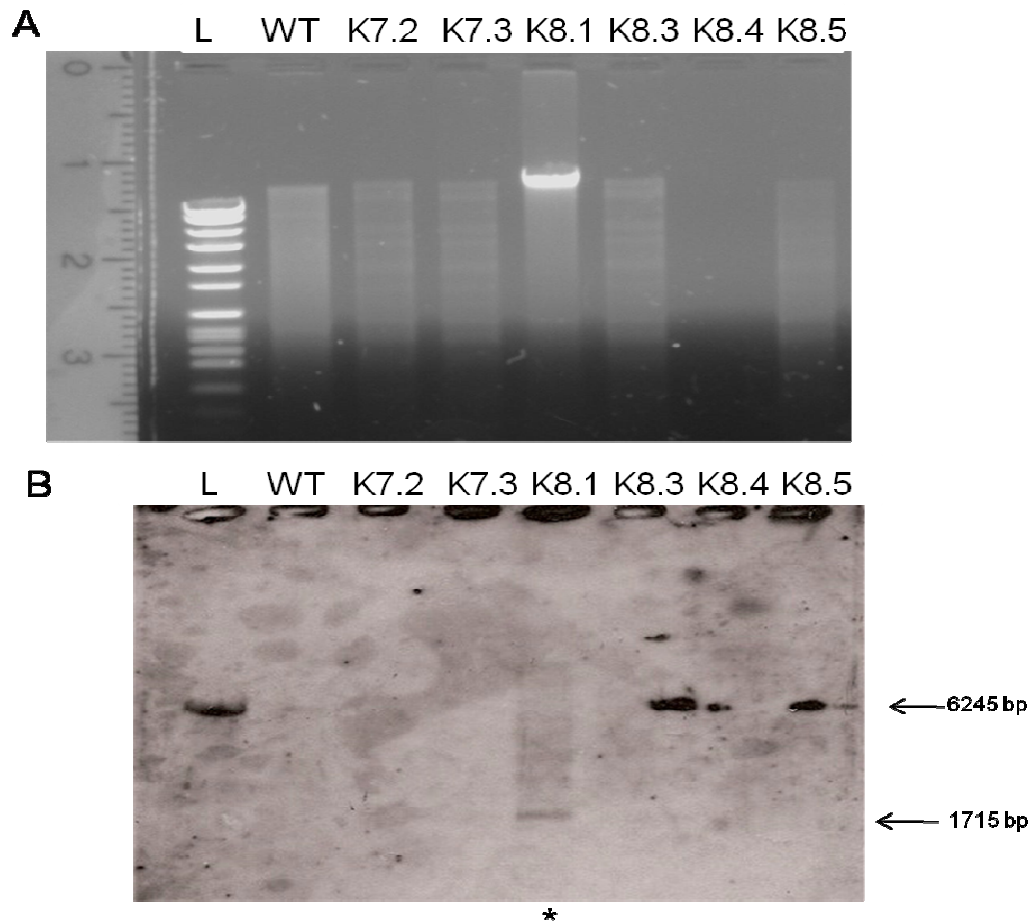
Figure 5.7: Identification of *A. fumigatus* Δ*gliK*[46645] by Southern blot analysis. (A) DNA double digested with *BamH*I and *Hind*III for probing by Southern blot with the 3'*gliK* probe and (B) corresponding Southern blot. Lane L: Molecular weight marker ladder (Roche VIII), Lane 1: ATCC46645, Lanes 2 & 3: single spored sample K7, named K7.2 & K7.4, Lanes 4 – 7: single-spored sample K8, named K8.1, K8.3, K8.4 and K8.5. Transformant K8.1 is marked with * below the respective lane.

To further clarify this result, transformant K8.1 was re-analysed by an alternative restriction digestion using *Pvu*II (Figure 2.10). This alternative analysis resulted in a clear blot for interpretation. Figure 5.8 depicts the Southern blot where the wild-type signal (1926 bp) and the mutant signal (2408 bp) can be easily distinguished. This

confirmed that that transformant K8.1 contains a targeted deletion of *gliK* in the *A. fumigatus* strain ATCC46645.

Figure 5.8: Identification of *A. fumigatus* Δ*gliK*[46645] by Southern blot analysis. (A) DNA digested with *Pvu*II for probing with the 5'*gliK* probe and (B) corresponding Southern blot. Lane L: Molecular weight marker dig labelled ladder (Roche VII), Lane 1: ATCC46645 (1926 bp), Lane 2: Δ*gliK*[46645] (2408 bp).

5.2.3.2 *gliK* deletion in the ATCC26933 strain

The ATCC26933 transformation was conducted by the same method and with the same constructs as for the ATCC46645 transformation. Screening for the mutant was conducted by Southern blot analysis, and the Δ*gliK*[46645] strain (K8.1) was used as a positive control on the blot (Figure 5.9). Of the eight transformants screened, three transformants, K2.1, K2.2 and K2.8, retained the wild-type signal (1926 bp), and two (K2.4 and K2.6) retained the wild-type signal, as well as other ectopic integration bands. Three transformants gave the correct size band (2408 bp) which

indicated a successful targeted transformation, namely K2.3, K2.5 and K2.7. These three transformants also had no other ectopic integration bands, nor the wild-type signal. This confirmed that the transformants were targeted deletions of *gliK* in the *A. fumigatus* strain ATCC26933.

Figure 5.9: Identification of *A. fumigatus* Δ*gliK*[26933] by Southern blot analysis. (A) DNA digested with *Pvu*II for probing with 5'*gliK* for Southern blot analysis and (B) corresponding Southern blot. Lane L: Molecular weight marker dig labelled ladder (Roche VII), Lane 1: ATCC26933 (1926 bp), Lane 2: Δ*gliK*[46645] (2408 bp), Lanes 3 – 10: possible transformants of ATCC26933, named K2.1 – K2.8. Transformants K2.3, K2.5 and K2.7 are marked by * below the respective lanes.

To further confirm the positive transformants, the transformants, K2.3, K2.5, and K2.7 were probed with the *gliK* coding region probe (Figure 2.13) and analysed by Southern blot to confirm the absence of *gliK* in the transformant strains (Figure 5.10). The wild-type signal is faint but can been seen at 2120 bp in lane 1. The

transformant of $\Delta gliK^{46645}$ is located in lane 2 and as expected does not result in any signal. Only one of the three possible transformants resulted in the expected signal absence, indicative of the deletion of *gliK*. This is transformant K2.3, located in lane 3. The other two possible transformants, K2.5 and K2.7 yielded non-specific binding. This result confirms that the transformant K2.3 contains targeted deletion of *gliK*.

Figure 5.10: Identification of *A. fumigatus* $\Delta gliK^{26933}$ by Southern blot analysis. (A) DNA digested with *Xba*I for probing with the *gliK* coding region probe and (B) corresponding Southern blot. Lane L: Molecular weight marker dig labelled ladder (Roche VII), Lane 1: ATCC26933 (2120 bp), lane 2: $\Delta gliK^{46645}$, Lane 3 – 5: possible transformants of ATCC26933, named K2.3, K2.5 and K2.7. Transformant K2.3 is marked by * below the respective lane.

5.2.3.3 Complementation of *gliK* into the Δ*gliK*^{46645} strain

Once it had been established that *gliK* was successfully deleted from the ATCC46645 strain, it was important to reintroduce the gene back into the mutant strain, to establish if any of the phenotype deficiencies may be restored. This ensures that any differences observed between the wild-type and the mutant can be attributed to the product of the gene. The reintroduction of *gliK* to the Δ*gliK*^{46645} strain, was carried out as described in Section 2.2.7.2, where the DNA encoding the *gliK* gene was cloned into TOPO and linearized with a unique restriction enzyme (*Ale*I) (Figure 2.7), creating a linear fragment homologous to the 3' flanking region of the *ptrA* gene, which if targeted homologous recombination occurs will reintroduce the *gliK* gene into the genome of *A. fumigatus* Δ*gliK*^{46645} after the *ptrA* gene.

The region encoding *gliK* was PCR amplified using primers detailed in Table 2.4, resulting in a 3528 bp fragment (Figure 5.11 (A)). The PCR product ws gel extracted and purified. The PCR product was cloned into TOPO vector as described in Section 2.2.7.2. To verify the cloning, the modified vector was digested with the restriction enzymes *Xma*I and *Xho*I which upon successful cloning would result in distinct fragments of 4201 bp and 3257 bp (Figure 5.11 (B)). After confirmation of successful cloning, the TOPO vector containing the *gliK* fragment was linearised by digestion with the restriction enzyme *Ale*I (Figure 5.11 (C)).
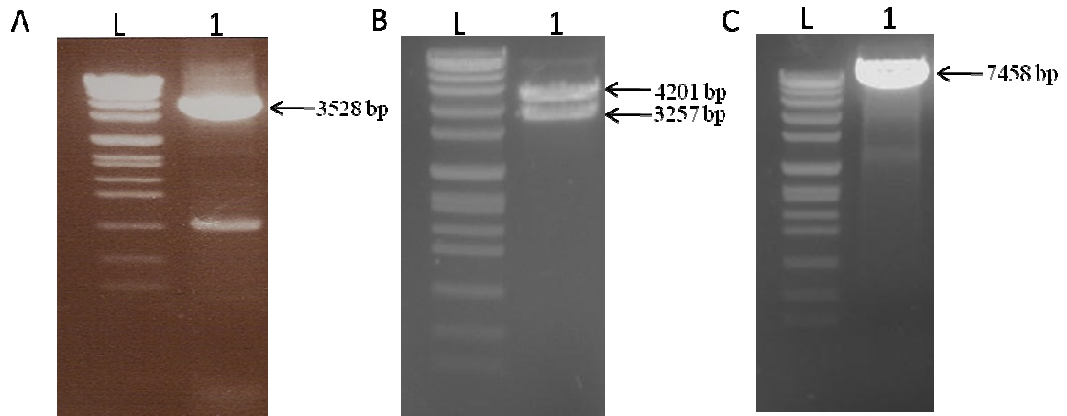
Figure 5.11: Constructs for complementation of *gliK* into the genome of *ΔgliK*^{46645}. (A) PCR amplification of the *gliK* region (3528 bp), (B) Digestion of the TOPO vector incorporating the *gliK* region with *Xma*I and *Xho*I to confirm the cloning of *gliK* into TOPO (4201 bp and 3257 bp), (C) linearization of the TOPO vector incorporating *gliK* by digestion with *Ale*I (7458 bp).

The selection marker employed in this transformation was phleomycin resistance, available in the plasmid pAN8-1. As this method is dependent on a unique restriction site in the TOPO vector containing the *gliK* gene, it was impossible to also incorporate the selection marker into the TOPO vector, along with the *gliK* gene (Figure 5.12). Therefore, the pAN8-1 plasmid was co-transformed in circular form with the linear TOPO vector containing *gliK*.
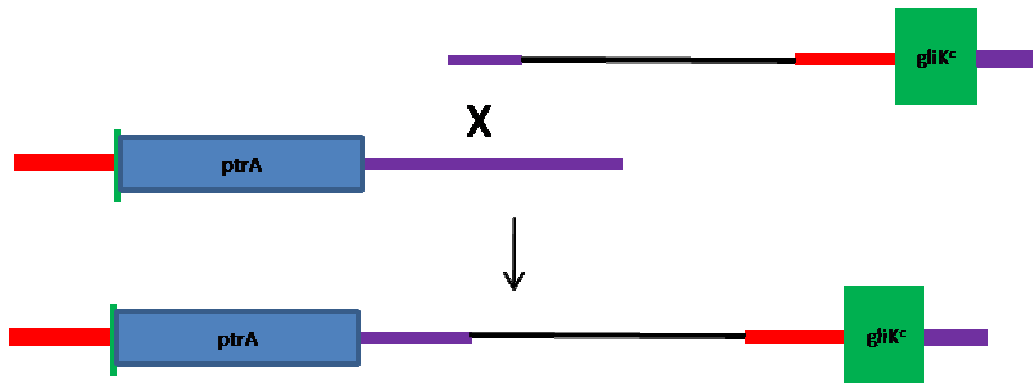
Figure 5.12: Schematic of the transformation for the complementation of *gliK* into the *A. fumigatus ΔgliK^46645* genome. The red shape depicts the 5' flanking region of *gliK*. The Green shape depicts the *gliK* gene. The purple shape depicts the 3' flanking region. The blue shape depicts the pyrithamine resistance cassette excised from the plasmid pSK275. The black shape depicts the Topo cloning vector.

Screening for the complemented *gliK* was carried out by Southern blot analysis following selection on phleomycin as described previously, and the results shown in Figure 5.13. Transformants KC5 and KC8, showed no integration of the *gliK*, remaining as *gliK* mutant strains (2408 bp). Whereas transformants KC3, KC4 and KC6, showed a targeted integration of the *gliK* gene (1625 bp) but also had an ectopic band, close to the size of the wild-type strain (1926 bp), KC2 had the same pattern as these transformants, with an additional lower band. Transformants KC1, KC7 and KC9, illustrate perfect examples of the *gliK^c* gene integration in a targeted fashion into the *A. fumigatus ΔgliK^46645* strain (2408 bp and 1625 bp).
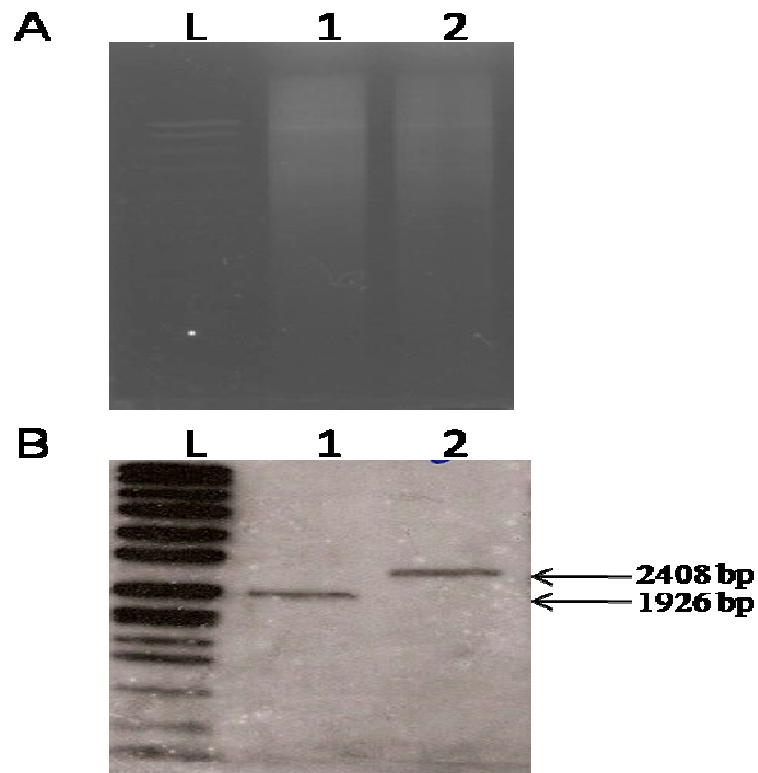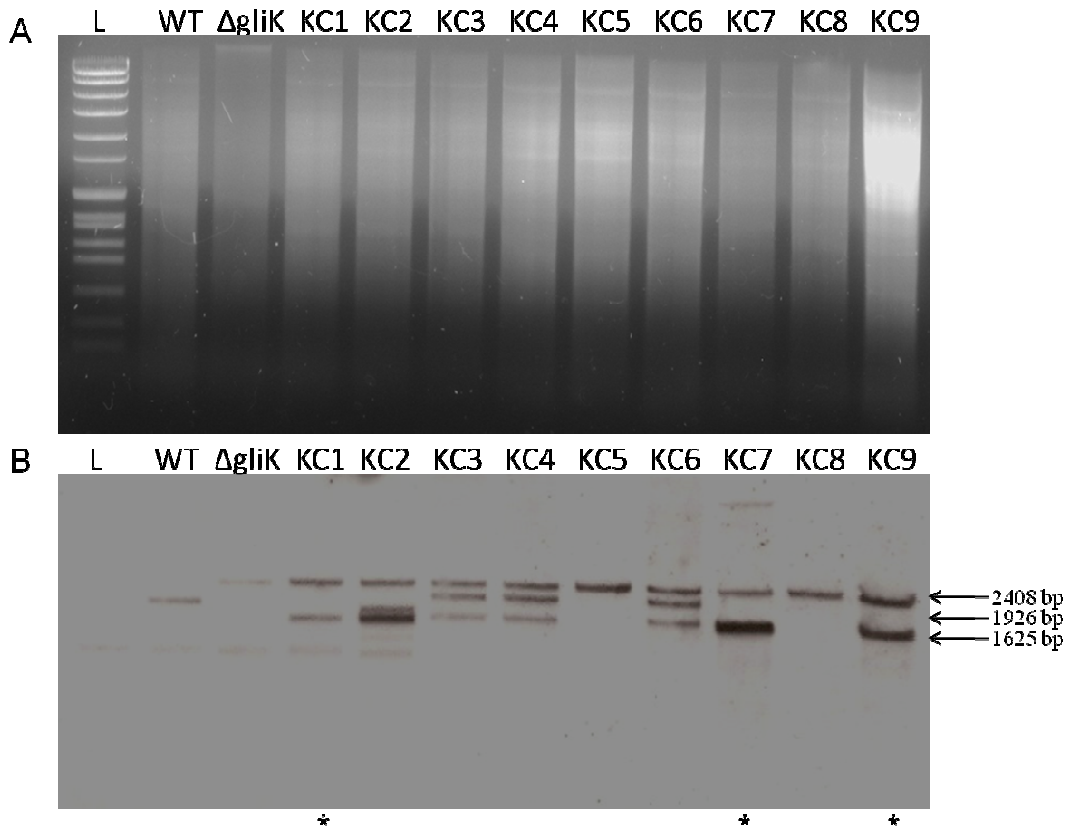
Figure 5.13: Identification of *A. fumigatus gliK^c* by Southern blot analysis. (A) DNA digested with *Pvu*II for probing with 5' *gliK* for Southern blot analysis and (B) corresponding Southern blot. Lane L: Molecular weight marker ladder (Roche VII), Lane 1: ATCC26933 (1926 bp), Lane 2: Δ*gliK*^46645 (2408 bp), Lanes 3 – 11: possible transformants encoding the complemented *gliK^c* (1625 bp and 2408 bp), named KC1 – KC9. Transformants KC1, KC7 and KC9 are marked by * below their respective lanes.

The Southern blot was repeated with the KC1, KC7 and KC9 transformants to clarify the result observed in Figure 5.13. The repeat Southern analysis confirmed that the three transformants each had the expected banding pattern (fragment sizes) that indicates the reintroduction of the *gliK* gene into the Δ*gliK* strain (Figure 5.14), to yield *A. fumigatus gliK^c*.
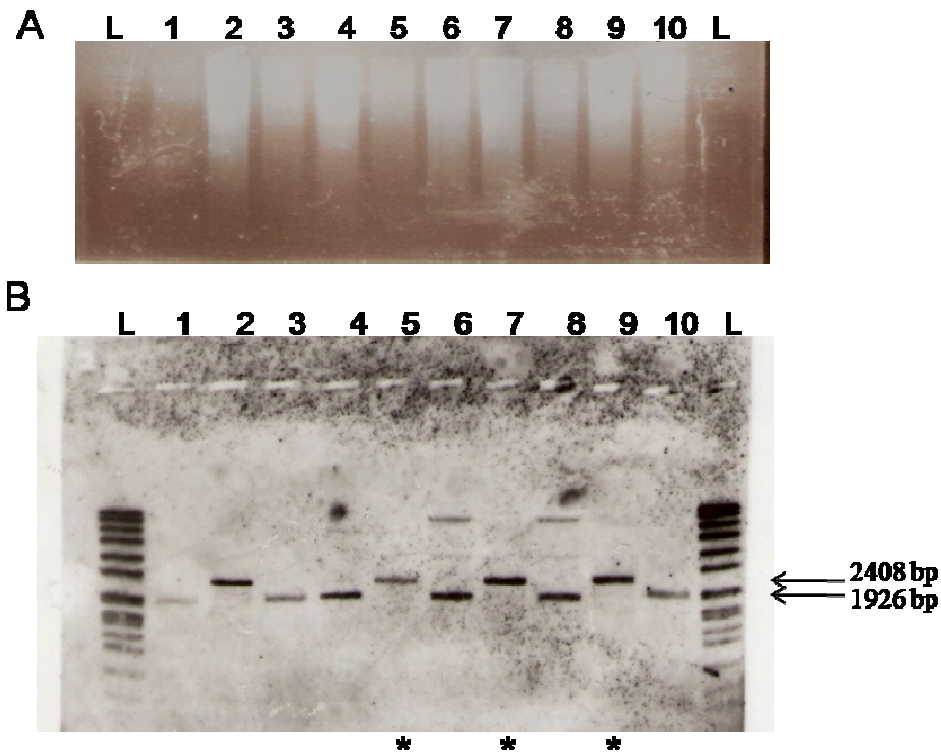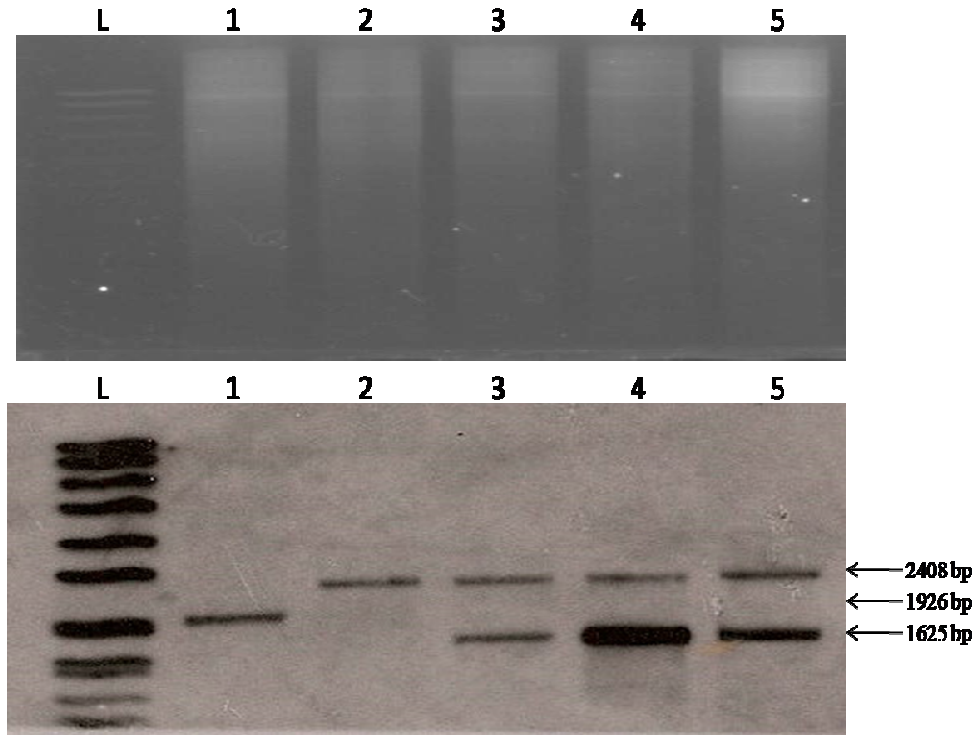
Figure 5.14: Identification of *A. fumigatus gliK*^{c} by Southern blot analysis. (A) DNA digested with *Pvu*II for probing with 5' *gliK* for Southern blot analysis and (B) corresponding Southern blot. Lane L: Molecular weight marker dig labelled ladder (Roche VII), Lane 1: ATCC26933 (1926 bp), Lane 2: Δ*gliK*^{46645} (2408 bp), Lanes 3 – 5: transformants encoding the complemented *gliK*^{c} (1625 bp & 2408 bp), named KC1, KC7 and KC9.

To verify the complemented strains, the transformants were screened with another probe, namely the 3' *gliK* probe (Figure 2.12). This analyses integrations which were positive for complementation when probed with the 5' *gliK* probe, as those not confirmed by the 3' *gliK* probe could be a false positive, as the full construct would not be integrated in a targeted manner. The transformants were probed with the *3'gliK* probe and analysed by Southern blot (Figure 5.15), where the wild-type band had an expected fragment size of 3212 bp, Δ*gliK* had a fragement sze of 2032 bp and the complemented strain had a two fragment sizes of 2032 bp and 6038 bp. The transformants that were previously determined by the 5' *gliK* Southern analysis to be positive for the *gliK*^{c} integration, KC1, KC7 and KC9, all had different

banding patterns in the 3' *gliK* Southern blot analysis. Transformants KC7 and KC9, had strong additional bands visible with the 3' *gliK* probe, whereas KC1 did not. This transformant, KC1, was taken to be the best representation of the complementation transformation, as it had a perfect representation of the complementation in the 5' analysis and no additional bands in the 3' analysis.
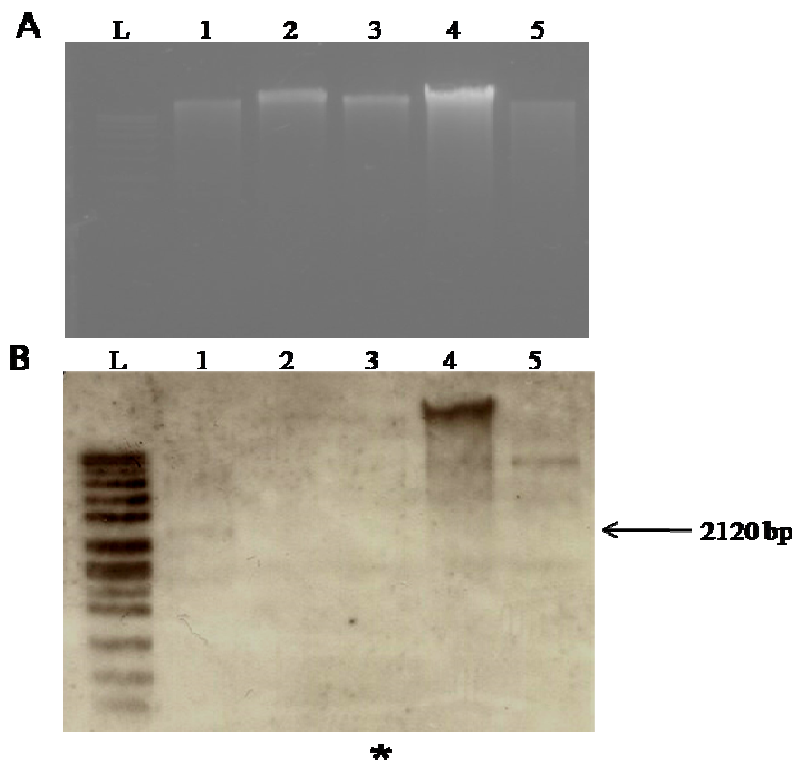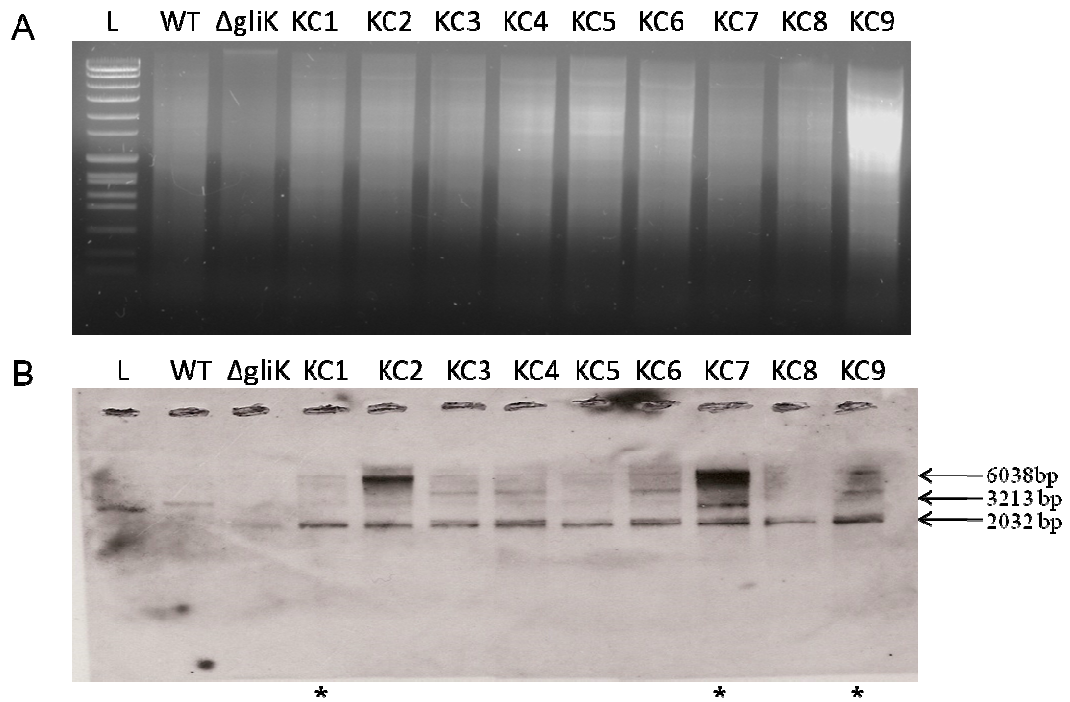

Figure 5.15: Identification of *A. fumigatus gliK^c* by Southern blot analysis. (A) DNA digested with *Sal*I for probing with 3' *gliK* for Southern blot analysis and (B) corresponding Southern blot. Lane L: Molecular weight marker ladder (Roche VII), Lane 1: ATCC46645 (3212 bp), Lane 2: Δ*gliK*^46645 (2032 bp), Lanes 3 – 11: possible transformants encoding the complemented *gliK^c* (2032 bp & 6038 bp), named KC1 – KC9. Transformants KC1, KC7 and KC9 are marked by * below the respective lanes.

To further verify the reintroduction of the *gliK* gene into the mutant, the wild-type, Δ*gliK*^46645 and *gliK^c*, were probed for a region of the *gliK* gene that was deleted (Figure 5.16). All the strains had a background signal at a high molecular size, of

unknown origin. The wild-type and the *gliK^c* strains contained the expected *gliK*

signal at 2120 bp, whereas the mutant contained no evidence of *gliK* presence,

thereby confirming the reintroduction of the *gliK* gene into the genome of *A.*

fumigatus Δ*gliK*^46645 and also the absence of the *gliK* gene in the mutant strain.
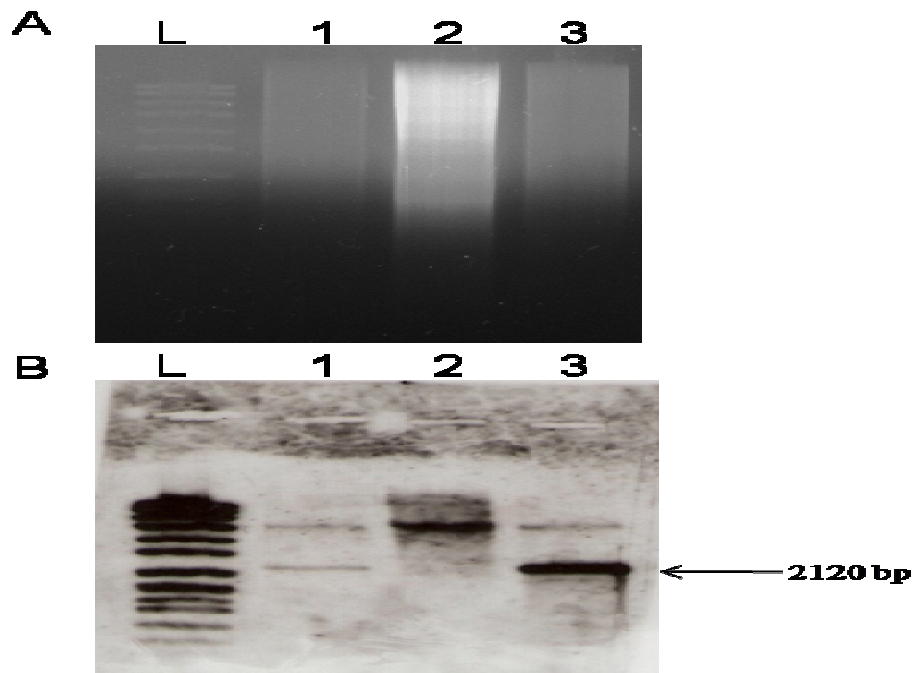
Figure 5.16: Identification of *A. fumigatus gliK^c* by Southern blot analysis. (A) DNA digested with *Xba*I for probing with *gliK* coding probe for Southern blot analysis & (B) corresponding Southern blot. Lane L: Molecular weight marker dig labelled ladder (Roche VII), Lane 1: ATCC46645 (2120 bp), Lane 2: Δ*gliK*^46645, Lane 3: *gliK^c* (2120 bp).

5.2.4 Real time PCR expression levels of *gliK*

Gene expression can be quantified relative to a constitutively expressed gene,

usually a housekeeping gene. In this project, the gene expression quantification is a

relative quantification compared to the constitutively expressed Calmodulin gene

(*calm*) (AFUA_4G10050) (Burns *et al.,* 2005). This gene is expressed at the same

level regardless of time-point, media, or additives. The expression of calmodulin is

adjusted to 1 and the expression of the gene of interest is expressed as a ratio compared to calmodulin expression.

Firstly, the expression of *gliK* was measured in *A. fumigatus* ATCC46645 in different liquid media types, namely, Sabouraud media, Minimal media (MM) and Aspergillus Minimal media (AMM). The cultures were grown for 24, 48 and 72 hr, respectively (Figure 5.17).
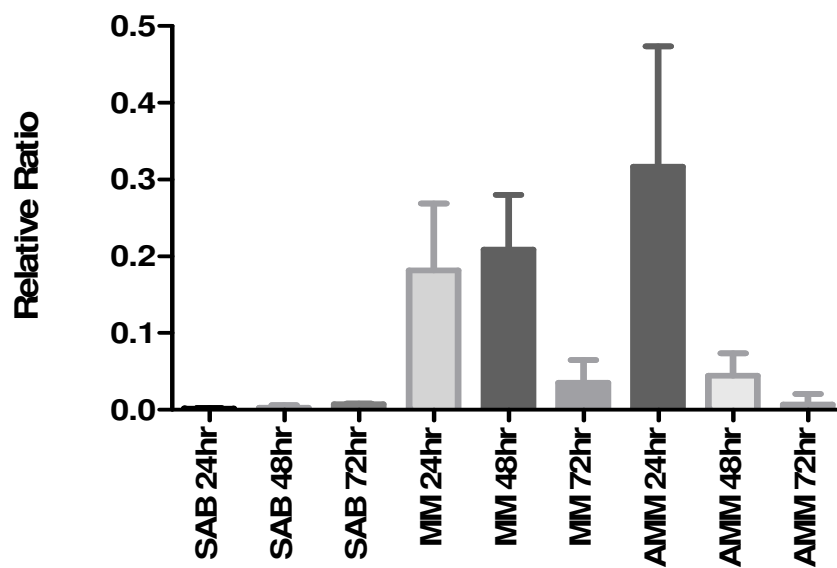
Figure 5.17: qRT-PCR analysis of *gliK* expression at 24, 48 and 72 hr in *A. fumigatus* ATCC46645 cultured in various media at 37 °C.

Expression of *gliK* never reached over a ratio of 1 indicating that it is expressed at a much lower level than calmodulin. The results show that *gliK* expression is highest in AMM media at 24 hr. Interestingly, *gliK* expression is absent in the Sabouraud media at all time points. The expression of *gliK* in MM media is approximately the same at 24 and 48 hr, whereas, the expression level drops dramatically at 72 hr ($P < 0.1$). In AMM cultures, the highest expression of *gliK* was at 24 hr which reduced considerably at 48 hr ($P < 0.01$) and is barely detectable at 72

hr (P < 0.001). This indicates that *gliK* expression is highest in minimal media and at early time-points during culture.

Secondly, the deletion of *gliK* from the genome in the $\Delta gliK^{46645}$ strain should result in absence of *gliK* expression. As culturing in AMM gave the greatest expression of *gliK*, this media was chosen to confirm the absence of *gliK* expression in *A. fumigatus* $\Delta gliK^{46645}$ (Figure 5.18).
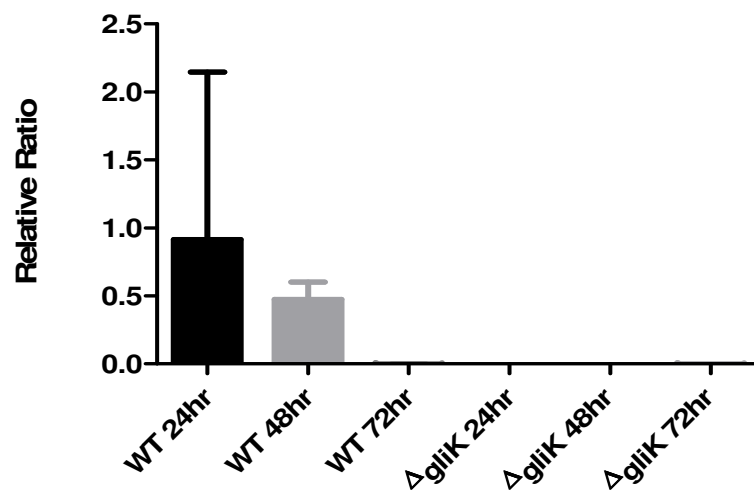
Figure 5.18: qRT-PCR analysis of *gliK* expression in *A. fumigatus* ATCC46645 and $\Delta gliK^{46645}$, respectively, in AMM at selected time points at 37 °C.

gliK was expressed in *A. fumigatus* ATCC46645 at 24 and 48 hr time points, whereas the $\Delta gliK^{46645}$ strain did not express *gliK*, thereby confirming the deletion of *gliK* from the genome.

As *gliK* is located adjacent to the transporter gene, *gliA*, the integrity and expression of *gliA* (AFUA_6G09710) was verified by RT-PCR in *A. fumigatus* ATCC46645, $\Delta gliK$ and *gliK*[c] to determine if the deletion of *gliK* and subsequent reinsertion of *gliK* disrupted the expression of this adjacent gene. RT-PCR was

conducted using the house-keeping gene Calmodulin (*calm*) (Burns *et al.,* 2005) as a control to verify that the samples used were gDNA free as *gliK* has a predicted intron of 50 bp, and such a small size difference is difficult to visualise by DNA electrophoresis. Also, *gliA* has no predicted introns, resulting in the same amplification size of cDNA or gDNA. Therefore, a gDNA control for *gliK* and *gliA* would not serve any purpose in this study. The genomic DNA amplification of *calm* results in a band of 617 bp, whereas the cDNA amplification of *calm* results in a band of 348 bp, due to the removal of the intron during cDNA synthesis. The amplification of *gliK* cDNA results in a band of 370 bp, and the amplification of *gliA* results in a band of 155 bp (Figure 5.19).
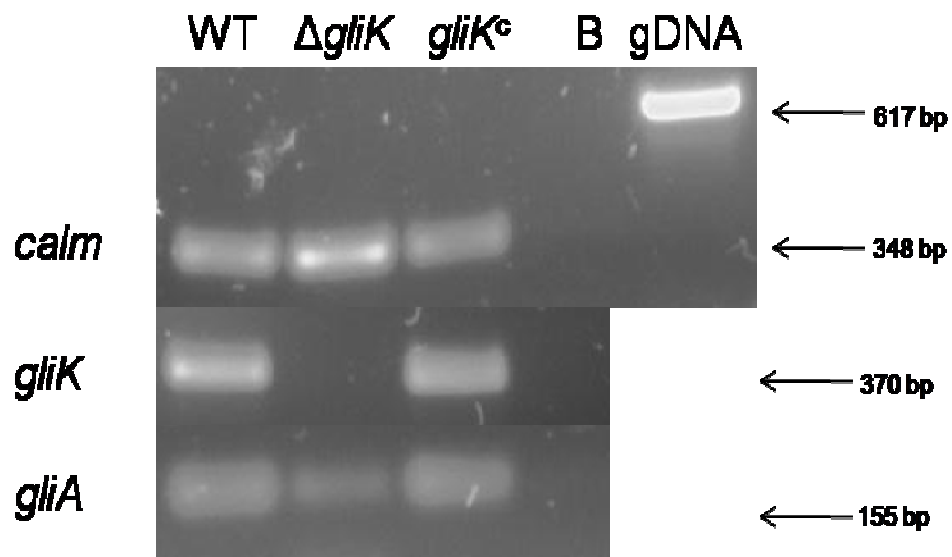
Figure 5.19: RT-PCR analysis of *gliK* and *gliA* expression in *A. fumigatus* ATCC46645, Δ*gliK*[46645] and *gliK*[c] respectively.

The expected bands were observed for all samples. *gliK* expression was observed in the wild-type and complimented strain, with a lack of expression in the mutant strain. *gliA* expression was observed in all strains, verifying that the deletion and reinsertion of *gliK* did not disrupt the expression of *gliA*.

As *gliK* is a component of the gliotoxin biosynthetic cluster, located adjacent to the transporter gene, *gliA*, the application of exogenous gliotoxin may have an impact on the expression of *gliK*. Liquid cultures of *A. fumigatus* ATCC46645 in AMM were spiked with gliotoxin (5 µg/ml final) at 21 hr and the cultures harvested at 24 hr (Schrettl *et al.,* 2010). The expression of *gliK* was determined in *A. fumigatus* ATCC46645 with and without gliotoxin presence (Figure 5.20).
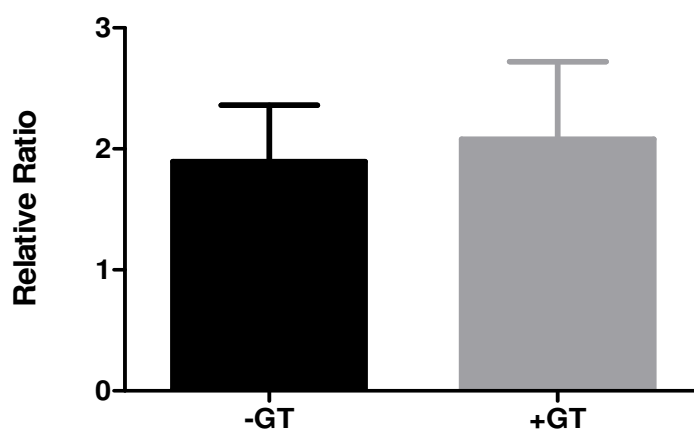
Figure 5.20: qRT-PCR analysis of *gliK* expression in *A. fumigatus* ATCC46645 in AMM at 24 hr at 37 °C, with and without exogenous gliotoxin spiked into the media. Column 1: *gliK* expression in *A. fumigatus* ATCC46645 strain; Column 2: *gliK* expression in *A. fumigatus* ATCC46645 strain spiked with 5 µg/ml gliotoxin.

The expression of *gliK* in *A. fumigatus* ATCC46645 did not significantly increase in the presence of gliotoxin. This may indicate that *gliK* expression is not dramatically controlled by the presence of gliotoxin. As gliotoxin is produced by the fungus itself, the concentration used may not have been sufficient to induce *gliK* expression.

AMM liquid cultures of *A. fumigatus* ATCC46645 were spiked with hydrogen peroxide (1 mM) at 21 hr and the culture was harvested at 24 hr. The expression of *gliK* was detected (Figure 5.21), whereby exposure of *A. fumigatus* to hydrogen peroxide caused an increase in *gliK* expression from a relative ratio of 0.1665 to 3.193 (P = 0.0101).
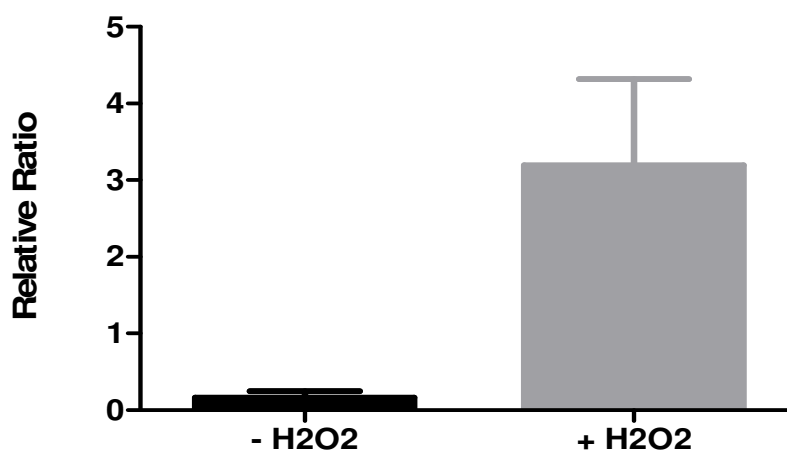
Figure 5.21: qRT-PCR analysis of *gliK* expression in *A. fumigatus* ATCC46645 in AMM at 24 hr at 37 $^{\circ}$C, with and without hydrogen peroxide spiked into the media. Column 1: *gliK* expression in *A. fumigatus* ATCC46645 strain; Column 2: *gliK* expression in *A. fumigatus* ATCC46645 strain spiked with 1 mM hydrogen peroxide (final concentration).

5.2.5 Plate assays

5.2.5.1 Gliotoxin Plate assays

Schrettl *et al.* (2010) have recently shown that *A. fumigatus* is capable of self-protection against gliotoxin, and that deletion of *gliT* from the gliotoxin biosynthetic cluster can render the mutant strain sensitive to exogenous gliotoxin. In plate assays where *A. fumigatus* wild-type and Δ*gliK* strains were grown on agar containing gliotoxin (0 – 20 µg/ml), both Δ*gliK* mutants were significantly more sensitive to gliotoxin (p < 0.001), and the reduced growth rate was seen at every time point of the assay, where the greatest difference in growth was seen at 72 hr (Figure 5.22 and

238

Figure 5.23). After 72 hr growth on AMM plates, there is a significant decrease in the radial growth of *A. fumigatus* Δ*gliK*[46645] strain compared to the wild-type strain when gliotoxin was present in the media (Figure 5.22). The difference is highly significant when the gliotoxin concentration is increased to 10 and 20 μg/ml, respectively ($p < 0.001$). *A. fumigatus* ATCC46645 also exhibited a decrease in radial growth (~20 %) at the highest gliotoxin concentration used (20 μg/ml), compared to the media without gliotoxin, indicating that *A. fumigatus* wild-type is sensitive to high concentrations of gliotoxin, under the experimental conditions used.
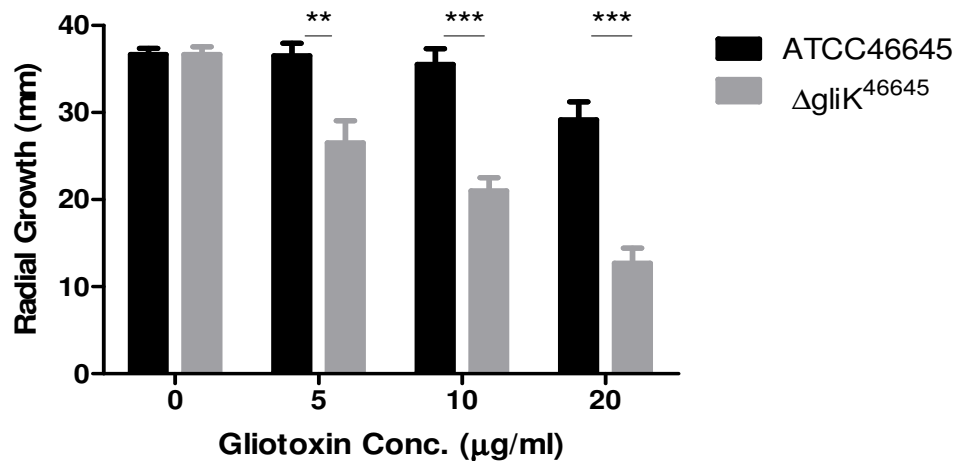
Figure 5.22: Effect of gliotoxin on the growth of *A. fumigatus* ATCC46645 and *ΔgliK*[46645], respectively. Significant growth inhibition of *A. fumigatus* Δ*gliK*[46645] is evident at 72 hr ($n = 3$).

The decrease in radial growth due to the presence of exogenous gliotoxin was also observed in *A. fumigatus* Δ*gliK*[26933] mutant strain at all gliotoxin concentrations tested (Figure 5.23). This decreased radial growth was highly significant at 10 and 20 μg/ml gliotoxin, respectively ($p < 0.001$). Similar to *A. fumigatus* ATCC46645, ATCC26933 showed a decrease in growth ability in gliotoxin (20 μg/ml), where

there was a reduction in radial growth of 21 % compared to the media without gliotoxin.
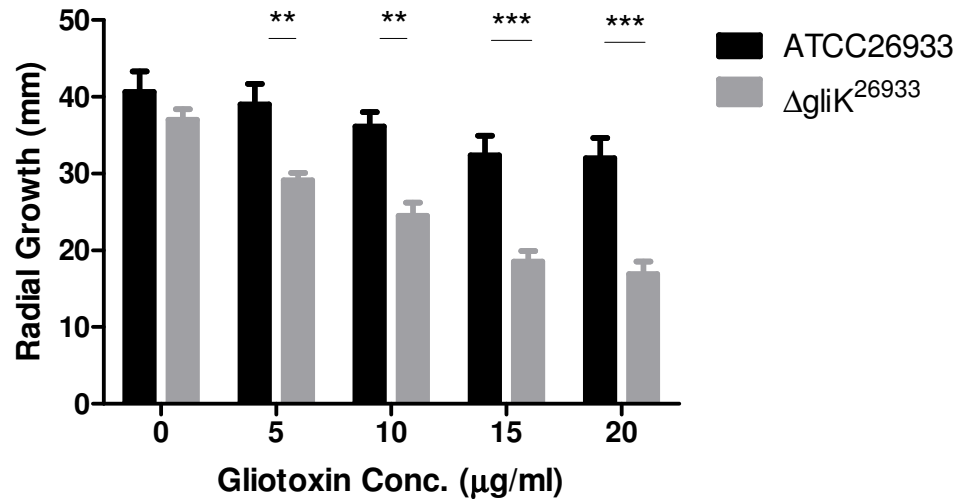
Figure 5.23: Effect of gliotoxin on the growth of *A. fumigatus* ATCC26933 and $\Delta gliK^{26933}$, respectively. Significant growth inhibition of *A. fumigatus* $\Delta gliK^{26933}$ is evident at 72 hr ($n = 4$).

5.2.5.2 Hydrogen peroxide susceptibility assays

After 72 hr growth on AMM plates, there was a significant difference in the radial growth of the *A. fumigatus* $\Delta gliK^{46645}$ strain compared to the wild-type strain when hydrogen peroxide (2 mM) was present ($p < 0.01$) (Figure 5.24). This concentration of hydrogen peroxide rendered the mutant strain incapable of any growth. Neither strain was capable of growth at 5 mM hydrogen peroxide. At the lower hydrogen peroxide concentration (1 mM), both strains were capable of equivalent radial growth.
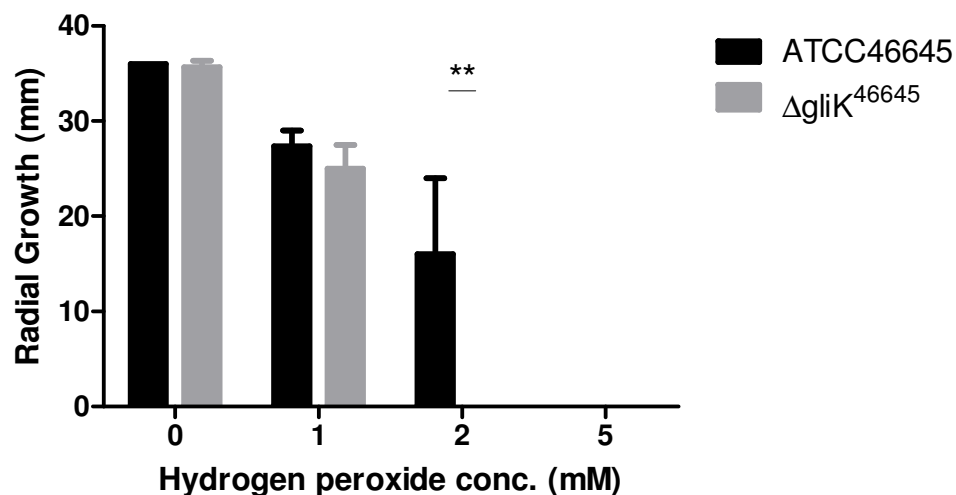
Figure 5.24: Effect of hydrogen peroxide on the growth of *A. fumigatus* ATCC46645 and Δ*gliK*[46645], respectively. Significant growth inhibition of *A. fumigatus* Δ*gliK*[46645] is evident at 72 hr ($n = 3$).

A. fumigatus Δ*gliK*[26933] showed the same pattern of growth on hydrogen peroxide plate assays, as the Δ*gliK*[46645] strain (Figure 5.25). There was significantly different radial growth at 2 mM hydrogen peroxide between the *A. fumigatus* ATCC26933 and Δ*gliK*[26933] strains ($p < 0.01$), as the mutant strain was incapable of any growth at this concentration. This inability of the mutant strain to grow was also observed at 3 mM hydrogen peroxide, but this was not found to be significant as the wild-type growth was also severely diminished.
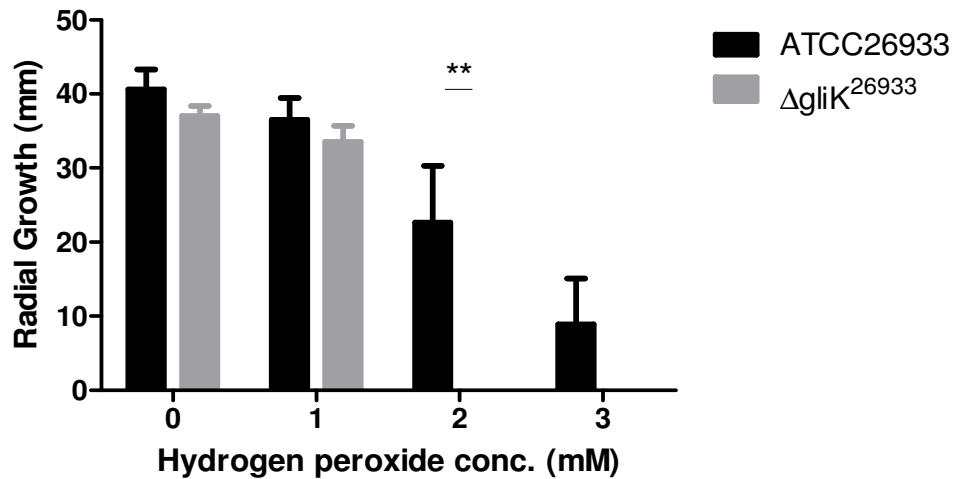
Figure 5.25: Effect of hydrogen peroxide on the growth of *A. fumigatus* ATCC26933 and Δ*gliK*[26933], respectively. Significant growth inhibition of *A. fumigatus* Δ*gliK*[26933] is evident at 72 hr ($n = 4$).

5.2.5.3 Voriconazole Plate assays

After 72 hr on AMM plates in the presence of voriconazole (0 – 0.25 μg/ml), there was no significant growth difference between the *A. fumigatus* ATCC46645 and Δ*gliK*[46645] strains (Figure 5.26). Neither strain was capable of growth on the 0.25 μg/ml concentration of voriconazole.
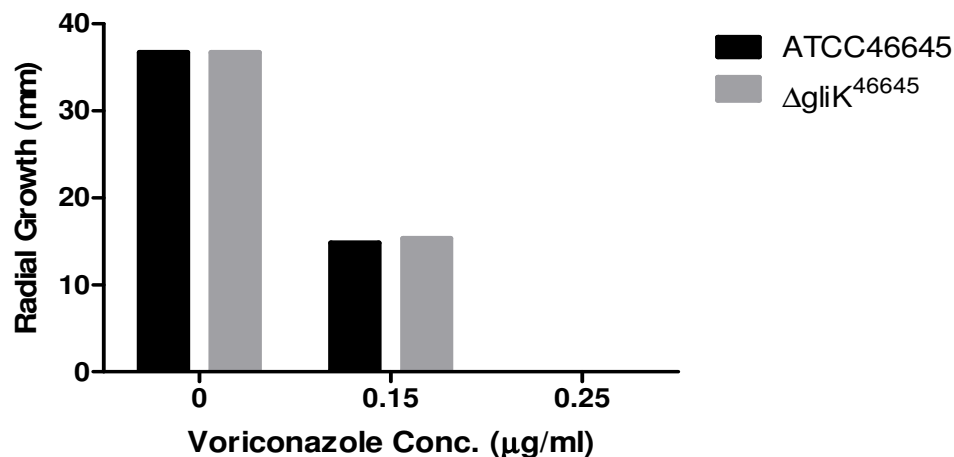
Figure 5.26: Effect of voriconazole on the growth rate of *A. fumigatus* ATCC46645 and $\Delta gliK^{46645}$, respectively. No significant growth inhibition of *A. fumigatus* $\Delta gliK^{46645}$ is evident ($n = 3$).

After 72 hr growth on AMM plates, there was a marginal decrease in radial growth of the $\Delta gliK^{26933}$ strain compared to that of the ATCC26933 observed on the higher concentrations of voriconazole (0.15 µg/ml and 0.25 µg/ml), but this difference in radial growth was not found to be significant (Figure 5.27). Interestingly, at the lower concentration (0.05 µg/ml), the radial growth of the mutant strain was greater than that of the wild-type strain. Again, this difference was not significant.
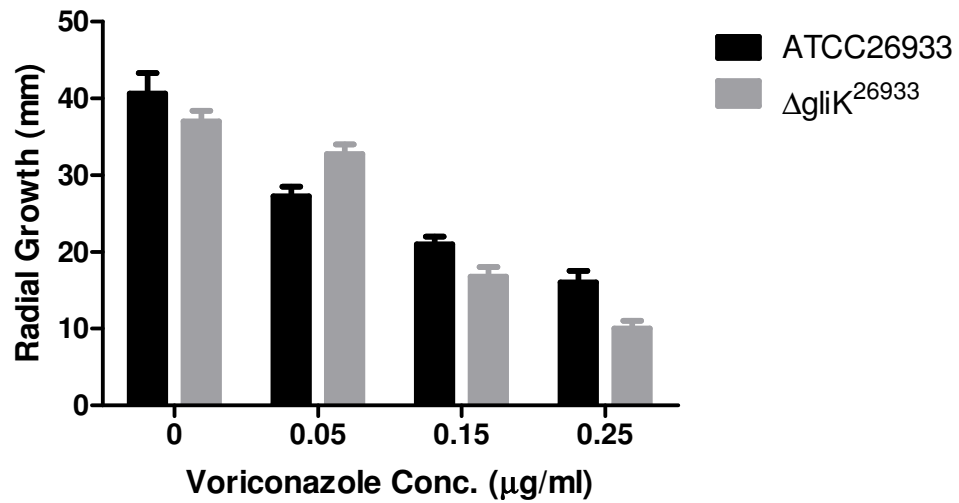
Figure 5.27: Effect of voriconazole on the growth of *A. fumigatus* ATCC26933 and Δ*gliK*[26933], respectively. No significant growth inhibition of *A. fumigatus* Δ*gliK*[26933] is evident (*n* = 4).

5.2.6 RP-HPLC analysis of gliotoxin production

As gliotoxin is a secreted from *A. fumigatus*, supernatants were collected from *A. fumigatus* wild-type and Δ*gliK* liquid cultures and subjected to organic extraction as described in Section 2.2.10. Organic extracts were fractionated by Reverse Phase - High Performance Liquid Chromatography (RP-HPLC) to determine whether the *A. fumigatus* Δ*gliK* strains could produce gliotoxin. Initial results revealed that *A. fumigatus* ATCC46645 did not produce significant amounts of gliotoxin and therefore it was difficult to determine if the removal of *gliK* had an impact on gliotoxin production (Figure 5.28). The gliotoxin standard was detected at a retention time of 14.41 min (A_{254nm}). *A. fumigatus* ATCC46645 produced a small peak at a retention time 14.37 min, which can be identified as gliotoxin. The analysis of the *A. fumigatus* Δ*gliK*[46645] showed that this strain did not produce a metabolite that corresponded to gliotoxin.

As the *A. fumigatus* ATCC46645 strain produces gliotoxin in such small quantities, the *A. fumigatus* ATCC26933 strain was employed, as this was a known producer of gliotoxin. RP-HPLC analysis of the *A. fumigatus* ATCC26933 strain showed clear gliotoxin production, resulting in a peak observed at a retention time of 15.216 min, comparable to the standard gliotoxin peak (15.243 min) (Figure 5.29). The RP-HPLC gradient conditions were altered, which resulted in the elevated retention time of gliotoxin, compared to the previous analysis (15.25 min compared to 14.4 min). The mutant, Δ*gliK*[26933] produced a metabolite corresponding to gliotoxin at the expected retention time, 15.267 min but at a very low level. A new metabolite with a retention time of 12.975 min was evident in cultures from *A. fumigatus* Δ*gliK*[26933].
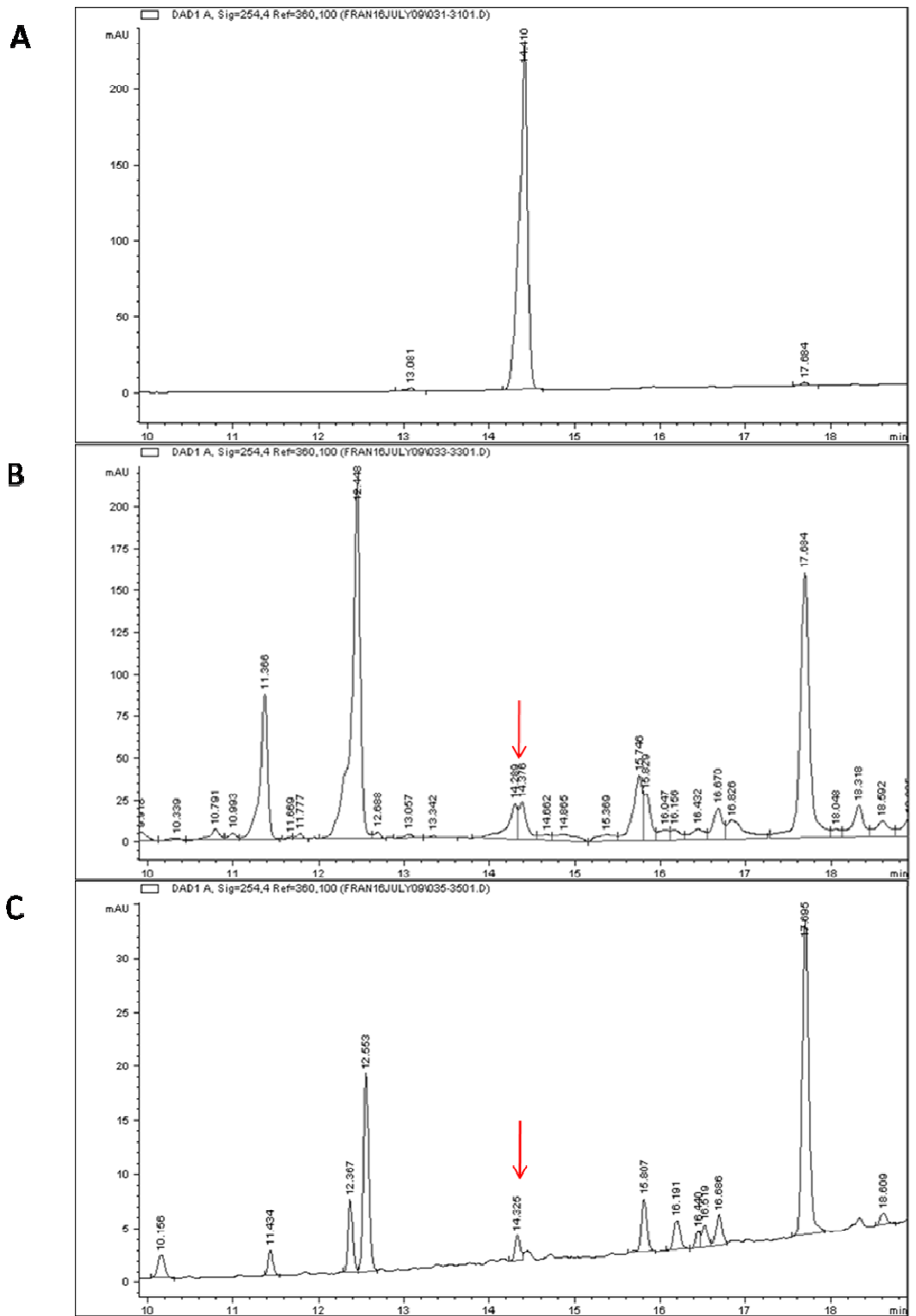
Figure 5.28: HPLC chromatograms detailing the fractionation of metabolites from A. *fumigatus* liquid cultures for the identification of gliotoxin production. Detection at 254nm. (A) standard gliotoxin with a retention time of 14.4 min, (B) ATCC46645 with a gliotoxin peak at the retention time of 14.376 min, and (C) Δ*gliK*[46645] lacking in a corresponding gliotoxin peak. Note the increased sensitivity of detection for C, compared to B.

246
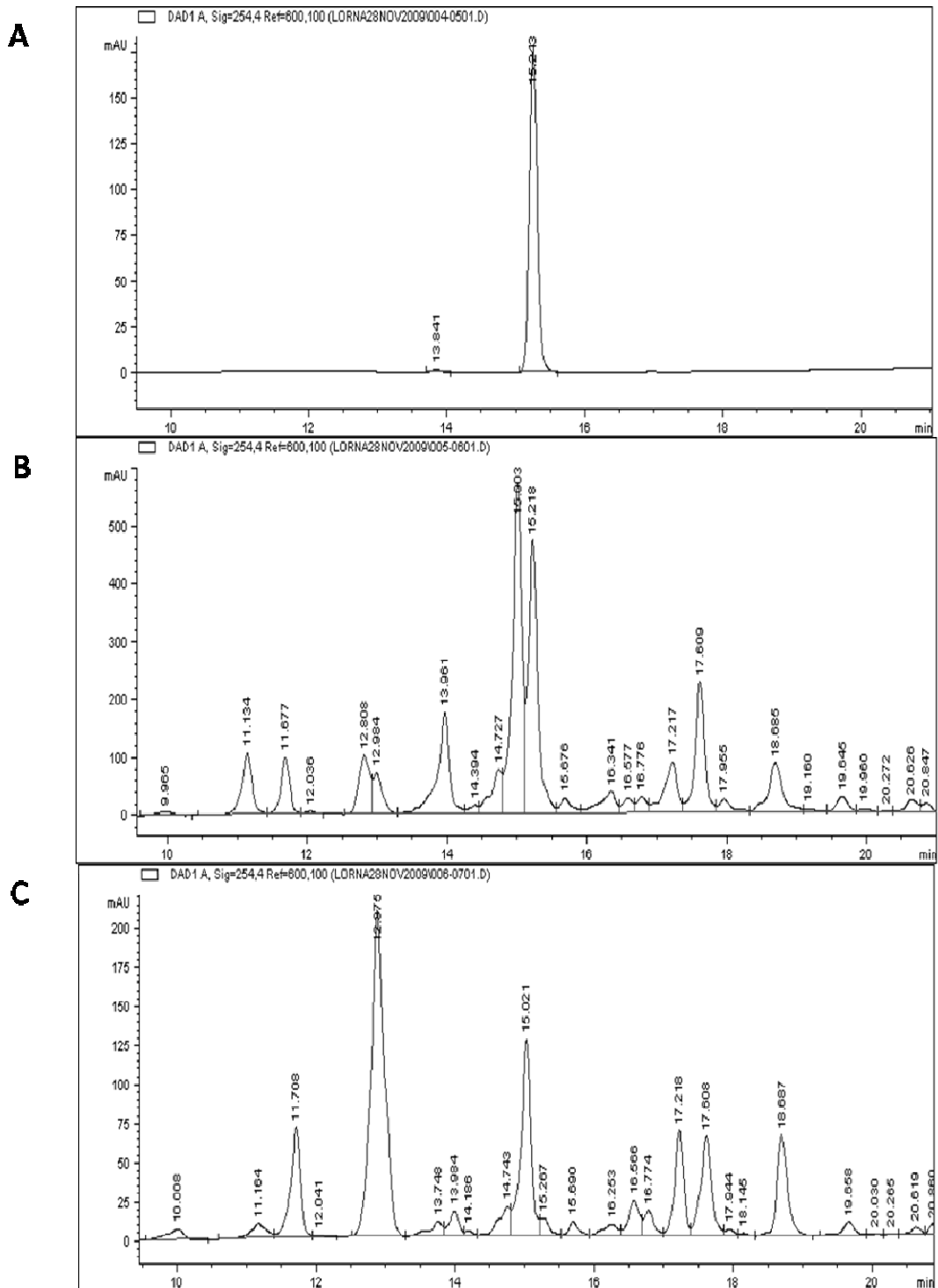
Figure 5.29: HPLC chromatograms detailing the fractionation of metabolites from A. *fumigatus* liquid cultures for the identification of gliotoxin production. Detection at 254nm. (A) standard gliotoxin with a retention time of 15.2 min, (B) ATCC26933 with a 15.2 min retention time peak, and (C) Δ*gliK*[26933], illustrating virtual absence of gliotoxin secretion at 15.2 min.

To confirm the results observed for altered gliotoxin production, organic extracts were treated with sodium borohydride to generate the dithiol form of gliotoxin (reduced gliotoxin; Figure 5.1). Sodium borohydride reduces the disulphide bridge to yield the dithiol form. Davis *et al.* (2010) showed that this reduction decreases the retention time of gliotoxin by approximately 1 min.

For the ATCC46645 analysis, the standard gliotoxin produced a peak at a retention time of 14.4 min. Once reduced, this peak shifted to a retention time of 13.38 min. It was unclear in *A. fumigatus* ATCC46645 if the peak barely detectable at 14.4 min retention time was gliotoxin (Figure 5.30). As the peak was so small, the reduction effect is unclear with very little changing in the reduced sample. The mutant strain, *A. fumigatus* Δ*gliK*[46645], did not produce a peak at 14.4 min, and therefore chemical reduction did not lead to any conclusive results to determine the effect of the *gliK* deletion.

For the analysis of *A. fumigatus* ATCC26933, the standard gliotoxin was detected at the retention time of 15.2 min. Once reduced, gliotoxin had a shorter retention time of 14.1 min. *A. fumigatus* ATCC26933 showed a corresponding peak to the gliotoxin standard at the expected retention time of 15.2 min. After reduction, the dithiol form of gliotoxin was detectable at the shorter retention time of 14.1 min. Thereby, confirming the production of gliotoxin in the ATCC26933 strain. Additionally, the peak observed at 15.0 min was also reduced. The mutant strain, Δ*gliK*[26933], exhibited a minor peak at the 15.2 min retention time which when reduced, was unclear if the reduction had any effect on this metabolite. The peak observed at 15.0 min was clearly reduced. In addition, the Δ*gliK*[26933] strain produces a larger peak, with a retention time of 12.9 min, than that observed in the wild-type strain (Figure 5.31).
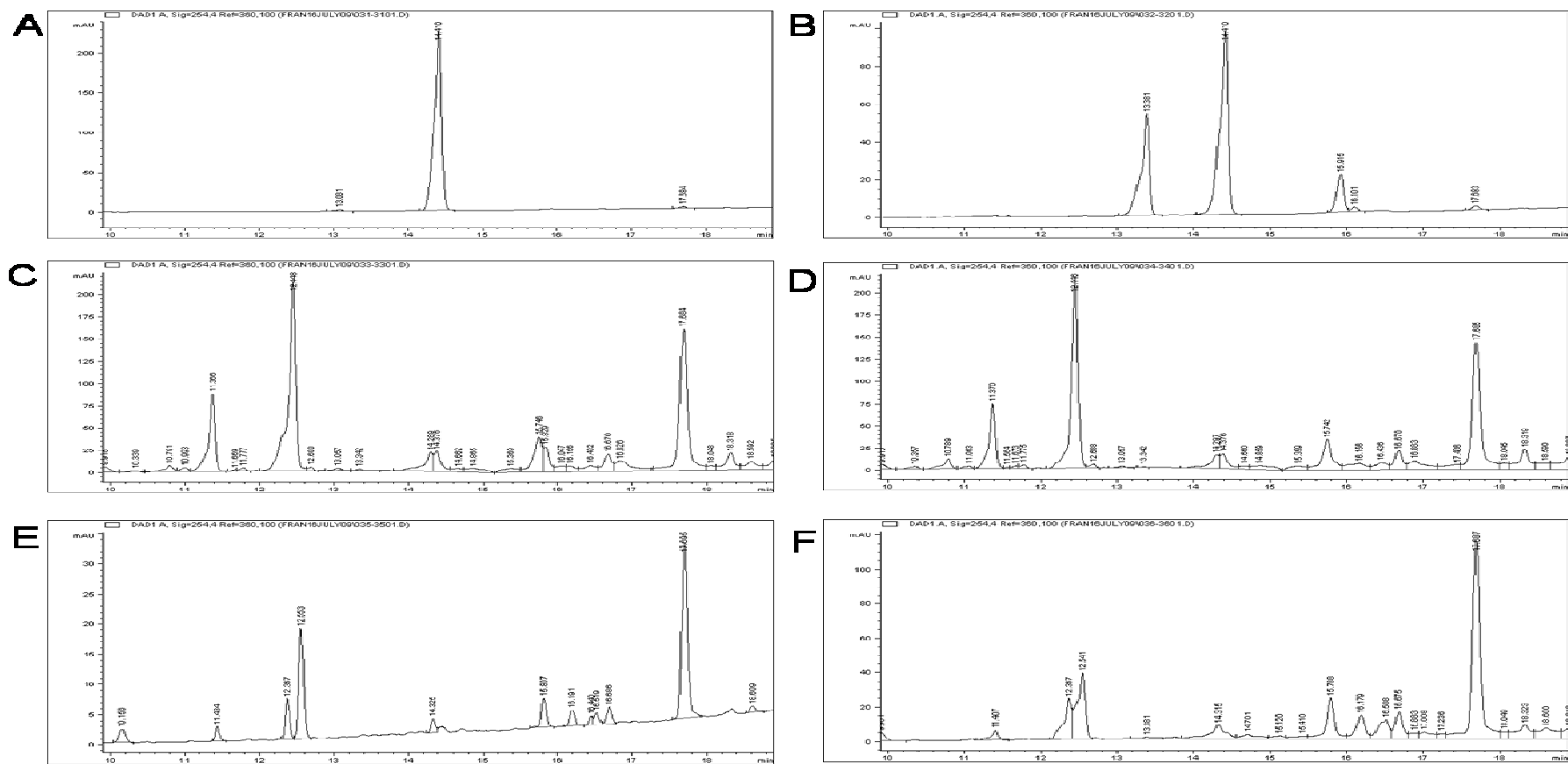
Figure 5.30: HPLC chromatograms of the fractionation of metabolites from A. *fumigatus* liquid cultures for the identification of gliotoxin production by reduction with sodium borohydride. (A & B) Unreduced and reduced Standard gliotoxin, with retention time peaks at 14.4 min and 13.38 min, respectively. (C & D) Unreduced and reduced ATCC46645, where the peak at the retention time 14.4 min did not alter by reduction, (E & F) Unreduced and reduced $\Delta gliK^{46645}$, where the peak at retention time 14.4 min did not alter by reduction.
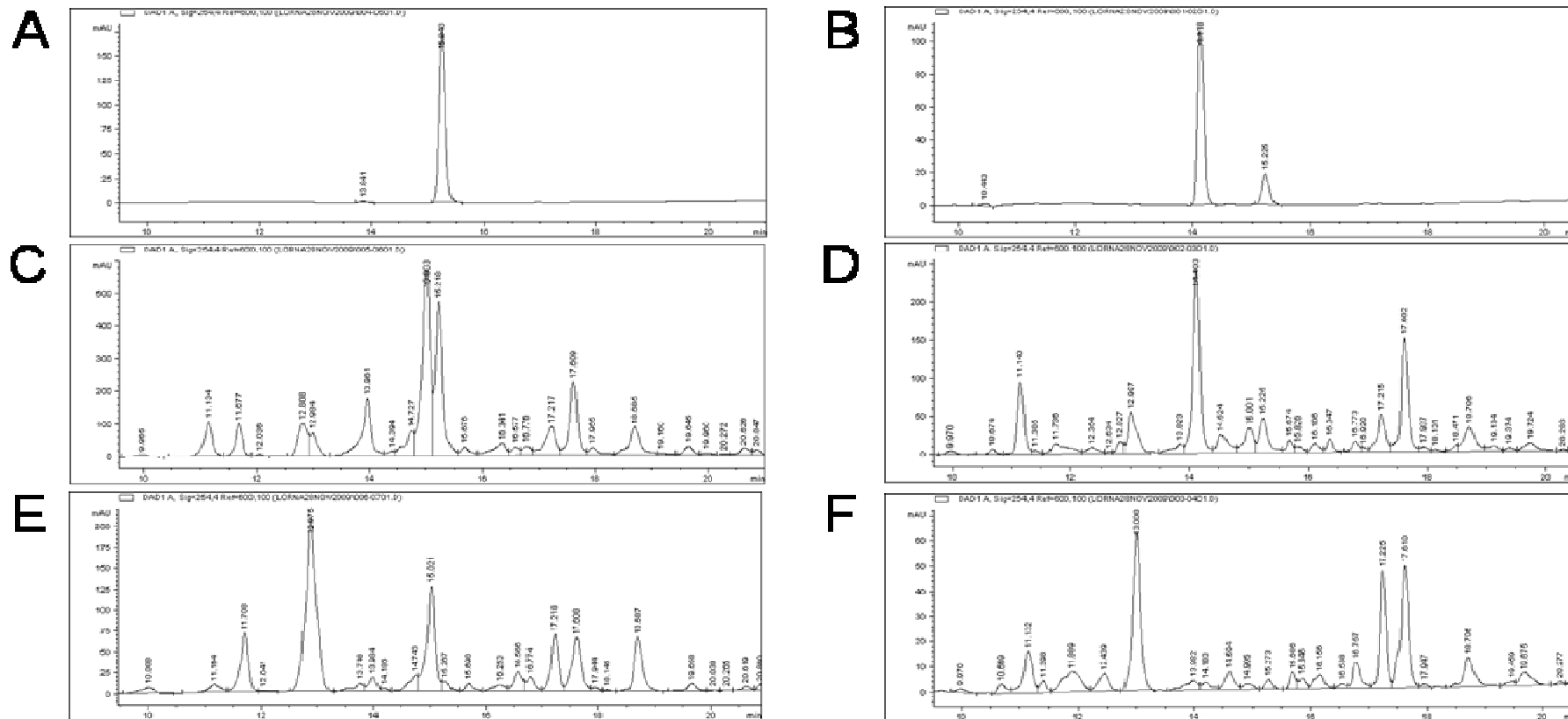
Figure 5.31: HPLC chromatographs of the fractionation of metabolites from A. *fumigatus* liquid cultures for the identification of gliotoxin production by reduction with sodium borohydride. (A & B) Unreduced and reduced Standard gliotoxin, with retention time peaks at 15.2 min and 14.1 min, respectively. (C & D) Unreduced and reduced ATCC26933, where the corresponding gliotoxin peak at the retention time 15.2 min was reduced to a lower retention time of 14.1 min, (E & F) Unreduced and reduced $\Delta gliK^{26933}$ where the peak at retention time 15.02 min was reduced.

5.2.7 Complementation analysis

The reinsertion of the *gliK* gene back into the *A. fumigatus* $\Delta gliK^{46645}$ can potentially recover the strain from the deficiencies of the mutation. qRT-PCR analysis confirmed that the expression of *gliK* had been restored in the complemented strain (Figure 5.32). The expression of *gliK* in the complemented strain was higher than the original wild type which may indicate that *gliK* may have reinserted into sites other than the targeted region. Although previous plate assays involving *gliK* had shown that the mutant strains are sensitive to gliotoxin (Section 5.2.5.1), the complemented strain did not return to full growth capabilities in the presence of gliotoxin (Figure 5.33). The complemented and mutant strains retained the same sensitivity to gliotoxin compared to the wild-type, and there was no significant difference in growth between the mutant and the complemented strains at any of the gliotoxin concentrations. Therefore, the reinsertion of the *gliK* gene has not recovered the wild-type phenotype, indicating that the inserted *gliK* is not functioning as in the original.
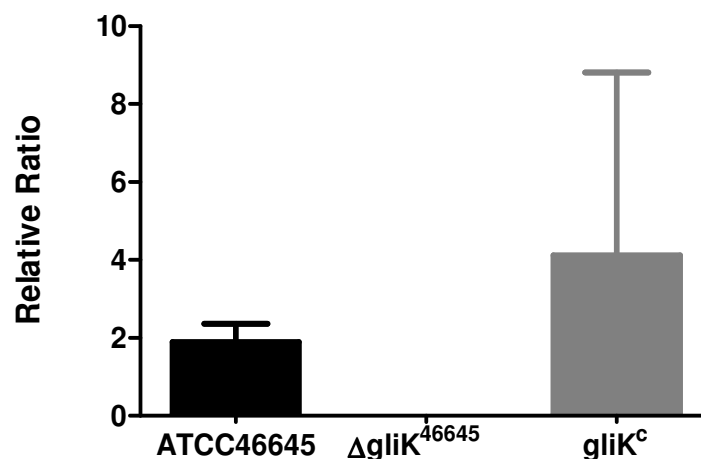
Figure 5.32: qRT-PCR analysis of *gliK* expression in *A. fumigatus* ATCC46645, $\Delta gliK^{46645}$, and *gliK^c* in AMM at 24 hr at 37 °C.
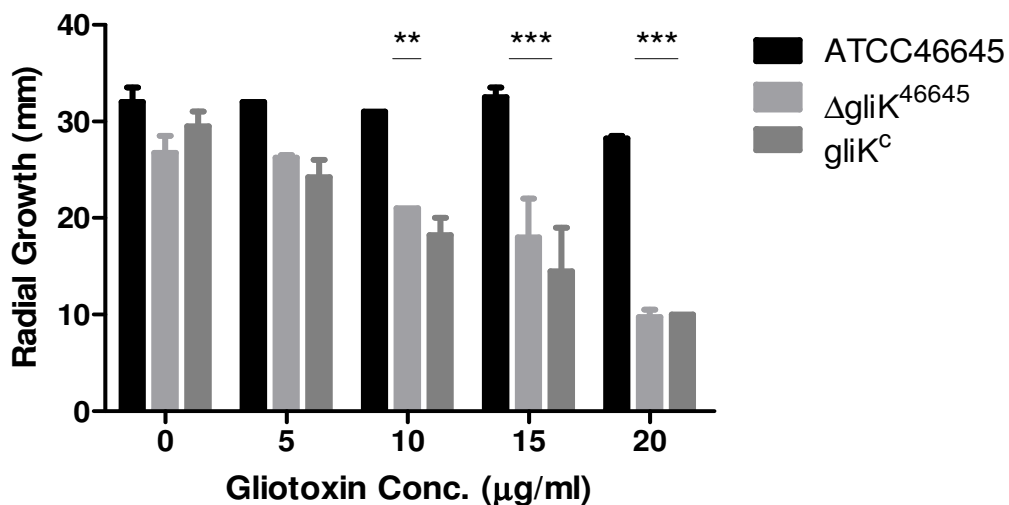
Figure 5.33: Effect of gliotoxin on the growth of *A. fumigatus* ATCC46645, *ΔgliK*⁴⁶⁶⁴⁵, and *gliK*ᶜ respectively ($n = 2$).

*gliK*ᶜ was also cultured in liquid media and the supernatant was examined for gliotoxin production by RP-HPLC. As the background strain is ATCC46645, a small producer of gliotoxin, it was not expected that the *gliK*ᶜ would produce a vast amount of gliotoxin. Nevertheless, the organic extract was subjected to reduction by sodium borohydride, as previously described. The RP-HPLC analysis of the *gliK*ᶜ cultures showed that that the peak at retention time of 14.4 min, was the same as the wild-type potential gliotoxin (Figure 5.34). The *gliK*ᶜ analysis showed that the complemented strain produces a peak at a retention time of 13.9 min, which was not observed in the *A. fumigatus* ATCC46645 or Δ*gliK*⁴⁶⁶⁴⁵ strains.
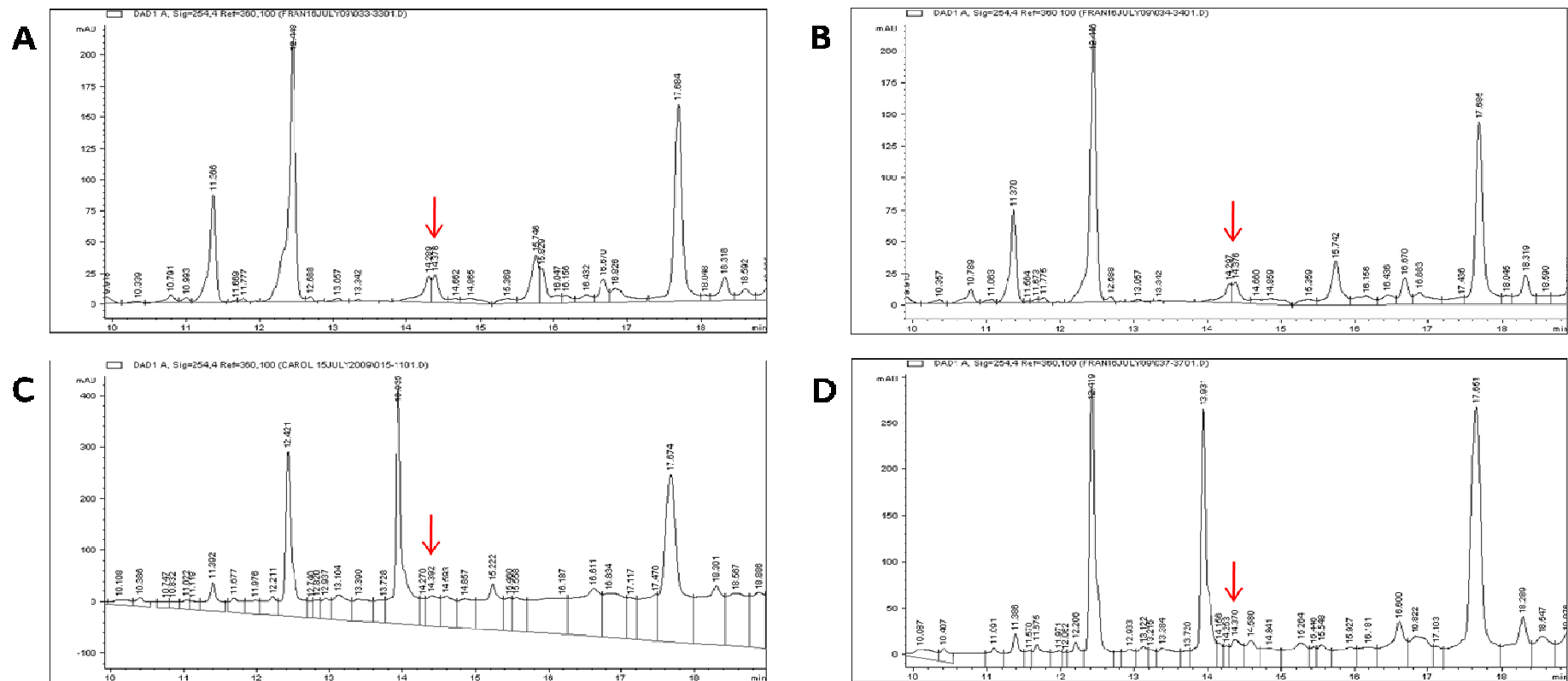
Figure 5.34: HPLC chromatograms of the fractionation of metabolites from A. *fumigatus* liquid cultures for the identification of gliotoxin production by reduction with sodium borohydride. (A & B) Unreduced and reduced ATCC46645, where the corresponding peak to the gliotoxin standard at the retention time 14.4 min was not reduced, (C & D) unreduced and reduced *gliK*^c where there was no corresponding gliotoxin peak at retention time 14.4 min. The peak at 13.9 min was partially reduced.The peak which corresponded to the gliotoxin peak is highlighted by a red arrow.

5.2.8 Gliotoxin uptake assay

Gliotoxin has been shown to have an impact on the expression of genes within the gliotoxin biosynthetic cluster, whereby the addition of gliotoxin to *A. fumigatus* Δ*gliP* strain restored the expression of all the other genes within the gliotoxin biosynthetic cluster (Cramer *et al.,* 2006a). Also, the transporter genes contained in the sirodesmin biosynthetic cluster of *L. maculans* can impart self-protection against the toxin (Gardiner *et al.,* 2005b), indicating that the presence of the toxin can induce expression of certain genes within the cluster. Schrettl *et al.* (2010) have described that *A. fumigatus* Δ*gliT* is unable to sustain growth in the presence of gliotoxin confirming that *gliT* protects against exogenous gliotoxin and therefore represents a mechanism within the fungus to self-protect against gliotoxin presence. Similarly, the plate assays previously described in this chapter show that the Δ*gliK* strains, regardless of background, are significantly more sensitive to the presence of gliotoxin, than wild-type, and therefore *gliK* may be involved in protection against gliotoxin toxicity in *A. fumigatus*. As gliotoxin clearly affects *A. fumigatus,* it was important to establish the baseline production of gliotoxin and also to investigate if *gliK* might have a role in gliotoxin uptake or release (efflux).

The RP-HPLC analysis showed that *A. fumigatus* ATCC46645 is capable of producing gliotoxin in very small quantities (Section 5.2.6). To further investigate the production of gliotoxin by this strain, the gliotoxin production was examined by analysing the gliotoxin production by RP-HPLC and taking into account the quantity of the mycelia mass produced, as detailed in Section 2.2.14. It was confirmed that the ATCC46645 strain produced a residual amount of gliotoxin, (mean ± SEM) 0.3 ± 0.13 ng/mg mycelia (Figure 5.35). *A. fumigatus* Δ*gliK*[46645] did not produce gliotoxin to the same extent as the wild-type strain, but it did produce a residual amount of

gliotoxin, 0.032 ± 0.02 ng/mg mycelia (Figure 5.35) (P = 0.001). This indicates that *gliK* may not be involved directly in the biosynthesis in gliotoxin, but that its deficiency is detrimental to the export, secretion or uptake of gliotoxin.
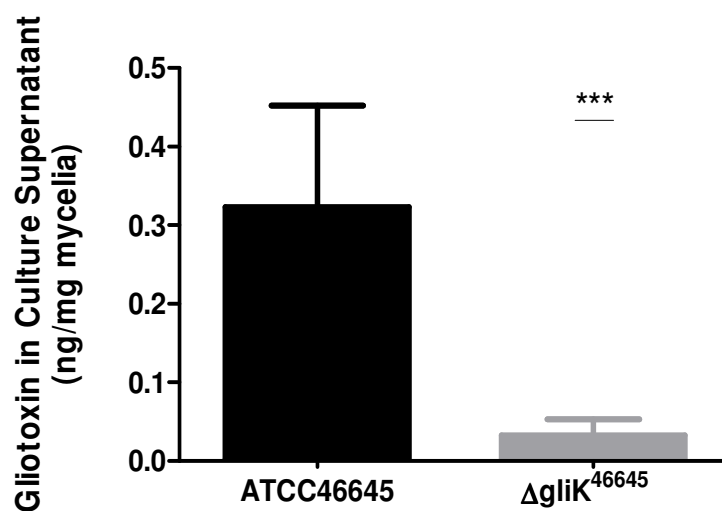
Figure 5.35: Gliotoxin production in AMM liquid cultures from strains ATCC46645 and Δ*gliK*[46645].

Given the low extent of secretion of significant amounts of gliotoxin by *A. fumigatus* ATCC46645 and Δ*gliK*[46645], it was decided to evaluate the uptake of relatively high concentrations of exogenously added gliotoxin to both wild-type and Δ*gliK*[46645] strains in liquid culture (5 μg/ml for 0 – 45 min). The extracts were then analysed by RP-HPLC to determine the amount of gliotoxin still remaining in the supernatant and gliotoxin uptake was related to mycelial mass. It was observed that significantly less gliotoxin was present in culture supernatants of *A. fumigatus* Δ*gliK*[46645] compared to ATCC46645 after gliotoxin exposure, at 15 min (P = 0.0102), and 30 min (P = 0.0045) suggesting that gliotoxin is either (i) removed more rapidly from the supernatant or (ii) is effluxing more slowly from the mycelia of *A. fumigatus* Δ*gliK*[46645] (Figure 5.36). After 45 min post-spiking of gliotoxin into the

cultures, the level of gliotoxin increases in the Δ*gliK* cultures, possibly because alternative efflux mechanisms had been activated.
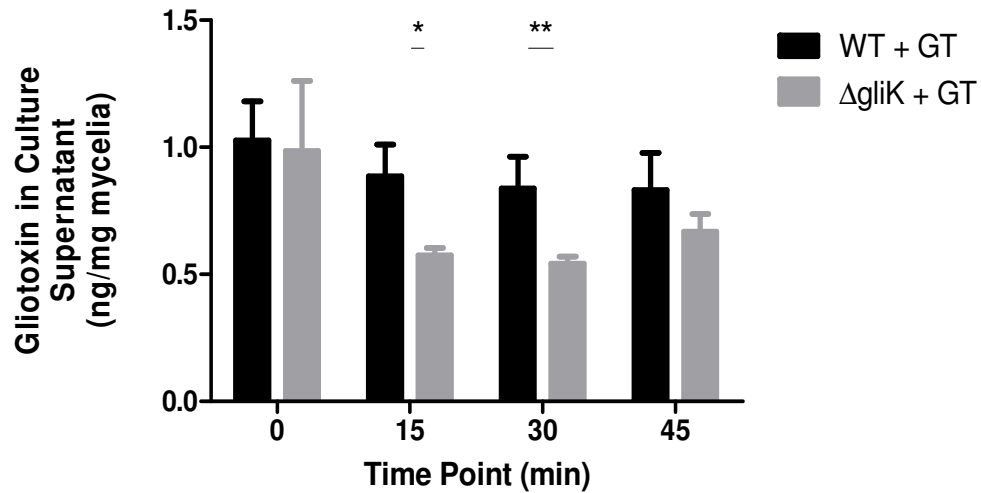
Figure 5.36: The amount of gliotoxin remaining in culture supernatants at time point intervals after exposure of *A. fumigatus* ATCC46645 and Δ*gliK*^{46645} to gliotoxin (5 μg/ml) over a 0 – 45 min duration.

The uptake rate of gliotoxin from the supernatant by the mycelia of the wild-type and mutant strain was calculated at 15 min intervals (Figure 5.37) where the first 15 min after gliotoxin application, *A. fumigatus* Δ*gliK*^{46645} exhibited a gliotoxin uptake rate of 31.443 pg/mg mycelia/min, over three times that of *A. fumigatus* ATCC46645 (9.337 pg/mg mycelia/min) (P = 0.0039). The wild-type strain had a relatively constant level of gliotoxin over 45 min in the supernatant, indicating that the wild-type strain displayed a balance between uptake and efflux of gliotoxin. In *A. fumigatus* Δ*gliK*^{46645}, gliotoxin levels began to stabilise in the supernatant after the initial uptake in the first 15 min of exposure. Thus, it appears that deletion of *gliK* has disrupted a gliotoxin efflux mechanism in *A. fumigatus* and points to a role for *gliK* in gliotoxin secretion. If *gliK* was a component of a gliotoxin uptake

mechanism, then one would have expected constant, or elevated, gliotoxin levels in

A. fumigatus Δ*gliK*[46645] spiked culture supernatants.
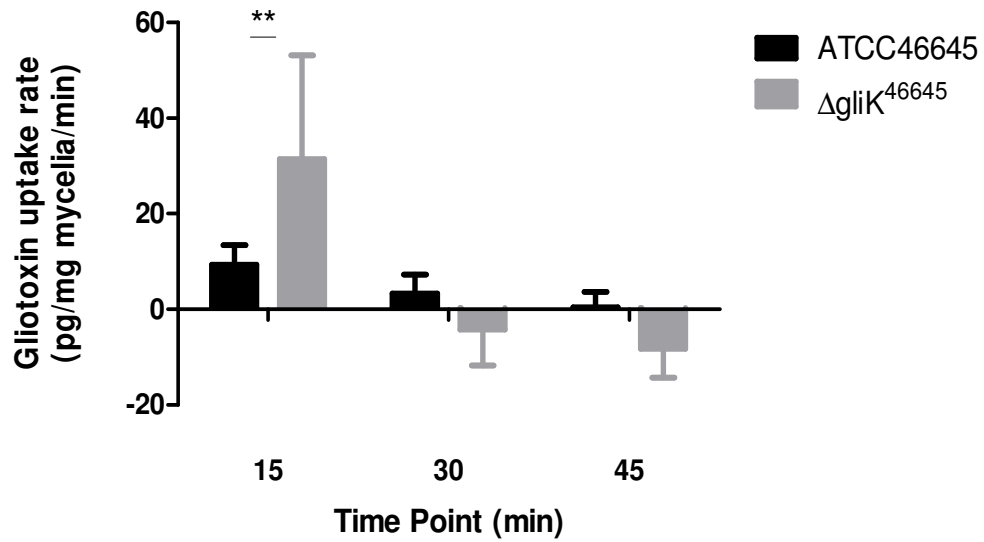
Figure 5.37: Gliotoxin uptake rate by *A. fumigatus* ATCC46645 and Δ*gliK*[46645] in liquid cultures at selected time points.

5.3 Discussion

Many fungi produce metabolites which are toxic to the producer, which leads to the question of how the fungus protects itself from the deleterious effects of its own metabolites. These species, including *A. fumigatus,* have incorporated efficient resistance mechanisms for protection against the specific metabolite. Efflux pathways exhibit such functions; transporting the toxin in/out of the cell, inhibiting the toxic effect of the metabolite or sensing of internal toxin levels (Andrade *et al.,* 2000; Del Sorbo *et al.,* 2000; Gardiner *et al.,* 2005b). The gliotoxin biosynthetic cluster contains 13 genes and only certain genes have been characterised, mainly those involved in the formation of, or self-protection against, gliotoxin (Kupfahl *et al.,* 2006; Bok *et al.,* 2006a; Cramer *et al.,* 2006a; Scharf *et al.,* 2010) or those that were identified by homology to genes in other ETP producing species (Gardiner and Howlett*,* 2005a; Gardiner *et al.,* 2005b). Although orthologs to *gliK* exist in other fungi, bioinformatic analysis of *gliK* in terms of comparative function prediction or conserved domain analysis has provided no clue as to its function (Patron *et al.,* 2007). Recently, certain genes in the gliotoxin biosynthetic cluster have been associated with protection against gliotoxin, such as *gliT*, the thioredoxin reductase, which has been shown to play a self-protecting role against gliotoxin as disruption of this gene renders the fungus completely sensitive to exogenous gliotoxin in plate assays (5 μg/ml)(Schrettl *et al.,* 2010) and in inhibition assays (3 mM) (Scharf *et al.,* 2010). The gliotoxin transporter, *gliA*, was shown to confer resistance to gliotoxin in the *L. maculans* Δ*sirA* (Gardiner *et al.,* 2005b). Interestingly, GliA was unable to extend this resistance to sirodesmin, indicating that the transport mechanisms of the gliotoxin MFS transporter, GliA, and the sirodesmin ABC transporter, SirA, are specific for the molecules that they recognise. Here, the deletion of *gliK* in *A.*

fumigatus ATCC46645 and ATCC26933 resulted in strains that became highly sensitive to exogenous gliotoxin and hydrogen peroxide, but were unaffected by exposure to the anti-fungal voriconazole. Hence, *gliK*, which appears to facilitate gliotoxin efflux, may, directly or indirectly, play a role in self-protection against the toxicity of gliotoxin. Furthermore, gliotoxin production was severely diminished in *A. fumigatus* Δ*gliK*[46645] and in Δ*gliK*[26933], in particular. Finally, it was demonstrated that exogenous gliotoxin entered the mycelia at a significantly faster rate in *A. fumigatus* Δ*gliK*[46645] (31.443 pg/mg mycelia/ min) than ATCC46645 (9.337 pg/mg mycelia/min) (P = 0.0039). Combined, these observations strongly suggest that *gliK* is a component of a gliotoxin efflux mechanism in *A. fumigatus*, since involvement in uptake would have results in exogenous gliotoxin levels in Δ*gliK* greater than those of wild-type.

As described in Chapter 3, gene deletion carried out by the bi-partite transformation process increases the rate of targeted integration whilst reducing the number of ectopic and partial integrations (Nielsen *et al.*, 2006). Complementation of the gene deletion is carried out by using a linearised plasmid containing the gene of interest for homologous recombination, with a separate selection marker which is co-transformed. To investigate if the restoration of the *gliK* gene into the Δ*gliK*[46645] strain would return the wild–type phenotype of self-protection against gliotoxin, a complemented strain was generated. Although the Southern blot analysis confirmed the reinsertion of the *gliK,* qRT-PCR and RT-PCR showed that the gene was expressed and RT-PCR of the adjacent gene, *gliA*, verified that the deletion and reinsertion of *gliK* did not disrupt the expression of the transporter gene, subsequent phenotypic analysis (gliotoxin sensitivity) revealed that the *gliK* complementation

did not resolve the mutant phenotype. Although this indicates that the *gliK* complementation process did not fully restore the function of the gene, the reason remains unclear. However a number of possibilities arise: (i) The selection marker for complementation (phleomycin) was co-transformed with intact *gliK* into *A. fumigatus* Δ*gliK*[46645], possibly resulting in insertion into the genome at random locations. This could have had detrimental effects on *A. fumigatus* in the presence of gliotoxin, as the location(s) of the insertion cannot be determined and this additional disruption may have caused pleiotropic effects that went undetected; (ii) As the reintroduction of *gliK* was confirmed to occur after the *ptrA* selection marker used in the original mutation, this shift in location may have hindered either gene integrity, transcription or control by the cluster transcription factor, *gliZ* (Bok *et al*., 2006). In the expression analysis by real time PCR, the expression of *gliK* in the *gliK^c* strain was higher than the wild-type which may indicate that *gliK* reinserted more than once into the genome during transformation. Maiya *et al* (2006) have also concluded that the increased transcription observed in their complementation of *ftmA*, a gene involved in the biosynthesis of fumitremorgin, resulted from the high copy number due to ectopic integration and/or high transcription activity at the site of integration.

The maximum yield of metabolite is highly influenced by the growth conditions, especially the culture media (Kosalec *et al.,* 2005b). Consequently, assessment of *gliK* expression, under different culture conditions, was undertaken to establish the best conditions for assessment of the relationship between *gliK* expression and gliotoxin production. *gliK* expression was found to be highest at 24 hr in AMM and this time point and media was used in all subsequent *gliK* expression analysis, RP-HPLC and gliotoxin secretion studies. *gliK* expression was also evident in MM at 24

and 48 hr, though it had decreased by 72 hr, indicating that *gliK* is normally expressed early on in cultures and may not be required in the latter stages of fungal culture. *gliK* expression was undetectable in Sabouraud media at any time point, and in *A. fumigatus* Δ*gliK*[46645], thereby confirming absence of gene presence in the latter.

It now appears that three systems may operate in *A. fumigatus* to either protect against gliotoxin or mediate efflux from the cell. Although a statistically significant difference in growth rates was observed between *A. fumigatus* wild-type(s) and respective Δ*gliK* strains, addition of gliotoxin did not completely suppress growth of Δ*gliK*[46645] and Δ*gliK*[26933], even at high concentrations of gliotoxin (20 μg/ml). This indicates that the protective role of GliT (Schrettl *et al.,* 2010) is capable of detoxifying gliotoxin, possibly in conjunction with GliA functionality as efflux pump (Gardiner *et al.,* 2005b) under these conditions which, in turn, may part-compensate for the loss of GliK, provided that the amount of gliotoxin does not exceed the levels with which the cell can cope.

Although exogenous gliotoxin (5 μg/ml) had no effect on *gliK* expression in *A. fumigatus* ATCC46645, we found that 3 hr exposure to hydrogen peroxide induced a nineteen fold increase in *gliK* expression (P = 0.0101). Moreover, exposure of *A. fumigatus* wild-type and Δ*gliK*[26933]/Δ*gliK*[46645] to hydrogen peroxide also resulted in a differential growth response. Here, increased mutant sensitivity to hydrogen peroxide (2 mM) was observed whereby the mutant strains were incapable of any growth, unlike both wild-type strains which exhibited approximately 50 % growth. If gliotoxin efflux was impaired in *A. fumigatus* Δ*gliK*, then these observations suggest that elevated levels of intracellular gliotoxin may potentiate hydrogen peroxide-

mediated oxidative stress. Moreover, although not demonstrated herein, they imply that gliotoxin efflux may result from hydrogen peroxide exposure, possibly as a mechanism to control the intracellular redox balance. Indeed Schrettl *et al.* (2010) have noted the gliotoxin may play a role in regulating the redox status of *A. fumigatus*.

Conversely, no significant difference between the growth rate of wild-type and their respective mutant strains in the presence of the anti-fungal, voriconazole, was observed indicating that *gliK* does not play a role in antifungal resistance. Indeed, in the transcriptional profiling of certain genes during voriconazole exposure, *gliT* expression was not altered by the presence of voriconazole (da Silva Ferreira *et al.,* 2006b). Although this was the only gene from the gliotoxin biosynthetic cluster tested, it is likely that the gene expression of all the genes involved in gliotoxin biosynthesis were not differently expressed during exposure to voriconazole.

Gliotoxin identification by RP-HPLC is enabled by comparison of the retention times (Rt) of *A. fumigatus*-derived metabolites, generally in organic extracts, to that of a standard gliotoxin preparation (Belkacemi *et al.,* 1999; Kupfahl *et al.,* 2006). Davis *et al.* (2010) developed a new method for gliotoxin detection which worked by labelling the reduced form of gliotoxin with 5'-iodoacetamidofluorescein (5'-IAF) following prior sodium borohydride reduction. They avoided use of reductants such as GSH or DTT which resulted in diminished sensitivity of detection of labelled gliotoxin due to depletion of the alkylation agent (5'-IAF). Sodium borohydride has previously been used to reduce other metabolites of *Aspergillus spp.*, including sterigmatocystin and versicolorin A hemiacetals (Chen *et al.,* 1977) and aflatoxin

(Johnson *et al.,* 2008). Thus, Davis *et al.* (2010) have utilised reduction of the disulfide bridge of gliotoxin, via sodium borohydride, to improve the specificity of gliotoxin detection as formation of the reduced (dithiol) form of gliotoxin results in a decreased Rt of gliotoxin, by approximately 1 min, under identical RP-HPLC conditions. Therefore, sodium borohydride was used in our study to investigate the presence of, and provide extra confirmatory data for, gliotoxin production by *A. fumigatus* wild-type and Δ*gliK* strains, respectively.

Gliotoxin production by *A. fumigatus* ATCC46645 was at too low a level to reliably assess by RP-HPLC (+/- sodium borohydride reduction) if Δ*gliK*, had any effect on gliotoxin production. This was not the case for *A. fumigatus* ATCC26933, where the amount of gliotoxin produced was easily observed prior to reduction, and subsequent reduction confirmed gliotoxin presence by the appearance of the dithiol form at a reduced retention time (Bernardo *et al.,* 2003) in organic extracts of the wild-type culture supernatants. Gliotoxin secretion by the corresponding mutant, Δ*gliK*^{26933}, was effectively abolished, which was confirmed by absence of the reduced form of gliotoxin at the expected Rt of 14.1 min. However, both *A. fumigatus* Δ*gliK* strains were able to produce gliotoxin, albeit minimally (Figure 5.35), and so it can be deduced that *gliK* is not essential for gliotoxin biosynthesis. Based on these data, we hypothesise that *gliK* may be involved in gliotoxin efflux from, or less likely, uptake into, *A. fumigatus*.

The analysis of RP-HPLC fractionation of Δ*gliK*^{26933} showed an increase in an unknown peak at a retention time of 12.9 min, which was reduced in both wild-type and mutant strain. Other peaks observed in ATCC26933 fractionation identified metabolites which were reduced by sodium borohydride (13.9 and 15 min). It is

highly possible that these metabolites are unrelated to gliotoxin, as they are present in $\Delta gliK^{26933}$.

Based on our observations that (i) both *A. fumigatus* $\Delta gliK$ mutants acquired increased sensitivity to exogenous gliotoxin (5 μg/ml); (ii) exposure to hydrogen peroxide significantly induced *gliK* expression, while also impairing $\Delta gliK$ growth with respect to wild-type(s), and finally (iii) disruption of *gliK* resulted in a tenfold decrease in gliotoxin efflux in *A. fumigatus*- it is hypothesised that *gliK* may play a role in gliotoxin efflux from *A. fumigatus*. Consequently, it was decided to assess the relative uptake rates of exogenous gliotoxin by *A. fumigatus* ATCC46645 and $\Delta gliK^{46645}$ to indirectly investigate the role of *gliK* in gliotoxin efflux. Here, we reasoned that if $\Delta gliK^{46645}$ could uptake gliotoxin normally, but exhibit impaired efflux compared to wild-type, then the exogenous levels of gliotoxin should reduce more rapidly- and to a greater extent- in $\Delta gliK^{46645}$ cultures. These strains were selected because the low levels of endogenous gliotoxin produced (Schrettl *et al.,* 2010) would not interfere with measurement of exogenously added gliotoxin. Previous work (unpublished; Dr Stephen Carberry personal communication) had suggested that a 45 min experimental period would be optimal for assessment of gliotoxin uptake by *A. fumigatus*.

Data analysis indicated that 15 min after gliotoxin addition (5 μg/ml final), there was a significantly lower level of gliotoxin present in *A. fumigatus* $\Delta gliK^{46645}$ supernatants, compared to wild-type (P = 0.0102). This difference was also evident at 30 min after addition (P= 0.0045), but at 45 min the level of exogenous gliotoxin in supernatants of *A. fumigatus* $\Delta gliK^{46645}$ began to increase and no statistically significant difference in exogenous gliotoxin levels between mutant and wild-type

was apparent (wild-type vs $\Delta gliK^{46645:}$ 0.831 ± 0.356 ng/mg mycelia and 0.668 ± 0.171 ng/mg mycelia, respectively). This is possibly due to activation of the auto-protective *gliT* response which has also been proposed to facilitate gliotoxin efflux from *A. fumigatus* (Schrettl *et al.,* 2010). Assessment of gliotoxin efflux in an *A. fumigatus* Δ*gliK*:Δ*gliT* double mutant would confirm this speculation. Overall, we propose that exogenous gliotoxin levels drop rapidly (0 - 30 min) in *A. fumigatus* $\Delta gliK^{46645}$ due to an impaired efflux pathway, consequent to *gliK* deletion, and thus conclude that *gliK* is involved in gliotoxin efflux from *A. fumigatus*. We predict that *gliK* acts in association with with *gliA*, the MFS transporter (Gardiner and Howlett, 2005a), to maintain gliotoxin homeostasis in *A. fumigatus*, and to facilitate gliotoxin efflux under normal conditions but that *gliT*–mediated efflux (Schrettl *et al.,* 2010) occurs when *A. fumigatus* encounters elevated gliotoxin levels. If *gliK* was involved in gliotoxin uptake, then one would have observed either no change, or an elevation of exogenous gliotoxin levels in *A. fumigatus* $\Delta gliK^{46645}$. This was not observed.

Sirodesmin, another ETP toxin, is produced by *L. maculans* and biosynthesis is encoded by a multigene cluster analogous to that which encodes gliotoxin production in *A. fumigatus* (Gardiner *et al.,* 2005b). Deletion of *sirA*, the sirodesmin transporter gene also led to increased sensitivity to exogenous sirodesmin and gliotoxin. Interestingly, introduction of *A. fumigatus gliA* recovered resistance to exogenous gliotoxin (10 μM), but not sirodesmin, in *L. maculans* Δ*sirA:gliA*. Gardiner *et al.* (2005a) noted that production and secretion of sirodesmin actually increased by 39 % in *L. maculans* Δ*sirA* compared to wild-type and speculated about the presence of alternative toxin efflux mechanisms. Subsequently, Schrettl *et al.* (2010) proposed that, in addition to the role of *gliA* in gliotoxin efflux by *A. fumigatus*, *gliT* plays an

essential role as a component of the auto-protective strategy against the cytotoxic effects of the ETP toxin. Furthermore, we now predict that *gliK* is essential for the effective functionality of *gliA*-mediated gliotoxin efflux from *A. fumigatus*.

Genes, other than encoding MFS or ABC transporters, involved in the transportation of biosynthesised molecules have been well documented in bacteria where several genes that encode membrane pumps of MFS transporter types are tightly linked to one or more genes involved in the biosynthesis of the molecule which is being pumped (Neal and Chater, 1987; Guilfoile and Hutchinson, 1992; Pitkin *et al.,* 1996). Overlapping transporters have also been well documented such as in *C. nicotianae* where the ABC transporter ATR1 involved in cercosporin production worked along with a MFS transported CnCFP which was involved in the auto-resistance to cercosporin (Amnuaykanjanasin and Daub, 2009). Also, Bradshaw *et al* (2009) suggested that the MFS transporter encoded by *dotC* was not the major efflux pump for dothistromin and concluded that there are other factors besides DotC facilitating the efflux of the toxin.

Figure 5.38 details a proposed model for the role of GliK in gliotoxin efflux by *A. fumigatus*. Here, endogenous, or exogenous gliotoxin which enters the cell, cycles between the oxidised and reduced forms, in part controlled by GliT activity/availability and chemical reduction by intracellular GSH (Schrettl *et al.,* 2010). Gliotoxin secretion occurs when the oxidised form is transported out of the cell by the GliK/GliA-mediated efflux system. In the absence of GliK, the elevated amount of gliotoxin accumulating in the cell exceeds the capacity of the GliA efflux system and activates the GliT self-protection system. Concomitant alteration of the

redox state within the cell occurs (due to GSH oxidation to GSSG) and a significant

diminution in cell growth occurs, as we have observed (Figures 5.26 and 5.27).

Absence of GliT leads to a complete inability to growth in the presence of elevated

gliotoxin levels (Schrettl *et al.,* 2010).
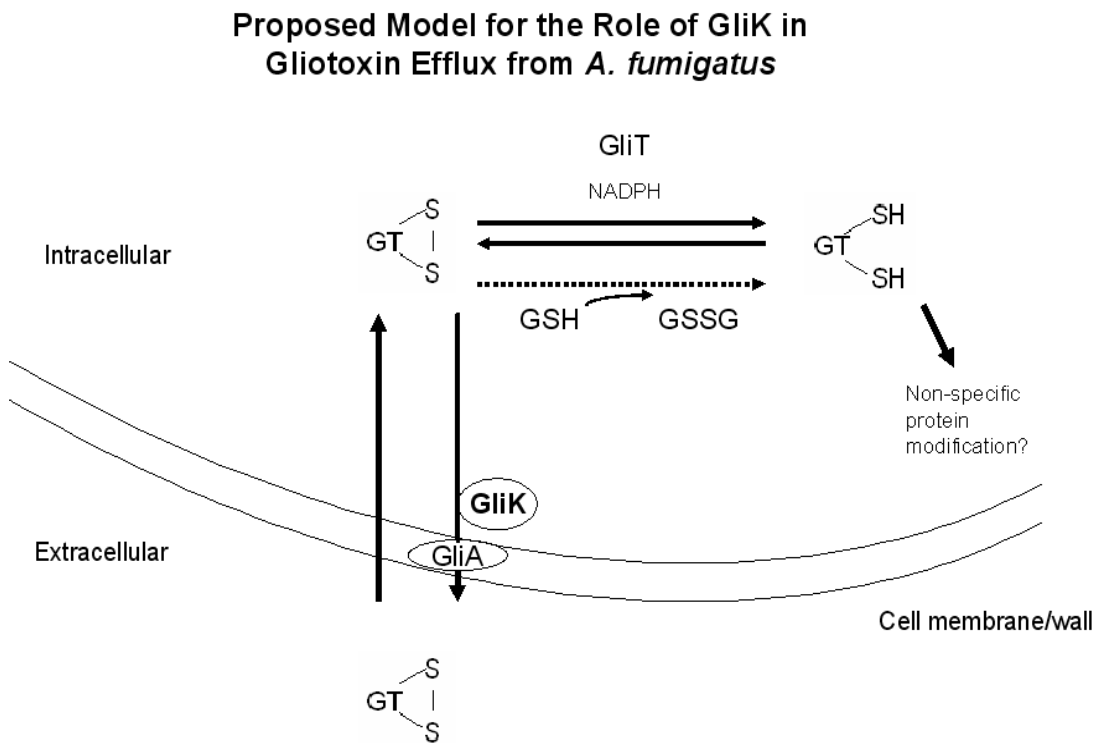
Figure 5.38: A proposed model for GliK functionality in gliotoxin efflux by *A. fumigatus*, based on experimental observations detailed herein (Schrettl *et al.,* 2010). In this model, GliK acts with GliA, and indirectly GliT, to mediate gliotoxin efflux. Absence of GliK would lead to increased gliotoxin levels in the cell, significantly hampering, but not overcoming the inducible GliT control the gliotoxin redox state. This would account for the impaired, but not absence of, growth observed for *A. fumigatus* Δ*gliK* mutants in the presence of gliotoxin. Note: Exogenous gliotoxin enters *A. fumigatus* via the cell membrane/wall by an, as yet, unidentified mechanism. Endogenous gliotoxin results from activity of the gliotoxin biosynthetic cluster (Gardiner and Howlett, 2005a).

In summary, targeted deletion of *A. fumigatus gliK*, a component of the gliotoxin biosynthetic cluster, in two fungal strains which produce low and high levels of gliotoxin, respectively, resulted in acquisition of (i) sensitivity to exogenous gliotoxin, (ii) increased sensitivity to hydrogen peroxide and (iii) impaired secretion of gliotoxin. We identify *gliK* as a component of the gliotoxin efflux system in *A. fumigatus* and predict that (i) hydrogen peroxide exposure may induce gliotoxin efflux, (ii) a Δ*gliK*:Δ*gliT* double mutant would be completely unable to efflux gliotoxin and (iii) increased intracellular gliotoxin levels due to Δ*gliK* cause an alteration in the redox status of *A. fumigatus* resulting in growth diminution. Future work will investigate these hypotheses.

CHAPTER 6

New Diagnostic Strategies for Detection of *A. fumigatus* Exposure in Humans

6. New Diagnostic Strategies for Detection of *A. fumigatus* Exposure in Humans

6.1 Introduction

A. fumigatus produces many metabolites that are secreted into the surrounding environment (Frisvad *et al.,* 2009). These secreted metabolites are recognisable by the immune system of the host and can alter the response of the immune system components in eliminating the infection. Pathogenic fungi avoid detection by the host immune response which aids the fungus in establishing growth and facilitating development (Toyotome *et al.,* 2009). As *A. fumigatus* infections occur for the most part in immunocompromised individuals, the immune response is unable to recognise the pathogen, resulting in a fatal infection (Latge, 1999). Hence, in parallel to understanding the fungus and the mechanisms it deploys to colonise the host, there is a drive to develop rapid and specific diagnostic tools to identify *A. fumigatus* infection at an early stage, so that a better outcome for the infected individual may result.

As described in Chapter 1, there are only a few diagnostic tests for the detection of the presence of *A. fumigatus*, (i) Biopsy, (ii) Galactomannan assay (de Repentigny *et al.,* 1987; Maertens *et al.,* 2007), (iii) PCR of *A. fumigatus* genes (Bretagne *et al.,* 1995; Yamakami *et al.,* 1996; Schabereiter-Gurtner *et al.,* 2007) and (iv) (1-3)β-glucan test (Mitsutake *et al.,* 1995; Krishnan-Natesan and Chandrasekar, 2008). Besides direct confirmation of biopsy examination, non-invasive diagnostic tests have shown limited success, with the galactomannan assay being the most reliable test (Scotter and Chambers, 2005). Therefore, test systems have been used in combination to try to increase the sensitivity and specificity of the available assays (Costa *et al.,* 2002), but there is still a need to improve the detection and diagnosis of *Aspergillus* related infections.

A. fumigatus is responsible for certain hypersensitivity respiratory disorders (Cockrill and Hales*,* 1999). In fact, some asthma related allergies are due to *A. fumigatus* allergic reactions (Agarwal*,* 2009). The human host response specific to *A. fumigatus* antigens includes increased levels of total IgE, *A. fumigatus* specific IgG and IgE, as well as a high eosinophil count (Gautam *et al.,* 2007). Of the predicted 10,000 proteins of *A. fumigatus*, only eight have been identified as positive allergens, namely, Aspf1, Aspf2, aspf3, Aspf4, Aspf6, glycoprotein (gp) 55, Aspf23 and an immune-dominant peptide of Aspf1 (Gautam *et al.,* 2008).

In immunocompromised patients, diagnosis of *A. fumigatus* infection is usually carried out by screening for the detection of circulating antigens, such as galactomannan and $(1\text{-}3)\beta$-glucans, as described in Chapter 1. Due to the lack of a full immune response in these patients, the usefulness of an antibody detection screening system seemed redundant, due to the defective antigen presentation function (Saugier-Veber *et al.,* 1993). However, the detection of anti-*Aspergillus* antibodies may be useful as a prognosis marker (Hope *et al.,* 2005). As native antigens cannot be always identified and isolated for use in creating specific antibodies, recombinant antigens can be produced using bacterial expression systems, usually *E. coli* – as noted for detection of anti-GliT IgG (Schrettl *et al.*, 2010). Such expression systems can be used to create recombinant antigens for use in serological investigations.

Here, recombinant GliK (encoded by AFUA_6G09700; Chapter 5) was generated, and produced using the PproEx™-Htb expression system. The recombinant protein can be isolated and used as the antigen in ELISA assays to determine if anti-GliK antibodies are present in human serum.

The aims of this chapter are to (i) clone and confirm expression of recombinant GliK in *E. coli,* and (ii) use an enzyme linked immunosorbant assay (ELISA) to evaluate the prevalence of GliK antibodies in human serum in a healthy cohort.

6.2 Results

6.2.1 Recombinant expression of GliK in *E. coli*

Separate from investigating the potential of TAFC as a diagnostic marker, a component of the gliotoxin biosynthetic cluster, GliK, was also examined. This was conducted by generating recombinant GliK, expressed in *E. coli.*

Primers were designed to amplify the *gliK* region and also to incorporate two restriction sites, *EcoR*I and *Hind*III into the forward and reverse primers, respectively, to allow for directional cloning into the pProEx™-Htb expression vector (Table 6.1). *A. fumigatus* cDNA was used as the template for the PCR amplification of the *gliK* gene.

Table 6.1: Primers used to amplify *gliK* gene.

Primer	(F/R)	Restriction site	Sequence (5' – 3')
gliK – F	Forward	*EcoR*I	AAGGAATTCAAATGGGGAAAGCAG
gliK – R	Reverse	*Hind*III	GAAAGCTTCTAAGCCGCCCTTCTAGA

cDNA synthesised from *A. fumigatus* was PCR amplified using *gliK* and calmodulin (*calm*) (Burns *et al.,* 2005) primers, separately and the *gliK* RT-PCR product was verified by gel electrophoresis (Figure 6.1). The *gliK* RT-PCR amplification only amplified the cDNA of the first PCR reaction, and very faintly,

the fourth PCR reaction. The *gliK* gene has a predicted intron of 50 bp (http://www.cadre-genomes.org.uk), and such a small size difference is difficult to determine by DNA electrophoresis, therefore the *calm* RT-PCR has confirmed that all four replicate PCR reactions are gDNA free as the cDNA template resulted in an amplification of a 348 bp product, rather than the gDNA amplification of 617 bp.
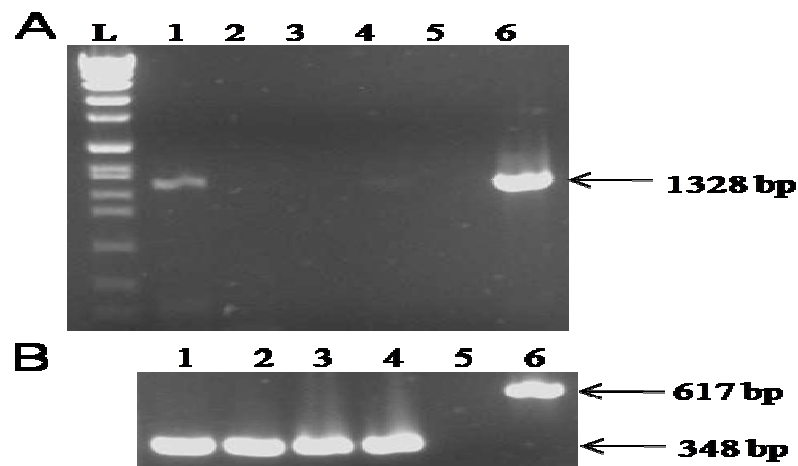
Figure 6.1: Reverse transcriptase PCR amplification of *A. fumigatus* ATCC46645 cDNA (A) using *gliK* primers Lane L: Molecular weight marker ladder (Roche VII), Lanes 1 - 4: cDNA amplification PCR product (1328 bp), Lane 5: Blank control, Lane 6: gDNA positive control (1328 bp) and (B) using *calmodulin* primers Lane L: Molecular weight marker ladder (Roche VII), Lanes 1 - 4: cDNA amplification PCR product (348 bp), Lane 5: Blank control, Lane 6: gDNA positive control (617 bp).

The *gliK* product was cloned into the pCR®II-TOPO® vector and transformed into *E. coli*. The resulting colonies were tested for integration of the DNA by restriction digest, using *Xba*I (Figure 6.2). The correct digestion pattern for the insertion of *gliK* cDNA into the TOPO vector was observed (5132 bp and 77 bp), and in the forward orientation. Digestion of the TOPO vector results in a linearization of the vector (3931 bp).
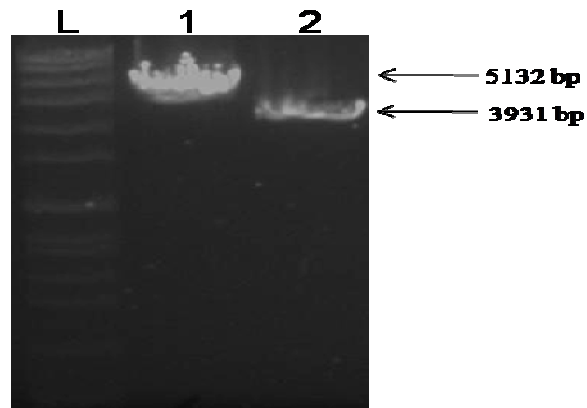
Figure 6.2: Restriction digest of *gliK* cloned into TOPO with *Xba*I. Lane L: Molecular weight marker ladder (Roche VII), Lane 1: Digested colony resulting in the expected band size of 5132 bp (the second band at 77 bp is not usually visible), Lane 2: TOPO vector linearised without *gliK* insertion (3931 bp).

After confirmation that *gliK* cDNA cloned correctly into TOPO, the pProEx™-Htb plasmid and the TOPO vector containing *gliK* were each digested with both *EcoR*I and *Hind*III, to result in the release of *gliK* from TOPO and also to open the pProEx™-Htb plasmid for subsequent ligation with the excised *gliK* (Figure 6.3).
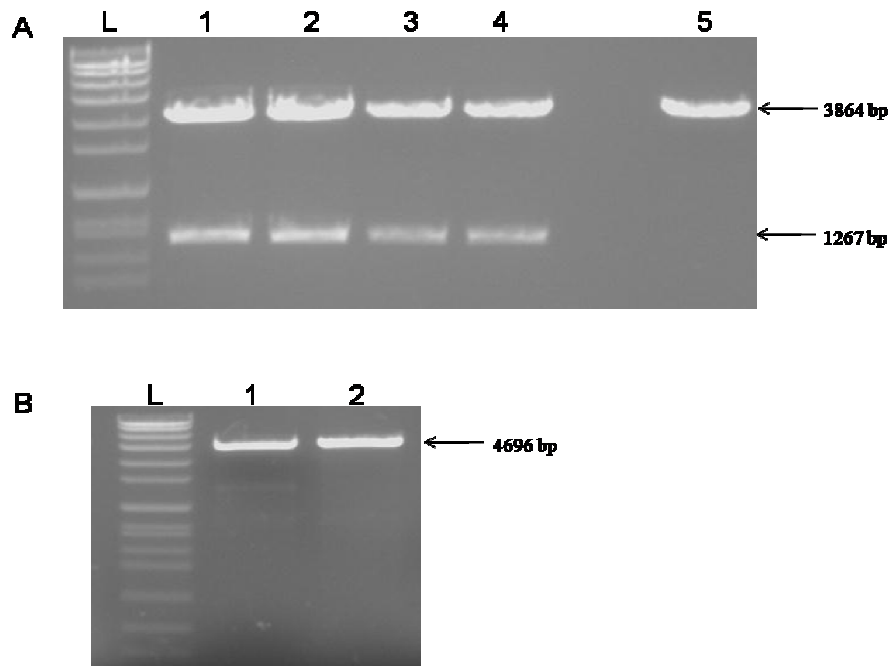
Figure 6.3: Restriction digests with *EcoR*I and *Hind*III to release *gliK* cDNA from TOPO and the opening of the pProEx™-Htb vector for ligation. (A) Digestion of *gliK*:TOPO. Lane L: Molecular weight marker ladder (Roche VII), Lane 1 - 4: *gliK* released from the TOPO vector (1267 bp) and the remaining vector (3864 bp), Lane 5: *gliK:*TOPO undigested (3864 bp) and (B) Digestion of pProEx™-Htb. Lane L: Molecular weight marker ladder (Roche VII), Lanes 1 – 2: digested pProEx™-Htb (4696 bp).

The appropriate *gliK* cDNA digested product was gel extracted and ligated to the digested pProEx™-Htb vector. The resultant ligation was used to transform *E. coli* DH5α. The colonies were screened by PCR for the *gliK* insertion (Figure 6.4) and the positive colonies resulted in an amplification product of 1328 bp. Not all colonies contained the plasmid and insert.
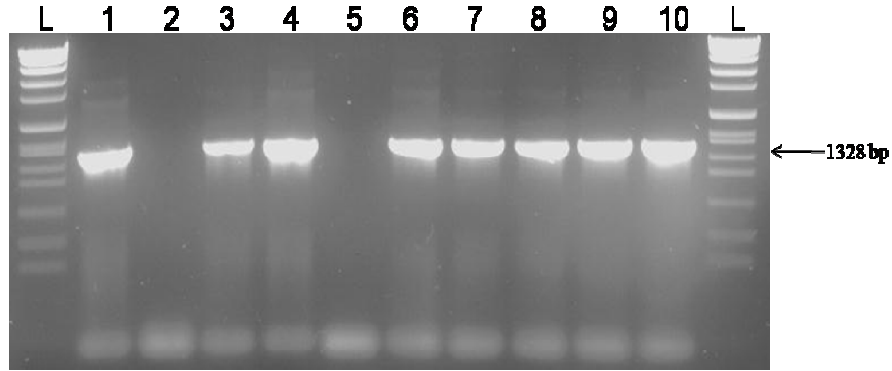
Figure 6.4: Colony PCR of transformed DH5α *E. coli* containing *gliK* cDNA within the pProEx-HtB vector. Lane L: Molecular weight marker ladder (Roche VII). Lanes 1 – 10: colonies screened by PCR for *gliK* (1328 bp), where colonies, with the exception of colonies 2 and 5, resulted in positive PCR amplification.

One of the positive clones was digested by the restriction enzymes, *BamH*I and *Pvu*I together, to confirm the insertion of the *gliK* cDNA sequence into the pProEx™-Htb plasmid (Figure 6.5). The pProEx™-Htb:*gliK* vector resulted in the expected banding pattern of 3749 bp and 2264 bp, whereas the pProEx™-Htb vector without the cDNA results in a banding pattern of 3749 bp and 1030 bp.
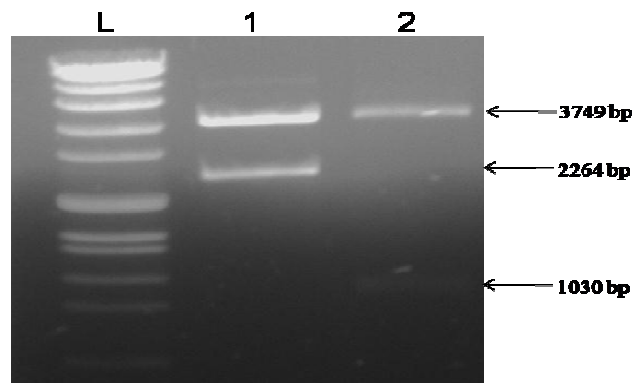
Figure 6.5: Restriction digests to confirm *gliK* integration into the pProEx™-Htb plasmid. Lane L: Molecular weight marker ladder (Roche VII), Lane 1: pProEx™-Htb:*gliK* digestion (3749 bp and 2264 bp), Lane 2: pProEx™-Htb only digestion (3749 bp and 1030 bp).

The restriction digestions and colony PCR confirmed the presence of the *gliK* gene in the pProEx™-Htb plasmid. The plasmid was sequenced to confirm that *gliK* remained in frame to enable protein expression. Sequence analysis was performed on a commercial basis (AGOWA, Germany), and was compared to the predicted sequences according to CADRE (http://www.cadre-genomes.org.uk), with ID AFUA_6G09700. The cDNA was sequenced from the M13 primer site which is incorporated in both the TOPO vector and the pProEx™-Htb plasmid. The sequencing of the *gliK* cDNA in the TOPO vector confirmed the correct sequence of *gliK* and also revealed that the intron predicted in the CADRE sequence was not a true intron (Figure 6.6). The sequencing of the *gliK* cDNA in the pProEx™-Htb plasmid confirmed that the *gliK* cDNA ligated and cloned correctly into the plasmid (Figure 6.7). There are five discrete residue changes, three of which result in an alteration of amino acid sequence (Table 6.2). The translated GliK protein sequence was aligned with the predicted protein sequence in CADRE and this alignment confirmed that the gene remained in-frame for protein expression (Figure 6.8).

```
Sequence_1: gliK in TOPO Sequenced

Sequence_2: gliK gDNA predicted from CADRE (AfuA_6g09700

Similarity : 631/631 (100.00 %)

Seq_1    1    ACGACTCACTATAGGGCGAATTGGGCCCTCTAGATGCATGCTCGAGCGGCCGCCAGTGTG    60

Seq_2    1    ------------------------------------------------------------     0


Seq_1   61    ATGGATATCTGCAGAATTCGCCCTTACAGAACGCAAAGAGCAAGCAACATGGGGAAAGCA   120
                                                            ||||||||||||
Seq_2    1    -----------------------------------------------ATGGGGAAAGCA    12


Seq_1  121    GCGTTGCAAGACCCTCATGGGGGAATCTGGTACTTTGCCTACGGCTCCAACTTACGCCTC   180
              ||||||||||||||||||||||||||||||||||||||||||||||||||||||||||||
Seq_2   13    GCGTTGCAAGACCCTCATGGGGGAATCTGGTACTTTGCCTACGGCTCCAACTTACGCCTC    72


Seq_1  181    TCGGTACTGGAGAATCGAGGCATCAAAGCACTGGATATCAAGGCCGTCATTGTCCCCTCA   240
               |||||||||||||||||||||||||||||||||||||||||||||||||||||||||||
Seq_2   73    TCGGTACTGGAGAATCGAGGCATCAAAGCACTGGATATCAAGGCCGTCATTGTCCCCTCG   132


Seq_1  241    CACTACCTGACCTTCGACATCTTTGGCATCCCGTACGCGGAACCTTCCTTTGCCAGCGTC   300
              ||||||||||||||||||||||||||||||||||||||||||||||||||||||||||||
Seq_2  133    CACTACCTGACCTTCGACATCTTTGGCATCCCGTACGCGGAACCTTCCTTTGCCAGCGTC   192


Seq_1  301    GCCCCCTTTGCCCGCGAGAAGAAAACCACCCTGCGACTGGGCGATTCACCCGCTTCTCGC   360
              ||||||||||||||||||||||||||||||||||||||||||||||||||||||||||||
Seq_2  193    GCCCCCTTTGCCCGCGAGAAGAAAACCACCCTGCGACTGGGCGATTCACCCGCTTCTCGC   252


Seq_1  361    GACGTTCCGCCGGTTCAGGGACTCGCCTATCTTTTAAATCCCAGGGATTACCGGCAGCTG   420
              ||||||||||||||||||||||||||||||||||||||||||||||||||||||||||||
Seq_2  253    GACGTTCCGCCGGTTCAGGGACTCGCCTATCTTTTAAATCCCAGGGATTACCGGCAGCTG   312


Seq_1  421    GTCATCAGCGAAGGCGGCGGCGTGGCTTACGATGAGGTCGAGGTCCATGCCTCGATCCTC   480
              ||||||||||||||||||||||||||||||||||||||||||||||||||||||||||||
Seq_2  313    GTCATCAGCGAAGGCGGCGGCGTGGCTTACGATGAGGTCGAGGTCCATGCCTCGATCCTC   372


Seq_1  481    GACAAGGACGGCAAACCCGACCCCGGCGCGACCCTGATTGCTCGGACCTTGCAAGCCAAG   540
              ||||||||||||||||||||||||||||||||||||||||||||||||||||||||||||
Seq_2  373    GACAAGGACGGCAAACCCGACCCCGGCGCGACCCTGATTGCTCGGACCTTGCAAGCCAAG   432


Seq_1  541    TACCCCTGGCGACCTAACGGTGCGCCCAGTGCGCGCTACCTGGTGAGCGGCCCCGGAACA   600
              ||||||||||||||||||||||||||||||||||||||||||||
Seq_2  433    TACCCCTGGCGACCTAACGGTGCGCCCAGTGCGCGCTACCTG<mark>gtgagcggccccggaaca</mark>   492


Seq_1  601    GAATCATGCTCTGCGATACTGATCGGAAACAGGGCCTCATCTCGACGGGGTGCAAACAGA   660
              ||||||||||||||||||||||||||||||||||||||||||
Seq_2  493    <mark>gaatcatgctctgcgatactgatcggaaacag</mark>GGCCTCATCTCGACGGGGTGCAAACAGA   552


Seq_1  661    ATGAGCCGCTCACGGCATACAGCGACTATATTGATTCCTTACCGGCCTATGAGCCGCCGA   720
              ||||||||||||||||||||||||||||||||||||||||||||||||||||||||||||
Seq_2  553    ATGAGCCGCTCACGGCATACAGCGACTATATTGATTCCTTACCGGCCTATGAGCCGCCGA   612


Seq_1  721    CATCCCTCCATGCCAAGG------------------------------------------   738
              ||||||||||||||||||
Seq_2  613    CATCCCTCCATGCCAAGGTGGGAGGTCTTCTTTTCCTGATGTTCTGGCGTCC          672
```

Figure 6.6: Alignment of sequence of *gliK* cDNA within the TOPO vector with the sequence predicted from CADRE. The sequenced cDNA contained the sequence of the predicted intron (highlighted in yellow), which indicates that this is not an intron, as predicted.

```
Sequence_1: gliK in pProEx Sequenced,
Sequence_2: gliK gDNA predicted
Similarity : 860/861 (99.88 %)

Seq_1  1    CCATCACCATCACGATTACGATATCCCAACGACCGAAAACCTGTATTTTCAGGGCGCCAT  60

Seq_2  1    ------------------------------------------------------------  0


Seq_1  61   GGGATCCGGAATTCAAATGGGGAAAGCAGCGTTGCAAGACCCTCATGGGGGAATCTGGTA  120
                           ||||||||||||||||||||||||||||||||||||||||||||||
Seq_2  1    ---------------ATGGGGAAAGCAGCGTTGCAAGACCCTCATGGGGGAATCTGGTA  44


Seq_1  121  CCTTGCCTACGGCTCCAACTTACGCCTCTCGGTCCTGGAGAATCGAGGCATCAAAGCACT  180
            |_||||||||||||||||||||||||||||||||_|||||||||||||||||||||||||
Seq_2  45   CTTTGCCTACGGCTCCAACTTACGCCTCTCGGTACTGGAGAATCGAGGCATCAAAGCACT  104


Seq_1  181  GGATATCAAGGCCGTCATTGTCCCCTCGCACTACCTGACCTTCGACATCTTTGGCATCCC  240
            ||||||||||||||||||||||||||||||||||||||||||||||||||||||||||||
Seq_2  105  GGATATCAAGGCCGTCATTGTCCCCTCGCACTACCTGACCTTCGACATCTTTGGCATCCC  164


Seq_1  241  GTACGCGGAACCTTCCTTTGCCAGCGTCGCCCCCTTTGCCCGCGAGAAGAAAACCACCCT  300
            ||||||||||||||||||||||||||||||||||||||||||||||||||||||||||||
Seq_2  165  GTACGCGGAACCTTCCTTTGCCAGCGTCGCCCCCTTTGCCCGCGAGAAGAAAACCACCCT  224


Seq_1  301  GCGACTGGGCGATTCATCCGCTTCTCGCGACGTTCCGCCGGTTCAGGGACTCGCCTATCT  360
            ||||||||||||||||_|||||||||||||||||||||||||||||||||||||||||||
Seq_2  225  GCGACTGGGCGATTCACCCGCTTCTCGCGACGTTCCGCCGGTTCAGGGACTCGCCTATCT  284


Seq_1  361  TTTAAATCCCAGGGATTACCGGCAGCTGGTCATCAGCGAAGGCGGCGGCGTGGCTTACGA  420
            ||||||||||||||||||||||||||||||||||||||||||||||||||||||||||||
Seq_2  285  TTTAAATCCCAGGGATTACCGGCAGCTGGTCATCAGCGAAGGCGGCGGCGTGGCTTACGA  344


Seq_1  421  TGAGGTCGGGGTCCATGCCTCGATCCTCGACAAGGACGGCAAACCCGACCCCGGCGCGAC  480
            ||||||||_|||||||||||||||||||||||||||||||||||||||||||||||||||
Seq_2  345  TGAGGTCGAGGTCCATGCCTCGATCCTCGACAAGGACGGCAAACCCGACCCCGGCGCGAC  404


Seq_1  481  CCTGATTGCTCGGACCTTGCAAGCCAAGTACCCCTGGCGACCTAACGGTGCGCCCAGTGC  540
            ||||||||||||||||||||||||||||||||||||||||||||||||||||||||||||
Seq_2  405  CCTGATTGCTCGGACCTTGCAAGCCAAGTACCCCTGGCGACCTAACGGTGCGCCCAGTGC  464


Seq_1  541  GCGCTACCTGGTGAGCGGCCCCGGAACAGAATCATGCTCTGCGATACTGATCGGGAACAG  600
            ||||||||||||||||||||||||||||||||||||||||||||||||||||||| |||||
Seq_2  465  GCGCTACCTGgtgagcggccccggaacagaatcatgctctgcgatactgatcggaaacag  524


Seq_1  601  GGCCTCATCTCGACGGGGTGCAAACAGAATGAGCCGCTCACGGCATACAGCGACTATATT  660
            ||||||||||||||||||||||||||||||||||||||||||||||||||||||||||||
Seq_2  525  GGCCTCATCTCGACGGGGTGCAAACAGAATGAGCCGCTCACGGCATACAGCGACTATATT  584


Seq_1  661  GATTCCTTACCGGCCTATGAGCCGCCGACATCCCTCCATGCCAAGGTGGGAGG        713
            |||||||||||||||||||||||||||||||||||||||||||||||||||||
Seq_2  585  GATTCCTTACCGGCCTATGAGCCGCCGACATCCCTCCATGCCAAGGTGGGAGG        638
```

Figure 6.7: Alignment of the sequence of *gliK* within the pProEx™-Htb plasmid with the sequence predicted from CADRE. Alterations of residues are highlighted in grey.

```
predicted    ------------------------MGKAALQDPHGGIWYFAYGSNLRLSVLENRGIKAL 35
sequenced    HHHHDYDIPTTENLYFQGAMGSGIQMGKAALQDPHGGIWYLAYGSNLRLSVLENRGIKAL 60
                                     **************:*******************

predicted    DIKAVIVPSHYLTFDIFGIPYAEPSFASVAPFAREKKTTLRLGDSPASRDVPPVQGLAYL 95
sequenced    DIKAVIVPSHYLTFDIFGIPYAEPSFASVAPFAREKKTTLRLGDSSASRDVPPVQGLAYL 120
             *********************************************.**************

predicted    LNPRDYRQLVISEGGGVAYDEVEVHASILDKDGKPDPGATLIARTLQAKYPWRPNGAPSA 155
sequenced    LNPRDYRQLVISEGGGVAYDEVGVHASILDKDGKPDPGATLIARTLQAKYPWRPNGAPSA 180
             ********************** ************************************

predicted    RYLV 159
sequenced    RYLV 184
             ****
```

Figure 6.8: Protein sequence of GliK translated from cloned cDNA. The cloned DNA is in frame with the N-terminal histidine affinity tag (part of which is underlined in green). The pProEx-Htb vector is underlined in Blue and the translated cDNA is underlined in red.

Three of the observed amino acids were not as predicted (Table 6.2). These discrete differences may be a result of the strain difference between the sequenced *A. fumigatus* strain AF293 and the strain used in this experiment, ATCC46645.

Table 6.2: Sequence of residues that result in a different protein sequence between the predicted protein sequence from CADRE (AF293) and the actual sequenced strain (ATCC46645)

Residue location	Sequenced (ATCC46645)		Predicated (AF293)	
	Residues	Amino acid	Residues	Amino acid
122	CTT	Leucine (L)	TTT	Phenylalanine (F)
317	TCC	Serine (S)	CCC	Proline (P)
429	GGG	Glycine (G)	GAG	Glutamic acid (E)

These changes may also indicate non-conserved aspects of the gene or they may be due to errors introduced during the amplification of the cDNA by PCR, even

though proof-reading *Taq* was used to reduce the possibility of such alterations occurring.

Detection of the protein expression of GliK in recombinant *E. coli* was carried out by induction using IPTG followed by SDS-PAGE and Western Blot analysis. Small scale cultures were induced and grown for 3 hr, with samples taken pre-induction and also at hourly time points. Both the SDS-PAGE and Western Blot analysis resulted in an approximate molecular mass of 30.5 kDa, which was expected of the recombinant GliK (rGliK) (Figure 6.9).

In order to check rGliK solubility, the cultures were induced as before with IPTG, cultured for 3 hr and then subjected to a series of purifications to determine the solubility of the protein, as described in Section 2.2.14. The extracts from the different stages of solubility were subjected to SDS-PAGE and Western blot analysis. Both the SDS-PAGE and the Western blot analysis showed the presence of rGliK at the correct molecular mass, 30.5 kDa. The recombinant protein was deemed to be insoluble in solubilisation buffers Triton X-100, and 2 M urea and was finally resuspended in 8 M Urea Buffer (Figure 6.10). The soluble protein was quantified by the Bradford protein assay, and was determined to be 5.69 mg/ml.
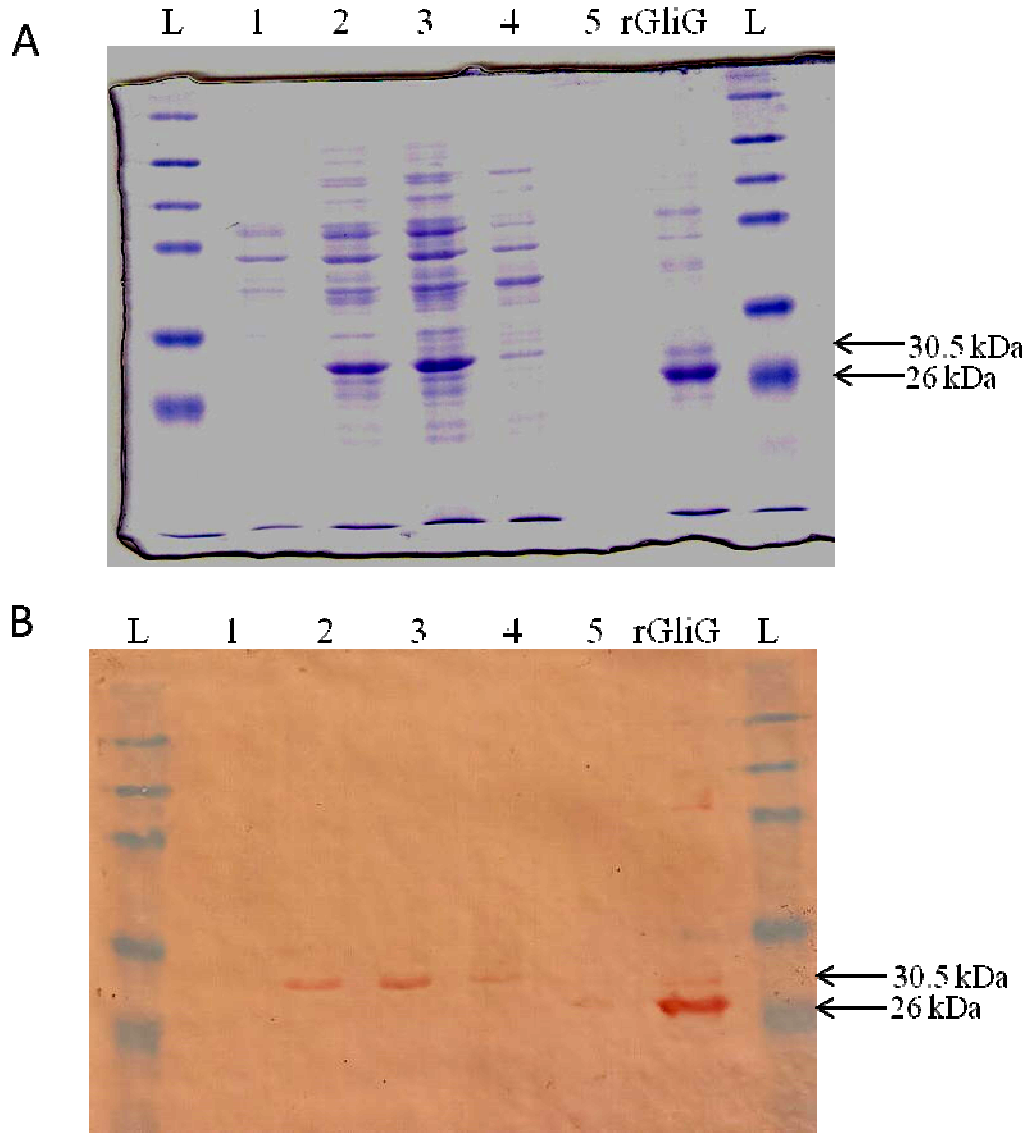
Figure 6.9: (A) SDS-PAGE and (B) Western blot analysis of recombinant GliK (rGliK) expression. Lane L contains the molecular mass marker; Lane 1 contains the non-induced cell extract; Lane 2 – 4 contains the cell extracts taken 1 – 3 hr post-induction (30.5 kDa); Lane 5 is empty; Lane 6 contains rGliG (26 kDa), a positive control (Davis *et al.,* submitted).
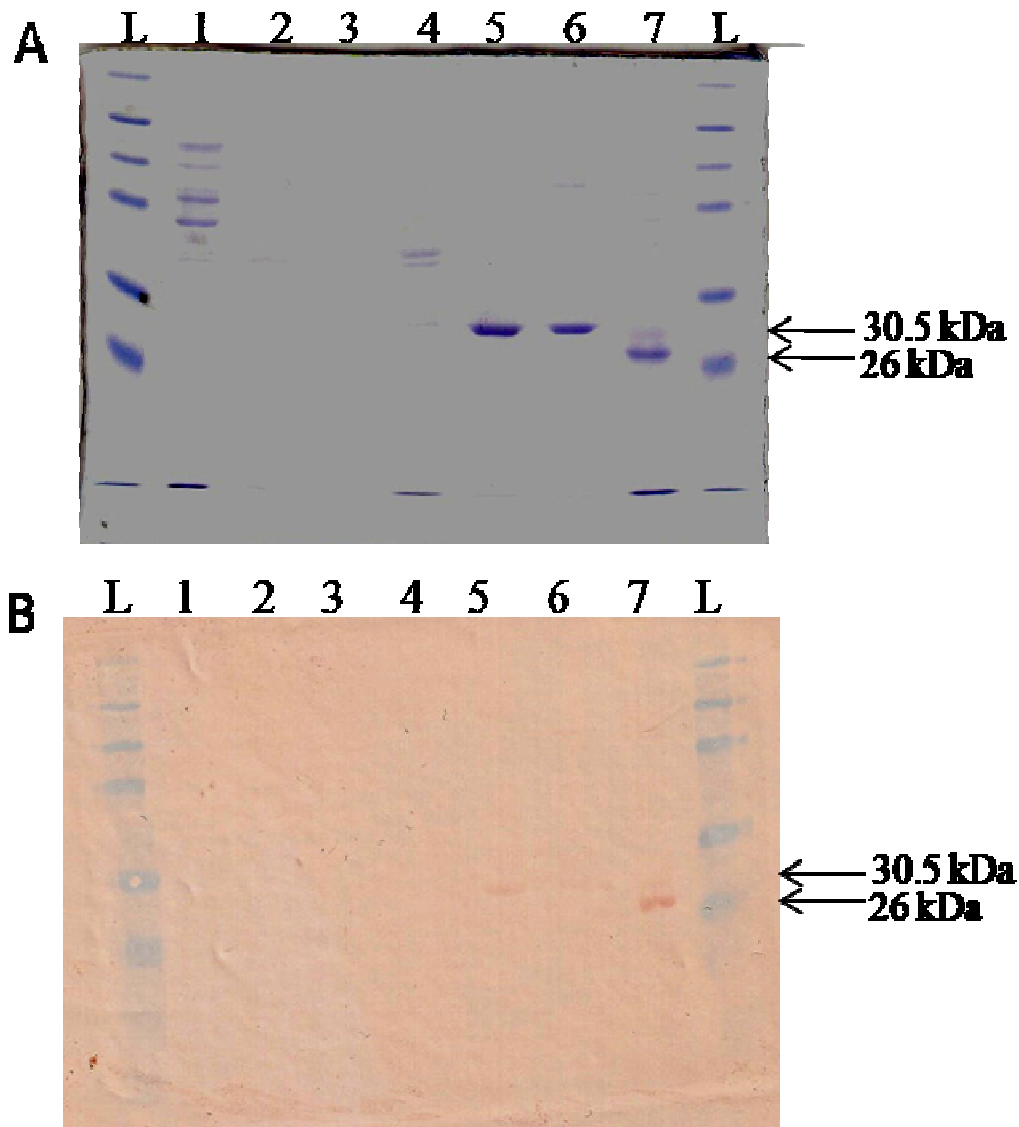
Figure 6.10: (A) SDS-PAGE and (B) Western blot analysis of rGliK solubility. Lane L contains the Molecular mass marker; Lanes 1 – 3 contain the Triton X-100 soluble protein; Lane 4 contains the 2 M Urea extract; Lanes 5 & 6 contain the 8 M Urea extract (30.5 kDa); Lane 7 contains rGliG (26 kDa), a positive control (Davis *et al.,* submitted).

6.2.2 Immunoreactivity of GliK

Previous immunoassays determined that there was a prevalence of anti-GliT and GliG IgG in human serum (Davis *et al.,* 2010; Schrettl *et al.,* 2010). Therefore, an assay was developed to determine if anti-GliK IgG were present in human serum. Microtitre plates were coated with the rGliK at a range of coating concentrations (0.5 - 8 μg/ml) to determine the optimum coating concentration (Figure 6.11). The dilutions were also carried out with and without 0.01 % (w/v) SDS. The purpose of the SDS is to facilitate homogenous coating of the antigen. The antigen was detected on the plate using an anti-His$_6$ monoclonal antibody (1/10000) and a goat anti-mouse IgG horseradish peroxidase (HRP) conjugate (1/5000). The substrate used was tetramethylbenzidine (TMB) and the reaction was stopped by the addition of 1 N Sulphuric acid solution. The optimum coating concentration for the rGliK antigen was determined to be 4 μg/ml in coating buffer containing 0.01 % (w/v) SDS, as no increased absorbance was observed as a result of increasing rGliK coating concentration.
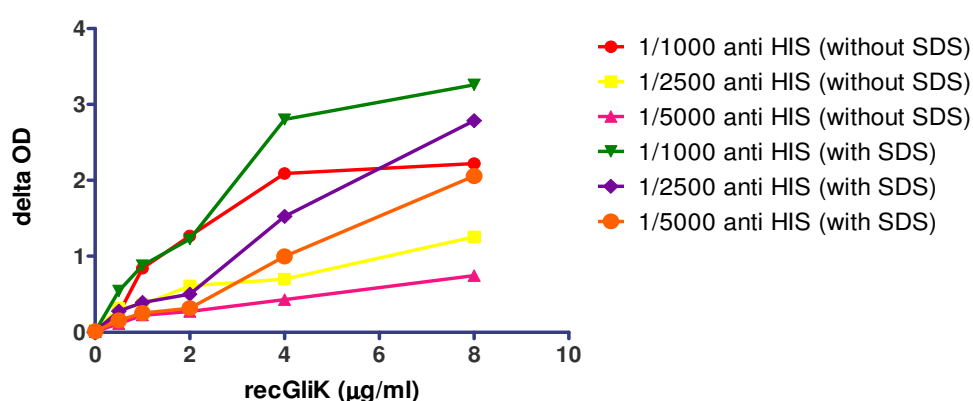
Figure 6.11: Optimisation of the coating concentration for the GliK ELISA. The microtitre plate was coated with the purified rGliK (0.5 – 8 μg/ml) diluted in carbonate buffer. The anti-His$_6$ monoclonal antibody was diluted in a range of carbonate buffer (1/1000, 1/2500 and 1/5000) either with or without 0.01 % (w/v) SDS.

The optimum concentration of rGliK (4 µg/ml) was coated onto 96 well plates, and human sera ($n = 71$) were screened by ELISA. Sera were assayed in duplicate on the microtitre plate, and repeated, resulting in two sets of results for each sample analysed (Figure 6.12).
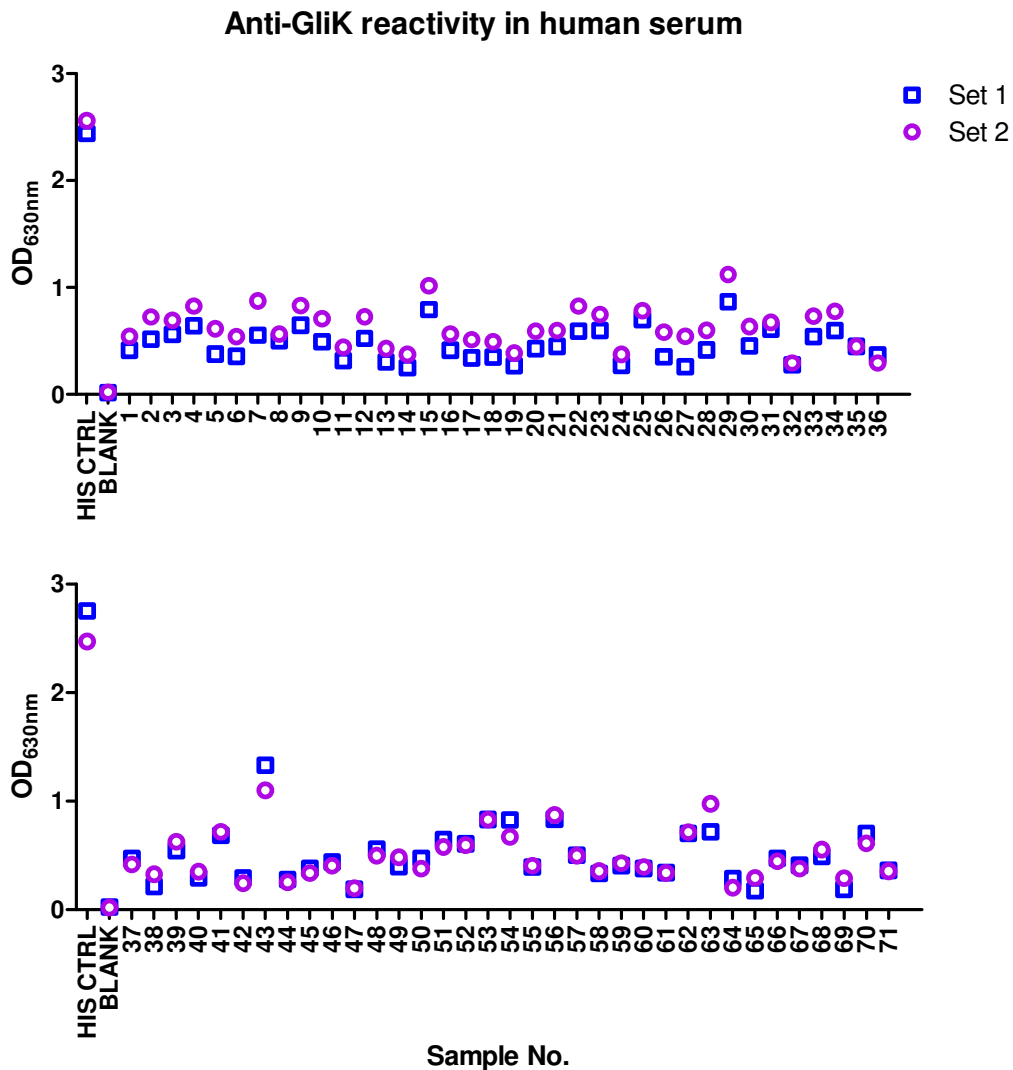
Figure 6.12: Detection of anti-GliK IgG in human serum. Samples 1 – 71 were screened, including an anti-His$_6$ positive control and a negative control.

ELISA results were expressed as index values (I.V.) representing specimen absorbance divided by the cut-off absorbance. The cut-off value for the GliK ELISA

was established by determining the absorbance values of the lowest ten values of the 71 samples. The cut-off value of the assay was defined by adding twice the standard deviation to the mean absorbance of the ten samples (Table 6.3). The established cut-off value was determined to be 0.339.

Table 6.3: Establishing the cut off valve of the rGliK ELISA

Assay	Mean of lowest ten samples	Standard deviation (STDEV)	2 X STDEV	Cut-off value
GliK ELISA	0.262	0.039	0.077	0.339

The results of the serum reactivity were calculated as Index Values (I.V.) as follows: the mean absorbance reading for each serum sample was divided by the cut-off value (0.339). An I.V. of greater than 1 was deemed to be seropositive, between 1 – 2 was deemed to be weakly seropositive, between 2 – 4 was deemed to be medium seropositive and greater than 4 was deemed to be highly seropositive. Of the serum samples screened ($n = 71$), 82 % (58/71) were seropositive; indicating that there is a prevalence of exposure to GliK in healthy individuals. None of the serum samples were highly seropositive, whereas the majority either displayed medium seropositivity (21 %) or weak seropositivity (61 %) reaction. Seronegative samples accounted for 18 % of the cohort tested (Figure 6.13).
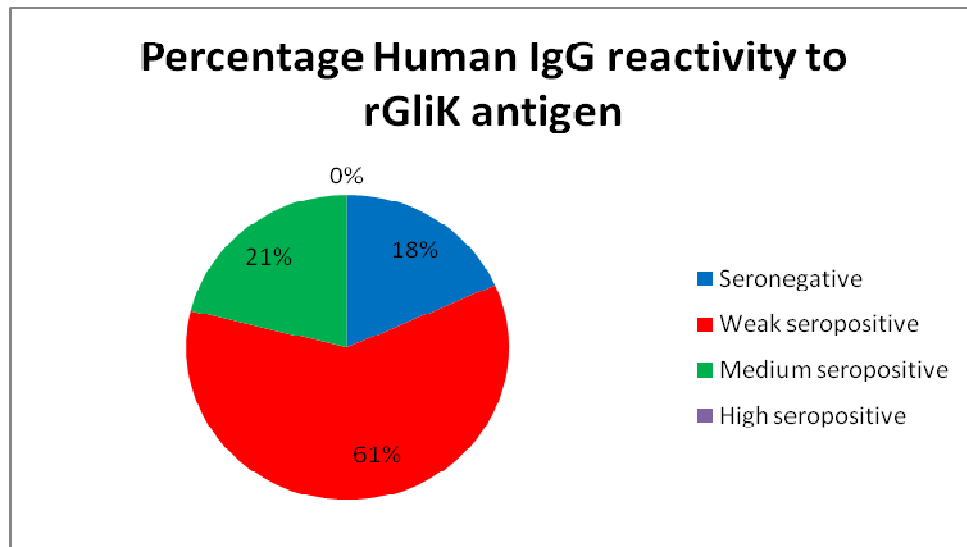
Figure 6.13: The Human IgG reactivity towards rGliK antigen. The total number of serum samples (*n* = 71). The seroreactivity toward the GliK antigen were further grouped into categories: Seronegative, an I.V. of less than 1, Weak seropositive, an I.V. of between 1 – 2, Medium seropositive, an I.V. of between 2 – 4 and High seropositive, an I.V. of higher than 4. Each category was scored as a percentage of the total number of serum samples screened.

6.3 Discussion

Secreted metabolites from *A. fumigatus* can potentially be used as a method of specific and sensitive detection of infection. Current detection of *Aspergillus* infection relies upon invasive procedures such as lung biopsy or broncoscopy procedures. Non-invasive methods have been limited to the detection of cell wall components of the fungus such as the β-galactomannan or (1-3)β-glucan. Alternative diagnosis tools are needed in the detection and diagnosis of *Aspergillus* infections. Here, a component of the gliotoxin biosynthetic cluster, GliK, was examined as potential diagnostic markers for the detection of *Aspergillus* infection.

Production of recombinant proteins has previously been used to characterise *A. fumigatus* protein function (Burns *et al.,* 2005; Davis *et al.,* 2010; Schrettl *et al.,*

286

2010), but this approach can also been used to characterise the prevalence of antibodies against such proteins in the human sera (Davis *et al.,* 2010). Here, *gliK*, a gene encoding an unknown protein in the gliotoxin biosynthetic cluster, was cloned into a bacterial expression system to induce production of this protein. It was verified that GliK expression was successful using the pProEx-Htb expression system to yield recombinant GliK (rGliK). The rGliK protein was insoluble in Triton X-100 and 2 M urea solubilisation buffers, but was successfully solubilised in 8 M urea buffer. The purified recombinant protein was used in an ELISA assay to investigate the seroprevalence of GliK antibodies. A random cohort of healthy sera samples ($n =$ 71) was screened in duplicate by ELISA, where rGliK was used as the antigen. It was discovered that there was a weak to medium seropositive reaction to the rGliK as 82 % (58/71) of the sera screened had anti-GliK antibodies present. This indicates that GliK interaction with healthy individuals is a common occurrence, and that the presence of GliK is capable of stimulating an immune response.

There is a need to extend the available diagnostic repertoire for the detection and diagnosis of *Aspergillus* infections, as there is an increase in the number of reported anti-fungal resistant strains (Denning and Hope*,* 2010; Schrettl *et al.,* 2010), as well as a delay in diagnosis of this potentially fatal infection (Maschmeyer *et al.,* 2007). *A. fumigatus* infection is the leading cause of fungal related fatalities, and early detection is the key to fighting this pathogen (Agarwal, 2009). Metabolites secreted from the fungus during infection may provide an opportunity to detect an infection if diagnostic assays were used to specifically screen for such metabolites (Hope *et al.,* 2005). Most of the metabolites produced by *A. fumigatus* are not recognised or detectable by the human immune system (Latge, 1999), which makes them suitable

as new diagnostic markers. Generation of recombinant antigens can be used in an ELISA which can screen human sera samples for the circulating anti-fungal antibodies. The ELISA procedure has been shown to be useful in the detection of antibodies associated with *A. fumigatus*, as the rGliK protein demonstrated that there is a prevalence of anti-GliK antibodies in healthy human sera.

CHAPTER 7

Discussion

7. Discussion

7.1 Establishment of a role for Pes1 in fumigaclavine C production in *A. fumigatus*

The sequencing of the genome of *A. fumigatus* has identified that genes involved in the biosynthesis of particular secondary metabolites are mainly found in clusters (Nierman *et al.,* 2005). In *A. fumigatus,* at least 26 secondary metabolite biosynthetic clusters have been identified, comprised of NRPS, PKS or DMAPP type genes (Keller *et al.,* 2005). However, the identification of the metabolites produced by many of these gene clusters is still unclear. Identification of NRP peptides is difficult as the substrate for the NRP synthetase may include fatty acids and α-hydroxy acids, as well as other non-proteogenic and proteogenic amino acids (Schwarzer *et al.,* 2003). NRP peptides can also undergo post-biosynthetic modifications, which can also make the link between NRP synthetase gene and corresponding peptide product harder to establish (Stack et al., 2007). In previous functional genomic analysis of *A. fumigatus*, genes of interest have either been part of a defined cluster, such as *gliP* of the gliotoxin biosynthetic cluster (Kupfahl *et al.,* 2006) or else a gene with a defined role, following identification of orthologs in other fungal species. For example, the role of *fgaPT2* in the biosynthesis of fumigaclavines in *A. fumigatus* was established by comparison to an ortholog in *C. purpurea*, *cpd1,* which had already been defined as the first step in the biosynthesis of the ergot alkaloid in this pathogen(Unsold and Li*,* 2005).

In previous work, expression of *pes1* has been altered by the deletion of other genes, such as *laeA*, encoding a global regulator (Perrin *et al.,* 2007). Such investigations have determined that *pes1* is under the same regulation as many of the secondary metabolite clusters but have not specifically examined the role of *pes1* in

A. fumigatus. Hence, the identification that *pes1* plays a role in the biosynthesis of the ergot alkaloid, fumigaclavine C, is the first time that a specific role for *pes1* in secondary metabolite biosynthesis has been elucidated.

Fumigaclavine C is produced in the conidia and therefore, most of the production of fumigaclavine C will be early in culture (Panaccione and Coyle, 2005), as the latter stages of culturing would contain more mycelia than conidia and therefore the amount of fumigaclavine C would diminish. Coyle *et al.* (2007) have noted that cultures grown on solid-based media produce more ergot alkaloids than cultures grown in liquid media, due to the higher level of conidia. In this thesis, analysis of *pes1* expression in *A. fumigatus* ATCC46645 showed that *pes1* was expressed at a higher level at 24 and 48 hr than 72 hr, regardless of media type, which is consistent with the predicted production time-frame of fumigaclavine C in liquid media cultures.

pes1 has been previously shown to be expressed during oxidative stress conditions (Reeves *et al.,* 2006). However in the present work, *pes1* expression was shown to be down-regulated in the presence of hydrogen peroxide (1 mM) in the strains *A. fumigatus* ATCC46645, Δ*sidD* and Δ*sidD:pes1*[c] after 24 hr incubation in AMM media. The down-regulation of *pes1* may be compensated for by the mycelial oxidative stress response components, such as the catalases (Paris *et al.,* 2003b).

Fumigaclavine C production is completely abolished in *A. fumigatus* Δ*pes1* strains. The fumigaclavine C biosynthetic cluster does not include *pes1* in *A. fumigatus* and we therefore propose that there has been extensive gene reorganisation in the cluster, which resulted in the migration of *pes1* onto chromosome 1, distant from the ergot alkaloid gene cluster located on chromosome 2. Gene rearrangement has also occurred within the cluster compared to the *C. purpurea* ergot alkaloid

biosynthetic cluster (Coyle and Panaccione, 2005), with which *A. fumigatus* shares similarity (Unsold and Li, 2005; Wallwey *et al.,* 2010). Therefore, *A. fumigatus* ergot alkaloid production is likely to be a result of cluster cross-talk between the genes within the ergot alkaloid biosynthetic cluster and the distantly located *pes1*. There has been extensive investigation into the fumigaclavine C biosynthetic pathway, but there are still a number of undefined reaction steps, and genes in the cluster with unknown functions (Unsold and Li, 2006; Rigbers and Li, 2008; Liu *et al.,* 2009; Coyle *et al.,* 2010; Wallwey *et al.,* 2010).

The cross-talk between *pes1* and the remainder of the fumigaclavine C encoding genes is an unusual arrangement in *A. fumigatus*, as generally the genes involved in the biosynthesis of a specific metabolite are all located adjacent to each other (Maiya *et al.,* 2006; Maiya *et al.,* 2007; Perrin *et al.,* 2007; Fedorova *et al.,* 2008; Fox *et al.,* 2008). Indeed, the majority of secondary metabolites are produced by defined clusters located near the telomeres (Keller *et al.,* 2005). However, there is an emergence of translocated or "orphan" genes identified distant from the cluster with which they co-operate to encode the biosynthesis of a specific metabolite. This is the case for the siderophore, erythrochelin, in *Saccharopolyspora erythraea*, which utilises two seemingly orphan NRP synthetase genes to synthesise the siderophore, in conjunction with genes found in a separate cluster (Lazos *et al.,* 2010). Also, in *A. fumigatus*, *sidA,* essential for the biosynthesis of both intracellular and extracellular siderophores, TAFC and FC, is located away from the siderophore biosynthetic cluster (Schrettl *et al.,* 2004). The genes involved in siderophore biosynthesis can be identified due to the availability of orthologs of the siderophore biosynthetic genes, and confirmed experimentally due to controlled expression regulated by iron availability (Reiber *et al.,* 2005). However, for NRP synthetase genes such as *pes1*,

no specific expression control has been identified, apart from the regulation by the global regulator of secondary metabolite production, LaeA, which controls a multitude of gene clusters (Bok and Keller, 2004) and the down-regulation of some NRP synthetase genes in the absence of the StuA transcription factor (Sheppard *et al.,* 2005). Therefore, the involvement of *pes1* in fumigaclavine C biosynthesis implies that there may be other orphan or cluster independent genes in the *A. fumigatus* genome which may be associated with the many previously identified metabolic biosynthetic processes, for which the full biosynthetic pathway is not completely understood.

Further to the findings presented herein with respect to NRP peptide interactions contributing to voriconazole resistance and the identification of a definite role for *pes1* in fumigaclavine C biosynthesis, a number of questions remain outstanding:

1. What is the molecular basis of the role played by fumigaclavine C in protecting against oxidative stress in *A. fumigatus ΔsidD* under iron-limiting conditions?

2. What is the precise role of Pes1 in fumigaclavine C production?

3. What is the amino acid substrate specificity of Pes1 modules ($n = 4$)?

4. To what extent is secondary metabolite/natural product cluster cross-talk occurring, and why?

7.2 Establishment of GliK involvement in gliotoxin efflux from *A. fumigatus*

Gliotoxin is a member of the ETP family and is one of the many secreted metabolites from *A. fumigatus.* Bioinformatic analysis identified a cluster of 13 genes which mediate gliotoxin biosynthesis (Gardiner and Howlett, 2005a; Schrettl *et al.,* 2010). *gliK*, encoding a protein of unknown function, is part of this cluster. Although orthologs of *gliK* exist in other fungi, the precise function in gliotoxin biosynthesis has remained elusive (Patron *et al.,* 2007). Recently, it has been identified that there are certain genes, for example *gliT*, within the cluster which confer protection against gliotoxin (Scharf *et al.,* 2010; Schrettl *et al.,* 2010). Also, the MFS transporter encoded by *gliA*, plays a role in protection against gliotoxin, as was demonstrated in a *L. maculans ΔsirA:gliA* strain (Gardiner *et al.,* 2005b).

Prior to the work carried out as part of this thesis, the exact role of *gliK* in gliotoxin biosynthesis or efflux was unclear. However, the efflux mechanism is proposed to be facilitated by the gliotoxin transporter, *gliA* (Gardiner *et al.,* 2005b), and also the gliotoxin oxidoreductase, *gliT* (Scharf *et al.,* 2010; Schrettl *et al.,* 2010). Herein, it is proposed that co-operation between these three genes facilitates the gliotoxin homeostasis in *A. fumigatus,* as well as gliotoxin efflux under basal conditions. In elevated exogenous gliotoxin conditions, *gliT*-mediated efflux occurs (Schrettl *et al.,* 2010). In the absence of GliK, there is a short-term accumulation of gliotoxin within mycelia, exceeding the capacity of the GliA efflux system. This internal level of gliotoxin is harmful to the organism, and activates the GliT self-protection activities (Schrettl *et al.,* 2010). This ability to react to an increase in intracellular gliotoxin is part of the self-protection system operated by the fungus. In the model proposed in this thesis (Figure 5.42), which is based on experimental

observation, GliK functions with GliA, and indirectly with GliT, to mediate the efflux of gliotoxin.

Identification of a role for a protein of unknown function, such as *gliK,* with no functionally annotated ortholog or identifiable domains was challenging. As *gliK* is located within the gliotoxin biosynthetic cluster, there was a likelihood that the protein played some role in gliotoxin production (Gardiner and Howlett*,* 2005a). Comparison of the gliotoxin biosynthetic genes to the sirodesmin biosynthetic genes of *L. maculans* showed that there was no ortholog of *gliK*, indicating that the protein was not likely to be necessary for gliotoxin biosynthesis (Gardiner and Howlett*,* 2005a). It has been noted that orthologs of *gliK* are only present in gliotoxin-producing organisms where there is a MFS type transporter, such as GliA (*A. fumigatus*), rather than an ABC type transporter, such as SirA (*L. maculans*) (Table 5.1)(Patron *et al.,* 2007).

The co-operation between GliA, an MFS transporter and GliK for the efflux of gliotoxin from *A. fumigatus* has ramifications for the production of other fungal toxins similar to gliotoxin. In particular, production of sirodesmin of *L. maculans* (Gardiner *et al.,* 2005b), dothstromin of *D. pini* (Bradshaw *et al.,* 2009), and aflatoxin of *A. parasiticus* (Chang *et al.,* 2004) do not rely solely on the transporter for each of their respective toxins, however other contributing factors have not yet been determined.

In the case of sirodesmin production in *L. maculans*, SirA, the ABC transporter is regulated by the transcription factor, SirZ, as well as the presence of sirodesmin itself. In Δ*sirA*, there was an elevated production of sirodesmin, which strongly suggests that there are other efflux mechanisms of sirodesmin (Gardiner *et al.,* 2005b). Dothstromin production in *D. pini* was unaffected by the absence of the MFS

transporter, DotC and this mutant was not sensitive to the presence of exogenous dothstromin (Bradshaw *et al.,* 2009). The authors note that there may be complex feedback regulation in the efflux and biosynthesis of the toxin, which has not yet been identified and elude to the possibility that compartmentalisation of the toxin may occur within the cell.

Intracellular vesicles, termed aflatoxisomes, have recently been shown to be involved in late-stage aflatoxin biosynthesis and export from *Aspergillus parasiticus* (Chanda *et al.,* 2009). These authors also demonstrated that aflatoxin biosynthesis was, in part, coordinated by Velvet (VeA) (Bayram *et al.,* 2008), a global regulator of *Aspergillus* secondary metabolism. Since VeA is primarily expressed under dark conditions, Chanda *et al*. (2009) have proposed that aflatoxin production may occur deep in soil to protect the fungal colony against predation by worms and insects, thereby ensuring survival of *A. parasiticus* in the environment. Given the auto-toxic (Schrettl *et al.*, 2010) and fungistatic effects of gliotoxin (Doyle *et al.,* 2010), it is conceivable that gliotoxin export also involves intracellular vesicular trafficking. However, although a role for intracellular vesicles involved in the intracellular transport of gliotoxin in *A. fumigatus* has been proposed (Schrettl *et al*., 2010), no experimental evidence has been provided to support this hypothesis. Now that a role of GliK in gliotoxin efflux has been identified, future GliK studies may resolve the gliotoxin storage/release mechanism in *A. fumigatus*. It is tempting to speculate that GliK may act as a targeting protein which directs gliotoxin-containing vesicles to the cell membrane prior to secretion.

CHAPTER 8

Bibliography

8. Bibliography

8.1 List of references

Agarwal, R. (2009). "Allergic bronchopulmonary aspergillosis." <u>Chest</u> **135**(3): 805-26.

Aguirre, J., Rios-Momberg, M., Hewitt, D. and Hansberg, W. (2005). "Reactive oxygen species and development in microbial eukaryotes." <u>Trends Microbiol</u> **13**(3): 111-8.

Alexander, N. J., McCormick, S. P. and Hohn, T. M. (1999). "TRI12, a trichothecene efflux pump from *Fusarium sporotrichioides*: gene isolation and expression in yeast." <u>Mol Gen Genet</u> **261**(6): 977-84.

Amitani, R., Taylor, G., Elezis, E. N., Llewellyn-Jones, C., Mitchell, J., Kuze, F., Cole, P. J. and Wilson, R. (1995). "Purification and characterization of factors produced by Aspergillus fumigatus which affect human ciliated respiratory epithelium." <u>Infect Immun</u> **63**(9): 3266-71.

Amnuaykanjanasin, A. and Daub, M. E. (2009). "The ABC transporter ATR1 is necessary for efflux of the toxin cercosporin in the fungus *Cercospora nicotianae*." <u>Fungal Genet Biol</u> **46**(2): 146-58.

Andrade, A. C., Van Nistelrooy, J. G., Peery, R. B., Skatrud, P. L. and De Waard, M. A. (2000). "The role of ABC transporters from *Aspergillus nidulans* in protection against cytotoxic agents and in antibiotic production." <u>Mol Gen Genet</u> **263**(6): 966-77.

Angelova, M. B., Pashova, S. B., Spasova, B. K., Vassilev, S. V. and Slokoska, L. S. (2005). "Oxidative stress response of filamentous fungi induced by hydrogen peroxide and paraquat." <u>Mycol Res</u> **109**(Pt 2): 150-8.

Antelo, L., Hof, C., Welzel, K., Eisfeld, K., Sterner, O. and Anke, H. (2006). "Siderophores produced by *Magnaporthe grisea* in the presence and absence of iron." <u>Z Naturforsch C</u> **61**(5-6): 461-4.

Baddley, J. W., Stroud, T. P., Salzman, D. and Pappas, P. G. (2001). "Invasive mold infections in allogeneic bone marrow transplant recipients." <u>Clin Infect Dis</u> **32**(9): 1319-24.

Bailey, A. M., Kershaw, M. J., Hunt, B. A., Paterson, I. C., Charnley, A. K., Reynolds, S. E. and Clarkson, J. M. (1996). "Cloning and sequence analysis of an intron-containing domain from a peptide synthetase-encoding gene of the entomopathogenic fungus *Metarhizium anisopliae*." <u>Gene</u> **173**(2): 195-7.

Baker, L. J., Dorocke, J. A., Harris, R. A. and Timm, D. E. (2001). "The crystal structure of yeast thiamin pyrophosphokinase." <u>Structure</u> **9**(6): 539-46.

Balibar, C. J. and Walsh, C. T. (2006). "GliP, a multimodular nonribosomal peptide synthetase in *Aspergillus fumigatus*, makes the diketopiperazine scaffold of gliotoxin." Biochemistry **45**(50): 15029-38.

Bayram, O., Krappmann, S., Ni, M., Bok, J. W., Helmstaedt, K., Valerius, O., Braus-Stromeyer, S., Kwon, N. J., Keller, N. P., Yu, J. H. and Braus, G. H. (2008). "VelB/VeA/LaeA complex coordinates light signal with fungal development and secondary metabolism." Science **320**(5882): 1504-6.

Beauvais, A. and Latge, J. P. (2001). "Membrane and cell wall targets in *Aspergillus fumigatus*." Drug Resist Updat **4**(1): 38-49.

Belaish, R., Sharon, H., Levdansky, E., Greenstein, S., Shadkchan, Y. and Osherov, N. (2008). "The *Aspergillus nidulans* cetA and calA genes are involved in conidial germination and cell wall morphogenesis." Fungal Genet Biol **45**(3): 232-42.

Belkacemi, L., Barton, R. C., Hopwood, V. and Evans, E. G. (1999). "Determination of optimum growth conditions for gliotoxin production by *Aspergillus fumigatus* and development of a novel method for gliotoxin detection." Med Mycol **37**(4): 227-33.

Ben-Ami, R., Lewis, R. E., Leventakos, K. and Kontoyiannis, D. P. (2009). "Aspergillus fumigatus inhibits angiogenesis through the production of gliotoxin and other secondary metabolites." Blood **114**(26): 5393-9.

Bernardo, P. H., Brasch, N., Chai, C. L. and Waring, P. (2003). "A novel redox mechanism for the glutathione-dependent reversible uptake of a fungal toxin in cells." J Biol Chem **278**(47): 46549-55.

Birchler, T., Seibl, R., Buchner, K., Loeliger, S., Seger, R., Hossle, J. P., Aguzzi, A. and Lauener, R. P. (2001). "Human Toll-like receptor 2 mediates induction of the antimicrobial peptide human beta-defensin 2 in response to bacterial lipoprotein." Eur J Immunol **31**(11): 3131-7.

Bok, J. W., Balajee, S. A., Marr, K. A., Andes, D., Nielsen, K. F., Frisvad, J. C. and Keller, N. P. (2005). "LaeA, a regulator of morphogenetic fungal virulence factors." Eukaryot Cell **4**(9): 1574-82.

Bok, J. W., Chung, D., Balajee, S. A., Marr, K. A., Andes, D., Nielsen, K. F., Frisvad, J. C., Kirby, K. A. and Keller, N. P. (2006a). "GliZ, a transcriptional regulator of gliotoxin biosynthesis, contributes to *Aspergillus fumigatus* virulence." Infect Immun **74**(12): 6761-8.

Bok, J. W., Hoffmeister, D., Maggio-Hall, L. A., Murillo, R., Glasner, J. D. and Keller, N. P. (2006b). "Genomic mining for *Aspergillus* natural products." Chem Biol **13**(1): 31-7.

Bok, J. W. and Keller, N. P. (2004). "LaeA, a regulator of secondary metabolism in *Aspergillus spp*." Eukaryot Cell **3**(2): 527-35.

Bolker, M., Basse, C. W. and Schirawski, J. (2008). "*Ustilago maydis* secondary metabolism-from genomics to biochemistry." Fungal Genet Biol **45 Suppl 1**: S88-93.

Bradshaw, R. E., Feng, Z., Schwelm, A., Yang, Y. and Zhang, S. (2009). "Functional Analysis of a Putative Dothistromin Toxin MFS Transporter Gene." Toxins **1**: 173-187.

Brakhage, A. A., Langfelder, K., Wanner, G., Schmidt, A. and Jahn, B. (1999). "Pigment biosynthesis and virulence." Contrib Microbiol **2**: 205-15.

Brennan, M., Thomas, D. Y., Whiteway, M. and Kavanagh, K. (2002). "Correlation between virulence of *Candida albicans* mutants in mice and *Galleria mellonella* larvae." FEMS Immunol Med Microbiol **34**(2): 153-7.

Bretagne, S., Costa, J. M., Marmorat-Khuong, A., Poron, F., Cordonnier, C., Vidaud, M. and Fleury-Feith, J. (1995). "Detection of *Aspergillus* species DNA in bronchoalveolar lavage samples by competitive PCR." J Clin Microbiol **33**(5): 1164-8.

Buckingham, S. J. and Hansell, D. M. (2003). "*Aspergillus* in the lung: diverse and coincident forms." Eur Radiol **13**(8): 1786-800.

Bunger, J., Westphal, G., Monnich, A., Hinnendahl, B., Hallier, E. and Muller, M. (2004). "Cytotoxicity of occupationally and environmentally relevant mycotoxins." Toxicology **202**(3): 199-211.

Burns, C., Geraghty, R., Neville, C., Murphy, A., Kavanagh, K. and Doyle, S. (2005). "Identification, cloning, and functional expression of three glutathione transferase genes from *Aspergillus fumigatus*." Fungal Genet Biol **42**(4): 319-27.

Caboche, S., Pupin, M., Leclere, V., Fontaine, A., Jacques, P. and Kucherov, G. (2008). "NORINE: a database of nonribosomal peptides." Nucleic Acids Res **36**(Database issue): D326-31.

Callahan, T. M., Rose, M. S., Meade, M. J., Ehrenshaft, M. and Upchurch, R. G. (1999). "CFP, the putative cercosporin transporter of *Cercospora kikuchii*, is required for wild type cercosporin production, resistance, and virulence on soybean." Mol Plant Microbe Interact **12**(10): 901-10.

Calvo, A. M., Wilson, R. A., Bok, J. W. and Keller, N. P. (2002). "Relationship between secondary metabolism and fungal development." Microbiol Mol Biol Rev **66**(3): 447-59.

Chamilos, G., Bignell, E. M., Schrettl, M., Lewis, R. E., Leventakos, K., May, G. S., Haas, H. and Kontoyiannis, D. P. (2010). "Exploring the concordance of *Aspergillus fumigatus* pathogenicity in mice and Toll-deficient flies." Med Mycol **48**(3): 506-10.

Chamilos, G., Lewis, R. E., Hu, J., Xiao, L., Zal, T., Gilliet, M., Halder, G. and Kontoyiannis, D. P. (2008). "*Drosophila melanogaster* as a model host to dissect the immunopathogenesis of zygomycosis." Proc Natl Acad Sci U S A **105**(27): 9367-72.

Chanda, A., Roze, L. V., Kang, S., Artymovich, K. A., Hicks, G. R., Raikhel, N. V., Calvo, A. M. and Linz, J. E. (2009). "A key role for vesicles in fungal secondary metabolism." <u>Proc Natl Acad Sci U S A</u> **106**(46): 19533-8.

Chang, P. K., Yu, J. and Yu, J. H. (2004). "aflT, a MFS transporter-encoding gene located in the aflatoxin gene cluster, does not have a significant role in aflatoxin secretion." <u>Fungal Genet Biol</u> **41**(10): 911-20.

Charlang, G., Ng, B., Horowitz, N. H. and Horowitz, R. M. (1981). "Cellular and extracellular siderophores of Aspergillus nidulans and Penicillium chrysogenum." <u>Mol Cell Biol</u> **1**(2): 94-100.

Chen, P. N., Kingston, D. G. and Vercellotti, J. R. (1977). "Reduction of sterigmatocystin and versicolorin A hemiacetals with sodium borohydride." <u>J Org Chem</u> **42**(22): 3599-3605.

Cockrill, B. A. and Hales, C. A. (1999). "Allergic bronchopulmonary aspergillosis." <u>Annu Rev Med</u> **50**: 303-16.

Conti, E., Stachelhaus, T., Marahiel, M. A. and Brick, P. (1997). "Structural basis for the activation of phenylalanine in the non-ribosomal biosynthesis of gramicidin S." <u>Embo J</u> **16**(14): 4174-83.

Cordonnier, C., Ribaud, P., Herbrecht, R., Milpied, N., Valteau-Couanet, D., Morgan, C. and Wade, A. (2006). "Prognostic factors for death due to invasive aspergillosis after hematopoietic stem cell transplantation: a 1-year retrospective study of consecutive patients at French transplantation centers." <u>Clin Infect Dis</u> **42**(7): 955-63.

Correia, T., Grammel, N., Ortel, I., Keller, U. and Tudzynski, P. (2003). "Molecular cloning and analysis of the ergopeptine assembly system in the ergot fungus *Claviceps purpurea*." <u>Chem Biol</u> **10**(12): 1281-92.

Costa, C., Costa, J. M., Desterke, C., Botterel, F., Cordonnier, C. and Bretagne, S. (2002). "Real-time PCR coupled with automated DNA extraction and detection of galactomannan antigen in serum by enzyme-linked immunosorbent assay for diagnosis of invasive aspergillosis." <u>J Clin Microbiol</u> **40**(6): 2224-7.

Cotter, G., Doyle, S. and Kavanagh, K. (2000). "Development of an insect model for the in vivo pathogenicity testing of yeasts." <u>FEMS Immunol Med Microbiol</u> **27**(2): 163-9.

Coyle, C. M., Cheng, J. Z., O'Connor, S. E. and Panaccione, D. G. (2010). "An old yellow enzyme gene controls the branch point between *Aspergillus fumigatus* and *Claviceps purpurea* ergot alkaloid pathways." <u>Appl Environ Microbiol</u> **76**(12): 3898-903.

Coyle, C. M., Kenaley, S. C., Rittenour, W. R. and Panaccione, D. G. (2007). "Association of ergot alkaloids with conidiation in *Aspergillus fumigatus*." Mycologia **99**(6): 804-11.

Coyle, C. M. and Panaccione, D. G. (2005). "An ergot alkaloid biosynthesis gene and clustered hypothetical genes from *Aspergillus fumigatus*." Appl Environ Microbiol **71**(6): 3112-8.

Cramer, R. A., Jr., Gamcsik, M. P., Brooking, R. M., Najvar, L. K., Kirkpatrick, W. R., Patterson, T. F., Balibar, C. J., Graybill, J. R., Perfect, J. R., Abraham, S. N. and Steinbach, W. J. (2006a). "Disruption of a nonribosomal peptide synthetase in *Aspergillus fumigatus* eliminates gliotoxin production." Eukaryot Cell **5**(6): 972-80.

Cramer, R. A., Jr., Stajich, J. E., Yamanaka, Y., Dietrich, F. S., Steinbach, W. J. and Perfect, J. R. (2006b). "Phylogenomic analysis of non-ribosomal peptide synthetases in the genus *Aspergillus*." Gene **383**: 24-32.

da Silva Ferreira, M. E., Heinekamp, T., Hartl, A., Brakhage, A. A., Semighini, C. P., Harris, S. D., Savoldi, M., de Gouvea, P. F., de Souza Goldman, M. H. and Goldman, G. H. (2007). "Functional characterization of the Aspergillus fumigatus calcineurin." Fungal Genet Biol **44**(3): 219-30.

da Silva Ferreira, M. E., Kress, M. R., Savoldi, M., Goldman, M. H., Hartl, A., Heinekamp, T., Brakhage, A. A. and Goldman, G. H. (2006a). "The akuB(KU80) mutant deficient for nonhomologous end joining is a powerful tool for analyzing pathogenicity in *Aspergillus fumigatus*." Eukaryot Cell **5**(1): 207-11.

da Silva Ferreira, M. E., Malavazi, I., Savoldi, M., Brakhage, A. A., Goldman, M. H., Kim, H. S., Nierman, W. C. and Goldman, G. H. (2006b). "Transcriptome analysis of *Aspergillus fumigatus* exposed to voriconazole." Curr Genet **50**(1): 32-44.

Dagenais, T. R., Giles, S. S., Aimanianda, V., Latge, J. P., Hull, C. M. and Keller, N. P. (2010). "*Aspergillus fumigatus* LaeA-mediated phagocytosis is associated with a decreased hydrophobin layer." Infect Immun **78**(2): 823-9.

Dagenais, T. R. and Keller, N. P. (2009). "Pathogenesis of *Aspergillus fumigatus* in Invasive Aspergillosis." Clin Microbiol Rev **22**(3): 447-65.

Davis, C. A., Carberry, S., Schrettl, M., Singh, I., Stephens, J., Kavanagh, K., Brougham, D. and Doyle, S. (2010). "Precursor Amino Acid Modification to a Methylenepiperazine-2,5-dione Is Essential for Gliotoxin Biosynthesis in *Aspergillus fumigatus*." (In Preparation).

de Repentigny, L., Boushira, M., Ste-Marie, L. and Bosisio, G. (1987). "Detection of galactomannan antigenemia by enzyme immunoassay in experimental invasive aspergillosis." J Clin Microbiol **25**(5): 863-7.

Del Bono, V., Mikulska, M. and Viscoli, C. (2008). "Invasive aspergillosis: diagnosis, prophylaxis and treatment." Curr Opin Hematol **15**(6): 586-93.

Del Sorbo, G., Schoonbeek, H. and De Waard, M. A. (2000). "Fungal transporters involved in efflux of natural toxic compounds and fungicides." Fungal Genet Biol **30**(1): 1-15.

Denning, D. W. (1998). "Invasive aspergillosis." Clin Infect Dis **26**(4): 781-803; quiz 804-5.

Denning, D. W. (2001). "Chronic forms of pulmonary aspergillosis." Clin Microbiol Infect **7 Suppl 2**: 25-31.

Denning, D. W., Anderson, M. J., Turner, G., Latge, J. P. and Bennett, J. W. (2002). "Sequencing the *Aspergillus fumigatus* genome." Lancet Infect Dis **2**(4): 251-3.

Denning, D. W. and Hope, W. W. (2010). "Therapy for fungal diseases: opportunities and priorities." Trends Microbiol **18**(5): 195-204.

Doyle, S. (2009). Nonribosomal Peptide Synthesis in Amino Acids, Peptides and Proteins in Organic Chemistry. Amino Acids, Peptides and Proteins in Organic Chemistry A. B. Hughes. Weinheim, Wiley-VCH. **2:** 631-650, ISBN: 978.3.527.32096.7.

Doyle, S., Molloy, E., Carberry, S., Schrettl, M., Kavanagh, K. and Jones, G. (2010 of Conference). Resistance of Aspergillus fumigatus to gliotoxin -a new selection marker strategy for fungal transformation. IMC9 The Biology of Fungi, Edinburgh, Conference 1 - 6 August 2010.

Dutton, J. R., Johns, S. and Miller, B. L. (1997). "StuAp is a sequence-specific transcription factor that regulates developmental complexity in *Aspergillus nidulans*." Embo J **16**(18): 5710-21.

Dyer, P. S. and Paoletti, M. (2005). "Reproduction in *Aspergillus fumigatus*: sexuality in a supposedly asexual species?" Med Mycol **43 Suppl 1**: S7-14.

Eichner, R. D., Al Salami, M., Wood, P. R. and Mullbacher, A. (1986). "The effect of gliotoxin upon macrophage function." Int J Immunopharmacol **8**(7): 789-97.

Eichner, R. D., Waring, P., Geue, A. M., Braithwaite, A. W. and Mullbacher, A. (1988). "Gliotoxin causes oxidative damage to plasmid and cellular DNA." J Biol Chem **263**(8): 3772-7.

Eisendle, M., Oberegger, H., Zadra, I. and Haas, H. (2003). "The siderophore system is essential for viability of *Aspergillus nidulans*: functional analysis of two genes encoding l-ornithine N 5-monooxygenase (sidA) and a non-ribosomal peptide synthetase (sidC)." Mol Microbiol **49**(2): 359-75.

Eisendle, M., Schrettl, M., Kragl, C., Muller, D., Illmer, P. and Haas, H. (2006). "The intracellular siderophore ferricrocin is involved in iron storage, oxidative-stress resistance, germination, and sexual development in *Aspergillus nidulans*." Eukaryot Cell **5**(10): 1596-603.

Ejzykowicz, D. E., Cunha, M. M., Rozental, S., Solis, N. V., Gravelat, F. N., Sheppard, D. C. and Filler, S. G. (2009). "The *Aspergillus fumigatus* transcription factor Ace2 governs pigment production, conidiation and virulence." <u>Mol Microbiol</u> **72**(1): 155-69.

El-Ganiny, A. M., Sanders, D. A. and Kaminskyj, S. G. (2008). "*Aspergillus nidulans* UDP-galactopyranose mutase, encoded by ugmA plays key roles in colony growth, hyphal morphogenesis, and conidiation." <u>Fungal Genet Biol</u> **45**(12): 1533-42.

Etxebeste, O., Markina-Inarrairaegui, A., Garzia, A., Herrero-Garcia, E., Ugalde, U. and Espeso, E. A. (2009). "KapI, a non-essential member of the Pse1p/Imp5 karyopherin family, controls colonial and asexual development in Aspergillus nidulans." <u>Microbiology</u> **155**(Pt 12): 3934-45.

Fallon, J. P., Reeves, E. P. and Kavanagh, K. (2010). "Inhibition of neutrophil function following exposure to the *Aspergillus fumigatus* toxin fumagillin." <u>J Med Microbiol</u> **59**(Pt 6): 625-33.

Fedorova, N. D., Khaldi, N., Joardar, V. S., Maiti, R., Amedeo, P., Anderson, M. J., Crabtree, J., Silva, J. C., Badger, J. H., Albarraq, A., Angiuoli, S., Bussey, H., Bowyer, P., Cotty, P. J., Dyer, P. S., Egan, A., Galens, K., Fraser-Liggett, C. M., Haas, B. J., Inman, J. M., Kent, R., Lemieux, S., Malavazi, I., Orvis, J., Roemer, T., Ronning, C. M., Sundaram, J. P., Sutton, G., Turner, G., Venter, J. C., White, O. R., Whitty, B. R., Youngman, P., Wolfe, K. H., Goldman, G. H., Wortman, J. R., Jiang, B., Denning, D. W. and Nierman, W. C. (2008). "Genomic islands in the pathogenic filamentous fungus *Aspergillus fumigatus*." <u>PLoS Genet</u> **4**(4): e1000046.

Fillinger, S., Chaveroche, M. K., van Dijck, P., de Vries, R., Ruijter, G., Thevelein, J. and d'Enfert, C. (2001). "Trehalose is required for the acquisition of tolerance to a variety of stresses in the filamentous fungus *Aspergillus nidulans*." <u>Microbiology</u> **147**(Pt 7): 1851-62.

Fischer, G., Muller, T., Schwalbe, R., Ostrowski, R. and Dott, W. (2000). "Species-specific profiles of mycotoxins produced in cultures and associated with conidia of airborne fungi derived from biowaste." <u>Int J Hyg Environ Health</u> **203**(2): 105-16.

Fleetwood, D. J., Scott, B., Lane, G. A., Tanaka, A. and Johnson, R. D. (2007). "A complex ergovaline gene cluster in epichloe endophytes of grasses." <u>Appl Environ Microbiol</u> **73**(8): 2571-9.

Flipphi, M., van de Vondervoort, P. J., Ruijter, G. J., Visser, J., Arst, H. N., Jr. and Felenbok, B. (2003). "Onset of carbon catabolite repression in Aspergillus nidulans. Parallel involvement of hexokinase and glucokinase in sugar signaling." <u>J Biol Chem</u> **278**(14): 11849-57.

Florent, M., Katsahian, S., Vekhoff, A., Levy, V., Rio, B., Marie, J. P., Bouvet, A. and Cornet, M. (2006). "Prospective evaluation of a polymerase chain reaction-ELISA targeted to *Aspergillus fumigatus* and *Aspergillus flavus* for the early

diagnosis of invasive aspergillosis in patients with hematological malignancies." J Infect Dis **193**(5): 741-7.

Foster, J. W. and Karow, E. O. (1945). "Microbiological Aspects of Penicillin: VIII. Penicillin from Different Fungi." J Bacteriol **49**(1): 19-29.

Fox, E. M., Gardiner, D. M., Keller, N. P. and Howlett, B. J. (2008). "A Zn(II)2Cys6 DNA binding protein regulates the sirodesmin PL biosynthetic gene cluster in *Leptosphaeria maculans*." Fungal Genet Biol **45**(5): 671-82.

Frandsen, R. J., Andersson, J. A., Kristensen, M. B. and Giese, H. (2008). "Efficient four fragment cloning for the construction of vectors for targeted gene replacement in filamentous fungi." BMC Mol Biol **9**: 70.

Frisvad, J. C., Rank, C., Nielsen, K. F. and Larsen, T. O. (2009). "Metabolomics of *Aspergillus fumigatus*." Med Mycol **47 Suppl 1**: S53-71.

Fujiwara, M., Ichinomiya, M., Motoyama, T., Horiuchi, H., Ohta, A. and Takagi, M. (2000). "Evidence that the Aspergillus nidulans class I and class II chitin synthase genes, chsC and chsA, share critical roles in hyphal wall integrity and conidiophore development." J Biochem **127**(3): 359-66.

Galagan, J. E., Calvo, S. E., Cuomo, C., Ma, L. J., Wortman, J. R., Batzoglou, S., Lee, S. I., Basturkmen, M., Spevak, C. C., Clutterbuck, J., Kapitonov, V., Jurka, J., Scazzocchio, C., Farman, M., Butler, J., Purcell, S., Harris, S., Braus, G. H., Draht, O., Busch, S., D'Enfert, C., Bouchier, C., Goldman, G. H., Bell-Pedersen, D., Griffiths-Jones, S., Doonan, J. H., Yu, J., Vienken, K., Pain, A., Freitag, M., Selker, E. U., Archer, D. B., Penalva, M. A., Oakley, B. R., Momany, M., Tanaka, T., Kumagai, T., Asai, K., Machida, M., Nierman, W. C., Denning, D. W., Caddick, M., Hynes, M., Paoletti, M., Fischer, R., Miller, B., Dyer, P., Sachs, M. S., Osmani, S. A. and Birren, B. W. (2005). "Sequencing of *Aspergillus nidulans* and comparative analysis with *A. fumigatus* and *A. oryzae*." Nature **438**(7071): 1105-15.

Gardiner, D. M., Cozijnsen, A. J., Wilson, L. M., Pedras, M. S. and Howlett, B. J. (2004). "The sirodesmin biosynthetic gene cluster of the plant pathogenic fungus Leptosphaeria maculans." Mol Microbiol **53**(5): 1307-18.

Gardiner, D. M. and Howlett, B. J. (2005a). "Bioinformatic and expression analysis of the putative gliotoxin biosynthetic gene cluster of *Aspergillus fumigatus*." FEMS Microbiol Lett **248**(2): 241-8.

Gardiner, D. M., Jarvis, R. S. and Howlett, B. J. (2005b). "The ABC transporter gene in the sirodesmin biosynthetic gene cluster of *Leptosphaeria maculans* is not essential for sirodesmin production but facilitates self-protection." Fungal Genet Biol **42**(3): 257-63.

Gardiner, D. M., Waring, P. and Howlett, B. J. (2005c). "The epipolythiodioxopiperazine (ETP) class of fungal toxins: distribution, mode of action, functions and biosynthesis." Microbiology **151**(Pt 4): 1021-32.

Gautam, P., Shankar, J., Madan, T., Sirdeshmukh, R., Sundaram, C. S., Gade, W. N., Basir, S. F. and Sarma, P. U. (2008). "Proteomic and transcriptomic analysis of *Aspergillus fumigatus* on exposure to amphotericin B." <u>Antimicrob Agents Chemother</u> **52**(12): 4220-7.

Gautam, P., Sundaram, C. S., Madan, T., Gade, W. N., Shah, A., Sirdeshmukh, R. and Sarma, P. U. (2007). "Identification of novel allergens of *Aspergillus fumigatus* using immunoproteomics approach." <u>Clin Exp Allergy</u> **37**(8): 1239-49.

Geiser, D. M., Klich, M. A., Frisvad, J. C., Peterson, S. W., Varga, J. and Samson, R. A. (2007). "The current status of species recognition and identification in *Aspergillus*." <u>Stud Mycol</u> **59**: 1-10.

Gifford, A. H., Klippenstein, J. R. and Moore, M. M. (2002). "Serum stimulates growth of and proteinase secretion by *Aspergillus fumigatus*." <u>Infect Immun</u> **70**(1): 19-26.

Groetzner, J., Kaczmarek, I., Wittwer, T., Strauch, J., Meiser, B., Wahlers, T., Daebritz, S. and Reichart, B. (2008). "Caspofungin as first-line therapy for the treatment of invasive aspergillosis after thoracic organ transplantation." <u>J Heart Lung Transplant</u> **27**(1): 1-6.

Grundmann, A., Kuznetsova, T., Afiyatullov, S. and Li, S. M. (2008). "FtmPT2, an N-prenyltransferase from *Aspergillus fumigatus*, catalyses the last step in the biosynthesis of fumitremorgin B." <u>Chembiochem</u> **9**(13): 2059-63.

Guilfoile, P. G. and Hutchinson, C. R. (1992). "The Streptomyces glaucescens TcmR protein represses transcription of the divergently oriented tcmR and tcmA genes by binding to an intergenic operator region." <u>J Bacteriol</u> **174**(11): 3659-66.

Guillemette, T., Sellam, A. and Simoneau, P. (2004). "Analysis of a nonribosomal peptide synthetase gene from *Alternaria brassicae* and flanking genomic sequences." <u>Curr Genet</u> **45**(4): 214-24.

Gulick, A. M. (2009). "Conformational dynamics in the Acyl-CoA synthetases, adenylation domains of non-ribosomal peptide synthetases, and firefly luciferase." <u>ACS Chem Biol</u> **4**(10): 811-27.

Haarmann, T., Machado, C., Lubbe, Y., Correia, T., Schardl, C. L., Panaccione, D. G. and Tudzynski, P. (2005). "The ergot alkaloid gene cluster in *Claviceps purpurea*: extension of the cluster sequence and intra species evolution." <u>Phytochemistry</u> **66**(11): 1312-20.

Haas, H. (2003). "Molecular genetics of fungal siderophore biosynthesis and uptake: the role of siderophores in iron uptake and storage." <u>Appl Microbiol Biotechnol</u> **62**(4): 316-30.

Haas, H., Eisendle, M. and Turgeon, B. G. (2008). "Siderophores in fungal physiology and virulence." <u>Annu Rev Phytopathol</u> **46**: 149-87.

Haas, H., Zadra, I., Stoffler, G. and Angermayr, K. (1999). "The *Aspergillus nidulans* GATA factor SREA is involved in regulation of siderophore biosynthesis and control of iron uptake." <u>J Biol Chem</u> **274**(8): 4613-9.

Hagiwara, D., Kondo, A., Fujioka, T. and Abe, K. (2008). "Functional analysis of C2H2 zinc finger transcription factor CrzA involved in calcium signaling in Aspergillus nidulans." <u>Curr Genet</u> **54**(6): 325-38.

Halliday, C., Hoile, R., Sorrell, T., James, G., Yadav, S., Shaw, P., Bleakley, M., Bradstock, K. and Chen, S. (2006). "Role of prospective screening of blood for invasive aspergillosis by polymerase chain reaction in febrile neutropenic recipients of haematopoietic stem cell transplants and patients with acute leukaemia." <u>Br J Haematol</u> **132**(4): 478-86.

Hamilton, A. J. and Gomez, B. L. (2002). "Melanins in fungal pathogens." <u>J Med Microbiol</u> **51**(3): 189-91.

Heinz, W. J. and Einsele, H. (2008). "Caspofungin for treatment of invasive aspergillus infections." <u>Mycoses</u> **51 Suppl 1**: 47-57.

Hicks, J. K., Yu, J. H., Keller, N. P. and Adams, T. H. (1997). "Aspergillus sporulation and mycotoxin production both require inactivation of the FadA G alpha protein-dependent signaling pathway." <u>Embo J</u> **16**(16): 4916-23.

Hissen, A. H., Chow, J. M., Pinto, L. J. and Moore, M. M. (2004). "Survival of Aspergillus fumigatus in serum involves removal of iron from transferrin: the role of siderophores." <u>Infect Immun</u> **72**(3): 1402-8.

Hope, W. W., Walsh, T. J. and Denning, D. W. (2005). "Laboratory diagnosis of invasive aspergillosis." <u>Lancet Infect Dis</u> **5**(10): 609-22.

Howard, D. H. (1999). "Acquisition, transport, and storage of iron by pathogenic fungi." <u>Clin Microbiol Rev</u> **12**(3): 394-404.

Howard, S. J., Cerar, D., Anderson, M. J., Albarrag, A., Fisher, M. C., Pasqualotto, A. C., Laverdiere, M., Arendrup, M. C., Perlin, D. S. and Denning, D. W. (2009). "Frequency and evolution of Azole resistance in *Aspergillus fumigatus* associated with treatment failure." <u>Emerg Infect Dis</u> **15**(7): 1068-76.

Hurne, A. M., Chai, C. L., Moerman, K. and Waring, P. (2002). "Influx of calcium through a redox-sensitive plasma membrane channel in thymocytes causes early necrotic cell death induced by the epipolythiodioxopiperazine toxins." <u>J Biol Chem</u> **277**(35): 31631-8.

Ichinomiya, M., Horiuchi, H. and Ohta, A. (2002a). "Different functions of the class I and class II chitin synthase genes, chsC and chsA, are revealed by repression of chsB expression in *Aspergillus nidulans*." <u>Curr Genet</u> **42**(1): 51-8.

Ichinomiya, M., Motoyama, T., Fujiwara, M., Takagi, M., Horiuchi, H. and Ohta, A. (2002b). "Repression of chsB expression reveals the functional importance of class

IV chitin synthase gene chsD in hyphal growth and conidiation of *Aspergillus nidulans*." Microbiology **148**(Pt 5): 1335-47.

Ichinomiya, M., Yamada, E., Yamashita, S., Ohta, A. and Horiuchi, H. (2005). "Class I and class II chitin synthases are involved in septum formation in the filamentous fungus Aspergillus nidulans." Eukaryot Cell **4**(6): 1125-36.

Jackson, J. C., Higgins, L. A. and Lin, X. (2009). "Conidiation color mutants of *Aspergillus fumigatus* are highly pathogenic to the heterologous insect host *Galleria mellonella*." PLoS One **4**(1): e4224.

Jander, G., Rahme, L. G. and Ausubel, F. M. (2000). "Positive correlation between virulence of Pseudomonas aeruginosa mutants in mice and insects." J Bacteriol **182**(13): 3843-5.

Jegorov, A., Hajduch, M., Sulc, M. and Havlicek, V. (2006). "Nonribosomal cyclic peptides: specific markers of fungal infections." J Mass Spectrom **41**(5): 563-76.

Jirakkakul, J., Punya, J., Pongpattanakitshote, S., Paungmoung, P., Vorapreeda, N., Tachaleat, A., Klomnara, C., Tanticharoen, M. and Cheevadhanarak, S. (2008). "Identification of the nonribosomal peptide synthetase gene responsible for bassianolide synthesis in wood-decaying fungus *Xylaria sp.* BCC1067." Microbiology **154**(Pt 4): 995-1006.

Johnson, D. N., Egner, P. A., Obrian, G., Glassbrook, N., Roebuck, B. D., Sutter, T. R., Payne, G. A., Kensler, T. W. and Groopman, J. D. (2008). "Quantification of urinary aflatoxin B1 dialdehyde metabolites formed by aflatoxin aldehyde reductase using isotope dilution tandem mass spectrometry." Chem Res Toxicol **21**(3): 752-60.

Johnson, L. (2008). "Iron and siderophores in fungal-host interactions." Mycol Res **112**(Pt 2): 170-83.

Jones, M. E. (1985). "Conversion of glutamate to ornithine and proline: pyrroline-5-carboxylate, a possible modulator of arginine requirements." J Nutr **115**(4): 509-15.

Kafer, E. and Mayor, O. (1986). "Genetic analysis of DNA repair in Aspergillus: evidence for different types of MMS-sensitive hyperrec mutants." Mutat Res **161**(2): 119-34.

Kato, N., Suzuki, H., Takagi, H., Asami, Y., Kakeya, H., Uramoto, M., Usui, T., Takahashi, S., Sugimoto, Y. and Osada, H. (2009). "Identification of cytochrome P450s required for fumitremorgin biosynthesis in *Aspergillus fumigatus*." Chembiochem **10**(5): 920-8.

Kavanagh, K. and Reeves, E. P. (2004). "Exploiting the potential of insects for in vivo pathogenicity testing of microbial pathogens." FEMS Microbiol Rev **28**(1): 101-12.

Keller, N. P., Turner, G. and Bennett, J. W. (2005). "Fungal secondary metabolism - from biochemistry to genomics." Nat Rev Microbiol **3**(12): 937-47.

Keszenman-Pereyra, D., Lawrence, S., Twfieg, M. E., Price, J. and Turner, G. (2003). "The npgA/ cfwA gene encodes a putative 4'-phosphopantetheinyl transferase which is essential for penicillin biosynthesis in *Aspergillus nidulans*." Curr Genet **43**(3): 186-90.

Khoufache, K., Puel, O., Loiseau, N., Delaforge, M., Rivollet, D., Coste, A., Cordonnier, C., Escudier, E., Botterel, F. and Bretagne, S. (2007). "Verruculogen associated with *Aspergillus fumigatus* hyphae and conidia modifies the electrophysiological properties of human nasal epithelial cells." BMC Microbiol **7**: 5.

Kidd, J. G. (1947). "Effects of an Antibiotic From Aspergillus fumigatus Fresenius on Tumor Cells in Vitro, and Its Possible Identity With Gliotoxin." Science **105**(2733): 511-513.

Kleinkauf, H. and Von Dohren, H. (1996). "A nonribosomal system of peptide biosynthesis." Eur J Biochem **236**(2): 335-51.

Koglin, A., Lohr, F., Bernhard, F., Rogov, V. V., Frueh, D. P., Strieter, E. R., Mofid, M. R., Guntert, P., Wagner, G., Walsh, C. T., Marahiel, M. A. and Dotsch, V. (2008). "Structural basis for the selectivity of the external thioesterase of the surfactin synthetase." Nature **454**(7206): 907-11.

Kontoyiannis, D. P., Lionakis, M. S., Lewis, R. E., Chamilos, G., Healy, M., Perego, C., Safdar, A., Kantarjian, H., Champlin, R., Walsh, T. J. and Raad, II (2005). "Zygomycosis in a tertiary-care cancer center in the era of *Aspergillus*-active antifungal therapy: a case-control observational study of 27 recent cases." J Infect Dis **191**(8): 1350-60.

Kosalec, I., Klaric, M. S. and Pepeljnjak, S. (2005a). "Verruculogen production in airborne and clinical isolates of *Aspergillus fumigatus Fres*." Acta Pharm **55**(4): 357-64.

Kosalec, I., Pepeljnjak, S. and Jandrlic, M. (2005b). "Influence of media and temperature on gliotoxin production in Aspergillus fumigatus strains." Arh Hig Rada Toksikol **56**(3): 269-73.

Kosman, D. J. (2003). "Molecular mechanisms of iron uptake in fungi." Mol Microbiol **47**(5): 1185-97.

Kragl, C., Schrettl, M., Abt, B., Sarg, B., Lindner, H. H. and Haas, H. (2007). "EstB-mediated hydrolysis of the siderophore triacetylfusarinine C optimizes iron uptake of *Aspergillus fumigatus*." Eukaryot Cell **6**(8): 1278-85.

Krappmann, S., Sasse, C. and Braus, G. H. (2006). "Gene targeting in *Aspergillus fumigatus* by homologous recombination is facilitated in a nonhomologous end-joining-deficient genetic background." Eukaryot Cell **5**(1): 212-5.

Krishnan-Natesan, S. and Chandrasekar, P. H. (2008). "Current and future therapeutic options in the management of invasive aspergillosis." Drugs **68**(3): 265-82.

Kubodera, T., Yamashita, N. and Nishimura, A. (2000). "Pyrithiamine resistance gene (ptrA) of *Aspergillus oryzae*: cloning, characterization and application as a dominant selectable marker for transformation." Biosci Biotechnol Biochem **64**(7): 1416-21.

Kubodera, T., Yamashita, N. and Nishimura, A. (2002). "Transformation of *Aspergillus sp.* and *Trichoderma reesei* using the pyrithiamine resistance gene (ptrA) of *Aspergillus oryzae*." Biosci Biotechnol Biochem **66**(2): 404-6.

Kupfahl, C., Heinekamp, T., Geginat, G., Ruppert, T., Hartl, A., Hof, H. and Brakhage, A. A. (2006). "Deletion of the gliP gene of Aspergillus fumigatus results in loss of gliotoxin production but has no effect on virulence of the fungus in a low-dose mouse infection model." Mol Microbiol **62**(1): 292-302.

Kupfahl, C., Michalka, A., Lass-Florl, C., Fischer, G., Haase, G., Ruppert, T., Geginat, G. and Hof, H. (2008). "Gliotoxin production by clinical and environmental Aspergillus fumigatus strains." Int J Med Microbiol **298**(3-4): 319-27.

Kuwayama, H., Obara, S., Morio, T., Katoh, M., Urushihara, H. and Tanaka, Y. (2002). "PCR-mediated generation of a gene disruption construct without the use of DNA ligase and plasmid vectors." Nucleic Acids Res **30**(2): E2.

Lamaris, G. A., Ben-Ami, R., Lewis, R. E., Chamilos, G., Samonis, G. and Kontoyiannis, D. P. (2009). "Increased virulence of Zygomycetes organisms following exposure to voriconazole: a study involving fly and murine models of zygomycosis." J Infect Dis **199**(9): 1399-406.

Lamaris, G. A., Ben-Ami, R., Lewis, R. E. and Kontoyiannis, D. P. (2008). "Does pre-exposure of *Aspergillus fumigatus* to voriconazole or posaconazole in vitro affect its virulence and the in vivo activity of subsequent posaconazole or voriconazole, respectively? A study in a fly model of aspergillosis." J Antimicrob Chemother **62**(3): 539-42.

Lambalot, R. H., Gehring, A. M., Flugel, R. S., Zuber, P., LaCelle, M., Marahiel, M. A., Reid, R., Khosla, C. and Walsh, C. T. (1996). "A new enzyme superfamily - the phosphopantetheinyl transferases." Chem Biol **3**(11): 923-36.

Larsen, T. O., Smedsgaard, J., Nielsen, K. F., Hansen, M. A., Samson, R. A. and Frisvad, J. C. (2007). "Production of mycotoxins by *Aspergillus lentulus* and other medically important and closely related species in section Fumigati." Med Mycol **45**(3): 225-32.

Latge, J. P. (1999). "*Aspergillus fumigatus* and aspergillosis." Clin Microbiol Rev **12**(2): 310-50.

Lau, A., Chen, S., Sorrell, T., Carter, D., Malik, R., Martin, P. and Halliday, C. (2007). "Development and clinical application of a panfungal PCR assay to detect and identify fungal DNA in tissue specimens." J Clin Microbiol **45**(2): 380-5.

Lautru, S. and Challis, G. L. (2004). "Substrate recognition by nonribosomal peptide synthetase multi-enzymes." Microbiology **150**(Pt 6): 1629-36.

Lazos, O., Tosin, M., Slusarczyk, A. L., Boakes, S., Cortes, J., Sidebottom, P. J. and Leadlay, P. F. (2010). "Biosynthesis of the putative siderophore erythrochelin requires unprecedented crosstalk between separate nonribosomal peptide gene clusters." Chem Biol **17**(2): 160-73.

Lee, B. N., Kroken, S., Chou, D. Y., Robbertse, B., Yoder, O. C. and Turgeon, B. G. (2005). "Functional analysis of all nonribosomal peptide synthetases in *Cochliobolus heterostrophus* reveals a factor, NPS6, involved in virulence and resistance to oxidative stress." Eukaryot Cell **4**(3): 545-55.

Lessing, F., Kniemeyer, O., Wozniok, I., Loeffler, J., Kurzai, O., Haertl, A. and Brakhage, A. A. (2007). "The *Aspergillus fumigatus* transcriptional regulator AfYap1 represents the major regulator for defense against reactive oxygen intermediates but is dispensable for pathogenicity in an intranasal mouse infection model." Eukaryot Cell **6**(12): 2290-302.

Lewis, R. E., Wiederhold, N. P., Lionakis, M. S., Prince, R. A. and Kontoyiannis, D. P. (2005). "Frequency and species distribution of gliotoxin-producing Aspergillus isolates recovered from patients at a tertiary-care cancer center." J Clin Microbiol **43**(12): 6120-2.

Lionakis, M. S. and Kontoyiannis, D. P. (2005). "Fruit flies as a minihost model for studying drug activity and virulence in *Aspergillus*." Med Mycol **43 Suppl 1**: S111-4.

Liu, X., Wang, L., Steffan, N., Yin, W. B. and Li, S. M. (2009). "Ergot Alkaloid Biosynthesis in *Aspergillus fumigatus*: FgaAT Catalyses the Acetylation of Fumigaclavine B." Chembiochem.

Lorenz, N., Wilson, E. V., Machado, C., Schardl, C. L. and Tudzynski, P. (2007). "Comparison of ergot alkaloid biosynthesis gene clusters in *Claviceps* species indicates loss of late pathway steps in evolution of *C. fusiformis*." Appl Environ Microbiol **73**(22): 7185-91.

Losada, L., Ajayi, O., Frisvad, J. C., Yu, J. and Nierman, W. C. (2009). "Effect of competition on the production and activity of secondary metabolites in *Aspergillus* species." Med Mycol **47 Suppl 1**: S88-96.

Mabey, J. E., Anderson, M. J., Giles, P. F., Miller, C. J., Attwood, T. K., Paton, N. W., Bornberg-Bauer, E., Robson, G. D., Oliver, S. G. and Denning, D. W. (2004). "CADRE: the Central Aspergillus Data REpository." Nucleic Acids Res **32**(Database issue): D401-5.

Machida, M., Asai, K., Sano, M., Tanaka, T., Kumagai, T., Terai, G., Kusumoto, K., Arima, T., Akita, O., Kashiwagi, Y., Abe, K., Gomi, K., Horiuchi, H., Kitamoto, K., Kobayashi, T., Takeuchi, M., Denning, D. W., Galagan, J. E., Nierman, W. C., Yu, J., Archer, D. B., Bennett, J. W., Bhatnagar, D., Cleveland, T. E., Fedorova, N. D., Gotoh, O., Horikawa, H., Hosoyama, A., Ichinomiya, M., Igarashi, R., Iwashita, K., Juvvadi, P. R., Kato, M., Kato, Y., Kin, T., Kokubun, A., Maeda, H., Maeyama, N., Maruyama, J., Nagasaki, H., Nakajima, T., Oda, K., Okada, K., Paulsen, I., Sakamoto, K., Sawano, T., Takahashi, M., Takase, K., Terabayashi, Y., Wortman, J. R., Yamada, O., Yamagata, Y., Anazawa, H., Hata, Y., Koide, Y., Komori, T., Koyama, Y., Minetoki, T., Suharnan, S., Tanaka, A., Isono, K., Kuhara, S., Ogasawara, N. and Kikuchi, H. (2005). "Genome sequencing and analysis of *Aspergillus oryzae*." Nature **438**(7071): 1157-61.

Madduri, K., Waldron, C. and Merlo, D. J. (2001). "Rhamnose biosynthesis pathway supplies precursors for primary and secondary metabolism in *Saccharopolyspora spinosa*." J Bacteriol **183**(19): 5632-8.

Maertens, J., Theunissen, K., Lodewyck, T., Lagrou, K. and Van Eldere, J. (2007). "Advances in the serological diagnosis of invasive *Aspergillus infections* in patients with haematological disorders." Mycoses **50 Suppl 1**: 2-17.

Maiya, S., Grundmann, A., Li, S. M. and Turner, G. (2006). "The fumitremorgin gene cluster of *Aspergillus fumigatus*: identification of a gene encoding brevianamide F synthetase." Chembiochem **7**(7): 1062-9.

Maiya, S., Grundmann, A., Li, S. M. and Turner, G. (2009). "Improved tryprostatin B production by heterologous gene expression in *Aspergillus nidulans*." Fungal Genet Biol.

Maiya, S., Grundmann, A., Li, X., Li, S. M. and Turner, G. (2007). "Identification of a hybrid PKS/NRPS required for pseurotin A biosynthesis in the human pathogen *Aspergillus fumigatus*." Chembiochem **8**(14): 1736-43.

Marr, K. A., Carter, R. A., Boeckh, M., Martin, P. and Corey, L. (2002). "Invasive aspergillosis in allogeneic stem cell transplant recipients: changes in epidemiology and risk factors." Blood **100**(13): 4358-66.

Maschmeyer, G., Haas, A. and Cornely, O. A. (2007). "Invasive aspergillosis: epidemiology, diagnosis and management in immunocompromised patients." Drugs **67**(11): 1567-601.

Matzanke, B. F., Bill, E., Trautwein, A. X. and Winkelmann, G. (1987). "Role of siderophores in iron storage in spores of *Neurospora crassa* and *Aspergillus ochraceus*." J Bacteriol **169**(12): 5873-6.

McDonagh, A., Fedorova, N. D., Crabtree, J., Yu, Y., Kim, S., Chen, D., Loss, O., Cairns, T., Goldman, G., Armstrong-James, D., Haynes, K., Haas, H., Schrettl, M., May, G., Nierman, W. C. and Bignell, E. (2008). "Sub-telomere directed gene expression during initiation of invasive aspergillosis." PLoS Pathog **4**(9): e1000154.

Meier, J. L. and Burkart, M. D. (2009). "The chemical biology of modular biosynthetic enzymes." Chem Soc Rev **38**(7): 2012-45.

Missall, T. A., Lodge, J. K. and McEwen, J. E. (2004). "Mechanisms of resistance to oxidative and nitrosative stress: implications for fungal survival in mammalian hosts." Eukaryot Cell **3**(4): 835-46.

Mitsutake, K., Kohno, S., Miyazaki, T., Yamamoto, Y., Yanagihara, K., Kakeya, H., Hashimoto, A., Koga, H. and Hara, K. (1995). "Detection of (1-3)-beta-D-glucan in a rat model of aspergillosis." J Clin Lab Anal **9**(2): 119-22.

Mootz, H. D., Schwarzer, D. and Marahiel, M. A. (2002). "Ways of assembling complex natural products on modular nonribosomal peptide synthetases." Chembiochem **3**(6): 490-504.

Morton, D. B., Dunphy, G. B. and Chadwick, J. S. (1987). "Reactions of hemocytes of immune and non-immune Galleria mellonella larvae to Proteus mirabilis." Dev Comp Immunol **11**(1): 47-55.

Moss, R. B. (2002). "Allergic bronchopulmonary aspergillosis." Clin Rev Allergy Immunol **23**(1): 87-104.

Mullbacher, A. and Eichner, R. D. (1984). "Immunosuppression in vitro by a metabolite of a human pathogenic fungus." Proc Natl Acad Sci U S A **81**(12): 3835-7.

Muller, G., Barclay, S. J. and Raymond, K. N. (1985). "The mechanism and specificity of iron transport in *Rhodotorula pilimanae* probed by synthetic analogs of rhodotorulic acid." J Biol Chem **260**(26): 13916-20.

Mylonakis, E. (2008). "Galleria mellonella and the study of fungal pathogenesis: making the case for another genetically tractable model host." Mycopathologia **165**(1): 1-3.

Nayak, S. K., Bagga, S., Gaur, D., Nair, D. T., Salunke, D. M. and Batra, J. K. (2001). "Mechanism of specific target recognition and RNA hydrolysis by ribonucleolytic toxin restrictocin." Biochemistry **40**(31): 9115-24.

Nayak, T., Szewczyk, E., Oakley, C. E., Osmani, A., Ukil, L., Murray, S. L., Hynes, M. J., Osmani, S. A. and Oakley, B. R. (2006). "A versatile and efficient gene-targeting system for *Aspergillus nidulans*." Genetics **172**(3): 1557-66.

Neal, R. J. and Chater, K. F. (1987). "Nucleotide sequence analysis reveals similarities between proteins determining methylenomycin A resistance in Streptomyces and tetracycline resistance in eubacteria." Gene **58**(2-3): 229-41.

Neilands, J. B. (1995). "Siderophores: structure and function of microbial iron transport compounds." J Biol Chem **270**(45): 26723-6.

Neville, C., Murphy, A., Kavanagh, K. and Doyle, S. (2005). "A 4'-phosphopantetheinyl transferase mediates non-ribosomal peptide synthetase activation in *Aspergillus fumigatus*." Chembiochem **6**(4): 679-85.

Nielsen, J. B., Nielsen, M. L. and Mortensen, U. H. (2008). "Transient disruption of non-homologous end-joining facilitates targeted genome manipulations in the filamentous fungus *Aspergillus nidulans*." Fungal Genet Biol **45**(3): 165-70.

Nielsen, M. L., Albertsen, L., Lettier, G., Nielsen, J. B. and Mortensen, U. H. (2006). "Efficient PCR-based gene targeting with a recyclable marker for *Aspergillus nidulans*." Fungal Genet Biol **43**(1): 54-64.

Nierman, W. C., Pain, A., Anderson, M. J., Wortman, J. R., Kim, H. S., Arroyo, J., Berriman, M., Abe, K., Archer, D. B., Bermejo, C., Bennett, J., Bowyer, P., Chen, D., Collins, M., Coulsen, R., Davies, R., Dyer, P. S., Farman, M., Fedorova, N., Fedorova, N., Feldblyum, T. V., Fischer, R., Fosker, N., Fraser, A., Garcia, J. L., Garcia, M. J., Goble, A., Goldman, G. H., Gomi, K., Griffith-Jones, S., Gwilliam, R., Haas, B., Haas, H., Harris, D., Horiuchi, H., Huang, J., Humphray, S., Jimenez, J., Keller, N., Khouri, H., Kitamoto, K., Kobayashi, T., Konzack, S., Kulkarni, R., Kumagai, T., Lafon, A., Latge, J. P., Li, W., Lord, A., Lu, C., Majoros, W. H., May, G. S., Miller, B. L., Mohamoud, Y., Molina, M., Monod, M., Mouyna, I., Mulligan, S., Murphy, L., O'Neil, S., Paulsen, I., Penalva, M. A., Pertea, M., Price, C., Pritchard, B. L., Quail, M. A., Rabbinowitsch, E., Rawlins, N., Rajandream, M. A., Reichard, U., Renauld, H., Robson, G. D., Rodriguez de Cordoba, S., Rodriguez-Pena, J. M., Ronning, C. M., Rutter, S., Salzberg, S. L., Sanchez, M., Sanchez-Ferrero, J. C., Saunders, D., Seeger, K., Squares, R., Squares, S., Takeuchi, M., Tekaia, F., Turner, G., Vazquez de Aldana, C. R., Weidman, J., White, O., Woodward, J., Yu, J. H., Fraser, C., Galagan, J. E., Asai, K., Machida, M., Hall, N., Barrell, B. and Denning, D. W. (2005). "Genomic sequence of the pathogenic and allergenic filamentous fungus *Aspergillus fumigatus*." Nature **438**(7071): 1151-6.

Niide, O., Suzuki, Y., Yoshimaru, T., Inoue, T., Takayama, T. and Ra, C. (2006). "Fungal metabolite gliotoxin blocks mast cell activation by a calcium- and superoxide-dependent mechanism: implications for immunosuppressive activities." Clin Immunol **118**(1): 108-16.

Ninomiya, Y., Suzuki, K., Ishii, C. and Inoue, H. (2004). "Highly efficient gene replacements in Neurospora strains deficient for nonhomologous end-joining." Proc Natl Acad Sci U S A **101**(33): 12248-53.

Novak, K. D., Peterson, M. D., Reedy, M. C. and Titus, M. A. (1995). "Dictyostelium myosin I double mutants exhibit conditional defects in pinocytosis." J Cell Biol **131**(5): 1205-21.

O'Gorman, C. M., Fuller, H. T. and Dyer, P. S. (2009). "Discovery of a sexual cycle in the opportunistic fungal pathogen *Aspergillus fumigatus*." Nature **457**(7228): 471-4.

Oberegger, H., Eisendle, M., Schrettl, M., Graessle, S. and Haas, H. (2003). "4'-phosphopantetheinyl transferase-encoding npgA is essential for siderophore biosynthesis in *Aspergillus nidulans*." Curr Genet **44**(4): 211-5.

Oberegger, H., Schoeser, M., Zadra, I., Abt, B. and Haas, H. (2001). "SREA is involved in regulation of siderophore biosynthesis, utilization and uptake in *Aspergillus nidulans*." Mol Microbiol **41**(5): 1077-89.

Oberegger, H., Schoeser, M., Zadra, I., Schrettl, M., Parson, W. and Haas, H. (2002a). "Regulation of freA, acoA, lysF, and cycA expression by iron availability in *Aspergillus nidulans*." Appl Environ Microbiol **68**(11): 5769-72.

Oberegger, H., Zadra, I., Schoeser, M., Abt, B., Parson, W. and Haas, H. (2002b). "Identification of members of the *Aspergillus nidulans* SREA regulon: genes involved in siderophore biosynthesis and utilization." Biochem Soc Trans **30**(4): 781-3.

Oide, S., Moeder, W., Krasnoff, S., Gibson, D., Haas, H., Yoshioka, K. and Turgeon, B. G. (2006). "NPS6, encoding a nonribosomal peptide synthetase involved in siderophore-mediated iron metabolism, is a conserved virulence determinant of plant pathogenic ascomycetes." Plant Cell **18**(10): 2836-53.

Ortel, I. and Keller, U. (2009). "Combinatorial assembly of simple and complex D-lysergic acid alkaloid peptide classes in the ergot fungus *Claviceps purpurea*." J Biol Chem **284**(11): 6650-60.

Pan, X. Q. and Harday, J. (2007). "Electromicroscopic observations on gliotoxin-induced apoptosis of cancer cells in culture and human cancer xenografts in transplanted SCID mice." In Vivo **21**(2): 259-65.

Panaccione, D. G. and Coyle, C. M. (2005). "Abundant respirable ergot alkaloids from the common airborne fungus *Aspergillus fumigatus*." Appl Environ Microbiol **71**(6): 3106-11.

Paris, S., Debeaupuis, J. P., Crameri, R., Carey, M., Charles, F., Prevost, M. C., Schmitt, C., Philippe, B. and Latge, J. P. (2003a). "Conidial hydrophobins of *Aspergillus fumigatus*." Appl Environ Microbiol **69**(3): 1581-8.

Paris, S., Wysong, D., Debeaupuis, J. P., Shibuya, K., Philippe, B., Diamond, R. D. and Latge, J. P. (2003b). "Catalases of *Aspergillus fumigatus*." Infect Immun **71**(6): 3551-62.

Patron, N. J., Waller, R. F., Cozijnsen, A. J., Straney, D. C., Gardiner, D. M., Nierman, W. C. and Howlett, B. J. (2007). "Origin and distribution of epipolythiodioxopiperazine (ETP) gene clusters in filamentous ascomycetes." BMC Evol Biol **7**: 174.

Perrin, R. M., Fedorova, N. D., Bok, J. W., Cramer, R. A., Wortman, J. R., Kim, H. S., Nierman, W. C. and Keller, N. P. (2007). "Transcriptional regulation of chemical diversity in *Aspergillus fumigatus* by LaeA." PLoS Pathog **3**(4): e50.

Pitkin, J. W., Panaccione, D. G. and Walton, J. D. (1996). "A putative cyclic peptide efflux pump encoded by the TOXA gene of the plant-pathogenic fungus *Cochliobolus carbonum*." <u>Microbiology</u> **142 (Pt 6)**: 1557-65.

Piva, T. J. (1994). "Gliotoxin induces apoptosis in mouse L929 fibroblast cells." <u>Biochem Mol Biol Int</u> **33**(3): 411-9.

Punt, P. J. and van den Hondel, C. A. (1992). "Transformation of filamentous fungi based on hygromycin B and phleomycin resistance markers." <u>Methods Enzymol</u> **216**: 447-57.

Qiao, J., Kontoyiannis, D. P., Calderone, R., Li, D., Ma, Y., Wan, Z., Li, R. and Liu, W. (2008). "Afyap1, encoding a bZip transcriptional factor of *Aspergillus fumigatus*, contributes to oxidative stress response but is not essential to the virulence of this pathogen in mice immunosuppressed by cyclophosphamide and triamcinolone." <u>Med Mycol</u> **46**(8): 773-82.

Qiao, J., Liu, W. and Li, R. (2010). "Truncated Afyap1 Attenuates Antifungal Susceptibility of *Aspergillus fumigatus* to Voriconazole and Confers Adaptation of the Fungus to Oxidative Stress." <u>Mycopathologia</u>.

Reeves, E. P., Messina, C. G., Doyle, S. and Kavanagh, K. (2004a). "Correlation between gliotoxin production and virulence of *Aspergillus fumigatus* in *Galleria mellonella*." <u>Mycopathologia</u> **158**(1): 73-9.

Reeves, E. P., Reiber, K., Neville, C., Scheibner, O., Kavanagh, K. and Doyle, S. (2006). "A nonribosomal peptide synthetase (Pes1) confers protection against oxidative stress in *Aspergillus fumigatus*." <u>FEBS J</u> **273**(13): 3038-53.

Reiber, K., Reeves, E. P., Neville, C. M., Winkler, R., Gebhardt, P., Kavanagh, K. and Doyle, S. (2005). "The expression of selected non-ribosomal peptide synthetases in *Aspergillus fumigatus* is controlled by the availability of free iron." <u>FEMS Microbiol Lett</u> **248**(1): 83-91.

Rementeria, A., Lopez-Molina, N., Ludwig, A., Vivanco, A. B., Bikandi, J., Ponton, J. and Garaizar, J. (2005). "Genes and molecules involved in *Aspergillus fumigatus* virulence." <u>Rev Iberoam Micol</u> **22**(1): 1-23.

Renshaw, J. C., Robson, G., Trinci, A. P., Wiebe, M. G., Livens, F. R., Collison, D. and Taylor, R. J. (2002). "Fungal siderophores:structures, functions and applications." <u>Mycol Res</u> **106**(10): 1123-1142.

Renwick, J., Daly, P., Reeves, E. P. and Kavanagh, K. (2006). "Susceptibility of larvae of *Galleria mellonella* to infection by *Aspergillus fumigatus* is dependent upon stage of conidial germination." <u>Mycopathologia</u> **161**(6): 377-84.

Revill, W. P., Bibb, M. J. and Hopwood, D. A. (1995). "Purification of a malonyltransferase from Streptomyces coelicolor A3(2) and analysis of its genetic determinant." <u>J Bacteriol</u> **177**(14): 3946-52.

Riederer, B., Han, M. and Keller, U. (1996). "D-Lysergyl peptide synthetase from the ergot fungus *Claviceps purpurea*." J Biol Chem **271**(44): 27524-30.

Rigbers, O. and Li, S. M. (2008). "Ergot alkaloid biosynthesis in *Aspergillus fumigatus*. Overproduction and biochemical characterization of a 4-dimethylallyltryptophan N-methyltransferase." J Biol Chem **283**(40): 26859-68.

Rock, F. L., Hardiman, G., Timans, J. C., Kastelein, R. A. and Bazan, J. F. (1998). "A family of human receptors structurally related to *Drosophila* Toll." Proc Natl Acad Sci U S A **95**(2): 588-93.

Rodriguez, P. L. and Carrasco, L. (1992). "Gliotoxin: inhibitor of poliovirus RNA synthesis that blocks the viral RNA polymerase 3Dpol." J Virol **66**(4): 1971-6.

Ruijter, G. J., Bax, M., Patel, H., Flitter, S. J., van de Vondervoort, P. J., de Vries, R. P., vanKuyk, P. A. and Visser, J. (2003). "Mannitol is required for stress tolerance in *Aspergillus niger* conidiospores." Eukaryot Cell **2**(4): 690-8.

Samel, S. A., Schoenafinger, G., Knappe, T. A., Marahiel, M. A. and Essen, L. O. (2007). "Structural and functional insights into a peptide bond-forming bidomain from a nonribosomal peptide synthetase." Structure **15**(7): 781-92.

Saugier-Veber, P., Devergie, A., Sulahian, A., Ribaud, P., Traore, F., Bourdeau-Esperou, H., Gluckman, E. and Derouin, F. (1993). "Epidemiology and diagnosis of invasive pulmonary aspergillosis in bone marrow transplant patients: results of a 5 year retrospective study." Bone Marrow Transplant **12**(2): 121-4.

Schabereiter-Gurtner, C., Selitsch, B., Rotter, M. L., Hirschl, A. M. and Willinger, B. (2007). "Development of novel real-time PCR assays for detection and differentiation of eleven medically important *Aspergillus* and *Candida* species in clinical specimens." J Clin Microbiol **45**(3): 906-14.

Schaffner, A., Douglas, H. and Braude, A. (1982). "Selective protection against conidia by mononuclear and against mycelia by polymorphonuclear phagocytes in resistance to *Aspergillus*. Observations on these two lines of defense in vivo and in vitro with human and mouse phagocytes." J Clin Invest **69**(3): 617-31.

Scharf, D. H., Remme, N., Heinekamp, T., Hortschansky, P., Brakhage, A. A. and Hertweck, C. (2010). "Transannular disulfide formation in gliotoxin biosynthesis and its role in self-resistance of the human pathogen Aspergillus fumigatus." J Am Chem Soc **132**(29): 10136-41.

Schrettl, M., Bignell, E., Kragl, C., Joechl, C., Rogers, T., Arst, H. N., Jr., Haynes, K. and Haas, H. (2004). "Siderophore biosynthesis but not reductive iron assimilation is essential for Aspergillus fumigatus virulence." J Exp Med **200**(9): 1213-9.

Schrettl, M., Bignell, E., Kragl, C., Sabiha, Y., Loss, O., Eisendle, M., Wallner, A., Arst, H. N., Jr., Haynes, K. and Haas, H. (2007). "Distinct roles for intra- and

extracellular siderophores during Aspergillus fumigatus infection." PLoS Pathog **3**(9): 1195-207.

Schrettl, M., Carberry, S., Kavanagh, K., Haas, H., Jones, G. W., O'Brien, J., Nolan, A., Stephens, J., Fenelon, O. and Doyle, S. (2010). "Self-protection against gliotoxin--a component of the gliotoxin biosynthetic cluster, GliT, completely protects *Aspergillus fumigatus* against exogenous gliotoxin." PLoS Pathog **6**(6): e1000952.

Schrettl, M., Kim, H. S., Eisendle, M., Kragl, C., Nierman, W. C., Heinekamp, T., Werner, E. R., Jacobsen, I., Illmer, P., Yi, H., Brakhage, A. A. and Haas, H. (2008). "SreA-mediated iron regulation in *Aspergillus fumigatus*." Mol Microbiol **70**(1): 27-43.

Schwarzer, D., Finking, R. and Marahiel, M. A. (2003). "Nonribosomal peptides: from genes to products." Nat Prod Rep **20**(3): 275-87.

Schwecke, T., Gottling, K., Durek, P., Duenas, I., Kaufer, N. F., Zock-Emmenthal, S., Staub, E., Neuhof, T., Dieckmann, R. and von Dohren, H. (2006). "Nonribosomal peptide synthesis in *Schizosaccharomyces pombe* and the architectures of ferrichrome-type siderophore synthetases in fungi." Chembiochem **7**(4): 612-22.

Scotter, J. M. and Chambers, S. T. (2005). "Comparison of galactomannan detection, PCR-enzyme-linked immunosorbent assay, and real-time PCR for diagnosis of invasive aspergillosis in a neutropenic rat model and effect of caspofungin acetate." Clin Diagn Lab Immunol **12**(11): 1322-7.

Segal, B. H. (2007). "Role of macrophages in host defense against aspergillosis and strategies for immune augmentation." Oncologist **12 Suppl 2**: 7-13.

Seifert, M., Nairz, M., Schroll, A., Schrettl, M., Haas, H. and Weiss, G. (2008). "Effects of the Aspergillus fumigatus siderophore systems on the regulation of macrophage immune effector pathways and iron homeostasis." Immunobiology **213**(9-10): 767-78.

Sheppard, D. C., Doedt, T., Chiang, L. Y., Kim, H. S., Chen, D., Nierman, W. C. and Filler, S. G. (2005). "The Aspergillus fumigatus StuA protein governs the up-regulation of a discrete transcriptional program during the acquisition of developmental competence." Mol Biol Cell **16**(12): 5866-79.

Simon, A., Kullberg, B. J., Tripet, B., Boerman, O. C., Zeeuwen, P., van der Ven-Jongekrijg, J., Verweij, P., Schalkwijk, J., Hodges, R., van der Meer, J. W. and Netea, M. G. (2008). "Drosomycin-like defensin, a human homologue of *Drosophila melanogaster* drosomycin with antifungal activity." Antimicrob Agents Chemother **52**(4): 1407-12.

Skory, C. D., Horng, J. S., Pestka, J. J. and Linz, J. E. (1990). "Transformation of *Aspergillus parasiticus* with a homologous gene (pyrG) involved in pyrimidine biosynthesis." Appl Environ Microbiol **56**(11): 3315-20.

Smedsgaard, J. (1997). "Micro-scale extraction procedure for standardized screening of fungal metabolite production in cultures." <u>J Chromatogr A</u> **760**(2): 264-70.

Smedsgaard, J. and Nielsen, J. (2005). "Metabolite profiling of fungi and yeast: from phenotype to metabolome by MS and informatics." <u>J Exp Bot</u> **56**(410): 273-86.

Smith, J. M., Tang, C. M., Van Noorden, S. and Holden, D. W. (1994). "Virulence of *Aspergillus fumigatus* double mutants lacking restriction and an alkaline protease in a low-dose model of invasive pulmonary aspergillosis." <u>Infect Immun</u> **62**(12): 5247-54.

Soderhall, K. and Cerenius, L. (1998). "Role of the prophenoloxidase-activating system in invertebrate immunity." <u>Curr Opin Immunol</u> **10**(1): 23-8.

Spikes, S., Xu, R., Nguyen, C. K., Chamilos, G., Kontoyiannis, D. P., Jacobson, R. H., Ejzykowicz, D. E., Chiang, L. Y., Filler, S. G. and May, G. S. (2008). "Gliotoxin production in *Aspergillus fumigatus* contributes to host-specific differences in virulence." <u>J Infect Dis</u> **197**(3): 479-86.

Stachelhaus, T., Huser, A. and Marahiel, M. A. (1996). "Biochemical characterization of peptidyl carrier protein (PCP), the thiolation domain of multifunctional peptide synthetases." <u>Chem Biol</u> **3**(11): 913-21.

Stachelhaus, T. and Marahiel, M. A. (1995). "Modular structure of genes encoding multifunctional peptide synthetases required for non-ribosomal peptide synthesis." <u>FEMS Microbiol Lett</u> **125**(1): 3-14.

Stachelhaus, T., Mootz, H. D. and Marahiel, M. A. (1999). "The specificity-conferring code of adenylation domains in nonribosomal peptide synthetases." <u>Chem Biol</u> **6**(8): 493-505.

Stack, D., Frizzell, A., Tomkins, K. and Doyle, S. (2009). "Solid Phase 4'-Phosphopantetheinylation: Fungal Thiolation Domains are Targets for Chemoenzymatic Modification." <u>Bioconjug Chem</u>.

Stack, D., Neville, C. and Doyle, S. (2007). "Nonribosomal peptide synthesis in Aspergillus fumigatus and other fungi." <u>Microbiology</u> **153**(Pt 5): 1297-306.

Steffan, N., Grundmann, A., Yin, W. B., Kremer, A. and Li, S. M. (2009). "Indole prenyltransferases from fungi: a new enzyme group with high potential for the production of prenylated indole derivatives." <u>Curr Med Chem</u> **16**(2): 218-31.

Steinbach, W. J., Cramer, R. A., Jr., Perfect, B. Z., Asfaw, Y. G., Sauer, T. C., Najvar, L. K., Kirkpatrick, W. R., Patterson, T. F., Benjamin, D. K., Jr., Heitman, J. and Perfect, J. R. (2006). "Calcineurin controls growth, morphology, and pathogenicity in *Aspergillus fumigatus*." <u>Eukaryot Cell</u> **5**(7): 1091-103.

Steller, S., Sokoll, A., Wilde, C., Bernhard, F., Franke, P. and Vater, J. (2004). "Initiation of surfactin biosynthesis and the role of the SrfD-thioesterase protein." <u>Biochemistry</u> **43**(35): 11331-43.

Strieker, M., Tanovic, A. and Marahiel, M. A. (2010). "Nonribosomal peptide synthetases: structures and dynamics." <u>Curr Opin Struct Biol</u> **20**(2): 234-40.

Stringer, M. A. and Timberlake, W. E. (1995). "dewA encodes a fungal hydrophobin component of the Aspergillus spore wall." <u>Mol Microbiol</u> **16**(1): 33-44.

Suen, Y. K., Fung, K. P., Lee, C. Y. and Kong, S. K. (2001). "Gliotoxin induces apoptosis in cultured macrophages via production of reactive oxygen species and cytochrome c release without mitochondrial depolarization." <u>Free Radic Res</u> **35**(1): 1-10.

Sugui, J. A., Pardo, J., Chang, Y. C., Zarember, K. A., Nardone, G., Galvez, E. M., Mullbacher, A., Gallin, J. I, Simon, M. M. and Kwon-Chung, K. J. (2007). "Gliotoxin is a virulence factor of *Aspergillus fumigatus*: gliP deletion attenuates virulence in mice immunosuppressed with hydrocortisone." <u>Eukaryot Cell</u> **6**(9): 1562-9.

Summers, R. G., Ali, A., Shen, B., Wessel, W. A. and Hutchinson, C. R. (1995). "Malonyl-coenzyme A:acyl carrier protein acyltransferase of *Streptomyces glaucescens*: a possible link between fatty acid and polyketide biosynthesis." <u>Biochemistry</u> **34**(29): 9389-402.

Sutton, P., Newcombe, N. R., Waring, P. and Mullbacher, A. (1994). "In vivo immunosuppressive activity of gliotoxin, a metabolite produced by human pathogenic fungi." <u>Infect Immun</u> **62**(4): 1192-8.

Tekaia, F. and Latge, J. P. (2005). "*Aspergillus fumigatus*: saprophyte or pathogen?" <u>Curr Opin Microbiol</u> **8**(4): 385-92.

Tepsic, K., Grunde-Cimerman, N. and Frisvad, J. (1997). "Growth and mycotoxin production by *Aspergillus fumigatus* strains isolated from a saltern." <u>FEMS Microbiology Letters</u> **157**: 9-12.

Thomas, A., Korb, V., Guillemain, R., Caruba, T., Boussaud, V., Billaud, E., Prognon, P., Begue, D. and Sabatier, B. (2010). "Clinical outcomes of lung-transplant recipients treated by voriconazole and caspofungin combination in aspergillosis." <u>J Clin Pharm Ther</u> **35**(1): 49-53.

Thornton, C. R. (2008). "Development of an immunochromatographic lateral-flow device for rapid serodiagnosis of invasive aspergillosis." <u>Clin Vaccine Immunol</u> **15**(7): 1095-105.

Thornton, C. R. (2010). "Detection of invasive aspergillosis." <u>Adv Appl Microbiol</u> **70**: 187-216.

Tojo, S., Naganuma, F., Arakawa, K. and Yokoo, S. (2000). "Involvement of both granular cells and plasmatocytes in phagocytic reactions in the greater wax moth, *Galleria mellonella*." <u>J Insect Physiol</u> **46**(7): 1129-1135.

Tomee, J. F. and Kauffman, H. F. (2000). "Putative virulence factors of *Aspergillus fumigatus*." Clin Exp Allergy **30**(4): 476-84.

Toyotome, T., Watanabe, A., Iwasaki, A. and Kamei, K. (2009). "[Strategy of Aspergillus fumigatus to evade attacks from host--projectile weapons and armor]." Nippon Ishinkin Gakkai Zasshi **50**(3): 139-45.

Tudzynski, P., Holter, K., Correia, T., Arntz, C., Grammel, N. and Keller, U. (1999). "Evidence for an ergot alkaloid gene cluster in *Claviceps purpurea*." Mol Gen Genet **261**(1): 133-41.

Unsold, I. A. and Li, S. M. (2005). "Overproduction, purification and characterization of FgaPT2, a dimethylallyltryptophan synthase from *Aspergillus fumigatus*." Microbiology **151**(Pt 5): 1499-505.

Unsold, I. A. and Li, S. M. (2006). "Reverse prenyltransferase in the biosynthesis of fumigaclavine C in *Aspergillus fumigatus*: gene expression, purification, and characterization of fumigaclavine C synthase FGAPT1." Chembiochem **7**(1): 158-64.

Valiante, V., Heinekamp, T., Jain, R., Hartl, A. and Brakhage, A. A. (2008). "The mitogen-activated protein kinase MpkA of Aspergillus fumigatus regulates cell wall signaling and oxidative stress response." Fungal Genet Biol **45**(5): 618-27.

Verdaguer, V., Walsh, T. J., Hope, W. and Cortez, K. J. (2007). "Galactomannan antigen detection in the diagnosis of invasive aspergillosis." Expert Rev Mol Diagn **7**(1): 21-32.

Vicentefranqueira, R., Moreno, M. A., Leal, F. and Calera, J. A. (2005). "The zrfA and zrfB genes of *Aspergillus fumigatus* encode the zinc transporter proteins of a zinc uptake system induced in an acid, zinc-depleted environment." Eukaryot Cell **4**(5): 837-48.

Wallner, A., Blatzer, M., Schrettl, M., Sarg, B., Lindner, H. and Haas, H. (2009). "Ferricrocin, a siderophore involved in intra- and transcellular iron distribution in *Aspergillus fumigatus*." Appl Environ Microbiol **75**(12): 4194-6.

Wallwey, C., Matuschek, M. and Li, S. M. (2010). "Ergot alkaloid biosynthesis in *Aspergillus fumigatus*: conversion of chanoclavine-I to chanoclavine-I aldehyde catalyzed by a short-chain alcohol dehydrogenase FgaDH." Arch Microbiol **192**(2): 127-34.

Walmsley, S. R., Print, C., Farahi, N., Peyssonnaux, C., Johnson, R. S., Cramer, T., Sobolewski, A., Condliffe, A. M., Cowburn, A. S., Johnson, N. and Chilvers, E. R. (2005). "Hypoxia-induced neutrophil survival is mediated by HIF-1alpha-dependent NF-kappaB activity." J Exp Med **201**(1): 105-15.

Walzel, B., Riederer, B. and Keller, U. (1997). "Mechanism of alkaloid cyclopeptide synthesis in the ergot fungus *Claviceps purpurea*." Chem Biol **4**(3): 223-30.

Wang, J., Machado, C., Panaccione, D. G., Tsai, H. F. and Schardl, C. L. (2004). "The determinant step in ergot alkaloid biosynthesis by an endophyte of perennial ryegrass." Fungal Genet Biol **41**(2): 189-98.

Waring, P. and Beaver, J. (1996). "Gliotoxin and related epipolythiodioxopiperazines." Gen Pharmacol **27**(8): 1311-6.

Weber, T. and Marahiel, M. A. (2001). "Exploring the domain structure of modular nonribosomal peptide synthetases." Structure **9**(1): R3-9.

Weindling, R. and Emerson, O. H. (1936). "The isolation of a toxic substance from the culture filtrate of *Trichoderma*." *Phytopathology* **26**: 1068-1070.

White, P. L., Linton, C. J., Perry, M. D., Johnson, E. M. and Barnes, R. A. (2006). "The evolution and evaluation of a whole blood polymerase chain reaction assay for the detection of invasive aspergillosis in hematology patients in a routine clinical setting." Clin Infect Dis **42**(4): 479-86.

White, T. C., Marr, K. A. and Bowden, R. A. (1998). "Clinical, cellular, and molecular factors that contribute to antifungal drug resistance." Clin Microbiol Rev **11**(2): 382-402.

Wiederhold, N. P., Thornton, C. R., Najvar, L. K., Kirkpatrick, W. R., Bocanegra, R. and Patterson, T. F. (2009). "Comparison of lateral flow technology and galactomannan and (1->3)-beta-D-glucan assays for detection of invasive pulmonary aspergillosis." Clin Vaccine Immunol **16**(12): 1844-6.

Willger, S. D., Grahl, N. and Cramer, R. A., Jr. (2009). "*Aspergillus fumigatus* metabolism: clues to mechanisms of in vivo fungal growth and virulence." Med Mycol **47 Suppl 1**: S72-9.

Willger, S. D., Puttikamonkul, S., Kim, K. H., Burritt, J. B., Grahl, N., Metzler, L. J., Barbuch, R., Bard, M., Lawrence, C. B. and Cramer, R. A., Jr. (2008). "A sterol-regulatory element binding protein is required for cell polarity, hypoxia adaptation, azole drug resistance, and virulence in *Aspergillus fumigatus*." PLoS Pathog **4**(11): e1000200.

Willingale, J., Perera, K. P. and Mantle, P. G. (1983). "An intermediary role for the tremorgenic mycotoxin TR-2 in the biosynthesis of verruculogen." Biochem J **214**(3): 991-3.

Yamada, A., Kataoka, T. and Nagai, K. (2000). "The fungal metabolite gliotoxin: immunosuppressive activity on CTL-mediated cytotoxicity." Immunol Lett **71**(1): 27-32.

Yamada, O., Na Nan, S., Akao, T., Tominaga, M., Watanabe, H., Satoh, T., Enei, H. and Akita, O. (2003). "dffA gene from *Aspergillus oryzae* encodes L-ornithine N5-oxygenase and is indispensable for deferriferrichrysin biosynthesis." J Biosci Bioeng **95**(1): 82-8.

Yamakami, Y., Hashimoto, A., Tokimatsu, I. and Nasu, M. (1996). "PCR detection of DNA specific for Aspergillus species in serum of patients with invasive aspergillosis." J Clin Microbiol **34**(10): 2464-8.

Yonus, H., Neumann, P., Zimmermann, S., May, J. J., Marahiel, M. A. and Stubbs, M. T. (2008). "Crystal structure of DltA. Implications for the reaction mechanism of non-ribosomal peptide synthetase adenylation domains." J Biol Chem **283**(47): 32484-91.

Yoshida, L. S., Abe, S. and Tsunawaki, S. (2000). "Fungal gliotoxin targets the onset of superoxide-generating NADPH oxidase of human neutrophils." Biochem Biophys Res Commun **268**(3): 716-23.

Young, C., McMillan, L., Telfer, E. and Scott, B. (2001). "Molecular cloning and genetic analysis of an indole-diterpene gene cluster from *Penicillium paxilli*." Mol Microbiol **39**(3): 754-64.

Yu, J. H., Hamari, Z., Han, K. H., Seo, J. A., Reyes-Dominguez, Y. and Scazzocchio, C. (2004). "Double-joint PCR: a PCR-based molecular tool for gene manipulations in filamentous fungi." Fungal Genet Biol **41**(11): 973-81.

Zhang, J., Li, S., Musa, S., Zhou, H. and Xiang, X. (2009). "Dynein light intermediate chain in Aspergillus nidulans is essential for the interaction between heavy and intermediate chains." J Biol Chem **284**(50): 34760-8.

9. Appendix I

9.1 Materials

9.1.1 Aspergillus Media and Agar

9.1.1.1 Sabouraud Dextrose Broth

Sabouraud-dextrose broth (30 g) (Oxoid, Cambridge, UK) was added to 1 L distilled water, and dissolved. The solution was autoclaved and stored at 4 $^{\circ}$C.

9.1.1.2 Sabouraud Agar

Sabouraud agar (65 g) (Oxoid, Cambridge, UK) was added to 1 L distilled water and dissolved. The solution was autoclaved, and allowed to cool to ~50 $^{\circ}$C. Agar (25 ml) was subsequently poured into 90 mm petri dishes, under sterile conditions. The plates were allowed to set and stored at 4 $^{\circ}$C.

9.1.1.3 Malt Extract Agar

Malt extract agar (50 g) (Difco, Maryland, USA) was added to 1 L distilled water, and dissolved. The solution was autoclaved, and allowed to cool to ~50 $^{\circ}$C. Agar (25 ml) was then poured into 90 mm petri dishes, under sterile conditions. The plates were allowed to set and stored at 4 $^{\circ}$C.

9.1.1.4 Aspergillus Minimal Media

9.1.1.4.1 50 X Salt Solution

KCl (26 g), MgSO$_4$.7H$_2$O (26 g), and KH$_2$PO$_4$ (76 g) was dissolved in 1 L distilled water and autoclaved. The solution was stored at 4 $^{\circ}$C.

9.1.1.4.2 100 X Ammonium Tartrate

Ammonium Tartrate (92 g) was dissolved in 1 L distilled water. The solution was autoclaved and stored at room temperature.

9.1.1.4.3 0.3 M L-Glutamine

L-glutamine (43.8 g) was dissolved in 800 ml distilled water. 1-2 drops of conc. HCl was added to aid dissolving. The pH was adjusted to pH 6.5 and the final volume was brought up to 1 L. The solution was filter sterilised and stored at room temperature.

9.1.1.5 Trace Elements

9.1.1.5.1 Trace Elements containing Iron

$Na_2B_4O_7.7H_2O$ (40 mg), $CuSO_4.5H_2O$ (400 mg), $FeSO_4.7H_2O$ (800 mg), $Na_2MoO.2H_2O$ (800 mg), and $ZnSO_4.7H_2O$ (8 g) were dissolved in order, in 800 ml distilled water allowing each to dissolve completely before addition of the next component. A few drops of conc. HCl was added to maintain the solution. The solution was then brought up to 1 L with distilled water, and filter sterilised.

9.1.1.5.2 Trace Elements without Iron

$Na_2B_4O_7.10H_2O$ (40 mg), $CuSO_4.5H_2O$ (400 mg), $MnSO_4.10H_2O$ (800 mg), $Na_2MoO.2H_2O$ (800 mg) and $ZnSO_4.7H_2O$ (8 g) were dissolved in order, in 800 ml distilled water allowing each to dissolve completely before addition of the next component. A few drops of conc. HCl was added to maintain the solution. The solution was then brought up to 1 L with distilled water, and filter sterilised.

9.1.1.6 Aspergillus Minimal Media Liquid

9.1.1.6.1 AMM Containing Iron

Salt solution (50 X, 20 ml), Ammonium Tartrate (100 X, 10 ml), and Glucose (10 g) were added to 800 ml distilled water. Trace elements containing Iron (1 ml) (Section 9.1.1.5.1) was added and the solution was adjusted to pH 6.8. The solution was brought to 1 L distilled water, mixed, autoclaved at 105 ^{o}C for 30 min and stored at room temperature.

9.1.1.6.2 AMM without Iron

Salt solution (50 X, 20 ml), Ammonium Tartrate (100 X, 10 ml), and Glucose (10 g) were added to 800 ml distilled water. Trace elements without Iron (1 ml) (Section 9.1.1.5.2) was added and the solution was adjusted to pH 6.8. The solution was brought to 1 L distilled water, mixed, autoclaved at 105 ^{o}C for 30 min and stored at room temperature.

9.1.1.6.3 MM containing Iron

Salt solution (50 X, 20 ml), glucose (10 g) and trace elements containing iron (1 ml) (Section 9.1.1.5.1) were added to 800 ml distilled water and dissolved. The pH of the solution was adjusted to pH 6.5 and made up to 1 L distilled water. The solution was autoclaved at 105 ^{o}C for 30 min. Filter sterilised L-glutamine (0.3 M, 66.3 ml) (Section 9.1.1.4.3) was added to the solution. The solution was stored at room temperature.

9.1.1.6.4 MM without Iron

Salt solution (50 X, 20 ml), glucose (10 g) and trace elements without iron (1 ml) (Section 9.1.1.5.2) were added to 800 ml distilled water and dissolved. The pH of the solution was adjusted to pH 6.5 and made up to 1 L distilled water. The solution was autoclaved at 105 ^{o}C for 30 minutes. Filter sterilised L-glutamine (0.3 M, 66.3 ml) (Section 9.1.1.4.3) was added to the solution. The solution was stored at room temperature.

9.1.1.7 Aspergillus Minimal Media Agar

9.1.1.7.1 AMM Agar

Agar (20 g) was added to 1 L of AMM Liquid media (Section 9.1.1.6.1 or 9.1.1.6.2). The solution was autoclaved and allowed to cool to about 50 ^{o}C and the agar mixture (25 ml) was poured into 90 mm petri dishes under sterile conditions and stored at 4 ^{o}C.

9.1.1.7.2 MM Agar

Agar (20 g) was added to 1 L of MM Liquid Media without added L-glutamine (Section 9.1.1.6.3 or 9.1.1.6.4). The solution was autoclaved and allowed to cool to about 50 $^{\circ}$C. L-glutamine (0.3 M; 66.3 ml) was mixed into the cooling agar solution and the agar mixture (25 ml) was poured into 90 mm petri dishes under sterile conditions and stored at 4 $^{\circ}$C.

9.1.1.8 Regeneration Agar

9.1.1.8.1 1.8 % (w/v) Regeneration Agar

Aspergillus salt solution (50 X; 20 ml), Ammonium Tartrate (100 X; 10 ml), and Trace elements (1 ml) (Section 9.1.1.5.1) were added to 800 ml distilled water and dissolved. The solution was adjusted to pH 6.8. Sucrose (342 g) was added and the solution was made up to 1 L distilled water. Agar (18 g) was added to the solution. The solution was autoclaved and kept at 65 $^{\circ}$C until required.

9.1.1.8.2 0.7% (w/v) Regeneration Agar

Aspergillus salt solution (50 X; 20 ml), Ammonium Tartrate (100 X; 10 ml), and Trace elements (1 ml) (Section 9.1.1.5.1) were added to 800 ml distilled water and dissolved. The pH of the solution was adjusted to pH 6.8. Sucrose (342 g) was added and the solution was made up to 1 L distilled water. Agar (7 g) was added to the solution. The solution was autoclaved and kept at 65 $^{\circ}$C until required.

9.1.2 Solutions for pH Adjustment

9.1.2.1 5 M Hydrochloric Acid (HCl)

Deionised water (40 ml) and hydrochloric acid (43.64 ml) were added slowly to a glass graduated cylinder. The final volume was adjusted to 100 ml. The solution was stored at room temperature.

9.1.2.2 5 M Sodium Hydroxide (NaOH)

NaOH pellets (20 g) were added to deionised water (80 ml) and dissolved using a magnetic stirrer. The final volume was adjusted to 100 ml. The solution was stored at room temperature.

9.1.3 Phosphate Buffer Saline

One PBS tablet (20 X) (Oxoid, Cambridge, UK) was added to 200 ml of distilled water, and dissolved by stirring. The solution was autoclaved and stored at room temperature.

9.1.4 Phosphate Buffer Saline-Tween 20 (PBST)

Tween-20 (0.5 ml) was added to 1 L PBS (Section 9.1.3). The solution was stored at room temperature.

9.1.5 Phosphate Buffer Saline-Tween 80 (PBST-80)

Tween-80 (0.5 ml) was added to 1 L PBS (Section 9.1.3). The solution was stored at room temperature.

9.1.6 Plate assays

Plate assay additives were prepared as stock solutions in either water or methanol. Iron solutions were stored at room temperature, bathophenanthrolinedisulfonic acid disodium salt (BPS), voriconazole, hydrogen peroxide, and menadione solutions were stored at 4 ^{o}C. Gliotoxin and amphothericin B solutions were stored at -20 ^{o}C. Further details are provided in Table 9.1.

Table 9.1: Plate assay additives.

Plate Additive		Stock	Diluents	Conc. in plate	Vol/50 ml Agar
Iron	FeCl$_3$	1 mM	Water	10 μM	500 μl
		75 mM	Water	1.5 mM	1 ml
	FeSO$_4$	1 mM	Water	10 μM	500 μl
		75 mM	Water	1.5 mM	1 ml
Batho-phenanthroline-disulfonic acid disodium salt	BPS	10 mM	Water	200 μM	1 ml
Hydrogen peroxide	H$_2$O$_2$	1 M	Water	1 mM	50 μl
			Water	2 mM	100 μl
			Water	3 mM	150 μl
			Water	4 mM	200 μl
Voriconazole	Vrc	100 μg/ml	Water	0.15 μg/ml	15 μl
			Water	0.25 μg/ml	25 μl
Menadione		20mM	Methanol	10mM	25μl
				20mM	50μl
				30mM	75μl
Gliotoxin	GT	1 mg/ml	Methanol	5 μg/ml	250 μl
			Methanol	10 μg/ml	500 μl
			Methanol	20 μg/ml	1 ml
Ampothericin B	Amp B		Water	0.15μg/ml	30μl
				0.25μg/ml	50μl
				0.5μg/ml	100μl

9.1.7 Luria-Bertani Broth

LB Broth (25 g) (Difco, Maryland, USA) was dissolved in 1 L distilled water and dissolved. The solution was autoclaved and stored at 4 $^{\circ}$C.

9.1.8 Luria-Bertani Agar

LB Agar (40 g) (Difco, Maryland, USA) was dissolved in 1 L distilled water. The solution was autoclaved, and allowed to cool to ~50 $^{\circ}$C. Agar (25 ml) was then

poured into 90 mm petri dishes, under sterile conditions and allowed to set. They were stored at 4 ^{o}C.

9.1.9 80 % (v/v) Glycerol

Glycerol (80 ml) was added to 20 ml deionised water. The solution was autoclaved and stored at 4 ^{o}C.

9.1.10 Antibiotics and Supplements

All antibiotics were supplied by Sigma-Aldrich, with the exception of hygromycin B (Melford Laboratories Ltd, Suffolk, U.K). Antibiotics were prepared in water and stored at -20 ^{o}C, with the exception of hygromycin B, which was stored at 4 ^{o}C. Further details are provided in Table 9.2.

Table 9.2: Common antibiotics and supplements with working concentrations

Antibiotic	Diluent	Stock concentration	Typical working conc.
Ampicillin	water	100 mg/ml	100 μg/ml
Hygromycin B	water	420 mg/ml	250 μg/ml
Pyrithiamine	water	100 μg/ml	100 ng/ml
Phleomycin	water	25 mg/ml	40 μg/ml

9.1.11 *E. coli* transformation buffers
9.1.11.1 5 M Potassium Acetate

Potassium acetate (4.907 g) was dissolved in distilled water (10 ml).

9.1.11.2 0.2 M Acetic Acid

Acetic acid (1 ml, 17.48 M) was added to distilled water (86.4 ml).

9.1.11.3 RF1

Potassium acetate (3 ml, 5 M) (Section 9.1.11.1), Calcium chloride dihydrate (0.75 g), and glycerol (75 g) were added to 450 ml distilled water. The pH was adjusted to pH 5.92 with 0.2 M acetic acid (Section 9.1.11.2). Rubidium chloride (6 g) and $MnCl_2.4H_2O$ (4.95 g) were added to the solution and the final volume was brought to 500 ml with distilled water. The solution was filter-sterilised and stored at 4 ^{o}C.

9.1.11.4 RF2

Rubidium chloride (0.6 g), calcium chloride dihydrate (5.5 g), MOPS (1.05 g) and glycerol (75 g) were added to 400 ml distilled water. The pH was adjusted to 6.8 with 5 M NaOH (Section 9.1.2.2). The final volume brought up to 500 ml. The solution was filtered sterilised and stored at 4 ^{o}C.

9.1.12 DNA Electrophoresis Reagents

9.1.12.1 50 X Tris-Acetate Buffer (TAE)

Trizma base (242 g) was added to 57.1 ml glacial acetic acid and 100 ml of 0.5 M EDTA, pH 8.0. The volume was adjusted to 1 L with distilled water. The solution was stored at room temperature.

9.1.12.2 1 X Tris-Acetate Buffer (TAE)

50 X TAE (20 ml) (Section 9.1.12.1) was added to distilled water (980 ml). The solution was stored at room temperature.

9.1.12.3 Ethidium Bromide

Ethidium bromide was supplied at 10 mg/ml of which 3 µl was used per 100 ml agarose gel.

9.1.12.4 6 X DNA Loading Dye

Loading dye (Promega, Southampton, UK) was used at the concentration supplied.

9.1.13 RNA Electrophoresis Reagents

9.1.13.1 RNA Glassware

All glassware required for RNA reagent preparation was soaked in 5% (v/v) HCl overnight and rinsed with DEPC water (Section 9.1.13.2).

9.1.13.2 Diethylpyrocarbonate H_2O (DEPC)

DEPC (1 ml) was added to 1 L distilled water in a pre-treated 1L Duran bottle (Section 9.1.13.1). The bottle was placed on a magnetic stirrer, and allowed to stir overnight. The solution was autoclaved and stored at room temperature.

9.1.13.3 10 X Formaldehyde Agarose (FA) Buffer

MOPS (41.9 g), sodium acetate (6.8 g) and 0.5 M EDTA pH 8 (20 ml) were dissolved in 800 ml DEPC water (Section 9.1.13.2). The pH of the solution was adjusted to pH 7.0 and the final volume brought up to 1 L with DEPC water. The solution was autoclaved and stored at room temperature.

9.1.13.4 1 X Formaldehyde Agarose (FA) Running Buffer

FA gel buffer (10 X, 100 ml), 37 % (v/v) (12.3 M) formaldehyde (20 ml) and DEPC water (Section 9.1.13.2) (880 ml) were added to a pre-treated 1 L Duran bottle (Section 9.1.13.1). The solution was stored at room temperature.

9.1.13.5 5 X RNA Loading Buffer

Bromophenol Blue (25 mg), 0.5 M EDTA pH 8.0 (80 μl), 37 % (v/v) (12.3 M) formaldehyde (750 μl), glycerol (2 ml), formamide (3.084 ml) and 10X FA Buffer (4 ml) (Section 9.1.13.3), were added together. The buffer was stored at 4 ^{o}C for three months.

9.1.14 10 % (w/v) Sodium Dodecyl Sulphate (SDS)

SDS (10 g) was added to 100 ml deionised water, and dissolved. The solution was stored at room temperature. If SDS precipitated, the solution was incubated at 37 ^{o}C until the SDS went back into solution.

9.1.15 0.3 M Sodium Acetate

Sodium acetate (2.46 g) was dissolved in 100 ml distilled water. The solution was mixed and stored at room temperature.

9.1.16 Transformation Reagents

9.1.16.1 0.7 M Potassium Chloride

KCl (26.1 g) was dissolved in 500 ml distilled water. The solution was autoclaved and stored at room temperature.

9.1.16.2 25 mM Potassium Phosphate Monobasic

KH$_2$PO$_4$ (1.7 g) was dissolved in 500 ml distilled water.

9.1.16.3 25 mM Potassium Phosphate dibasic

K$_2$HPO$_4$ (0.87 g) was dissolved in 200 ml distilled water.

9.1.16.4 Lysis Buffer and Lytic Enyzmes

9.1.16.4.1 Lysis Buffer

KCl (26.1 g) was dissolved in 25 mM KH$_2$PO$_4$ (350 ml) (Section 9.1.16.2). The pH was adjusted to pH 5.8 with 25 mM K$_2$HPO$_4$ (Section 9.1.16.3). The solution was brought to 500 ml with distilled water.

9.1.16.4.2 Lysis Buffer containing Lytic Enzymes

Lytic enzymes from *Trichoderma* harzianum (0.45 g) were added to 15 ml lysis buffer (Section 9.1.16.4.1) and filter sterilised with a 0.45 μm filter, changing the filter after every 10 ml.

9.1.16.5 Buffer L6

Sorbitol (72.88 g), Tris-HCl (0.484 g), and $CaCl_2.2H_2O$ (0.588 g) were dissolved in 400 ml distilled water. The pH was adjusted to pH 7.5. The solution was autoclaved and stored at room temperature.

9.1.16.6 Buffer L7

PEG 6000 (60 g) was added to distilled water (40 ml). Tris-HCl (0.157 g) and $CaCl_2.6H_2O$ (0.219 g) was added. Conc. HCl was added to aid dissolution. The pH was adjusted to pH 7.5, the solution was autoclaved and stored at room temperature.

9.1.17 Southern Blot reagents

9.1.17.1 Transfer buffer

Sodium hydroxide (0.6 M; 16 g) and Sodium chloride (0.4 M; 35.07 g) were dissolved in 800 ml distilled water. The volume was adjusted to 1 L with distilled water.

9.1.17.2 20 X SSC

Sodium chloride (175.3 g) and Sodium citrate (88.2 g) were added to distilled water (800 ml). The pH was adjusted to pH 7 and the volume brought up to 1 L distilled water. The solution was autoclaved and stored at room temperature.

9.1.17.3 2 X SSC

SSC (100 ml, 20 X) (Section 9.1.17.2) was added to 900 ml distilled water and stored at room temperature.

9.1.17.4 Dig Buffer 1 (10 X)

Malic Acid (23.22 g) and NaCl (17.5 g) were added to 180 ml distilled water. The pH was adjusted to pH 7.5. Pellets of NaOH were added to aid dissolving. The volume was brought to 200 ml with distilled water. The solution was stored at room temperature.

9.1.17.5 Dig Buffer (1 X)

Malic Acid (2.322 g) and NaCl (1.75 g) were added to 180 ml distilled water. The pH was adjusted to pH 7.5. Pellets of NaOH were added to aid dissolving. The volume was brought to 200 ml with distilled water. The solution was stored at room temperature.

9.1.17.6 Blocking Reagent

Blocking Reagent was obtained from Roche Applied Science (Mannheim, Germany).

9.1.17.6.1 10 % (w/v) Blocking Reagent

Blocking reagent (50 g) (Section 9.1.17.6) was dissolved in 500 ml Dig Buffer 1 (10X) (Section 9.1.17.4). The solution was mixed by stirring and slight heating. The solution was then autoclaved and stored at 4°C.

9.1.17.7 10 % (w/v) Laurosarcosine

Lauroylsarcosine (1 g) was dissolved in 10 ml distilled water.

9.1.17.8 High SDS/Blocking Buffer

Sodium Dodecyl Sulphate (SDS) (35 g), formamide (250 ml), SSC (20 X, 125 ml) (Section 9.1.17.2), Blocking reagent (10 % (w/v), 100 ml) (Section 9.1.17.6.1), and Lauroylsarcosine (10 % (w/v), 5 ml) (Section 9.1.17.7) were added to 1 L distilled water. The solution was mixed and stored at 4°C. Before use the solution was pre-heated at 65°C for 15 minutes.

9.1.17.9 1 X SSC/0.1 % (w/v) SDS

SSC (20 X, 50 ml) (Section 9.1.17.2) and 4 ml of 10 % (w/v) SDS (Section 9.1.14) was added to distilled water (946 ml). The solution was mixed and stored at room temperature.

9.1.17.10 Dig Wash Buffer (0.3 % (v/v) Tween-20 in Dig Buffer 1)

Tween 20 (0.15 g) was added to Dig Buffer 1 (1 X, 50 ml) (Section 9.1.17.5). The solution was mixed and filter sterilised.

9.1.17.11 Dig Buffer 2

Dig Buffer 1 (1 X) (Section 9.1.17.5) (20 ml) and Blocking reagent (Section 9.1.17.6) (2 g) was mixed and filter sterilised and used immediately.

9.1.17.12 Dig Buffer 3

Tris-HCl (1.575 g), NaCl (0.584 g) and $MgCl_2$ (1.02 g) was dissolved in distilled water (90 ml). The pH was adjusted to pH 9.5 and the final volume brought up to 100 ml. The solution was filtered sterilised and then stored at room temperature.

9.1.17.13 Anti-Digoxigenin-Alkaline Phosphatase (AP), Fab fragment conjugate

Anti-Digoxigenin- AP, Fab fragments (Roche, Mannheim, Germany) (2 μl) was added to 20 ml Dig Buffer 2 (Section 9.1.17.11).

9.1.17.14 Chemiluminescent substrate phosphatase detection (CSPD) Substrate

CSPD (50 μl) (Roche, Mannheim, Germany) was added to Dig Buffer 3 (5 ml) (Section 9.1.17.12).

9.1.18 Chemicals for Photography

9.1.18.1 Developer Solution

The Developer (Kodak) was diluted 1/4 in distilled water and stored in a tinfoil covered Duran in a dark room.

9.1.18.2 Fixer Solution

The fixer solution (Kodak) was diluted 1/5 in distilled water and stored in a tinfoil covered Duran in a dark room.

9.1.19 Organic Extraction Buffer

Ethyl Acetate (300 ml), dichloromethane (200 ml) and Methanol (100 ml) were mixed together and stored in a Duran covered in tinfoil and stored at 4 ^{o}C.

9.1.20 HPLC Reagents

9.1.20.1 Solvent A: 0.1 % (v/v) Trifluroacetic acid (TFA) in HPLC grade water

TFA (1 ml) was added to HPLC Grade Water (1 L) in a darkened Duran.

9.1.20.2 Solvent B: 0.1 % (v/v) Trifluroacetic acid (TFA) in HPLC grade Acetonitrile

TFA (1 ml) was added to HPLC Grade Acetonitrile (1 L) in a darkened Duran.

9.1.21 Triacetylfusarinine C (TAFC) Conjugation Reagents

9.1.21.1 BSA (6 mg/ml)

BSA (62 mg) was dissolved in PBS (103 ml) (Section 9.1.3).

9.1.21.2 Sulfo N-hydroxysulfosuccinimidyl-4-azidobenzoate (HSAB) preparation

HSAB (6 mg) was dissolved in DMSO (150 μl), in a 15 ml Falcon tube covered in tinfoil. PBS (Section 9.1.3) was added to bring the solution up to 3 ml.

9.1.22 Protein Induction and Purification Reagents

9.1.22.1 1 M Isopropyl β-D-Thiogalactopyranoside (IPTG) Solution.

IPTG (0.238 g) was dissolved in 1 ml distilled water. The solution was filter sterilised and stored at -20 ^{o}C.

9.1.22.2 Lysis Buffer

Trizma base (3.02 g), EDTA (0.186 g), Sodium chloride (2.92 g) and Glycerol (50 ml) were dissolved in 400 ml distilled water. The pH was adjusted to pH 8.0. The final volume was made up to 500 ml with deionised water, and stored at 4 ^{o}C.

9.1.22.3 Lysozyme Stock

Lysozyme (10 mg) was dissolved in 1 ml distilled water.

9.1.22.4 Sodium Deoxycholate (120mM)

Sodium deoxycholate (50 mg) was added to 1 ml distilled water.

9.1.22.5 Wash Buffer

Trizma base (3.02 g), EDTA (0.186 g), Sodium Chloride (2.92 g) and Triton-X-100 (20 ml) were dissolved in 400 ml distilled water. The pH was adjusted to pH 8.0, and the final volume was made up to 500 ml with deionised water, and stored at 4 ^{o}C.

9.1.22.6 2 M Urea Buffer

Trizma base (3.02 g), Urea (60 g), and EDTA (0.186 g) were dissolved in 300 ml deionised water and the pH was adjusted to pH 8.0. The final volume was made up to 500 ml with deionised water, and stored at 4 ^{o}C.

9.1.22.7 8 M Urea Buffer

Trizma base (3.02 g), Urea (240 g), and EDTA (0.186 g) were dissolved in 300 ml deionised water. The pH was adjusted to pH 8.0. The final volume was made up to 500 ml with deionised water, and stored at 4 ^{o}C.

9.1.23 SDS-PAGE Reagents

9.1.23.1 1.5 M Tris-HCl, pH 8.8

Trizma base (18.15 g) was dissolved in 75 ml deionised water. The pH was adjusted to pH 8.8 and the volume brought up to 100 ml with deionised water. The solution was stored at 4 ^{o}C.

9.1.23.2 0.5 M Tris-HCl, pH 6.8

Trizma base (6.05 g) was dissolved in 75 ml deionised water. The pH was adjusted to pH 6.8 and the solution was brought to a final volume of 100 ml with deionised water. The solution as stored at 4 ^{o}C.

9.1.23.3 10 % (w/v) Ammonium Persulphate

Ammonium persulphate (0.1 g) was added to 1 ml deionised water. The solution was stored at 4 ^{o}C, and used immediately.

9.1.23.4 30 % (w/v) Acrylamide/Bis

Protogel (National Diagnostics, Hessle Hull, England) was obtained which contained 30 % (w/v) acrylamide: 0.8% (w/v) Bis-acrylamide.

9.1.23.5 0.5 % (w/v) Bromophenol Blue

Bromophenol blue (0.1 g) was added to deionised water (20 ml). The solution was stored at 4 ^{o}C.

9.1.23.6 Lysis Buffer

NaH$_2$PO$_4$.2H$_2$O (1.5 g) and Sodium Chloride (4.3 g) were dissolved in 250 ml distilled water. The solution was stored at room temperature.

9.1.23.7 5 X Solubilisation Buffer

Glycerol (10 ml) was added to deionised water (4 ml), containing 1.6 ml of 10 % (w/v) SDS and 1 ml of 0.5 M Tris-HCl, (pH 6.8). The solution was mixed and then 2-mercapthoethanol (0.4 ml) was added along with 0.2 ml of 0.5% (w/v) bromophenol blue solution (Section 9.1.23.5). The solution was stored at room temperature.

9.1.23.8 5 X Electrode Running Buffer

Trizma base (15 g), glycine (72 g) and SDS (5 g) were dissolved in deionised water (800 ml). The final volume was adjusted to 1 L. The solution was stored at room temperature.

9.1.23.8.1 1 X Electrode Running Buffer

5 X Electrode Running Buffer (200 ml) (Section 9.1.23.8.1) was added to 800 ml distilled water. The solution was stored at room temperature.

9.1.23.9 Coomassie Blue Stain Solution

Coomassie® Brilliant Blue R (2.5 g), glacial acetic acid (100 ml), methanol (450 ml) and deionised water (50 ml) were added to a glass bottle and mixed. The solution was brought to a final volume of 1 L and the solution was stored at room temperature.

9.1.23.10 Destain Solution

Glacial acetic acid (100 ml) and methanol (150 ml) was added to 750 ml deionised water. The solution was stored at room temperature.

9.1.24 Western Blot Reagents

9.1.24.1 Towbin Electrotransfer Buffer

Trizma base (30.3 g) and glycine (144 g) were added to 3 L deionised water and 1 L methanol. The pH was adjusted to between 8 – 8.5 and the final volume brought to 5 L with deionised water. The solution was stored at room temperature.

9.1.24.2 Blocking Solution

Marvel® (Powdered Milk) (5 g) was added to 100 ml PBST (Section 9.1.4).

9.1.24.3 Substrate Buffer (0.1 M Tris-HCl, pH 7.6)

Trizma base (12.1 g) was added to 800 ml deionised water. The pH was adjusted to pH 7.6 and the final volume was brought up to 1 L with deionised water. The solution was stored at room temperature.

9.1.24.4 AEC Substrate Buffer Components

9.1.24.4.1 0.2 M Acetic acid Solution

Acetic acid (11.45 ml, 17.48 M) was added to 1 L distilled water. The solution was kept at room temperature.

9.1.24.4.2 0.2 M Sodium acetate Solution

Sodium acetate (27.2 g) was added to 1 L distilled water. The solution was kept at room temperature.

9.1.24.4.3 AEC Substrate Buffer

Acetic acid (148 ml, 0.2 M) (Section 9.1.24.4.1) was mixed with Sodium acetate (352 ml, 0.2 M) (Section 9.1.24.4.2). The pH was adjusted to 5, if required and the final volume was brought to 1 L with distilled water. The solution was stored at room temperature.

9.1.24.4.4 AEC Substrate

3-Amino-9-Ethylcarbazole (AEC) (1 tablet) was dissolved in N,N-Dimethylformamide (1 ml) and vortexed until dissolved.

9.1.24.4.5 AEC Substrate Solution

AEC Substrate (1 ml, Section 9.1.24.4.4) was added to 25 ml AEC Substrate Buffer (Section 9.1.24.4). Once mixed, Hydrogen peroxide (10 μl) was added to the solution. The solution was used immediately.

9.1.24.5 DAB Solution

3, 3' –diaminobenzidine (DAB) (1 tablet) was dissolved in Substrate Buffer (15 ml) (Section 9.1.24.3). Hydrogen Peroxide (7 μl) was added and the solution was used immediately.

9.1.25 ELISA Buffers and Reagents

9.1.25.1 1X Carbonate Buffer

Na_2CO_3 (5.3 g) was dissolved into 900 ml distilled water. $NaHCO_3$ (4.2 g) was added and the pH was adjusted to pH 9.6 with 5 M HCl (Section 9.1.2.1). The final volume was brought up to 1 L with distilled water.

9.1.25.2 ELISA Blocking Buffer

Sucrose (10 g) and BSA (1 g) was added to 100 ml Carbonate Buffer (Section 9.1.25.1).

9.1.25.3 ELISA Antibody Buffer

BSA (1 g) was added to PBST (100 ml) (Section 9.1.4)

9.1.25.4 HRP-conjugated human IgG

HRP-conjugated human IgG (2 μl) was added to ELISA Antibody Buffer (20 ml) (Section 9.1.25.3) and kept on ice until required.

9.1.25.5 Tetramethylbenzidine (TMB) Substrate

Tetramethylbenzidine (TMB) Substrate was used according to manufacturer's instructions. TMB was used at room temperature and kept out of light, as it is light sensitive.

9.1.25.6 ELISA Stop solution (1N H_2SO_4)

Sulphuric acid (6.9 ml) was added to distilled water (250 ml) in a fume hood, using a glass graduated cylinder. The solution was stored in a glass Duran at room temperature.